

# Model Predictive Load Frequency Control Methods with Battery Energy Storage in Future Power Systems



The  
University  
Of  
Sheffield.

**Abidemi Solomon Ajiborisha**

Department of Automatic Control and Systems Engineering  
University of Sheffield

This dissertation is submitted for the degree of  
*Doctor of Philosophy*

September 2021



*Dedicated to my family*

*In loving memory of my father Engineer M.O. Ajiborisha. You said it daddy,  
"books are a thinking man's tools"*



## Acknowledgements

I thank God for His provision of health, wisdom, and strength that saw me through to the completion of this thesis. I am a living testimony of His grace and mercy.

I would like to express my gratitude to my supervisor, Dr Paul Trodden for his guidance and support during the course of my PhD programme. You helped in firming and bringing my ideas, brining them together to make this work complete. In addition I would like to thank my second supervisor, Dr Anthony Rossiter, for his guidance and wise words. I greatly appreciate the assistance of all who contributed to the success of my program, my peers, those within my research group and especially my sponsor: the Petroleum Technology Development Fund (PTDF) Nigeria.

Finally, I would like to say a great thank you to my loving parents and siblings for all their support and encouragement as I pursued my doctorate degree. You were always there when I needed you. Thank you all and God bless.



## Abstract

The power grid is undergoing a transition process characterised by increased inter-connectedness and heterogeneity. This makes maintaining its reliability and quality of supply indicated by a key service known as load frequency control (LFC), a more complex task due to the need for flexible control methods which can effectively multiple energy resources working towards a common objective. Battery energy storage systems (BESS) are key devices that can support LFC. This thesis is concerned with the development of model predictive load frequency control (MPLFC) strategies incorporating battery energy storage systems. A review of the MPLFC applications within legacy and future grids is given including BESS LFC applications. A model consisting of generators and BESS which includes all dynamic subsystem interactions is then developed using the deregulated power system framework. Centralised model predictive load frequency control is applied to this system for the cases of both contracted loads and uncontracted load demands occurring in the network. Limits on subsystem inputs, incremental generator rates, BESS power and energy are considered including BESS state of charge management. The centralised model is a large scale heterogeneous system of coupled subsystems performing a common task of LFC but having different control loops. For independent flexible controller design decentralised control is often desirable. Hence, local decentralised MPC controllers are designed for the BESS and generator subsystems. However, this requires creating suitable decomposed prediction models, from a system of strongly connected subsystems of power generators. In addition, the design process should have stability guarantees despite the dynamics ignored in the decentralised prediction models without compromising control performance. A model decomposition technique that explicitly accounts for all dynamic interactions, while ensuring overlapping information is incorporated in local controllers is adopted. Stability is guaranteed using the inherent robustness property of MPC with the assumption that interacting dynamics ignored by the decentralised controllers are within established interaction bounds linked to inertia of the power system. Simulations show stability is achieved when this approach is applied to LFC. This work is then extended to account for the temporal nature of the future grid characterised by slow

and fast states. A multi time scale hierarchical MPC algorithm is developed where the challenge for MPC in multi time scale systems is selecting a suitable sampling time that ensures acceptable dynamics responses at each time scale. Hence, multirate sampling is employed to account for two timescales. The algorithm was then extended the case of decentralised lower controllers for independent systems with strong dynamic coupling. Simulations show that the LFC objective of regulating the frequency deviation to zero is achieved with the proposed methods.

# Table of contents

<b>List of figures</b>	<b>xiii</b>
<b>List of tables</b>	<b>xvii</b>
<b>Nomenclature</b>	<b>xix</b>
<b>1 Introduction</b>	<b>1</b>
1.1 The Power System . . . . .	1
1.2 Frequency Control in Power Systems . . . . .	4
1.3 Motivation . . . . .	5
1.4 Thesis Scope . . . . .	9
1.5 List of Publications . . . . .	10
1.6 Thesis Outline . . . . .	10
<b>2 Background and Literature Review</b>	<b>13</b>
2.1 Background on Frequency Control . . . . .	14
2.1.1 Frequency Control Loops and Dynamic Models . . . . .	16
2.1.1.1 Primary Control Loop . . . . .	16
2.1.1.2 Secondary Control (LFC) Loop . . . . .	21
2.1.1.3 Tertiary control . . . . .	26
2.1.2 Two area LFC example . . . . .	27
2.2 Model Predictive Control Background/Review . . . . .	30
2.2.1 Centralised MPC Design . . . . .	31
2.2.1.1 Prediction Model . . . . .	31
2.2.1.2 Prediction Equations . . . . .	31
2.2.1.3 Cost Function . . . . .	32
2.2.1.4 Constraints . . . . .	33
2.2.1.5 Dual-mode MPC . . . . .	34
2.2.1.6 Feasibility and Terminal Regions . . . . .	36

2.2.2	Decentralised MPC . . . . .	39
2.2.3	Distributed MPC . . . . .	41
2.2.3.1	Non iterative DMPC . . . . .	44
2.2.3.2	Iterative DMPC . . . . .	44
2.2.4	Hierarchical MPC . . . . .	45
2.3	Battery Energy Storage Systems - BESS . . . . .	48
2.3.1	Potential Applications in Future Power Systems . . . . .	49
2.3.2	Frequency Regulation Applications . . . . .	51
2.4	System Decomposition . . . . .	54
2.4.1	Distributed Optimisation Decomposition . . . . .	55
2.4.2	Overlapping Decomposition . . . . .	56
2.5	Model Predictive Load Frequency Control Review . . . . .	58
2.5.1	Model Predictive Load Frequency Control . . . . .	58
2.6	Model Predictive Control in Future Power Grids . . . . .	62
2.6.1	MPC Application in Future Power Systems . . . . .	62
2.6.1.1	Centralised . . . . .	63
2.6.1.2	Distributed . . . . .	64
2.6.1.3	Hierarchical . . . . .	65
2.7	Conclusion . . . . .	68
<b>3</b>	<b>Load Frequency Control with Battery Energy Storage</b>	<b>71</b>
3.1	Introduction . . . . .	71
3.2	Development of BESS Model Supporting Load Frequency Control . . . . .	73
3.2.0.1	State Space representation . . . . .	76
3.3	Deregulated power system with BESS . . . . .	77
3.3.1	Interconnection of GENCOs and DISCOs . . . . .	78
3.3.2	GENCO dynamic model . . . . .	81
3.3.3	Scheduled inter-area transfers and tie-line dynamics . . . . .	83
3.3.4	Area frequency dynamics and control error . . . . .	83
3.3.5	Different area capacities . . . . .	85
3.3.6	State-space model and discrete-time prediction model . . . . .	86
3.4	MPC formulation for LFC . . . . .	87
3.4.1	Prediction equations . . . . .	87
3.4.2	Controller Objective Function . . . . .	88
3.4.3	System Constraints . . . . .	89
3.4.3.1	Battery Constraints . . . . .	89
3.4.3.2	Generation Constraints . . . . .	90

3.4.3.3	Input Constraints . . . . .	91
3.4.4	Centralised Solution . . . . .	92
3.5	Numerical simulation and discussion . . . . .	92
3.5.1	Case I—No uncontracted load demands . . . . .	94
3.5.2	Case II—Uncontracted load demands . . . . .	99
3.6	Net Energy Neutrality and Energy Recovery . . . . .	104
3.6.1	Impact of energy recovery . . . . .	105
3.7	Conclusion . . . . .	108
<b>4</b>	<b>Decentralised Predictive Load Frequency Control with Battery Energy Storage</b>	<b>111</b>
4.1	Introduction . . . . .	111
4.2	Centralised Model Development . . . . .	113
4.2.1	Model Dynamics . . . . .	113
4.2.2	The Control problem . . . . .	115
4.3	Model Decomposition Methodology . . . . .	117
4.3.1	Structured system model . . . . .	118
4.3.2	Discretisation . . . . .	119
4.3.3	Model Expansion and Decomposition . . . . .	120
4.3.4	Decomposition of Power System Model . . . . .	123
4.4	Decentralized MPC formulation . . . . .	126
4.5	Stability analysis . . . . .	131
4.6	Decentralised MPC scheme LFC in Smart Power System . . . . .	135
4.6.1	Tracking Targets . . . . .	136
4.7	Simulations and Discussion . . . . .	137
4.7.1	Scenario 1 - Decentralised Forward Euler . . . . .	137
4.7.2	Scenario 2 - ceMPC, eDMPC, meDMPC and zDMPC LFC . . . . .	143
4.8	Conclusion . . . . .	148
4.9	Proofs . . . . .	150
4.9.1	Mixed Euler–ZOH discretization . . . . .	150
4.9.2	Deriving a discrete-time model . . . . .	150
4.9.3	Lemma 1 . . . . .	151
4.9.4	Lemma 2 . . . . .	155
4.9.5	Lemma 5 . . . . .	156
4.9.6	Theorem 1 . . . . .	156
4.9.7	Corollary 1 . . . . .	158
4.9.8	Theorem 2 . . . . .	158

---

<b>5</b>	<b>Hierarchical Predictive Load Frequency Control with Battery Energy Storage</b>	<b>159</b>
5.1	Introduction . . . . .	159
5.2	Hierarchical Model Predictive Control . . . . .	161
5.3	Two Layer Hierarchical LFC Structure . . . . .	163
5.3.1	Upper Layer Controller Design . . . . .	164
5.3.2	Lower layer Controller Design . . . . .	167
5.3.3	Clarification of Open Loop Dynamic Behaviour . . . . .	172
5.4	Numerical Simulations . . . . .	174
5.4.1	Impact of Shifting and Multirate sampling . . . . .	174
5.4.2	Hierarchical Load Frequency Control . . . . .	178
5.5	The Decentralised Case . . . . .	182
5.6	Numerical Simulation and Discussion . . . . .	186
5.7	Conclusion . . . . .	188
<b>6</b>	<b>Conclusion and Future Work</b>	<b>191</b>
6.1	Conclusions and Contributions . . . . .	191
6.2	Future Research Directions . . . . .	195
	<b>References</b>	<b>199</b>
	<b>Appendix A Appendix</b>	<b>217</b>
A.1	Chapter 3 . . . . .	218
A.1.1	Deregulated Power System Model - BESS . . . . .	218
A.1.2	Deregulated Power System Model - No BESS . . . . .	220
A.2	Chapter 4 . . . . .	221
A.2.0.1	Transformation Matrices . . . . .	221

# List of figures

1.1	The evolutionary process of the transition to a future smart grid adopted from [6]. New technologies can encompass transmission, distribution and commercial or residential levels of the future grid at large, medium and small scales respectively . . . . .	3
1.2	Power System Generation Control adapted from [14] with new technologies included in a future grid scenario.Red lines indicate power flow and blue lines communications flow. Controls signals generation references (or local feedback) for each type of generator . . . . .	6
2.1	Frequency control loops with activation times and pattern adapted from [37]. The three loops in the upper section from left to right in light red, red and green are primary, secondary and tertiary control loops and are activated in the same order following a frequency excursion event. The lower section shows the characteristics of each loop, the subsequent response pattern of the three loops and their coordinated responses graphically. Time control is used in maintaining accurate synchronous time. . . . .	15
2.2	Schematic of the complete primary loop adapted from [15] made up of speed governing, turbine, generator and load . . . . .	17
2.3	Generator-Load model. . . . .	19
2.4	Turbine Model . . . . .	20
2.5	Speed Governor Model. . . . .	21
2.6	Line diagram of two area system with parameter and variables of each interconnected area . . . . .	23
2.7	Block diagram model for control area i . . . . .	26
2.8	Frequency response in areas 1 and 2 where a deviation still exists with PFC only . . . . .	27

2.9	Mechanical power output of generators where only PFC is insufficient to match the load in area 1 . . . . .	28
2.10	Area control errors of areas 1 and 2 where PFC alone is insufficient to achieve an ACE of zero . . . . .	29
2.11	Tie line flow where only PFC does not drive the tie-line to zero . . . . .	29
2.12	Decentralised control structure showing $S_N$ interacting subsystems. Local controllers $M_i$ do not communicate with each other. . . . .	39
2.13	Distributed MPC with M referring to controllers and S subsystems . . . . .	42
3.1	Battery model . . . . .	75
3.2	Single line diagram of a two-area deregulated power system comprising conventional thermal generators and battery energy storage in each area. The MW capacity of area 2 is larger than that of area 1 . . . . .	79
3.3	The power system with GENCOs, DISCOs and BESS in each area based on the deregulated framework. . . . .	80
3.4	Frequency deviations for areas 1 and 2, case 1 . . . . .	94
3.5	Area control error for areas 1 and 2, case 1 . . . . .	95
3.6	Output power of all generators both areas, Case 1 . . . . .	96
3.7	Generation rate constraint of all generators in area 1 and 2, Case 1 . . . . .	96
3.8	Inputs to areas 1 and 2, and tie-line flow case 1 . . . . .	97
3.9	BESS output power and State of Charge in percentages in areas 1 and 2, case 1 . . . . .	97
3.10	BES inputs and State of Charge(pu) areas 1 and 2, case 1 . . . . .	98
3.11	Frequency and ACE in areas 1 and 2, case 2 . . . . .	99
3.12	Unscheduled load changes in areas 1 and 2, Case 2 . . . . .	100
3.13	Output powers of all generators in both areas, Case 2 . . . . .	100
3.14	Generation rate constraint of all generators in area 1 and 2, Case 2 . . . . .	101
3.15	Inputs to areas 1 and 2 and tie-line flow case 2 . . . . .	102
3.16	BESS output power and state of charge in percentages in areas 1 and 2, case 2 . . . . .	102
3.17	BES inputs and State of Charge(pu) areas 1 and 2, case 2 . . . . .	103
3.18	Change in the energy recovery time of the BESS as a result of weight adjustments indicated by the coloured lines:black (0.01),blue(10),green(100),red(500) and black dash line(1000) in the legend for areas 1 and 2 . . . . .	106
3.19	Frequency deviation in area 1 and Tie-line in area one and two for different weights on $Q_{soc}$ . Top: $Q_{soc} = 0.01$ . Bottom: $Q_{soc} = 1000$ . . . . .	107

3.20	Output power deviation of GENCOs 1 and 4 for different weights on $Q_{soc}$ . Top: $Q_{soc} = 0.01$ . Bottom: $Q_{soc} = 1000$ . . . . .	107
4.1	The centralised model power system consisting of BESS and generators. Local control is achieved by a centralised controller in response to a common frequency represented by $\Delta\omega$ . . . . .	114
4.2	Model with decentralised controllers . . . . .	116
4.3	Surface plot showing the dependence on mechanical starting time $M$ and system damping $D$ . . . . .	135
4.4	Frequency deviation in response to a load disturbance . . . . .	138
4.5	Generator power outputs . . . . .	139
4.6	Battery power outputs . . . . .	139
4.7	Battery state of charge outputs . . . . .	140
4.8	Battery state of charge outputs in pu . . . . .	140
4.9	Generator reference inputs . . . . .	141
4.10	Battery control inputs. . . . .	141
4.11	generation rate constraints. . . . .	142
4.12	Sample of bounds for both the generator and BESS. . . . .	142
4.13	Frequency deviation in response to a load disturbance . . . . .	143
4.14	Generator power outputs . . . . .	144
4.15	Battery power outputs . . . . .	144
4.16	Battery state of charge outputs . . . . .	145
4.17	Battery state of charge outputs in pu . . . . .	145
4.18	Generator reference inputs . . . . .	146
4.19	Battery control inputs. . . . .	147
4.20	generation rate constraints. . . . .	148
5.1	The hierarchical control structure. The upper layer controller generates target references for the lower layer controller . . . . .	165
5.2	Depiction of the connection between both timescales. The slow timescale is $k_s$ with sampling interval $T_s$ for the upper layer while the fast timescale coincident with that of the nominal model is $k$ with sampling interval $T$ . Hence $T_s = Tv$ and $k = k_s v$ . Red lines indicate the direction of information flow. . . . .	170
5.3	The shifting procedure used to calculate the references for each hold of the upper layer input for $v$ number of time steps of the lower layer input	171
5.4	Open loop step response of the power system dynamic to a load disturbance	173

---

5.5	The effect of shifting on the frequency and generator output. Top shifting, bottom no shifting. . . . .	175
5.6	The effect of shifting on battery performance. Top shifting, bottom no shifting. . . . .	175
5.7	The effect of shifting on system inputs. Top with shifting, bottom no shifting. . . . .	176
5.8	The effect of noise on BESS system on frequency and generator output. Top: high level input only. Bottom: hierarchical input . . . . .	176
5.9	The effect of noise on BESS systems. Top: high level input only, bottom: hierarchical input . . . . .	177
5.10	The effect noise on the BESS system on both its and the generators inputs. Top: high level input only. Bottom: hierarchical input. . . . .	177
5.11	The disturbance sequence . . . . .	179
5.12	Frequency deviation and generator outputs comparing centralised and hierarchical control . . . . .	179
5.13	Battery dynamics for centralised and hierarchical control . . . . .	180
5.14	Systems inputs: Generator Top, BESS Bottom. Dotted lines are the input constraints . . . . .	181
5.15	The hierarchical control structure. The upper layer sends reference trajectories to lower layer decentralised controllers designed at the nominal timescale. . . . .	183
5.16	Frequency deviation and generator outputs comparing centralised and hierarchical control . . . . .	187
5.17	Battery dynamics for centralised and hierarchical control . . . . .	188
5.18	Systems inputs: Generator Top, BESS Bottom. . . . .	189

# List of tables

2.1	Parameters used in the simulation of the two area power system . . . . .	27
2.2	Categorisation of distributed MPC. Fully connected schemes involve communication between all controllers while partial schemes are based on neighbour to neighbour communication. Iterative control involves information exchange several times within a sampling interval while for non iterative, information exchange occurs only once within a sampling interval. In independent controllers a local cost function is used by each controller while for cooperating controllers a cost function relating to the global cost is used by each controller . . . . .	42
3.1	Nomenclature of Parameters . . . . .	78
3.2	Parameters of the two area deregulated model . . . . .	92
3.3	Weights and the corresponding costs for the case of BESS and no BESS. Regulations refers to the costs of regulation only <i>i.e</i> frequency and ACE while full systems refers to total system costs. . . . .	105
4.1	The power systems parameters . . . . .	138
4.2	Comparison of the average computation times and cost for the centralised, decentralised zero order hold, decentralised mixed Euler and decentralised Euler MPC controllers . . . . .	147
5.1	Parameters of the power system . . . . .	174
5.2	Parameters of the power system . . . . .	178
5.3	Comparison of the average computation times and cost for centralised and hierarchical MPC . . . . .	181
5.4	Parameters of the power system . . . . .	186
5.5	Comparison of the average computation times and cost for centralised, centralised hierarchical and decentralised hierarchical MPC . . . . .	187



# Nomenclature

## Roman Symbols

AC Alternating Current

ACE Area Control Error

BESS Battery Energy Storage Systems

CMPC Centralised Model Predictive Control

CPS Control Performance Standard

DeMPC Decentralised Model Predictive Control

DISCO Distribution Company

DMPC Distributed Model Predictive Control

EMPC Explicit Model Predictive Control

ESC Energy Service Company

FCMPC Feasible Cooperation Model Predictive Control

GENCO Generation Company

GRC Generation Rate Constraint

ISO Independent System Operator

LFC Load Frequency Control

MPC Model Predictive Control

MPLFC Model Predictive Load frequency Control

MTDC Multi-terminal HVDC

NERC North American Electricity Reliability Corporation

NMPC Nonlinear Model Predictive Control

NNMPC Nominal Nonlinear Model Predictive Control

RNMPC Robust Nonlinear Model Predictive Control

ROCOF Rate of change of Frequency

SCMPC Stability Constrained Model Predictive Control

TRANSCO Transmission System Company

TSO Transmission System Operator

VSC Voltage Source Converters

# Chapter 1

## Introduction

This thesis aims to develop model predictive based control strategies for the load frequency control of future power grids supported by battery energy storage systems. As a result of the drive for affordable and reliable energy supply, the power system is undergoing significant changes, characterised by the increasing integration of new generation technologies. Traditional control methods would have to be adjusted to enable new technologies, such as battery storage systems to participate in load frequency control. This chapter sets the stage for the work carried out in this thesis with an overview of the transition of the power system, load frequency control, motivation and related aims linked to model predictive control and a description of the scope and objectives of this thesis.

### 1.1 The Power System

The electric power system is one of the largest interconnected networks in the world, It is of fundamental importance in modern society. It is an expansive, dynamic and complex system of many individual components networked together which generate, transmit and distribute electrical power over large geographical areas [1]. However, the configuration of the grid is gradually changing driven by a combination of technological, political and economic factors necessitating the need for novel approaches to power system management.

Conceptually within the traditional vertically integrated framework large power networks were made up of several energy companies with each one responsible for all the controls and devices necessary for the security, efficiency and reliability of the system under their area of jurisdiction [2]. The basic operating structure of the power system, mostly still in use today, is as follows:

1. Electricity is generated by large power plants and transmitted at high voltage levels.
2. Interconnected transmission lines convey this high voltage electricity over long distances.
3. These high voltages are stepped down to medium levels using transformers at distribution substations.
4. Over localised networks the voltages are further stepped down to low levels suitable for different categories of end users.

The conventional electricity system was based on this structure. The management and control of the designated areas in this legacy system was by utility companies who are responsible for the entire process of generation, transmission and distribution of electricity. The actions of a utility were limited to their balancing (control) area and all contractual agreements including the supply of energy were limited to their area of control. Hence, the design and control requirements for this system were well established and in terms of complexity manageable. This basic structure remained the standard procedure for operating power systems for decades. However, in recent times, there has been significant changes in the practices used in the planning, operation, control and regulatory structure that govern the power industry [3]. These changes in the regulatory framework were key drivers in the evolution of the power system.

The process of deregulation began a change in the models and algorithms required for control of the power grid. Under deregulation, generation, transmission, and distribution facilities belong to generation (GENCOs), transmission (TRANSCO) and distribution (DISCO) operating companies respectively. GENCOs are independent owners of large generating power plants that sell energy. TRANSCO own and manage transmission networks. They are responsible for the management and maintenance of all assets related to the transmission network. DISCOs own distribution networks which supply energy to end users. Sometimes, they are managed by distribution system operators (DSOs) having similar levels of responsibility as TRANSCO only in this case with respect to the distribution network. In most instances, due to the critical nature of the transmission system, it is still managed by one single operator *i.e* one TRANSCO referred to as the transmission system operator (TSO) or independent system operator (ISO) such as National Grid in the United Kingdom or Statnett in Norway. These networks are characterised by highly bidirectional power flows [4] requiring new modelling methodologies which accommodate the deregulated structure in their design [5].

The recent change taking place in the power system relates to the area of information and communication technology. This process is expected to create a future power system with certain key features such as the ability to integrate new generation technologies, optimise network asset usage, accommodate new market dynamics, be environmentally friendly and increase overall grid efficiency, safety and reliability. This transition process and increasing complexity of the grid is depicted in Figure 1.1. Here we see that beyond the standard large scale power plants of the traditional grid, different generation technologies work together to ensure the smooth operation of the power system and can be installed at both transmission and distribution levels based on their capacities and controlled from the corresponding control centres.

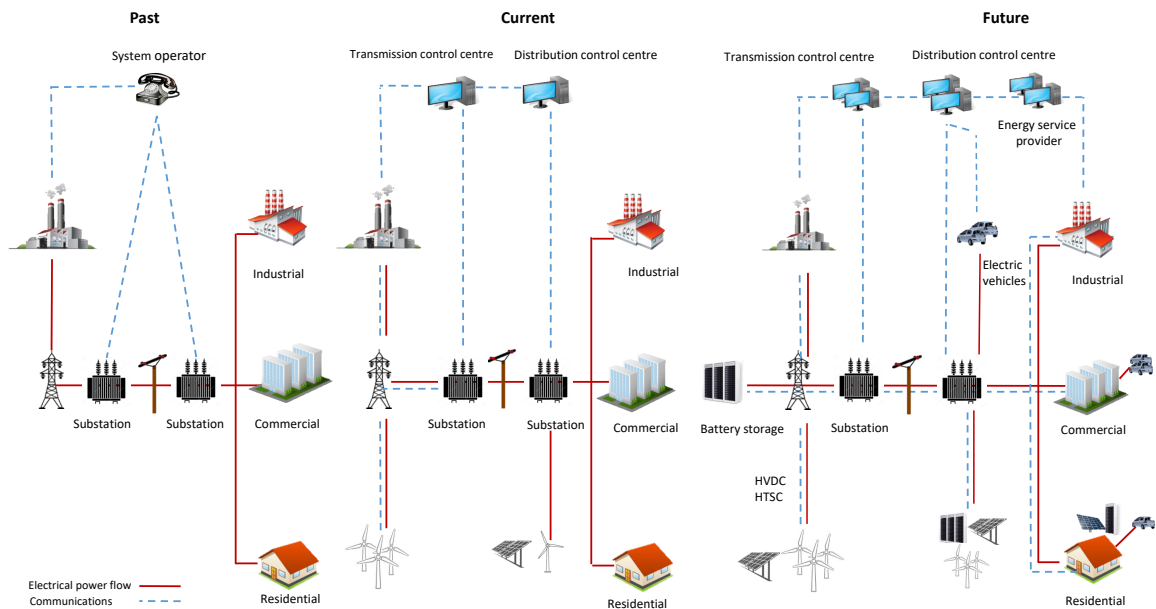


Fig. 1.1 The evolutionary process of the transition to a future smart grid adopted from [6]. New technologies can encompass transmission, distribution and commercial or residential levels of the future grid at large, medium and small scales respectively

However, for the future grid to function properly some enabling technologies are required [7–9]. These include high speed, bidirectional adaptive communication networks, real-time decision making for smart control and optimisation, advanced computing and non centralised control. These intelligent technologies would provide: improved interfaces and decision support; better human machine interaction; enable real time smart decision making; self healing; and improve the overall knowledge and efficiency of the grid.

## 1.2 Frequency Control in Power Systems

The stability of the power system is dependent on its initial operating condition and on the nature of the corresponding disturbance. It is therefore a function of the motion of the system around an equilibrium set (the initial operating conditions) and indicates the ability of the system to continue operation following a disturbance [10]. The value of the nominal operating point of the system frequency is dependent on the geographic region. This is 50Hz in the United Kingdom. Over the course of a day the total power demand varies continuously in a predictable manner. Typically, these changes in demand which are large and slow are met by a process known as unit commitment. This determines the modes of operations of generators which have been scheduled for use a day ahead. A committed unit is one that has been turned on and is synchronised with the grid. Here, the generation schedules are sent out once a day giving the operating schedule for the day. This is implemented considering system constraints such as physical generator ramp rates, transmission line congestion limits, voltage constraints, in addition to costs, pricing and other economic considerations [11–13]. Following unit commitment, economic dispatch indicating generator actual power output is implemented next at shorter intervals of about 30 minutes and used to determine the optimal generation unit to be dispatched in order to meet the schedule derived from the unit commitment operation subject to constraints in meeting the system load demand. Considering these constraints is necessary for the safe and secure operation of the power system.

The process of unit commitment and economic dispatch however, do not account for real time power supply and load imbalances. Efficient operation of the power system requires generation and demand to be closely matched at every time instant necessitating adjustments in generation outputs *i.e* real-time power supply and load balancing at minimal cost. Thus, these load changes which are smaller and faster are met using a process that allows quicker generation control for system frequency control. Following an instantaneous disturbance, generators react to restore balance between the electrical demand and the mechanical power output of the system. For an increase in demand the first move to rectify this change is from inertial response of rotating machines such as turbines and motors (frequency sensitive) due to a loss of kinetic energy. For steam turbine driven generators representing large rotating masses, this means that the normally equal electrical and mechanical torques which determine the rotational speed and nominal operating frequency of the system become unequal with the electrical torque exceeding the mechanical torque. Since the effect of the

mechanical torque is to increase the system speed and the electrical torque to slow it down, the system would begin to slow down leading to a subsequent drop in frequency albeit to a non nominal stable operating point with an increase in generator output but at fixed operating set points. This is primary frequency control which is proportional action local to generators and takes place within 15 seconds.

These small disturbances are usually dealt with without the need for significant variation in the power generated or load consumed in the system. For a situation where there is a sudden loss of generation or the connection of a large load, the power system becomes unbalanced due to a power supply-demand load mismatch [1]. For the system frequency to be restored to its nominal value, the mechanical torque must be increased. This would lead to an increase in rotational speed and bring the system back to the equilibrium state of equal mechanical and electrical torques with constant speed. This is readily achieved by resetting the operational set points of participating units thereby regulating the production of torque in response to frequency deviations within 30 seconds. This is secondary frequency control which is centralised in a balancing area. The focus of this thesis on this level of control. It is also known as load frequency control. It typically incorporates the faster primary control response at the transmission level which in Figure 1.1 is via the transmission control centre. The process of resetting the set points of generators is known as tertiary control. This is done either manually or automatically following purely economic dispatch calculations in vertically integrated markets but normally includes additional bilateral contracts settlements by the system operator[1] in deregulated markets.

### 1.3 Motivation

A major feature of the future grid is the integration of new generation technologies. However, this modifies the structure of the power system particularly with the modifications increasingly characterised by a reduction in the use of conventional power generation. As was shown in Section 1.2 these generators are primarily responsible for balancing generation and load demand through the process of LFC. However, most renewable generation technologies are characterised by variability and uncertainty in their power outputs making the prediction of their future behaviour non deterministic and their control complex. In this scenario of increased uncontrollable renewable generation and reduced conventional power supplies there is increased uncertainty in the disturbance and correspondingly in the power imbalance of the system with its reduced inertia. This leads to an increase in the frequency of changes in power patterns

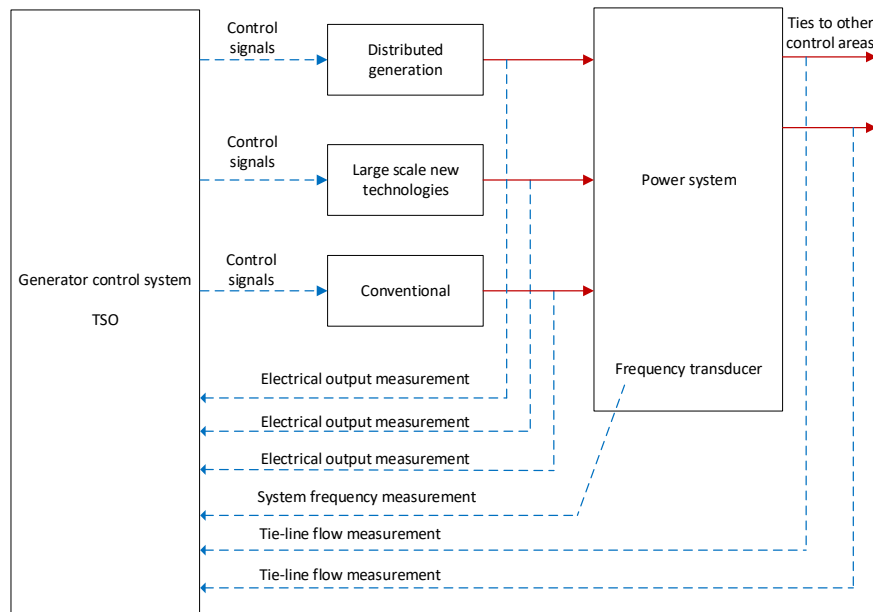


Fig. 1.2 Power System Generation Control adapted from [14] with new technologies included in a future grid scenario. Red lines indicate power flow and blue lines communications flow. Controls signals generation references (or local feedback) for each type of generator

creating more issues with stability in the implementation of LFC [15, 16]. Coupled with the reduction in system inertia, power reserves available for active power control needed for LFC are also reduced. This means that the future grid would increasingly need to rely on new technologies with active power that can be effectively controlled. This would lead to the addition of such new technologies to the generation control structure and a depiction of this future grid scenario is given in Figure 1.2. A technology that is increasingly used for this purpose and the device of focus in this thesis is grid scale battery energy storage systems.

The frequency regulation market for conventional generation is mature and various forms of contractual agreements such as bilateral, poolco or mixed have been adequately covered in the literature [17–19] and represented in the deregulated energy market. Initially, this was not the case for storages. In some instances the market structure was even unfavourable for storage participation in frequency regulation [20]. To create a favourable market for BESS, various orders like the Federal Energy Regulatory Commission (FERC) order 755 in the United States, were created. These enabled

fast responding storages such as BESS to receive performance remunerations. Further additional orders, such as the FERC orders 841 and 845, respectively allowed BESS to provide capacity, ancillary and energy services and permitted them to be included in the class of generating units with their spare capacity utilised on the transmission systems [21]. In Europe, the ENTSO-E (Germany and Netherlands) signal for primary frequency response also provides a means for BESS to participate in frequency regulation. Significant growth in BESS has also been seen in the UK with several consultative smart initiatives like the 'Upgrading our Energy System - Smart Systems and Flexibility plan' report of the national regulator Ofgem outlining several requirements for the integration of BESS and other smart devices into the power grid in an economically and technically efficient manner [22]. In fact, the European Union has identified BESS as devices that can fill the 'flexibility gap' with a Strategic Energy Technology (SET) Plan report in the BATSTORM project leading to recommendations on the way forward for the integration of battery systems into the grid [23].

Beyond the standard LFC framework some ISO's have introduced special regulation signals such as the PJM-RegD (a faster signal that can be followed by fast units), ISO-NE energy neutral and MISO-AGC enhancement for storage units [24]. These regulatory and signal changes now allow storage assets to enjoy the same remuneration benefits as conventional generators for providing ancillary services [25, 26] including applications where for example their ability to allow an offset in time between energy production and consumption can be effectively utilised [27]. Furthermore, they promoted a growth in the use of BESS within the power system. In particular these developments show that BESS can be combined with conventional generators for the implementation of load frequency control.

However, the use of BESS for LFC raises some new challenges in the power system. Conventional generators are still by and large responsible for LFC and their speed of rotation is what determines the power systems nominal operating frequency. For BESS participating in LFC their operation would need to be in response to changes in this frequency for them to effectively contribute to LFC. In addition, the behaviour of the BESS when supporting LFC being carried out by the generators should be such that they do not in anyway contribute to a worsening in the quality of power system frequency. This is possible because the functional classification of BESS is not specific and could change from generation to consumption during operation. Further performance degradation is possible if the control design does not account for the physical system constraints of all generating subsystems. Therefore, in the first instance, a dynamical model that is an aggregation of the generators and BESS is required. This

model should account for any interactions between the generators and BESS in relation to frequency deviations for the effective implementation of LFC. In other words the same information should be fed back to both subsystems devices and any centralised controller should have full model visibility of both subsystems [28]. This centralised model then forms a benchmark from which further design considerations within the future grid are addressed.

In such a large scale complex system, where the implementation of LFC is based on heterogeneous generating sources, independent behaviour of the component device subsystems supported by local controllers is often desirable influenced by factors such as high state dimensionality, geographic spread and ease of computation. In particular, such a design approach enables individual subsystems to remain operational without significant performance degradation since their design and subsequent behaviour is not dependent on information from other subsystems. This can be achieved through non centralised control techniques but with the challenge of managing the non centralised behaviour of the BESS and generators during controller design. [29–31]. The adopted method could be decentralised without any communication or collaborative [32, 33] characterised by information sharing between controllers. Completely independent controller design is particularly challenging for device subsystems in LFC because of the strong coupling due to the common shared objective of frequency regulation by both subsystems. That is the BESS and generator subsystems are strongly coupled through the frequency dynamic of the grid. Completely decentralised design could lead to unacceptable LFC performance except information about the coupling dynamic is incorporated in each controller design. For this to be achieved a suitable technical decomposition methodology [34, 35] which ensures independent but coherent dynamic response of both subsystems is required. Another added complexity in LFC using BESS and generators is the centralised model now has two time scales. Frequency control loops in LFC design is normally dependent on the time constants related to the generators and controller synthesis can be implemented within a single timescale. However, when fast acting BESS are included in the controller design LFC is now subject to two time scales. With the increasing addition of BESS to the grid this timescale consideration could be increasingly relevant in future control designs to ensure that acceptable LFC performance is achieved.

In view of the above challenges regarding LFC in a future power system this thesis aims to develop control strategies for load frequency control using model predictive control (MPC). The decision to use MPC is due to the fact that (MPC) is an advanced control methodology that uses predictions of future system behaviour to determine

optimal inputs at each instant in time while systematically accounting for physical system constraints. MPC also has multivariable and multi input-output capabilities making it suitable for large scale power system design consisting of several inputs and outputs both at the device and area levels using a single centralised controller. In addition MPC also lends itself to non centralised formulations and can be synthesized in decentralised or distributed formats. Hence with regards to LFC, MPC can be used for systematic controller design. MPC can therefore accommodate the integration of BESS into the traditional LFC framework due to its inherent multi input-output property. In addition, physical constraints on generators and BESS can be systematically handled. MPC can also be adapted to decentralised design for heterogeneous power sources. Furthermore, multi timescale formulations are achievable. Finally, due to these features of MPC, the key objective of LFC which is the restoration of frequency to its nominal value and for interconnected systems all tie line flows to their scheduled values following changes in load demand placed on the power system can be readily achieved.

## 1.4 Thesis Scope

In light of the motivations and aims given in Section 1.3 the scope of this thesis is focused on the development of model predictive control based algorithms to tackle the operational challenges relating to the use of BESS and conventional generators for LFC. The main objectives are:

1. Highlight the range of model predictive control formulations and their applications to LFC in conventional and future grids including regulatory policies that promote the potential applications of BESS in power systems with a focus on LFC support.
2. The development of a future grid model within the deregulated framework enabling BESS to participate in load frequency control while accommodating power and energy constraints on the BESS. Generation rate and input constraints are implemented on the GENCOs using centralised MPC.
3. Apply a different approach in decomposing a future power system which cannot be easily decomposed into weakly interconnected systems using the standard balancing area approach such that the groupings or aggregations of the system is based on devices rather than control areas while accounting for the common coupling information between subsystems in a single area.

4. Develop decentralised model predictive load frequency control for the generator and BESS subsystems linked via the frequency state with guarantees stability based on power system parameters which define disturbance bounds. Achieve acceptable LFC performance despite the loss of coordination between controllers due to no inter controller communication exchange.
5. Propose a hierarchical multirate model predictive load control algorithm designed to accommodate the temporal differences in the response of BESS and generator systems (fast and slow state) which make the use of a single sampling rate time challenging. The design is applicable to systems with non separable dynamics.
6. Develop a multi timescale model predictive control load frequency control method based on hierarchical control where the basic sampling rate is based on the battery system rather than on the generators. In addition the communication requirements are minimal with only top down information sharing occurring in the hierarchy.

## 1.5 List of Publications

- A. Ajiborisha and P. Trodden, “Model predictive load frequency control of a deregulated power system with battery energy storage,” in 2019 IEEE Conference on Control Technology and Applications (CCTA), pp. 196–202, IEEE, 2019.
- A. Ajiborisha and P. Trodden (xxxx), “Stable decentralised predictive load-frequency control with battery energy storage,” *Submitted*
- A. Ajiborisha and P. Trodden (xxxx). “Hierarchical model predictive load frequency control with battery energy storage,” *To be submitted*

## 1.6 Thesis Outline

The contributions made in each chapter of this thesis are presented here:

**Chapter 2** The basics of load frequency is covered in the first section of this chapter. The dynamical equations that represent LFC in the traditional power system structure are derived and an example of LFC is shown. Furthermore, a formulation of the centralised MPC format used in this thesis is given. In addition to this decentralised, distributed and hierarchical architectures with their basic attributes are defined. These sections clearly define the LFC problem and the various architectures for solving it in

order to allow a clearer and more detailed review of the literature. Following this, a review on battery energy storage systems; the different multi-use purposes of a BESS within the power system and applications specific to load frequency control is given. This review showed the importance of BESS for power frequency control applications in future grids. From this analysis the relevant decomposition techniques that facilitate non centralised control design and the applicability to LFC is reviewed. The chapter concludes with a review of model predictive load frequency control applications in power systems with a further section on applications of MPC within the context of a future grid using the different MPC architectures presented.

**Chapter 3** The review in Chapter 2 showed the feasibility of using BESS for MPLFC. Chapter 3 provides a novel MPLFC application using BESS systems which handles BESS controllability limitations but at the same time provides visibility to the controller for state of charge management preserving system reliability in the presence of load disturbances. This model development is implemented within the deregulated market framework. Centralised MPC design was used to achieve coordinated behaviour between the GENCOs and BESS with both subsystems responding to changes in frequency. The BESS dynamics are included in the model and are not treated as external disturbances to be rejected by the controller. Coordination between the BESS and GENCOs led to improved system dynamical performance with better generator transient dynamics seen from reduced peaks and smoother behaviour with less operation at ramp limits. This translates to a reduction in the stresses on GENCOs and the power system introduced by new market dynamics. In addition, the controllability constraints of the BESS related to their limited power and energy capacities including their inter-temporal dependencies are handled effectively. GENCOs are driven to their contracted values with DISCOs in the presence of both contracted and uncontracted disturbances even with generation rate and input constraints. This chapter solved the issues of new dynamic interaction, constraint limitation and control rethink required for future grid LFC design. This work was based on [36] as a contribution to this thesis.

**Chapter 4** This Chapter proposes a decentralised MPLFC based on the model developed in Chapter 3 outside of the deregulated structure. The key contributions here are two fold. First the issue of system decomposition in future power systems where the assumption of weak interconnection between areas cannot be applied within a single area since the groupings for non centralised design are based on devices rather than swing dynamics of coherent generators. For this reason a single area was considered to highlight this unique requirement. A approach that solves this problem was therefore

adopted for model decomposition. However, to ensure BESS responsiveness to frequency deviation the inclusion principle was used to provide the common frequency dynamic to both subsystems. This preserved the dynamic interaction created by the model developed in Chapter 3, defining clear control boundaries but using device rather than area groupings. The second contribution was the decentralised controlled system was stable due to the guarantees of stability provided by the design of decentralised controllers. Stability is based on the inherent robustness of MPC without resorting to robust by design and this was linked to the physical properties of power systems relating to inertia and loading damping subject to clearly defined interaction disturbance bounds including the impact of discretisation on prediction accuracy. Simulations were carried out comparing three discretisation based decentralised MPLFC controllers and the objective of LFC were achieved.

**Chapter 5** In this chapter the model used in Chapter 4 is extended to the case of multi-rate dynamic considerations. MPLFC is designed for systems where the dynamics are not clearly separable due to a strong coupling between subsystems. For the special case of a common dynamic being the source of coupling, a hierarchical scheme is designed to account for the slow and fast update rates requiring multi-rate sampling to guarantee acceptable dynamic responses in both the slow and fast time scales due to different BESS and generator speeds. Particular to the LFC problem, this chapter proposes a novel hierarchical multi-rate algorithm for the generator and BESS states including the use of a steady state target calculator to handle changes in targets based caused by changes in load disturbances. The centralised hierarchical method is then extended to the case of lower level decentralised controllers developed in Chapter 4 for subsystems linked by a common state which in the context of LFC is the frequency. A novel hierarchical multirate decentralised overlapping control algorithm for subsystems linked by a common dynamic was implemented using decentralised controllers and the objectives of LFC was achieved.

**Chapter 6** is for concluding statements and contributions. Future research directions are also presented providing insights into some of the opportunities for building upon the work done in this thesis.

# Chapter 2

## Background and Literature Review

The aim of this chapter is to introduce the background knowledge required for load frequency control in power systems. In Chapter 1 the structural changes that drive the development of a future power system and the subsequent requirements and importance of power balancing supported by BESS from the perspective of LFC in order to maintain stability were introduced. Hence the need for advanced control methodologies with desirable technical properties suitable for the management and control of the future power system were highlighted.

In this chapter the focus is on load frequency control, model predictive control, model predictive load frequency control (MPLFC), system decomposition, and BESS applications in power systems. First, the technical aspects and a detailed model of the component parts of the traditional power system used for LFC is detailed in Section 2.1. In Section 2.2 centralised model predictive control formulation and a review of decentralised, distributed and hierarchical architectures of MPC is also presented. This is then followed by Section 2.3 with a review of a battery energy storage systems which is the principal new technology integrated into the traditional grid in this thesis. An explanation on potential future uses and LFC applications show the usefulness and show relevance of BESS in load frequency control. Section 2.4 is a review on the decomposition methods that facilitate non centralised control design application in LFC. This is then followed by 2.5 with a review of applications of model predictive load frequency control in the literature within the traditional power system network. Section 2.6 is a review of MPC applications in smart power systems themed as the future grid characterised by new technologies such as heat pumps, wind turbines, battery storage and microgrids using different MPC architectures.

## 2.1 Background on Frequency Control

An overview of the need for frequency control and the immediate actions taken by generators following a disturbance in the system was given in Section 1.2. That overview made it clear that the fundamental function of load frequency control is to maintain balance in the supply and demand of electrical power. This entire process of active power balance in the power system is used in maintaining a specific operating frequency. Within a given balancing area, the generators are assumed to all swing with a common frequency which is in turn dependent on their synchronous speed and inertia. This enables them to supply the required power needed to maintain a balance in generation and load. Since the frequency is a common factor local to an area in the power system, a change in active power in any part of the system has an impact on the local area frequency.

In Section 1.1 the traditional power network based on the vertically integrated framework was explained. This structure is hierarchical in nature and involves different voltage levels from very high to low. In Section 1.2 it was shown that frequency control in power systems can be split into primary and secondary control. A third level is tertiary control. There it was also revealed that this categorisation is not arbitrary and is based on measurable time dependent factors such as the duration of instability following its occurrence or the time taken for the restoration of system equilibrium. Hence each level of control is of necessity implemented on a different time scale for varying purposes. Functionally, based on a bottom up approach the categories can also be classified into frequency containment, restoration and replacement [38] which is also representative of the speed of response at each level in the hierarchy.

The three different levels of the hierarchy therefore create separate control loops in the power system. Considering the complexity of the power system, with the large number of devices, the dynamics tend to vary over different time scales. Using the varying dynamical responses of the devices whose transients decay at different rates it is possible to de-couple various control loops [16, 1]. These variations in the speed of response are generally categorised into three types of stability; rotor angle, voltage and frequency stability. Hence despite the complexity of the power system it is possible to study each of the control loops separately since they are decoupled from each other as a result of their different time scales of operation. Correspondingly, the three frequency control loops can also be analysed individually based on active response over differing timescales. In Figure 2.1 all the frequency control loops are shown represented in a nested fashion and the activation pattern of each loop following a disturbance is

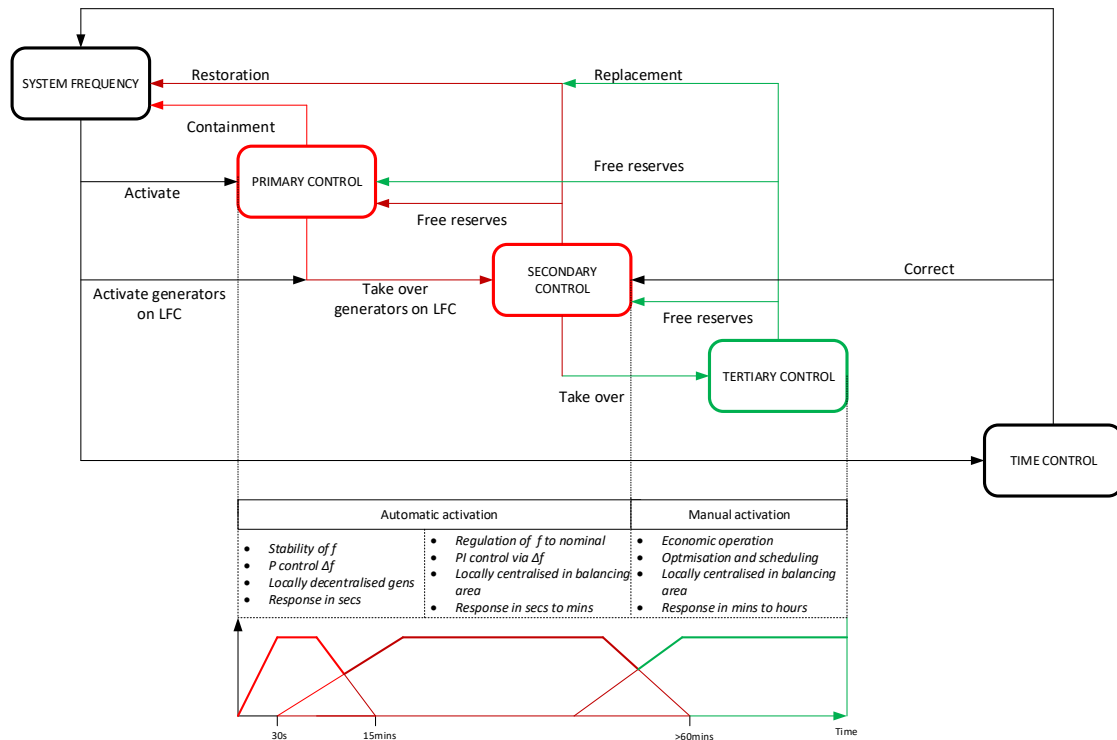


Fig. 2.1 Frequency control loops with activation times and pattern adapted from [37]. The three loops in the upper section from left to right in light red, red and green are primary, secondary and tertiary control loops and are activated in the same order following a frequency excursion event. The lower section shows the characteristics of each loop, the subsequent response pattern of the three loops and their coordinated responses graphically. Time control is used in maintaining accurate synchronous time.

also depicted. The first response is primary control to contain the frequency within pre-specified bounds and occurs within a few seconds. This prevents frequency runaway in the system. Then generators on LFC take over in the process of secondary control allowing other generators which responded during primary control to return to their scheduled values. The process of LFC is the focus of this research work. Finally tertiary control is implemented to determine new economic operating points with the timing control used to ensure global synchronisation of synchronous generators. The synchronous time is proportional to the integral of frequency and is necessary for electric clocks and other devices which depend on accurate frequency for their operations [15]. Traditionally, tertiary control is usually performed offline based on economic considerations. Tertiary control is not considered in this thesis.

### 2.1.1 Frequency Control Loops and Dynamic Models

In this section the different frequency control loops and models of the component parts associated with each of the control loops necessary for balancing the demand and supply of real power is presented. The time scale separation of frequency, rotor and voltage dynamics makes it possible to use a decoupled control design approach. Hence when deriving models this difference in speed makes it possible to ignore the fast responses associated with the rotor angle and voltage, while designing simplified linearised models for the slower response which is the frequency [16]. As a result, in traditional load frequency balancing, simplified models of the generator, load, prime mover and the governor are developed and combined to get a representation of a balancing area. These simplified models make it possible to perform LFC analysis conveniently. More detailed models increase complexity and might prove to be quite unsuitable for frequency studies. The loops associated with frequency control and the models related to each loop are detailed and developed respectively in the next segments of this section.

#### 2.1.1.1 Primary Control Loop

Primary control is the first mitigating action taken to maintain system stability following a frequency excursion event. It sits at the lowest level of the frequency control hierarchy and is the fastest of three control loops. For units taking part in AGC, whenever there is a change in demand, primary frequency control is activated. It is a continuous service implemented by an increase in the power output of the generator due to the action of turbines governors [1]. Primary control is localised within the power station and the power output of participating generation units are adjusted by an increase in the flow of the primary energy source (steam or gas) to the turbine. During this process the reference values of all generators are kept constant and proportional control is used to achieve frequency containment. The complete primary loop is shown in Figure 2.2 and consists of the dynamics models used in accomplishing this level of control which are explained next.

#### Generator-Load Model

The model used in representing the generator and load is derived by considering the process of speed governing of the synchronous generator. If initially the assumption is for a single generator supplying a local load, the net torque of the generator is the difference between the mechanical and electrical torques. When these two are equal the

speed of the generator is steady and does not change. LFC analysis is usually based on changes in load demand and this approach is adopted in this thesis. Following for instance an increase in load, the electrical torque exceeds the mechanical torque which leads to a reduction in the rotational speed of the machine based on the equations of motion. In order for equilibrium to be restored the mechanical torque would have to be increased. This response to load change by the generator i.e the relationship between mechanical and electrical torque due to changes in speed is used in determining the generator load model. The equation relating rotor speed and torque is:

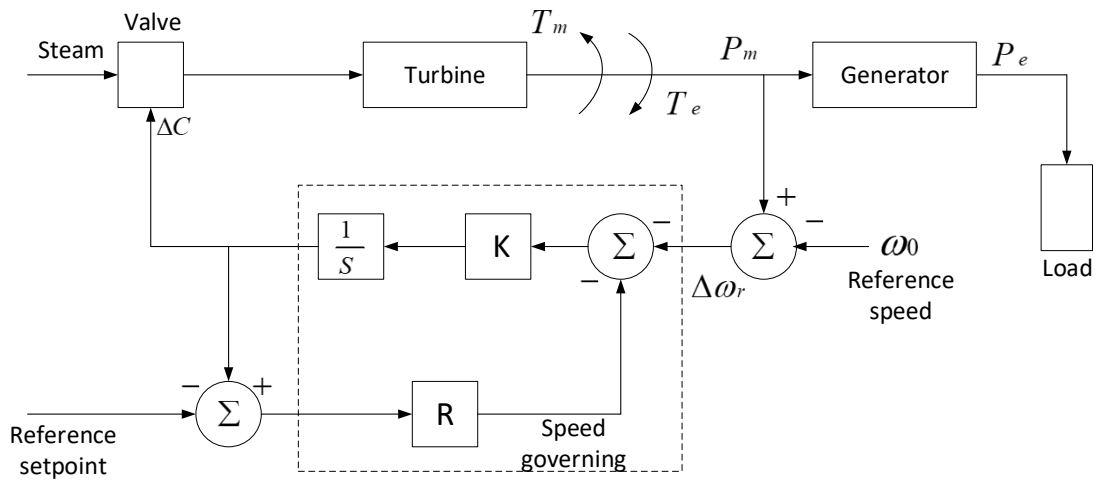


Fig. 2.2 Schematic of the complete primary loop adapted from [15] made up of speed governing, turbine, generator and load

$$\frac{T_m - T_e}{2Hs} = \Delta\omega \quad (2.1)$$

In Figure 2.1  $\Delta\omega$  is the deviation in rotor speed (pu),  $T_e$  is the electrical torque (pu),  $T_m$  the mechanical torque (pu),  $H$  the inertia constant (MW-sec/MVA), and  $s$  the Laplace operator. The expression given by (2.1) can be written in terms of power rather than torque which is more suitable for LFC studies. The relationship between power and torque is given by  $P = \omega T$ . In LFC studies the consideration is for small deviations from steady states values. Hence considering a small perturbation  $\Delta$  from the initial values which are in turn represented by the subscript  $o$  i.e  $(\omega_o, T_o, P_o)$ , the power-torque relationship can be rewritten as:

$$P_o + \Delta P = (\omega_o + \Delta\omega)(T_o + \Delta T) \quad (2.2)$$

Expanding this equation and selecting only the perturbed parts while neglecting all higher terms related to them gives the perturbed equation

$$\Delta P = \omega_o \Delta T + T_o \Delta \omega \quad (2.3)$$

This perturbed equation can be expanded by combining the power-torque equation and torque-speed relationship in (2.1) leading to

$$\Delta P_m - \Delta P_e = \omega_o (\Delta T_m - \Delta T_e) + (T_{mo} - T_{eo}) \Delta \omega \quad (2.4)$$

At steady state both mechanical and electrical torques are equal, therefore

$$\Delta P_m - \Delta P_e = (\Delta T_m - \Delta T_e) \Delta \omega_o \quad (2.5)$$

The initial value of speed,  $\omega_o = 1$  with speed expressed in per unit (pu). Hence the electrical and mechanical torques can now be replaced by electrical and mechanical power. Therefore

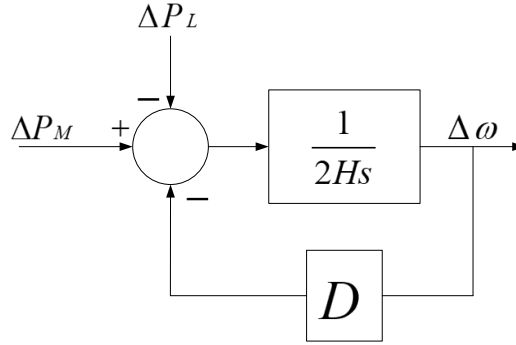
$$\Delta P_m - \Delta P_e = (\Delta T_m - \Delta T_e) \quad (2.6)$$

In Figure 2.2 the electrical power  $P_e$  supplied by the generator is equal to the load demand. In a power system the load is made up different types electrical devices. Lighting and heating loads are resistive in nature, with their power output independent of frequency while motor loads tend to be frequency sensitive. The characteristic of the frequency-dependent composite load is therefore represented by

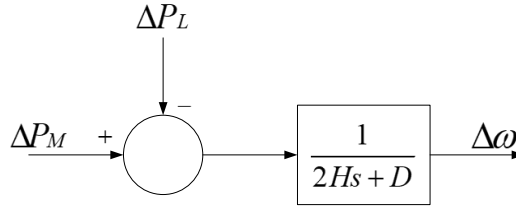
$$\Delta P_e = \Delta P_L + D \Delta \omega \quad (2.7)$$

In (2.7)  $\Delta P_L$  is the nonfrequency-sensitive load change,  $D \Delta \omega$  the frequency-sensitive load change, and  $D$  is the load-damping constant. The load damping constant  $D$  in  $MW/Hz$  determines by how many percent the load changes for a percentage change in frequency. For example, if  $D$  is equals to 1.5, this means the load changes by 1.5 percent for a 1 percent change in frequency. The complete reduced generator load model is given in Figure 2.3 which is represented by (2.8) after combining (2.1),(2.6) and (2.7)

$$\Delta P_M - \Delta P_L = 2Hs \Delta \omega + D \Delta \omega \quad (2.8)$$



(a) Model with composite load



(b) Complete reduced schematic model.

Fig. 2.3 Generator-Load model.

In the absence of a speed governor the response of the system to changes in load is determined by the inertia and damping constants [15]

### Turbine-Prime Mover

The prime mover is used for generating mechanical power. Different sources of the primary supply of energy for driving the generator unit exist and these include sources of energy such as water for hydro turbines or the burning of other primary fuels such as coal, gas or nuclear energy for use in steam and gas turbines. In the case of steam turbines they can be classed as either reheat or non-reheat. For this investigation the focus would be on steam turbines of the non-reheat type. A simplified model can be represented by the block diagram in Figure 2.4. This model expresses the relationship between the output mechanical power and the valve position set by the governor which determines how much steam is injected into the turbine as depicted in Figure 2.2. The terms  $T_T$  and  $\Delta P_V$  represent the charging time constant of the turbine and the valve position as shown in Figure 2.4 and which can be represented by the transfer function in (2.9)

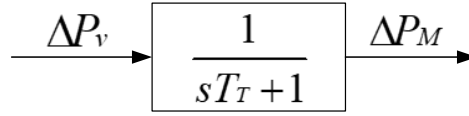


Fig. 2.4 Turbine Model

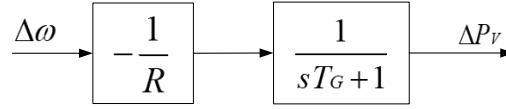
$$\frac{\Delta P_M}{\Delta P_V} = \frac{1}{1 + T_T s} \quad (2.9)$$

### Speed-Governor

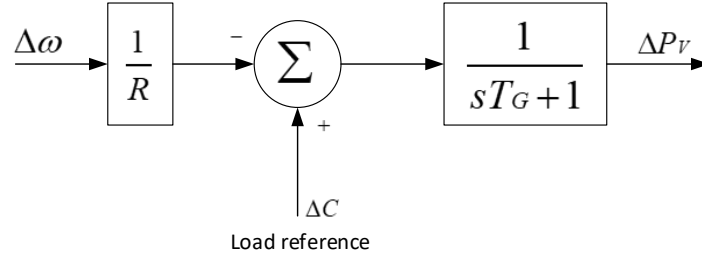
In order to supply power at the nominal system frequency, the prime mover is expected to run at a reference speed at steady state. However, with an increase in load the electrical power demand in the system is greater than the mechanical power leading to a loss of kinetic energy and a subsequent drop in speed. This loss of speed is rectified by the use of a governing system which is able to sense the drop in speed (frequency) and then move the steam valve so as to increase the mechanical power output, thereby restoring frequency to a region within the immediate vicinity (a fixed range which is dependent on the power system) of its nominal value. This prevents frequency runaway in the presence of a load disturbance. This process is known as speed governing and is depicted in Figure 2.2. The integral controller only stops sending the control signal  $\Delta C$  to the steam valve when the error  $\Delta\omega$  reduces to zero. In a multi-generator system their governors are non isochronous *i.e* the load is shared among generators participating in LFC [14, 15]. The converse is the case for isochronous generators.

The speed-droop characteristic of the individual governors in a multi-generator system therefore determine how much each generator contributes to load balancing in the event of a speed deviation and is achieved by the additional loop around the integral controller in Figure 2.2 which is used for speed deviation correction. This is in the form of a proportional controller with a gain of  $1/R$  and the output of each generator can then be varied by changing their load reference set points. The reduced block diagram of the speed - governor is given in Figure 2.5a where  $T_G = \frac{1}{KR}$  is the governor time constant and  $R$  in  $MW/Hz$  is generator droop.

The droop  $R$  is used in determining what percentage change in speed will cause the governor valve to move from fully open to fully closed *i.e* 100 percent valve movement. The values of these parameters are given in per unit (pu). The per unit system is used in power system analysis to simplify calculations by taking all measurements to a



(a) Reduced speed governor schematic.



(b) Load reference set point for generator output control.

Fig. 2.5 Speed Governor Model.

common base which is usually equal to the capacity of an area. Since all quantities are fractions of a common base it makes it easier to compare their relative magnitudes in calculations

### 2.1.1.2 Secondary Control (LFC) Loop

The previous section describing speed governing is generally referred to as the primary control loop. This process does not restore a power network to the nominal frequency following a load disturbance. This is because, speed governing only adjusts generator output in proportion to a change in speed. This is a fixed relationship. In order to adjust this setting a load reference set point is used which provides a means of controlling the output power of a generating unit. This is normally accomplished using a speed changer which leads to a change in generator output. To achieve this a supplementary control loop is added to the governor and turbines to achieve frequency restoration. In application, it is much slower than primary control. The reduced governor block diagram including the load reference set point is shown in Figure 2.5b. This can be represented by (2.10) where  $\Delta P_C$  is the load reference set point

$$\Delta P_V = \left( \Delta P_C - \frac{\Delta \omega}{R} \right) \frac{1}{1 + sT_G} \quad (2.10)$$

Each of the models can be expressed mathematically as dynamic state variables (converting from Laplace to continuous time) suitable power system analysis using the

each of models derived in Figures 2.3,2.4, and 2.5. These relevant mathematical models are derived from (2.8),(2.9) and (2.10) [39]. Hence, for the speed governor, (2.10) can be written as

$$\Delta \dot{P}_V = \frac{1}{T_G}(\Delta P_C - \Delta P_V - \frac{1}{R}\Delta\omega) \quad (2.11)$$

The turbine state dynamic variable model can be derived from (2.9) giving

$$\Delta \dot{P}_M = \Delta P_{Msat} \frac{1}{T_T}(\Delta P_V - \Delta P_M) \quad (2.12)$$

In power systems, the ramping up or down of the generator is limited by a generation rate constraint (GRC)  $\Delta P_{Msat}$ . This is because generating units are limited in the rate at which they can change their outputs. If units operate outside their rated capacity, they could be affected by their limiting thermal and mechanical stresses [40, 14]. Therefore for units undergoing fast changes in load it would be beneficial to their operations and longevity if the rate of change of their power outputs could be limited. The complete overall generator-load dynamic derived from (2.8) is

$$\Delta \dot{\omega} = \frac{1}{2H}(\Delta P_M - \Delta P_L - D\Delta\omega) \quad (2.13)$$

In this thesis the focus is on the composite regulating characteristics of generating units in a control area. Therefore generators in an area are assumed to all rotate at a common speed. This assumption an area can be represented by a common frequency i.e  $\Delta\omega = \Delta f$ . Equally the load damping and inertia constants can be represented by single equivalents. This is the coherency assumption and the LFC loop can therefore be used in representing a single area. This is possible since the focus is on the total performance of all generators in the system, therefore coherent response is assumed for all units [15, 16]. As a result voltage dynamics, transmission line performance including inter machine and inter area oscillations can be neglected.

However, not all generating units in a power station or equally in an area must necessarily take part in frequency control. Selected units which take part must therefore retain an adequate amount of additional generation capacity known as *spinning reserve* by being partly loaded which gives them sufficient spare capacity to participate in frequency regulation. The set points are sent from a control centre. Therefore, unlike primary frequency control, LFC is not localised within the power station. The control centre can be the TSO/ISO and leads to a change in the operating point of generators on LFC, thereby increasing their mechanical torque and by extension electrical output [15]. In a single area LFC is therefore implemented by using an integral controller

which acts on the new load reference sent to the generators by changing the speed setting [41]. This provides the reset action which restores frequency to its nominal value.

### Multi-Area LFC

The assumption of coherency of a group of generators which are now assumed to *swing* with a common frequency is used in the classification of control areas. Generators in an area collectively handle any disturbances within the area with a unison effort and in general make up a common pool managed by a TSO [42]. It is also possible for a combination of control areas to be considered as a single large control area with respect to another similarly large control area with both areas swinging against each other. Individual areas are connected by tie lines which make it possible for power to be exchanged profitably between areas [14]. This tie-line flow is based on a scheduled agreement and normally the operating costs of the selling utility is taken into consideration. A schematic of two interconnected areas is shown in Figure 2.6.

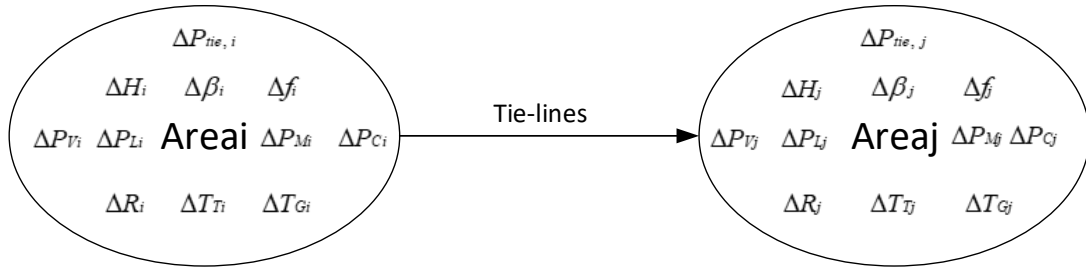


Fig. 2.6 Line diagram of two area system with parameter and variables of each interconnected area

Therefore, in an interconnected system the swing dynamic also includes inter area tie line flow. So in addition to controlled generation maintaining the nominal frequency within an area, the scheduled interchange of power between areas must also be maintained. The process by which these two objectives i.e control of generation and frequency is automatically achieved is referred to as load frequency control [15]. Hence multi-area LFC is usually implemented to:

- keep system frequency fairly constant (frequency control)
- ensure scheduled power flow between control areas is maintained (tie-line control)

- make sure the power allocation among generating units reflect the dispatching needs of an area.

While initially LFC was implemented manually, over the years different schemes for automation have evolved due to among other factors a combination of the increasing temporal and spatial nature of the system and the subsequent desire for improved optimal performance [40, 43]. The increasing heterogeneous nature of the grid also necessitates the need for new design and control approaches to LFC.

### Complete Network Representation

In the complete network representation of an interconnected area  $i$  the overall incremental power balance equation now includes the tie-line power flow. This overall power balance can be represented using the mismatch between mechanical power and the composite load given as:

$$\Delta P_{Mi} - \Delta P_{Li} - \Delta P_{tie,i} = 2H_i \frac{d\Delta f_i}{dt} + D_i \Delta f_i \quad (2.14)$$

which dynamically is

$$\Delta \dot{f}_i = \frac{1}{2H_i} (\Delta P_{Mi} - \Delta P_{Li} - D \Delta f_i - \Delta P_{tie,i}) \quad (2.15)$$

For a single area,  $\Delta P_{tie}$  is zero and can be omitted from (2.15).

The tie-line flow between areas  $i$  and  $j$  at steady state assuming power flow in the same direction is

$$P_{tieij} = \frac{|V_i||V_j|}{X_{ij}} \sin(\delta_{i_o} - \delta_{j_o}) \quad (2.16)$$

In (2.16),  $\delta_{i_o}$  and  $\delta_{j_o}$  are the nominal phase angles of the respective areas in radians, the reactance of the tieline between both areas is  $X_{ij}$  and the voltages at the equivalent terminals between them is  $V_i$  and  $V_j$ . Unity values are assumed at steady state for  $|V_i|$  and  $|V_j|$ . In addition  $X_{ij}$  is assumed to be much greater than the line resistance  $R_{ij}$ . Perturbing (2.16) to obtain the deviations from steady state (equilibrium point) of the tie-line and phase angles leads to

$$P_{tie,ij_o} + \Delta P_{tie,ij} = \frac{1}{X_{ij}} \sin[(\delta_{i_o} + \Delta\delta_i) - (\delta_{j_o} + \Delta\delta_j)] \quad (2.17)$$

Then,

$$\Delta P_{tie,ij} = A_{ij}(\delta_i - \delta_j) \quad (2.18)$$

where  $A_{ij} = \frac{1}{X_{ij}} \cos(\delta_{i_0} - \delta_{j_0})$

Using the relationship between frequency and phase angular deviation i.e  $\Delta f_i = \frac{1}{2\pi} \frac{d}{dt}(\Delta \delta_i)$

$$\Delta P_{tie,ij} = T_{ij} \left( \int \Delta f_i - \int \Delta f_j \right) \quad (2.19)$$

where  $T = 2\pi A_{ij}$  is the synchronising tie-line coefficient. Expressing 2.19 in Laplace form

$$\Delta P_{tie,ij} = \frac{T_{ij}}{s} (\Delta f_i - \Delta f_j) \quad (2.20)$$

If the capacities areas of  $i$  and  $j$  are represented by  $Pr_i$  and  $Pr_j$ , then the relationship between them can be expressed using  $\alpha_{ij} = \frac{Pr_i}{Pr_j}$ . It is the capacity ratio of the areas and it's value is 1 for equal area capacities. For a two area system  $P_{tie,ij}$  must be equal to the negative of  $P_{tie,ji}$  [39, 42]. Therefore, the following relationship exists for tie-line flow between the two areas

$$\Delta P_{tie,ji} = -\alpha_{ij} \frac{T_{ji}}{s} (\Delta f_i - \Delta f_j) \quad (2.21)$$

For an area  $i$  connected to  $N$  areas i.e  $j = 2, 3, \dots, N, i = 1$  and  $j \neq i$  assuming unity capacity ratio.

$$\Delta P_{tie,i} = \sum_{j=2,3..N} \frac{T_{ij}}{s} (\Delta f_i - \Delta f_j) \quad (2.22)$$

$$\dot{\Delta P}_{tie,i} = \sum_{j=2,3..N} T_{ij} (\Delta f_i - \Delta f_j) \quad (2.23)$$

As noted previously, in order to restore the frequency deviation to zero after a load change, the supplementary loop is used to add the reset control to the governor. This forces the deviation to zero by adjusting the reference set point i.e the speed position of generators [14]. Traditionally this is achieved using an integral controller. In the presence of a tie-line in multi-area systems the net power flow interchange must also be maintained. The tie-line deviation is therefore also added to the supplementary loop to accomplish complete LFC. This creates what is referred to as the area control error (ACE) which is a linear combination of the frequency and tie line deviation. The ACE for an area  $i$  is;

$$ACE_i = \Delta P_{tie,i} + \beta_i \Delta f_i \quad (2.24)$$

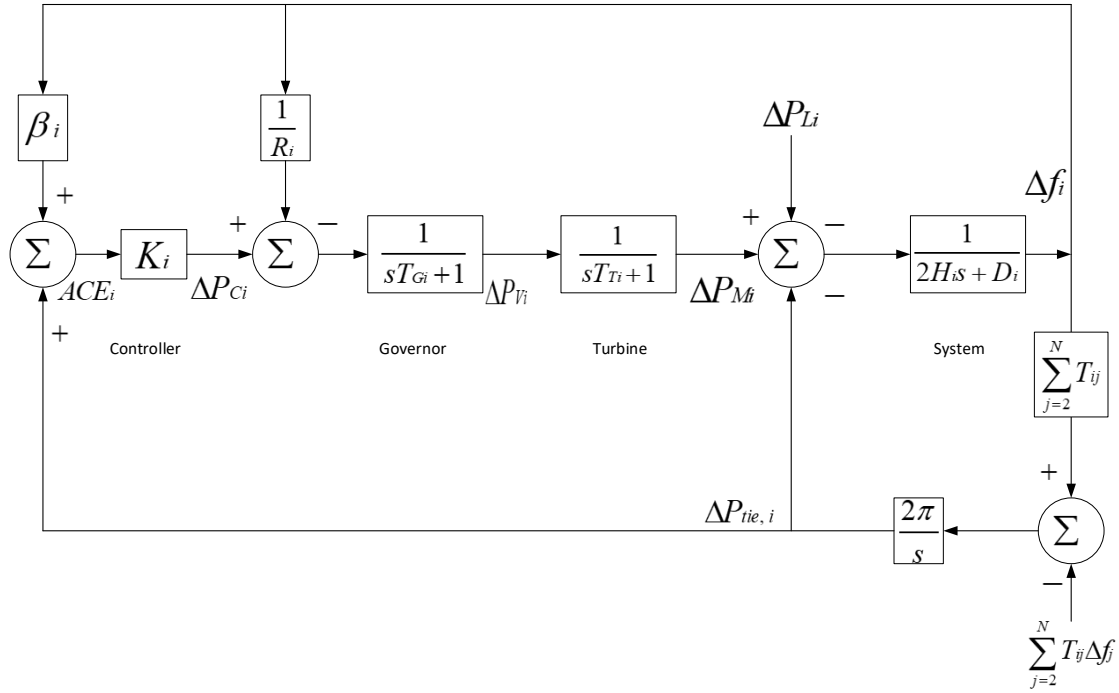


Fig. 2.7 Block diagram model for control area  $i$

$\beta_i$  is the frequency bias factor of area  $i$ . Therefore for an interconnected network the LFC signal sent to the controllers for individual areas is actually the ACE signal. Hence

$$\Delta P_{Ci} = K_i ACE_i \quad (2.25)$$

Within an area this signal is split among the different generation units taking part in LFC according to their participation factors. By combining all the model components developed in the preceding sections, the complete dynamic model representation of an area shown in Figure 2.7 is obtained.

### 2.1.1.3 Tertiary control

Tertiary control is the slowest all three control loops. Its implementation in any network is dependent on the prevailing market structure in place. In a liberalised market, tertiary control is through an energy market (bilateral contracts, etc.) while in the vertically integrated structure it is mainly through optimal power flow considerations or economic dispatch [1]. It is used to generate the set points for generating units participating in

secondary control and to manage the connection or disconnection of units on tertiary control either manually or automatically for frequency replacement.

### 2.1.2 Two area LFC example

In this section, for the purpose of illustration, an example of a two area LFC based on the traditional structure is implemented. Simulations were done using Matlab/Simulink. The areas are identical and can each be represented by the transfer function diagram given in Figure 2.7. The parameters for this simulation are given in Table 2.1 and selected using the values in [16] as a guide. Note that all capacities are expressed in per units with the megawatts omitted.

$Area_i$	$D_i(\text{pu/Hz})$	$2H_i(\text{pu s})$	$R_i(\text{Hz/pu})$	$T_{Gi}(\text{s})$	$T_{Ti}(\text{s})$	$\beta_i(\text{pu/Hz})$	$T_{ij}(\text{pu/Hz})$
1	0.08	0.25	2.5	0.08	0.50	0.48	0.25
2	0.10	0.20	3	0.06	0.44	0.43	0.25

Table 2.1 Parameters used in the simulation of the two area power system

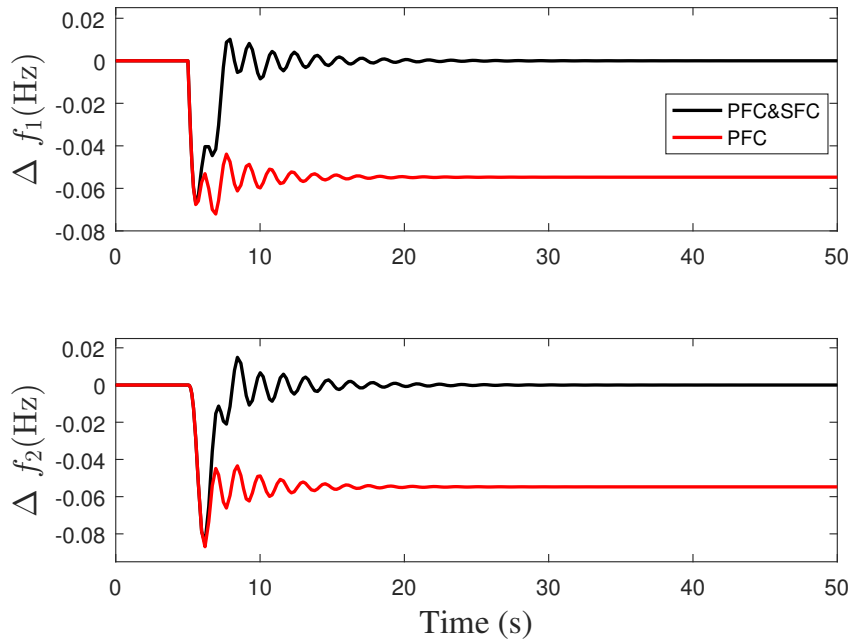


Fig. 2.8 Frequency response in areas 1 and 2 where a deviation still exists with PFC only

Since the areas are of capacity,  $\alpha_{12}$  is equal to 1 and  $\Delta P_{tie,1} = -\Delta P_{tie,2}$ . A load disturbance of  $0.05\text{pu}$  occurs in area one five seconds into the simulation. This

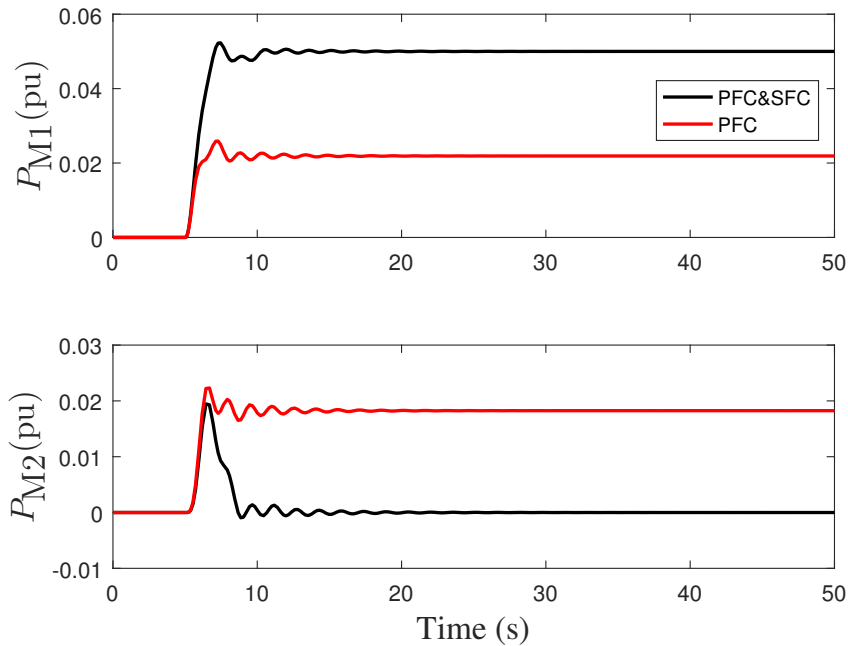


Fig. 2.9 Mechanical power output of generators where only PFC is insufficient to match the load in area 1

disturbance remains constant and is sustained after its occurrence. The values of the integral gains were obtained by tuning and are  $K_1 = 0.55$  and  $K_2 = 0.4$  for area 1 and 2 respectively. The response of the two area system to this disturbance is shown in Figures 2.8,2.9,2.10 and 2.11 with primary control only and a combination of both primary and secondary control.

The frequency response is shown in Figure 2.8 where it can be seen that the main objective of restoring the deviation in frequency to zero following the load disturbance of  $0.05pu$  at 5 seconds is achieved in both areas 1 and 2 when primary and secondary control *i.e* PFC and SFC are applied. However, the action of primary control only could not achieve this objective. The response of the generators in both areas is shown in Figure 2.9. Here it can be seen that generators in both areas respond to the load disturbance. This is primary control by governor action. However, when the system is at steady state only the generator in area 1 where the disturbance occurred, is generating the additional capacity needed to meet the load. Zero ACE is achieved in areas 1 and 2 by a combination PFC and SFC. But for PFC only, the ACE of area 1 is not driven to zero at steady state as seen in Figure 2.10. Tie-line power change is also compensated for during the frequency containment phase as shown in Figure 2.11. Here the tie-line flow is driven to zero which is the desired steady value only with the

use of PFC and SFC. The control loops used in the frequency control of power systems have thus been demonstrated using this example.

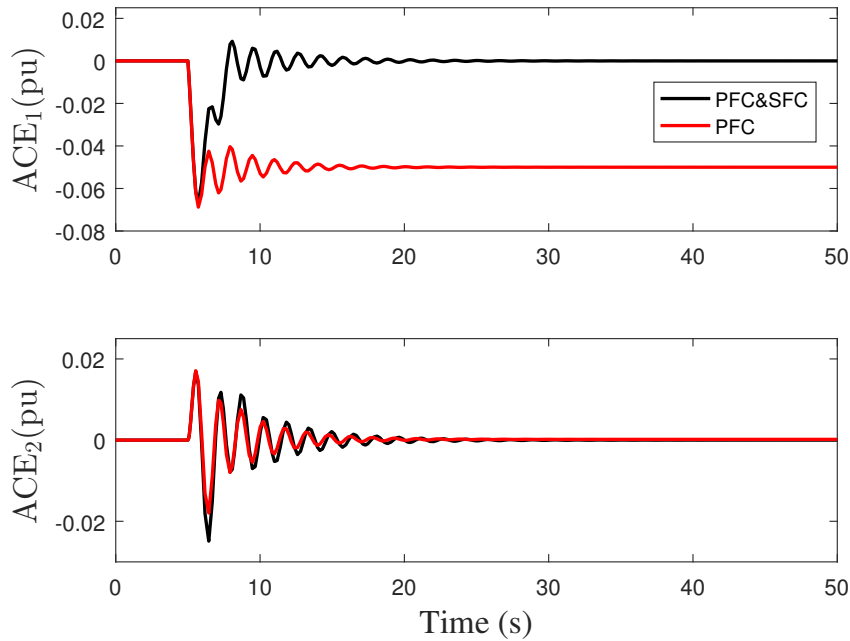


Fig. 2.10 Area control errors of areas 1 and 2 where PFC alone is insufficient to achieve an ACE of zero

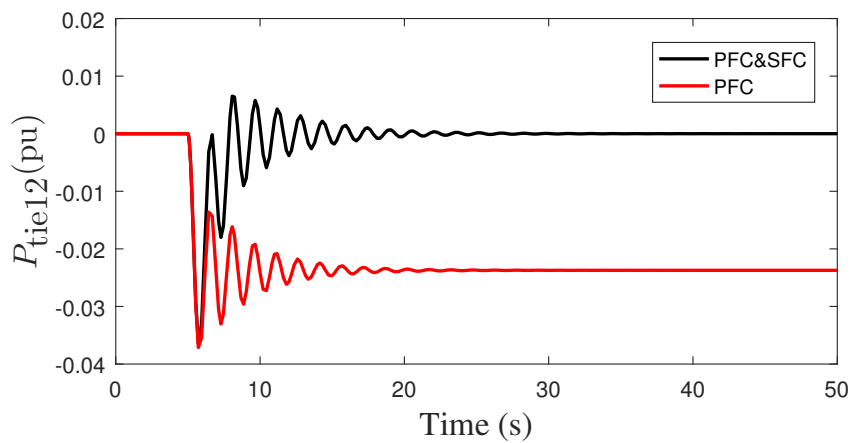


Fig. 2.11 Tie line flow where only PFC does not drive the tie-line to zero

## 2.2 Model Predictive Control Background/Review

In Section 1.4 of Chapter 1, the reason for the adoption of model predictive control for load frequency control within the context of the future power system was explained. This section gives the background necessary for the implementation of MPC. The concept of MPC and the formulation used in this thesis is given. In addition, a review of the different broad categories of MPC from the centralised, decentralised, distributed to hierarchical approaches is explained.

MPC is one of the most popular advanced control techniques used in industrial applications [44, 45]. MPC is well developed with guarantees of features such as stability, feasibility, robustness, non-linearities and so on well covered in the literature [46, 47]. Some of the main features of MPC that make it of particular attraction to industrial practitioners include: MPC uses predictions of the future behaviour of the system to determine the optimal input to apply at the current time, this property of prediction which is based on a set of future inputs makes it possible for the controller to handle system constraints explicitly and systematically, it can also be used to handle large scale multi-variable, multi input output systems with several interacting components, the values of the decision variables being determined are optimal since the problem is formulated as an optimisation one.

In implementation, a model is required of the system to be controlled. Based on this model, predictions of the behaviour of the system over a horizon into the future with a set of admissible inputs which are dependent on either measurements or estimates of the current states of the system is used to determine an optimal control input that meets a given target or matches an expected dynamic behaviour. The predictions explicitly account for any constraints that the system might be subjected to over the prediction horizon and the input is determined by minimising a cost function which is a reflection of the objective to be achieved via optimal control. Only the current input is applied to the system. At the next sampling instant the entire process is repeated based on new measurements or estimates of the state or behaviour of the system.

The use of new information at the next sampling instant induces a feedback in MPC and the repetitive prediction process is known as receding horizon control. As a result, nominal MPC has a degree of robustness making it possible to obtain a stable dynamic performance of the system under control notwithstanding any parameter or disturbance uncertainties. The predictions in this case can be seen as unbiased [48]. Different models can be used for MPC such as transfer function and finite impulse/step response models. Some of these models such as the transfer function one are considered

to be less amenable to multivariable plants while others such as the step response could be limited to applications with stable or large order plants [49]. State space models in most cases offer a simple design framework and links to classical linear quadratic control making them suitable for MPC where often a simplified model that is accurate enough is required for implementation.

## 2.2.1 Centralised MPC Design

The most generic form of MPC is the centralised formulation. An MPC controller is made up several component parts and these are explained next.

### 2.2.1.1 Prediction Model

The first requirement in the design of an MPC controller is a prediction model. In this thesis the model considered is represented by a linear time invariant state space, discrete time equation which is given by:

$$\begin{aligned}x_{k+1} &= Ax_k + Bu_k \\ y_k &= Cx_k\end{aligned}\tag{2.26}$$

where  $x \in R^n$  is the vector of systems states,  $u \in R^m$  the vector of inputs and  $y \in R^p$  the vector of outputs. The pair  $(A, B)$  is assumed to be stabilisable and  $(A, C)$  detectable. In terms of prediction, model (2.26) is the one step ahead prediction of the system. For simplicity it is also assumed a measurement of the states is available at each sampling instant.

### 2.2.1.2 Prediction Equations

Model (2.26) is used to generate the  $N$  step ahead open loop predictions into the future where  $N \in Z^+$  is the prediction horizon. This procedure which involves iterating the system model to a fixed horizon  $N$ , see [48] for details, can be represented in matrix form by (2.31).

$$\underbrace{\begin{bmatrix} x_{k+1} \\ x_{k+2} \\ x_{k+3} \\ \vdots \\ x_{k+N} \end{bmatrix}}_{\mathbf{x}} = \underbrace{\begin{bmatrix} A \\ A^2 \\ A^3 \\ \vdots \\ A^N \end{bmatrix}}_{\mathbf{F}} x_k + \underbrace{\begin{bmatrix} B & 0 & 0 & 0 & \dots & 0 \\ AB & B & 0 & 0 & \dots & 0 \\ A^2B & AB & B & 0 & \dots & 0 \\ \vdots & \vdots & \vdots & \vdots & \vdots & \vdots \\ A^{N-1}B & A^{N-2}B & A^{N-3}B & A^{N-4}B & \dots & B \end{bmatrix}}_{\mathbf{G}} \underbrace{\begin{bmatrix} u_k \\ u_{k+1} \\ u_{k+2} \\ \vdots \\ u_{k+N-1} \end{bmatrix}}_{\mathbf{u}} \quad (2.27)$$

The output predictions for  $N$  steps can be obtained by multiplying the state predictions by the output. This can be written as:

$$y_{k+N} = CA^N x_k + CA^{N-1}Bu_k + CA^{N-2}Bu_{k+1} + \dots + CBu_{k+N-1} \quad (2.28)$$

A compact form of (2.27) can then be represented by:

$$\mathbf{x} = \mathbf{F}x_k + \mathbf{G}\mathbf{u} \quad (2.29)$$

### 2.2.1.3 Cost Function

The next component in MPC is the cost function which can be written using several suitable cost functions. In this thesis a quadratic form is adopted. This represents a performance index for the system to be controlled either towards the origin for regulation or to a target in the case of tracking. For simplicity, we initially focus on the case of regulation to the origin. For an infinite horizon problem this cost can be defined as:

$$J_{x_k, u_k} = \frac{1}{2} \sum_{i=0}^{\infty} \{x_{k+i+1}^\top Q x_{k+i+1} + u_{k+i}^\top R u_{k+i}\} \quad (2.30)$$

The matrix  $Q$  is symmetric and positive semi definite while  $R$  is also symmetric but positive definite.  $Q \in R^{n \times n}$  and  $R \in R^{m \times m}$  are weighting matrices for the states and inputs respectively. The optimisation problem defined by equation (2.30) is of an infinite horizon which would require obtaining an the optimal solution to the problem over an infinite number of degrees of freedom. Similarly it would also require minimisation of an infinite number of tracking errors [48]. In the absence of constraints this problem is tractable. The solution is the same as what is obtainable using dynamic programming. This can be represented by the fixed control law

$$u_k = -Kx_k \quad (2.31)$$

One of the key benefits of MPC is systematic constraint handling. The definition and formulation of constraints is covered next.

#### 2.2.1.4 Constraints

For systematic constraint handling several different types of constraints can be defined during the design stage of MPC. Both state and inputs constraints can be defined in general by  $u_k \in \mathbb{U} \subset \mathbb{R}^m$  and  $x \in \mathbb{X} \subset \mathbb{R}^n$  where  $\mathbb{U}$  and  $\mathbb{X}$  are prescribed sets. More specifically, the input constraints are often defined by upper and lower bounds which can be written in the form:

$$\begin{aligned} u^{\min} &\leq u_k \leq u^{\max} \\ x^{\min} &\leq x_k \leq x^{\max} \end{aligned} \quad (2.32)$$

The inputs and state constraints can be represented in linear inequality form by:

$$\underbrace{\begin{bmatrix} I_{m \times m} \\ -I_{m \times m} \end{bmatrix}}_{P_u} u_{k+i} \leq \underbrace{\begin{bmatrix} u^{\max} \\ -u^{\min} \end{bmatrix}}_{q_u} \quad (2.33)$$

$$\underbrace{\begin{bmatrix} I_{n \times n} \\ -I_{n \times n} \end{bmatrix}}_{P_x} x_{k+i} \leq \underbrace{\begin{bmatrix} x^{\max} \\ -x^{\min} \end{bmatrix}}_{q_x} \quad (2.34)$$

By propagating the constraints given in (2.33),(2.34) up to the prediction horizon we obtain:

$$\underbrace{\begin{bmatrix} P_u & \mathbf{0} & \cdots & \mathbf{0} \\ \mathbf{0} & P_u & \cdots & \mathbf{0} \\ \vdots & \vdots & \ddots & \vdots \\ \mathbf{0} & \mathbf{0} & \cdots & P_u \end{bmatrix}}_{\tilde{P}_u} \underbrace{\begin{bmatrix} u_k \\ u_{k+1} \\ \vdots \\ u_{k+N-1} \end{bmatrix}}_{\mathbf{u}} \leq \underbrace{\begin{bmatrix} q_u \\ q_u \\ \vdots \\ q_u \end{bmatrix}}_{\tilde{q}_u} \quad (2.35)$$

$$\underbrace{\begin{bmatrix} P_x & \mathbf{0} & \cdots & \mathbf{0} \\ \mathbf{0} & P_x & \cdots & \mathbf{0} \\ \vdots & \vdots & \ddots & \vdots \\ \mathbf{0} & \mathbf{0} & \cdots & P_x \end{bmatrix}}_{\tilde{\mathbf{P}}_x} \underbrace{\begin{bmatrix} x_{k+1} \\ x_{k+2} \\ \vdots \\ x_{k+N} \end{bmatrix}}_{\mathbf{x}} \leq \underbrace{\begin{bmatrix} q_x \\ q_x \\ \vdots \\ q_x \end{bmatrix}}_{\tilde{\mathbf{q}}_u} \quad (2.36)$$

Which can be written compactly as

$$\begin{aligned} \tilde{\mathbf{P}}_u \mathbf{u} &\leq \tilde{\mathbf{q}}_u \\ \tilde{\mathbf{P}}_x \mathbf{x} &\leq \tilde{\mathbf{q}}_x \end{aligned} \quad (2.37)$$

The final constraint equation is obtained by substituting (2.29) into the state inequality of (2.36). Stacking both the state and input constraints of (2.37), the combined linear inequality is given by:

$$\underbrace{\begin{bmatrix} \tilde{\mathbf{P}}_u \\ \tilde{\mathbf{P}}_x G \end{bmatrix}}_{P_c} \mathbf{u}_k \leq \underbrace{\begin{bmatrix} \tilde{\mathbf{q}}_u \\ \tilde{\mathbf{q}}_x \end{bmatrix}}_{q_c} + \underbrace{\begin{bmatrix} \mathbf{0} \\ -\tilde{\mathbf{P}}_x F \end{bmatrix}}_{S_c} x_k \quad (2.38)$$

Giving

$$P_c \mathbf{u}_k \leq q_c + S_c x_k \quad (2.39)$$

### 2.2.1.5 Dual-mode MPC

The optimisation problem solved by (2.30) is intractable in the presence of constraints and for practical considerations it is convenient to define the cost over a finite horizon. This can be handled using the concept of dual mode which is used to define a tractable optimisation problem over an infinite horizon. The cost function is split into two parts or modes. One mode has the same degree of freedom as the number of control moves and is flexible. The second mode is assumed to have a stabilising fixed control law.

$$J_{x_k, u_k} = \underbrace{\frac{1}{2} \sum_{i=0}^{N-1} x_{k+i+1}^\top Q x_{k+i+1} + u_{k+i}^\top R u_{k+i}}_{\text{Mode 1}} + \underbrace{\frac{1}{2} \sum_{i=N}^{\infty} x_{k+i+1}^\top Q x_{k+i+1} + u_{k+i}^\top R u_{k+i}}_{\text{Mode 2}} \quad (2.40)$$

Mode 1 ( $J_1$ ) defines a stage cost and mode 2 ( $J_2$ ) a cost to go or terminal cost. Mode 2 can be defined by a fixed control law:

$$u_k = -Kx_k \quad (2.41)$$

Though the dual mode approach provides a way to handle the issue intractability of an infinite horizon problem, the choice of the embedded state feedback  $K$  now has an impact on the close loop dynamic behaviour of the system. A careful selection of this  $K$  guaranteeing stability and optimality is therefore important. In the literature this is determined as the solution to the discrete algebraic Riccati equation from optimal control theory which then defines the terminal feedback gain  $K$ .

Such a formulation can be used as infinite horizon cost function where the terminal cost is selected such that it is equal to the cost to go. To achieve this the terminal penalty  $P$  which defines the terminal cost is derived from the solution to the lyapunov equation using the stabilising optimal feedback gain  $K$  derived as the solution of an optimum standard control problem. The terminal cost  $J_2$  can be written as:

$$J_2 = x_{k+N}^\top P x_{k+N} \quad (2.42)$$

The compact form of (2.29) can now be substituted into the stage cost function in (2.40). The terminal cost can be derived from the last block diagonal of (2.27):

$$\mathbf{x}_{k+N} = F_N x_k + G_N \mathbf{u}_{k+N} \quad (2.43)$$

The combined cost can now be written as:

$$J(\mathbf{x}_k, \mathbf{u}_k) = \frac{1}{2} \sum_{i=0}^{N-1} \{x_{k+i+1}^\top Q x_{k+i+1} + u_{k+i}^\top R u_{k+i}\} + \frac{1}{2} x_{k+N}^\top P x_{k+N} \quad (2.44)$$

The complete finite horizon optimisation problem can be written as a quadratic programming one which is solvable by commercially available solvers in the form:

$$J_{\mathbf{u}(k)} = \frac{1}{2} \mathbf{u}^\top H \mathbf{u} + f^\top \mathbf{u} + c \quad (2.45)$$

Where  $H = (G^\top \mathbf{Q} G + \mathbf{R} + G_N^\top P G_N)$  and  $f = 2[G^\top \mathbf{Q} F + G_N^\top P F_N]x_k$ . The block diagonal matrices  $\mathbf{Q}$  and  $\mathbf{R}$  are obtained by the propagation the matrices  $Q$  and  $R$  over the finite horizon. All constant terms are represented by  $c$  and are not directly linked to the degree of freedom  $u$  so are not part of the optimisation problem.

The complete centralised MPC problem including constraints is now given by:

$$\begin{aligned}
J_{\mathbf{u}(k)} &= \frac{1}{2} \mathbf{u}^\top \mathbf{u} + f^\top \mathbf{u} + c \\
P_c \mathbf{u}_k &\leq \mathbf{q}_c + \mathbf{S}_c x_k
\end{aligned} \tag{2.46}$$

Note that the solution to (2.45) in the absence of the constraints of (2.46) is

$$\mathbf{u}^0 = -H^{-1} L x_k \tag{2.47}$$

which is time invariant, and a linear function of the state measurement, and the extraction and application of the first control in the  $\mathbf{u}^0$  sequence then defines the linear time invariant (LTI) law

$$u_k = K_N x_k \tag{2.48}$$

where  $K_N$  is obtained from the first  $m$  rows of (2.48). The MPC-controlled system is as a result LTI which may be analysed rigorously using the tools of linear system theory. However, in the presence of constraints the solution of (2.46) may not be written on the closed form of (2.48) (or indeed in any closed form), and has to be obtained numerically for each state  $x_k$ . This necessitates the need to solve the optimisation problem online at each new state. In this case the feedback control law induced by applying the first control in the optimal sequence is

$$u_k = \kappa_N(x_k) \tag{2.49}$$

where  $\kappa_N$  is a non linear function that does not usually admit a closed-form expression.

### 2.2.1.6 Feasibility and Terminal Regions

The MPC controlled closed loop system is consequently nonlinear, requiring the use of more sophisticated tools and methods in the analysis of its stability and performance. The key concepts are based on the feasibility, invariance and terminal regions. Feasibility means that the optimisation problem is solvable subject to constraints (2.39). For the optimisation to be recursively feasible the constraint inequalities of the MPC optimisation problem solved at the current time instant must be feasible at the next time instant. This is the concept of recursive feasibility. This holds true for dual mode algorithms in the absence of disturbance or target change. The presence of such changes lead to changes in the size of the feasible region which is now time varying.

However, the chances of infeasibility occurring is dependent on the magnitude of these changes in disturbances [48]. This may lead to a certain level of conservatism in the dual mode algorithm.

The trajectory of the mode 2 predictions is determined by the fixed control law of (2.41) which is unconstrained. In order to guarantee stability linked to the feasible behaviour of predictions in mode two, without recourse to long horizons, a terminal set is adopted. It is well known that the use of long horizons could prove to be computationally expensive in practical implementations. The terminal set is chosen to be a positive invariant maximal admissible set. This means that once the predicted state at the end of mode 1 is constrained to lie in this set, the trajectory of the state under mode 2 would always remain in this set [48, 50]. Assuming this region is represented by  $\mathcal{X}_{\mathcal{T}}$ . Then feasibility is guaranteed in mode two if:

$$\mathbf{x}_{k+N} \in \mathcal{X}_{\mathcal{T}} \quad (2.50)$$

Note that stability of the closed loop system using (2.49) is non-trivial. For example, it does not readily follow that  $\kappa_N$  is stabilizing under the same conditions with which the LQR control law is stabilizing – but the technical design conditions under which it can be made to be stabilizing are by now well established and widely known. However, this stability is purely nominal in nature; it assumes that the model is accurate. When this is not the case further analysis and/or design ingredients are required. Feasibility, invariance and the use of a terminal region further provide support for stability analysis in MPC. This is usually analysed using Lyapunov stability theorem [51, 50] for the nominal case. Some of these tools would be used in Chapter 4 of this thesis when inaccurate prediction models are used in order to establish stability.

The MPC formulation in the preceding sections is a centralised one. With this formulation the entire plantwide optimisation over all inputs is solved. Since all the required information is available in a single plantwide controller, no communication is required between controllers, signals only have to be transmitted between sensors and controllers and between controllers and actuators. The solutions are those of the systemwide control problem [51].

Centralised MPC however could pose several challenges when applied to large scale interconnected systems which are heterogeneous in nature. Since the underlying rationale in MPC is to solve an optimisation problem in real time within a sampling instant, large scale heterogeneous systems with a high number of state and decision variables as well as measurements could lead to an increase in the computation time needed to arrive at the optimal solution in real time and within the limits set by the

operating condition and dynamics of the systems [52, 53]. This challenge could also be compounded by the need for fast, flawless and reliable communication with significant storage requirements for the successful implementation of the centralised algorithm.

Additionally, large scale system may often consists of different sections owned and operated by several entities. These entities are responsible for the proper operation and functioning of their portions of the network and could be unwillingly to share information because they are competitors within the same market or for political reasons such as in power or large scale water networks. This would pose a constraint on information flow and could make the design of a centralised controller impractical.

Also the system's network could be flexible in the sense that some components are connected and disconnected from the network at different times. This could mean that a fixed centralised model is not available for MPC design and any model selected becomes invalid whenever a new subsystem is connected or disconnected. Such a situation could arise in smart grids having a large number of components [54, 2]. The increasing complexity of the smart grid makes the need for flexibility, adaptability and reliability crucial.

Finally, with centralised MPC the entire system susceptible to faults since a problematic sensor or actuator anywhere on the network could affect the entire system. This could also pose maintenance challenges when only specific sections of the network require work on them. Furthermore, a single controller means the system is susceptible to a single point of failure; if the central controller fails the entire system could go down. As a result of these and similar consideration non centralised control schemes have been developed over the years. Centralised MPC does however provide a comparable standard (a benchmark) for the other schemes.

In large scale systems made up of several component parts or increasingly device groupings such as the power grid, it is usually more convenient to split the overall problem into smaller local problems. This requirement has led to the use of non centralised schemes where the plantwide systems behaviour is achieved by the overall combination of the local control actions. The non centralised schemes can be broadly divided into: decentralised methods, which do not require any form of communication between local controllers where the controller design is done with the assumption that any interaction between local subsystems is negligible and distributed methods where partial or full communication between local controllers is required to account for the interactions among subsystems.

### 2.2.2 Decentralised MPC

Decentralised control involves the design of local subsystem controllers which have no information about the actions of any other subsystem's controller and optimises only their local objectives. It is the direct opposite of the centralised control algorithm. However, while reducing communication overheads when compared to centralised control, it introduces model error into the system since the inputs of the other controllers are not taken into account by the local controller's model [51].

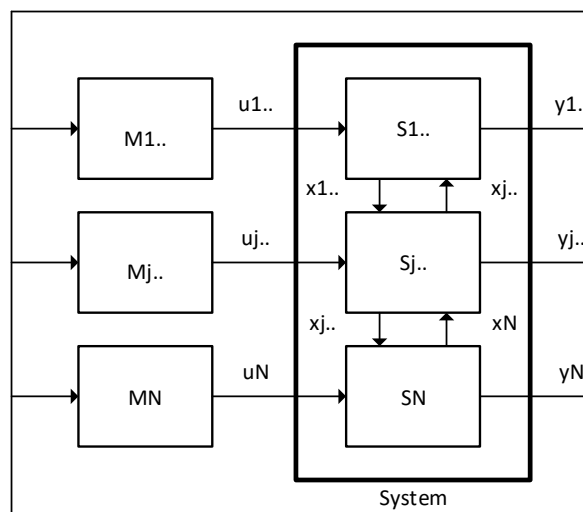


Fig. 2.12 Decentralised control structure showing  $S_N$  interacting subsystems. Local controllers  $M_i$  do not communicate with each other.

In implementation, the corresponding large scale system represented by (2.26) is decomposed into subsystems with individual inputs, states and outputs. This creates models of separate input output pairs for each subsystem and provides the basis for decentralised MPC (DeMPC) controller design for each subsystem which operates independently from the other subsystems. That is, the entire system is decomposed into  $N$  subsystems with individual controllers and it is assumed that there is no or negligible interaction between subsystems. In this way the controllers can then be designed independently for each subsystem  $i = 1, 2, \dots, M$ , with the input, states and output vectors respectively represented by  $u_i \in R^{n_i}$ ,  $x_i \in R^{m_i}$  and  $y_i \in R^{p_i}$ . This is depicted in Figure 2.12 with the dark highlighted box showing the system of subsystems and their corresponding local controllers, states, inputs and outputs. The evolution of the states of each subsystem following an input directly applied to it is given by

$$x_{k+1}^i = A_{ii}x_k^i + B_{ii}u_k^i + \sum_{j=1, j \neq i}^N A_{ij}x_k^j + B_{ij}u_k^j \quad (2.51)$$

This is the true subsystem dynamics with the interactions represented by the summation term. These are normally neglected leading to the decentralized model that may be directly used in an MPC controller deployed for each subsystem under the assumption of weak coupling between subsystems. Hence the model used in the design of a local subsystem MPC controller and its corresponding feedback control law is

$$\begin{aligned} x_{k+1}^i &= A_{ii}x_k^i + B_{ii}u_k^i \\ u_k^i &= \kappa^i(x_k^i) \end{aligned} \quad (2.52)$$

Hence there is a mismatch between the true system dynamics and the model used in the design of local controllers. The decentralised model excludes the possibility that  $A_{ij} \neq 0$ ,  $B_{ij} \neq 0$ . In the context of power system dynamics, this is equivalent to the assumption that the actions taken in area  $i$  have no influence on what happens in area  $j$  and that the frequency in each area has no influence on that of other areas.

However, in a future power system there are several interconnecting dynamics. The dynamical interactions (couplings) between these subsystems are often strong. Neglecting them could have undesirable effects on system performance and stability. Studies on this effect and other issues with decentralised control can be found in [55]. Another issue with decentralised control is that the standard stability analysis in MPC whereby the optimal cost is used as a Lyapunov function is not easily extended to the decentralised case [56] which could make such an analysis non-trivial. Hence DeMPC not only inherits but also compounds the main issues arising in decentralised control in particular stability. For example in the presence of constraints on subsystems inputs susceptibility to instability is higher while with state or output constraints the primary concern is infeasibility of the optimisation problem since it is possible for interaction induced disturbances to push a system outside its feasibility region.

An analysis of decentralised MPC can be found in [57] where stability was achieved for non-communicating decentralised controllers by the use of a contractive constraint in the optimisation problem for a non-linear discrete time system despite the presence of a decaying exogenous disturbance. Also in [58] plug and play decentralised MPC is used and stability is guaranteed by applying robust techniques to reject subsystem interactions even in the presence of model fluidity due to connecting/disconnecting subsystems. In [59] stable decentralised control of dynamically coupled independent

systems formed by decomposition of a large scale system into possibly overlapping sub models obtained using extraction matrices and subject to input constraints was developed and implemented.

In spite of these challenges decentralised control still provides the advantages of scalability, flexibility and adaptability (particularly when considering plug and play applications) when compared to centralised MPC. Also maintenance organisational issues are easier to handle [53] with less susceptibility to faults. The computation and communication requirements are also reduced when compared to centralised MPC.

### 2.2.3 Distributed MPC

Distributed MPC (DMPC) is the middle ground between centralised and fully decentralised MPC controllers. The key differentiating feature between the two architectures is that information is now shared between controllers in the distributed setting. Here the local controller is aware of the inputs and states of neighbouring controllers and optimises its local objective function with this information [51]. The knowledge of states and inputs of neighbouring controllers is usually in the form of their planned trajectories — actual states and inputs could also be shared. The availability of this information may improve the closed loop performance of distributed MPC in comparison to decentralised MPC. A general model for subsystem  $i$  and its control law which includes information from its neighbours  $j$  is given by:

$$x_{k+1}^i = A_{ii}x_k^i + B_{ii}^i u_k + \sum_{j=1, j \neq i}^N A_{ij}x_k^j + B_{ij}u_k^j \quad (2.53)$$

$$u_k^i = \kappa^i(x_k^i; z_k^i)$$

where  $z_k^i$  denotes the "information" gathered by subsystem  $i$  in order to evaluate its control law. This model now includes the interactions that were omitted from the decentralised model. This can be seen in Figure 2.13 where there is now information sharing between the controllers.

Distributed formulations offer promise particularly in future power networks and have been the subject of research in recent years. There have been several formulations of distributed MPC which can all be classed into several categories based on different criteria and have been formulated in various ways with their features depending on the application or expected performance. This has led to a wide variety of algorithms which has created a need for proper categorisation. In [53] distributed MPC algorithms

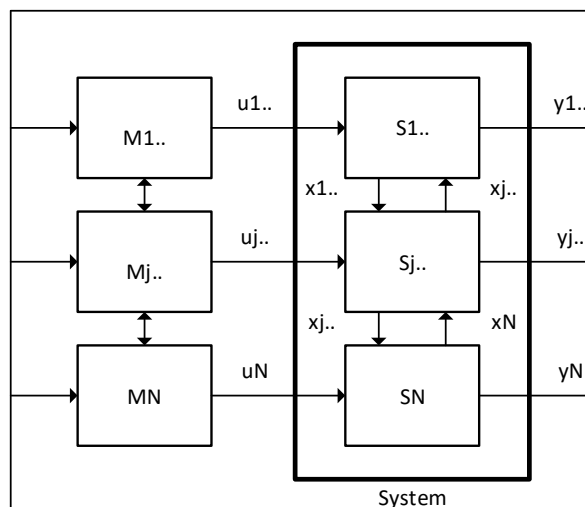


Fig. 2.13 Distributed MPC with M referring to controllers and S subsystems

were grouped based on three commonalities: process features, control architecture and theoretical attributes with each commonality having sub-features such as type of control, communication and optimality respectively. A simpler and more straightforward classification can be found in [56] where the classifications are done based on the level of communication, connectivity and type of controller behaviour. While it may not be exhaustive in its categorisation of distributed MPC algorithms, it nevertheless gives a clear picture of the key differentiating characteristics which can be represented as shown in Table 2.2.

Classification Type	Distributed Feature	
Communication topology	partially connected	Fully connected
Communication protocol	non iterative	iterative
Controller attitude	independent	cooperating

Table 2.2 Categorisation of distributed MPC. Fully connected schemes involve communication between all controllers while partial schemes are based on neighbour to neighbour communication. Iterative control involves information exchange several times within a sampling interval while for non iterative, information exchange occurs only once within a sampling interval. In independent controllers a local cost function is used by each controller while for cooperating controllers a cost function relating to the global cost is used by each controller

In terms of communication topology fully connected systems are those in which every controller exchanges information with all the other controllers in the network. For partially connected systems information exchange is only between a controller and a subset of the remaining controllers in a network. The partial communication topology is suitable for sparsely connected networks with possibly weak interconnections. Figure 2.13 is a partially connected DMPC system where communication is only between neighbouring controllers. Under communication protocol, the non iterative schemes are characterised by the exchange of information only once within a sampling interval between local controllers. Because of this reduced information exchange the communication overhead related to non iterative schemes is low making them quite suitable for practical applications where the optimisation problem is likely to be solved only once within a sampling time. On the other hand iterative schemes involve the exchange of information several times within a sampling interval. The aim is usually to iterate until some optimal criteria such as convergence is achieved. However, such algorithms also include mechanisms for terminating them if required before the end of a sampling interval. In the case of independent controllers each one solves a local cost function while for cooperating controllers each one solves a weighted portion (part of a convex combination) of global cost function.

In DMPC algorithms several different types of dynamic couplings can be considered depending on the problem being solved. Equation 2.53 has both state and input couplings indicated by  $A_{ij}x_k^j$  and  $B_{ij}u_k^j$  respectively. In a multi-area power system the coupling interaction is a state coupling represented by the tie-line when solving the LFC problem. In this instance the matrix  $B_{ij}u_k^j$  is equal to zero. In future power systems the dynamic state couplings between the various heterogeneous components are important in the design of decentralised or distributed controllers. In multi-area power systems consisting of only generators the natural coupling between area subsystems is the tie-line. This makes it easier to identify local subsystems suitable for any non centralised control design. However, if the inter-area subsystems are to be broken down into groupings based on heterogeneous generating sources such as in a future power grid such a natural identification of subsystems may prove to be challenging. This could pose challenges in the design of local controllers since the local models required for control design are not easily identifiable. Note that couplings could also be from cost functions and constraints when the subsystems are dynamically decoupled. Power systems however are mainly linked by dynamic states and this is the principal coupling considered in this thesis.

### 2.2.3.1 Non iterative DMPC

Non iterative MPC schemes can be formulated based on any of the communication topologies in Table 2.2. In addition, non iterative formulations do not have controllers that cooperate since the objective of each controller is local. They do not share a common global objective. However, each one is aware of the decisions of other controllers and these are treated as known disturbances to be compensated for by their local inputs. From the perspective of game theory the equilibrium obtained from the optimisation is a Nash equilibrium due to the conflicting objectives of each local controller. A consequence of this non corporative approach however is that the stability analysis of the centralised case is no more applicable. See [51] for details. An example can be found in [60] where stability was guaranteed by the use of contractive constraints computed offline. In this regard, several non iterative, non corporative schemes often adopt robust approaches [61]. Such an MPC approach can be found for example in [62] where stability is guaranteed by resorting to robust MPC with careful offline selection of the stabilising terminal weights and control gains. Reference states and inputs are exchanged between neighbours. Any unmodeled disturbances resulting from differences between the actual and transferred reference trajectories are rejected via the tube based approach. For problems having coupled constraints an example can be found in [63]. Here by an appropriate communication and constraint tightening method feasibility and stability were achieved in the presence of persistent but bounded disturbances. The non iterative schemes offer advantages in privacy, limited communication, and computational requirements.

### 2.2.3.2 Iterative DMPC

Iterative algorithms on the other hand can be non cooperative or non cooperative. The optimisation problems solved by each controller in the cooperative case is based on a common objective which is that of the entire plant system. Therefore, in terms of game theory the algorithm converges to the Pareto optimal [64]. The stability of the composite control obtained in this instance is similar to that achieved in the centralised scheme and provides theoretical guarantees. In addition, if the algorithm is able to converge within one sampling interval without early termination the optimal value obtained is similarly the same. However, algorithms have been developed that guarantee stability even with early termination [60]. Cooperative schemes require all subsystems to have knowledge of each others models which could create issues with privately owned systems with competing interests such as in obtainable in future power networks. Some

iterative schemes also employ distributed optimisation techniques such as in [65–69] where dual decomposition, gradient descent, and the alternating direction multiplier methods are used in solving the centralised problem in a distributed fashion. The process of iteration in iterative schemes increases the amount of communication required to achieve performances comparable to the centralised case due to the optimisation problem being solved several times within a sampling interval. This might make their implementation challenging in some practical applications such as LFC where convergence is in the order of a few seconds. A performance comparison of iterative and non iterative MPC based on robust methods can be found in [70]. Detailed descriptions of different distributed MPC architectures based on stability analysis, communication requirements, couplings and more can be found in [53] with theory and applications treated.

Distributed MPC provides the same advantages that are accrued from decentralised MPC and much more. The size of the optimisation problem solved is similar to the decentralised case smaller and than the centralised case. Other benefits include fault tolerance, an easier way to manage maintenance and organisational challenges relating to technical, commercial and privacy issues. They also offer the possibility of flexible operations related to plug and play [71, 72]. Compared to decentralised MPC they also offer better closed loop performance since the exchange of trajectory information between controllers and the subsequent use of this knowledge in determining local inputs improves overall performance system. However, the communication requirements also tend to be high and the design process to manage this is could be more involved. Also distributed approaches pose the additional challenge of selecting a suitable decomposition scheme [34] when this is not clearly apparent in the structure of the system to be controlled.

#### **2.2.4 Hierarchical MPC**

Another category of MPC is the hierarchical structure consisting of several levels with coordination and information exchange between layers. The higher level is used in generating references for the lower levels. The optimisation problem solved at this level could be over a longer time scale due to the need to meet certain economic criteria and hence require longer sampling intervals when compared to the subsequent lower level or levels. The references generated at the upper layer are then tracked by a properly designed lower layer controller having shorter sampling intervals; often characterised by faster dynamic models.

In the context of control, such multilayer schemes are usually designed using classical feedback cascaded control [56]. The assumption is that the different layers are clearly separated temporally making it possible to design independent decentralised controllers across the layers. An example of the cascaded design approach, based on a clear temporal decoupling of the different layers is the classic cascaded frequency control shown in Figure 2.1 and explained in Sections 2.1.1. A multilayer multiple timescale cascaded MPC for power system transmission planning/dispatch and control was implemented in [73]. Two MPCs work in parallel to solve the dispatch and frequency regulation problems respectively on different time scales with the higher layer setting the control references and state constraints for the lower layer. Two way communication was required in order to update the upper layer cost function thereby improving the overall grid performance.

Hierarchical MPC has historically being applied for plantwide optimisation and control in the process industry and is similar to the multilayer cascaded control approach. At the upper layer a real time optimisation (RTO) problem is solved based on a static nonlinear model of the system. The references generated at this layer should ideally be reachable (feasible) by the lower layer, exhibit model consistency with the lower layer and be updated periodically to account for unmodelled slow disturbances. This is fed to a supervisory layer possibly designed using MPC, which then feeds optimal setpoints to local PID controllers in charge of actuators. An application of this control structure can be found in the works of [74, 75]. Furthermore, attempts have been made to combine optimisation and economic MPC at the RTO layer [76] such that simplified linear dynamic models can be used at the upper layer. Hierarchical schemes employing economic cost functions at a layer can be found in [77, 78]. In the literature there is no clear cut classification for hierarchical MPC. However, for the purposes of this exposition, just like the case for distributed MPC, an iterative and non iterative methodology can be broadly adopted.

Focusing on applications using non iterative algorithms, in many instances the upper layer solving a long horizon problem at slower timescale is used for deriving optimal scheduled trajectories. They are used for scheduling/trajectory planning over a long time horizon based on a slow timescale model while a lower controller tracks the scheduled values from the upper layer. This approach was adopted for example in the control of vehicle thermal management systems in [79, 80]. Other schemes can be applied to autonomous/ensemble systems where the upper layer is based on a simplified or reduced order model of the systems. Decentralised controllers are then designed

for each system at the lower level [81–83]. Robust approaches are adopted in most of these applications to account for unplanned or ignored disturbances.

Hierarchical MPC has also been used for interconnected systems. A formulation allowing for reconfiguration by switching on/off of interconnected systems at the lower layer was reported in [84]. Convergence is obtained by resorting to robust approaches. A reduced order robust higher upper layer controller penalising state and input deviations from their nominal values was designed in [85]. Lower layer decentralised controllers then refined the controls decisions from the upper layer. A two layer distributed hierarchical control for an interconnected system was designed in [86]. Subsystems were decomposed into clusters and communicate with each cluster at a faster time scale in the lower layer. In the upper layer only cluster to cluster communication is performed at a slower time scale. In most of these non iterative schemes stability and improved performance were achieved by resorting to robust design requiring minimal communication with good convergence.

The iterative schemes are based on architectures which combine distributed optimisation techniques with hierarchical MPC. Like in distributed MPC, these methods split the optimisation problem between sub-models in a manner that integrates information relating to a neighbours optimal control problem. The primal dual optimisation method was applied in [87] where constraint tightening is used for systems coupled via dynamics and constraints to generate the primal feasible solution and the dual is by an approximate subgradient method with stability guaranteed using bounded suboptimality. Alternting direction of multipliers (ADMM) was used in [88] for hierarchical MPC design where the approach led to flexible plug and play. This allowed runtime changes in systems dynamics and objective functions. In [89] ADMM is used in designing a central entity that manages a group of microgrids ensuring line constraints are met. The use ADMM provided flexible operation, scalability and privacy between microgrids.

In this section a review of different MPC architectures has been given. From this, the versatility of MPC and its usefulness for different applications in various industries has been highlighted. However MPC still offers several challenges such as the basic requirement for a model, redundancy of the controller if there are changes to the underlying basic model and the need for special practitioners in industry[90]. While MPC is suitable for applications to large scale systems the review has shown that this is clearly dependent on the performance requirements of the control application such as operational time scale (seconds, minutes), communication overhead, computational time, convergence speed and system structure. In power systems, LFC is in the order of seconds and this has an impact on what kind of MPC formulation is adopted. In

addition, when considering decentralised/distributed control design for different energy sources in future grids the decomposition method adopted is also important. This thesis is focused on the integration of new generation technologies for LFC in future grids. The new technology of concern is battery energy storage systems which is reviewed in the next section BESS.

## 2.3 Battery Energy Storage Systems - BESS

Energy storage adds a new dimension to the power grid. Historically, for bulk storage systems the focus has been on large hydro stations and compressed air energy storage which provide base loading or ancillary services [29]. They are either located far from load centres for hydro plants or need specific geological formations for compressed air storage. These bulk systems were mainly used for the traditional grid. However, in the context of the future grid a main technology of choice are battery energy storage systems (BESS) which can either be installed as distributed resources mainly connected to the distribution grid, as part of virtual power plants or as large capacity grid connected utility scale devices at transmission level. It is expected that in future grids BESS can provide a wide range of services which would improve the operational flexibility, efficiency and reduce the economic costs for both generators and operators. Applications in the future grid could vary across various time scales for short, medium and long term use [91]. The growth in the use of BESS over recent years and the multi use functions they provide has seen the installation of several working grid connected BESS in different parts of the world. Early installations include the 20 MW/20 MWh system in Berlin [92] and more recently larger facilities such as the 30 MW/129 MWh in Hornsdale Australia [93] and the 34 MW/204 MWh and 30 MW/120 MWh systems in Rakkasho, Aomori, Japan and Escondido, California, United States respectively [94]. When used for power applications BESS can provide frequency regulation services due to their fast response and with their increasing capacity, modularity and scalability are integral for the successful implementation and development of future grids.

Battery energy storage systems when compared to other energy storage systems such as flywheels, pumped hydro, compressed air energy storage, fuel cells, cryogenic, and superconducting magnetic energy storage offer several advantages. These include faster response times, higher ramping rates, modularity, scalability, simple geographic location, moderate space requirements and ease of maintenance. In most applications BESS are combined with renewable generation and are regarded as critical assets for the successful integration and management of renewable generation technologies such

as solar PV panels and wind turbines into the power grid. In addition, grid scale connected BESS have the additional advantage of not being dependent of end user behaviour when compared to other non storage distributed energy resources such as demand response, thus eliminating the need for disutility considerations. They also require less costs in communication, aggregation, actuation and sensors in controller design making integration and coordination with conventional generators easier.

Nevertheless, even with these benefits BESS do have power and energy limitations which make the efficient management and control of these devices of critical importance if they are to participate effectively in LFC or else the system could experience reduced LFC performance when BESS reach their capacity limits. Control techniques that can accommodate requirements challenges are important for their grid integration.

### 2.3.1 Potential Applications in Future Power Systems

Energy storage technologies can be used for numerous purposes within the power system. BESS can in general be used for most of the applications energy storage systems are used for. In this section a non exhaustive list with a brief description of some of the proposed uses of BESS in future power networks is given

- Peak shaving - storage units can be charged during off peak hours and discharged during peaks hours to flatten the demand profile of large customers thereby reducing the demand charge they have receive from operators. Applications of BESS for this service can be found in [95–97]
- Arbitrage services - BESS can be used in providing several arbitrage services such as time of use tariffs for customers or bulk arbitrage as seen by generators. For customers, BESS can be used to absorb power when prices are low and sell when prices are high. Implementations of BESS for arbitrage services can be found in [98, 99]
- Frequency regulation - BESS can be used for transient stability enhancement which improves power quality and system stability. Also due to their fast response they can be used as frequency reserves for providing both primary and secondary frequency control and to reduce the frequency nadir following an excursion event by reducing the rate of change of frequency (ROCOF). Applications of BESS for this service can be found in [100, 101]
- Instantaneous reserves *i.e* black start which is the ability of a generator to start without an external source of supply. Generators (normally diesel operated)

which render these services are used to re-energise the power system following a major blackout. BESS can also be used to render this service though with their capacity limitations BESS use here could be constrained to a few minutes. Though MPC based optimisation examples are not common, applications of BESS for this service using multiobjective optimisation techniques can be found in [102, 103]

- Voltage regulation - Utilities provide reactive power into the grid in order to meet the power demand of reactive components thereby maintaining voltage stability. BESS can also use their ability to inject and absorb reactive power into the grid to improve the voltage stability of the grid. The fast response of BESS to changes in voltage is also of particular importance here as shown in [104–107]
- Power factor correction - Since a BESS can inject both active and reactive power into the grid, large customers could use the reactive power from a BESS installation to reduce their power factor charge [108]
- Reserve - The use of BESS for reserve can take several forms. BESS can serve as backups in customers premises which provide power to the grid in times of failures. This could help in reducing the costs associated with grid failures. Also reserve could be in the form of resource adequacy which is primarily implemented during extreme conditions as a form of capacity reserve. Instead of starting expensive peaking plants, BESS could offer this service for the short duration required. The short installation times of BESS makes their application for this service an attractive proposition. Spinning reserve generators are synchronised to the grid, unloaded and ready to meet demand. A BESS maintained at a fixed capacity can provide this service supporting system frequency while fast acting generators start up. Applications based on MPC can be found in [109–111]
- Grid upgrade deferral - similar to reserves services BESS can be ideally located in areas that experience significant stresses on transmission lines and other grid components during period of high demand. Rather than invest in line upgrades, BESS can mitigate the effect of increased line stresses which cause line overload thereby saving the costs associated with grid upgrades or even the need to design to maximum grid capacity. In [112, 113] MPC is used to coordinate BESS, conventional generators and controllable loads limiting line overloads and preventing the need for costly grid upgrades.

- Renewable capacity firming - during periods of peak demand renewable generation could be used to support conventional generators. However, due to their intermittent generation which follows the weather rather than demand, there is a disjoint between maximum demand and renewable production. BESS can be paired with renewable generation to make their production coincident with when peak demand occurs thereby improving their value and overall system reliability. In addition they could also assist with the dispatch of solar PV [114–117]

There are several more applications BESS can be used for in the power grid such as load following, long line stabilisation, power quality improvement and load levelling. The use of BESS to provide any of these services would depend on several factors such as network size, BESS capacity, investment costs, BESS type, proximity to the point of use of service, battery technology, efficiency cycle, discharge rate and many other factors. Some of the most common types of battery systems used are the lead-acid, redox flow, sodium-sulphur, nickel-cadmium, lithium-ion and flywheels which have found both commercial success and a certain level of technical maturity with known installations in service in different parts of the world.

### 2.3.2 Frequency Regulation Applications

An area of research in which the application of BESS has seen increasingly significant studies is in frequency control applications where it has previously been demonstrated that they have the potential to provide some of their most profitable applications [118]. An early experiment investigating the use of battery energy storage as another option for load frequency control and instantaneous reserve was carried out in [92]. To demonstrate the efficacy of BESS in LFC applications a 20 MW test facility was designed and operated over a period of two years. The technical and operational versatility of the BESS was proven. This work provided good operational experiences of issues such as charging methodology, maximum current, efficiency, cooling and battery service life. A simple digital control system was used to achieve both primary and secondary frequency control. Following the success of this experiment a decision was made to develop a full large scale facility power system studies. In [119] a 30 MW BESS unit for frequency regulation was used on an island power system. A first order transfer function approximation was used to model the BESS facility. The battery was shown to have the effect of reducing the maximum frequency deviation following a load disturbance on the system. In order to accommodate the capacity limits of the BESS, the system was allowed to fully discharge within 1100s and ceased to participate in load

frequency control after this time. A high pass filter was included in the control loop to prevent the BESS from continuously supplying power bidirectionally as a result of sustained frequency deviations. These early investigations were based on a centralised PI controller in single area power systems.

The use of BESS in multi-area power systems for frequency control can be found in several works. An application of BESS considering both generation rate and deadband constraints for LFC in a two area interconnected power system can be found in [120]. For a two area interconnected power system, control was via an integral controller with the optimal value of the controllers' gains determined by using a least square error algorithm. Both frequency and ACE feedback were used as the signals for BESS installed in both areas. A similar investigation was implemented in the work done in [121] for a two area interconnected system. The values of the integral gains were determined using the integral square error technique applied to the ACE of each area. The use of the BESS reduced peak deviations from sudden load perturbations, the steady state values of time error and inadvertent interchange accumulations. Similarly, for a two area interconnected system in [122], the use of batteries to suppress both frequency and tie line fluctuations caused by wind power generation using PI controllers was demonstrated. The LFC signal was shared between thermal and battery units for coordinated operation with battery capacity size shown to influence the performance of the systems with regards to the level of deviation suppression.

However, other control methods which require the use of filters in centralised and decentralised approaches do exist. A BESS is used to provide active power compensation in an isolated power system in [123]. A control algorithm was developed that enabled dynamic adjustable state of charge limits along with a procedure for optimal BESS sizing for frequency regulation. The BESS was able to improve the dynamic stability of the low inertia isolated system and the developed algorithm ensured a profitable operation with the state of charge (SOC) limits, reducing depth of discharge and thereby extending the BESS lifetime. In a small wind-battery-diesel power system a minimal observer based frequency control scheme was implemented by the coordinated operation of a wind turbine and a BESS in [124]. The generalised predictive control (GPC) pitch angle controller of the wind turbine generator reduced the low component of the frequency deviation while depending on state of charge level the PI controlled BESS reduced the high component via a high pass filter. Hence for this MIMO system decentralised controllers were designed for each subsystem which both respond to the load variation. This approach successfully reduced frequency deviations in the small isolated power system. A combination of lumped electric vehicles (EVs), heat

pump water heater, BESS and conventional generators were used to design a PI supplementary load frequency methodology in [125]. The LFC signal to the EV's in addition to passing through a high pass filter which does not completely cut long term frequency fluctuation, is also biased using half hourly average state of charge information in order to regulate the SOC of the lumped EVs using a PI controller. The proposed LFC method was able reduce the frequency deviation in the presence of wind and PV generation. A reduction in frequency deviation caused by renewable and load fluctuations by designing a robust control strategy in the presence of model uncertainties in a smart microgrid was implemented in [126]. Three control signals; a high frequency signal for BESS power control and two low frequency signals for diesel engine and SOC control are penalised separately. An iterative  $H_\infty$  and  $\mu$  analysis is used to design an optimal robust  $\mu$  synthesised controller. This designed robust MIMO controller achieved better frequency regulation compared to standard PID control.

Energy storage have been used in combination with conventional generators to achieve improved frequency control within the deregulated market setting in several works. The controller of choice in most instances is the traditional integral controller with the gains tuned using some intelligent means such as bacteria foraging, opposition based harmonic search optimisation, differential evolution for the case of a proportional integral derivative filter (PIDF). Also optimal Adaptive Neuro Fuzzy System (ANFIS) and optimal controller were also applied with [127–131] containing examples of these applications. The storage technology used is mainly the redox flow battery or super conducting magnetic energy store (SMES) and in most cases were power applications without any mechanisms for state of charge management.

From the preceding paragraphs in this section most of these frequency control applications mainly employ PI controllers, filtering methods and techniques for optimal tuning of the PI parameters. In the implementation of LFC different traditional control techniques have been used over the years. For example, there are the pioneering frequency based methods (classical control) using Nyquist, Bode and root locus approaches. Two key drawbacks of these methods were their characteristic large settling time and overshoots following a frequency deviation and their limited application to a linear range of operation [132]. With these drawbacks in mind new control methods which aimed to improve these characteristics were proposed and applied to the LFC problem such as in [133, 134]. Another category is made up of techniques that are categorised as intelligent methods. Typically, these are methods that use algorithms such as fuzzy Logic, artificial neural networks, neuro-fuzzy, or some combination of these methods with classical PID or other advanced optimisation techniques such as genetic

algorithms. These methods offer flexibility and can accommodate non-linearities such as generation rate constraints and a dead band. Examples of successful applications can be found in [135–138]. A third category of control techniques are approaches utilising optimal control methods such as robust control, adaptive, self tuning, and model predictive control. These methods offer features such as optimal feedback or cost control application (optimal control), parametric and process uncertainties handling (robust, adaptive methods and self tuning). In the integration of storage systems into the power grid for frequency regulation some of these control techniques as seen from the previous examples with the traditional PI in [92, 119, 121, 122], robust methods in [126], optimal control in [123, 131] and a combination of intelligent techniques with integral control in [127–130]. The limitations in the use of many of these techniques in solving the LFC problem are well known and detailed surveys of the different control techniques and their strengths and weaknesses can be found in [132, 139]. A drawback of most of these methods particularly PI controllers which in a sense are the industry standard is that they lack systematic constraint handling. MPC controllers do have this capability. However, more recently new optimisation based techniques have been adopted for use in the integration of intelligent loads for power system frequency control to tackle the problem of low system inertia and large power supply fluctuations caused by renewable generation. These new control techniques are in most cases characterised by the use of distributed optimisation.

## 2.4 System Decomposition

Modern large scale systems such as the future power grid are increasingly made of heterogeneous components and interconnected dynamics. In the analysis of such systems it is often preferable to decompose the system into smaller subsystems. A common approach is to decompose the system based on its inherent structure or physical properties. However, in future grids an additional grouping of subsystems based on heterogeneous sources is also possible. This kind of subsystem grouping however is not naturally evident as in the case of control area groupings. In particular, if these heterogeneous sources (controllable devices) are to contribute to LFC they should be able to receive a feedback of frequency enabling decentralised (autonomous) or distributed control. The feasibility of using frequency in this manner based on a fixed control law with a gain was investigated in [140]. Improved dynamic stability and transient performance was achieved using controllable loads. The key point to note is that for loads to participate in frequency control the swing dynamics must be available

to them which in turns is dependent on the decomposition methodology adopted. This has been tackled recently using distributed optimisation algorithms in decomposing the problem to be solved.

### 2.4.1 Distributed Optimisation Decomposition

Distributed optimisation algorithms decompose the large scale control problem using optimal decomposition methods. Here, following the construction of the global model for the large scale system, this model is not decomposed into smaller submodels. Rather the central optimisation problem to be solved is decomposed into decentralised problems which converge to the centralised solution. Here interesting algorithms including early precursors such as dual ascent, primal-dual sub-gradient, dual decomposition as well proximal algorithms from which splitting methods such as the douglas-rachford, peaceman-rachford and the alternating direction methods of multipliers (ADMM) are derived. Useful background information and details can be found in [141, 142]. A survey on the use of distributed optimisation and control algorithms in electric power systems can be found in [143]. In frequency control applications the swing dynamics was used as a primal dual algorithm for optimal load control in [144]. This method was based on a dualisation of the optimal problem which make the local frequency deviations often corresponding to lagrange multipliers and any branch flows available to loads subject to their end use disutility minimisations. Decentralised local optimal problems are solved and communication between controllers is used to establish global consensus, mitigating any inconsistencies in the shared variables. A similar approach was used in [145] for the case of distributed primal dual algorithm in frequency based optimal load control subject to power balance across the network. Loads were for used primary frequency control and global asymptotic stability was established. The same issue of integrating load side control while guaranteeing system stability and constraint satisfaction was investigated in [146] using distributed load side control. It was shown that the algorithm was globally stable and robust to changes in system parameters without violating operational constraints. Optimal load control is combined with LFC implemented by conventional generators in these works. The primal dual approach has also been extended to include dynamic markets and pricing with stability and convergence guarantees in [147, 148]. Though these methods converge to the optimal steady state, constraint satisfaction is only guaranteed at steady state. This could prove to be problematic in real power systems where generators and BESS are subject to hard constraints. However, the systematic constraint handling feature of MPC

guarantees recursive feasibility of the optimisation problem guaranteeing transient constraint satisfaction.

## 2.4.2 Overlapping Decomposition

Distributed optimisation algorithms provide a mechanism for solving the global problem in a decentralised/distributed manner. The objective function is separable and all shared variables are accounted for using splitting algorithms. Though these algorithms only guarantee stability at steady state by adopting MPC transient stability guarantees can be achieved. However, the stability properties are dependent on iterative consensus and sharing approaches sometimes characterised by slow convergence. Improving this could require large communication within a sampling time which might not be feasible in real time implementations. This could lead to inexact solutions [149] or require recourse to higher order algorithms [148]. A method that splits the swing dynamic between generators and controllable loads without decomposing the problem while providing the transient stability guarantees of MPC would prove useful. A decomposition technique that can split the centralised model rather than the optimisation problem into groupings of subsystems is the method of overlapping decomposition [150]. This technique splits the composite large scale system state transition matrix into disjoint subsystem matrices. Each of the subsystems contains their local states and the shared state. Decentralised local controllers which solve a local optimisation can then be designed for each subsystem. The mathematical framework on which the overlapping decomposition technique is based is known as the inclusion principle. This principle provides theoretical conditions ensuring that the expanded system model contains the same dynamical properties as the original model. These conditions are related to the expansion and contractibility of the state space of the model as well as the contractibility of the decentralised control laws of the disjoint subsystems [151]. For expansion of the state, input and output space the extension principle provides another mathematical framework [152]. With the extension principle, any controller designed in the expanded space is always contractible to original space.

The use of overlapping decompositions thus provides a framework for the design of decentralised/distributed controllers of interconnected subsystems within a large scale systems. Implicit in this approach is that the state space must contain all the relevant couplings in the global system model. Some of the early applications for frequency control applied this method to multi- area model decomposition [153, 154] or interarea oscillation damping using phase shifters [155, 156]. Recent applications using integral controllers for LFC in power systems consisting of BESS, wind turbines and

conventional generators can be found in [157]. In this thesis this method is combined with MPC for the design of decentralised local controllers for BESS systems which are able to respond to local area frequency changes. However, the robustness of MPC against ignored dynamics which constituent perturbations due to prediction mismatch has not been analysed in the literature. Hence in this thesis the non iterative MPC is adopted and overlapping decompositions are used in the integration of BESS systems for decentralised LFC control design. Sufficient conditions that guarantee stability would be established with convergence to the nominal steady state frequency of the system.

The deregulation process already introduced challenges in LFC management [17] and this coupled with the intermittency and variability of the renewable energy supply and the increasing decentralization and heterogeneity of the system they create make managing LFC a more challenging control problem. Grid-scale energy storage applications have the potential to improve the reliability and efficiency of the power system [158] with BESS in particular, being used in providing support for frequency regulation. However, with a future grid consisting of a combination of different sources of power the failure of a centralised controller creates an even more critical situation negating the benefits of integrating new technologies. A decentralised approach with independent controllers for conventional generators and BESS provides a robust fault tolerant system. In addition it reduces cost and is not subject to communication latency. The challenge is identifying and accounting for the interactions between generators and BESS for non centralised LFC controller design. Applications of MPC controlled BESS mainly focus on frequency regulation in combination with renewable energy resources. Direct coordinated control of BESS and conventional generators for LFC is rarely analysed. Two issues which arise however are: (a) how to decompose the global model such that both subsystems receive a feedback of frequency without recourse to splitting algorithms and their related iterative requirements (b) how to guarantee stability due to the lack of consensus, sharing and prediction mismatch as a result of decentralisation while achieving transient constraint satisfaction. As seen in this section, combining overlapping decompositions with MPC provides a means to solve these issues. Now that the motivation for MPC has been stated the next sections focus on model predictive load frequency control in future grids which is the central theme of this thesis.

## 2.5 Model Predictive Load Frequency Control Review

This section contains a review of model predictive load frequency control. Load frequency control via MPC in this context refers to LFC within the traditional vertical grid model. Here we show how MPC has been used for frequency control applications in the literature. In general the use of MPLFC control in this section does not include most of the new technologies that make up the smart grid; that is a future grid containing distributed energy resources and new devices such as battery energy storage systems, micro combined heat and power systems including new consumers such as thermostatically controlled loads and distributed generating units.

### 2.5.1 Model Predictive Load Frequency Control

Power systems tend to be geographically expansive consisting of several areas interconnected via long tie-lines. These interconnections are assumed to be weak and link generators which constitute a coherent group and hence define a control area. However, the definition of an area is relative and it is possible for a control area to be made of up several coherent groupings of generators [42]. Therefore, LFC is usually applied via decentralised control for each area using conventional PI controllers in power systems. This approach also helps in addressing privacy, market competition and other organisational concerns in power systems. In the same vein different configurations of MPC have been implemented in solving the LFC problem (MPLFC). In Section 2.2 these different configurations of MPC were explained and their relative strengths and weaknesses outlined. The centralised structure has been implemented in several works and following the aforementioned limitations of centralised approaches to large spatio-temporal systems the implementation of MPLFC have also focused extensively on non centralised techniques *ie* decentralised and distributed.

Centralised MPC schemes are often used as the benchmark in terms of performance when comparing various MPC configurations. As a result several centralised MPLFC works have been implemented in the literature. For example in [159] a functional MPC was presented. Simulations of the proposed MPC were characterised by reduced computational time, allowed the use of large horizons which improved prediction accuracy and without did not require additional tuning parameters when compared to classical MPC. Generation rate constraints were also taken into consideration in the controller design and with their the proper imposition LFC performance was improved

when compared to PI controllers. Similarly in [160] centralised MPC was applied to the Nordic system for frequency control. Though the MPC itself was not an economic MPC *ie* the objective function does not directly penalise an economic cost<sup>1</sup>, instead pricing is included in a quadratic manner in the objective function using a weighting matrix of the control input signals. Generation capacity, rate of change and tie-line limitations (maintained using slack variables see [162]) were considered with good flexible, coordinated and economic performance achieved when compared to standard PI controllers.

In modern electricity markets due to liberalisation, LFC is increasingly becoming price based [163] with balancing services affected by price bids due to the new arrangements between GENCOs, DISCOs and where applicable the system operator. Since accepted bids determine the direction of energy flow and hence have an impact on system balance, the ability to model these contracts and for controllers to maintain stability in the presence of them becomes more critical. An early formulation of LFC considering contractual arrangements was described in [5] for LFC of a two area system. Similar bilateral contracts consideration for LFC can also be found in [164–166]. In [167] load following and regulation contracts between GENCOs and DISCOs were introduced. However these contracts were not included in the MPLFC formulations. This was taken into consideration in [168] using the concept of DPM which represents agreements (via area and contract participation factors) between GENCOs and DISCOs for balancing services. GRC and load reference constraints were explicitly included in the MPC algorithm with no contract and contract violations scenarios simulated showing better constraint handling performance when compared to an LQR control LFC approach.

In Section 2.1 it was shown that one of the requirements of LFC in a multi-area power system is that individual areas take care of their local demands while maintaining tie-line flows at scheduled values. This is the principle of non intervention in LFC. With centralised control this would not be adhered to and for this reason decentralised MPLFC has also been implemented. In addition, centralised control is based on the assumption that wide area measurements are available via reliable and fast communication links which could create issues relating to computational volume/complexity and data confidentiality. Subsequently, decentralised MPLFC was implemented in [167] where control actions were constrained to reduce generator manoeuvring. Results similar to the centralised case were achieved. Decentralised

---

<sup>1</sup>Economic MPC aims to use feedback control to directly determine optimal economic plant performance rather than just meeting stability and steady state requirements see for example [161]

MPLFC was designed in [169]. The robustness of MPC to various load changes and parameter uncertainty (generator and other system parameters) was investigated with good robustness performance. The algorithm was decentralised, making it possible to design each controller independently. Here, it was shown that MPC was able to regulate both frequency and tie-line deviations to zero, giving desirable performance when compared to other conventional control techniques. Also, governor deadband and GRC were taken into consideration. Another application of decentralised MPLFC can be found in [170] where MPC is used for alternating current AGC control of areas connected via a multi terminal high voltage (MTDC) grid. The linear gain based MPC were able to accommodate voltage offsets improving the control of DC voltages and hence efficiency in the use and sharing of secondary reserves across the AC network. However, the performance of decentralised controllers is often dependent on the degree of dynamic couplings between subsystems in a network (such as tie-lines) and the methods that guarantee stability in the centralised case are difficult to establish.

Distributed MPC involves communication between decentralised controllers thereby improving control performance making them equally suitable for applications in large scale power systems. These algorithms aim produce similar performance and guarantees as the centralised structure with minimal communication overheads. For iterative schemes an early formulation of MPC can be found in [60] where a contractive constraint computed online is applied to the first state of the prediction. This guarantees stability of the MPC for a partially connected non iterative approach. This formulation was referred to as a stability constrained MPC (SC-MPC); frequency restoration and tie-line control were achieved. Turbine dynamics were also excluded from the model equation for each area and the use of a contractive constraint made the application quite conservative. In [171] a fully connected, iterative and cooperative MPC referred to as feasible cooperation MPC (FC-MPC) was proposed that guaranteed stability and gave performances close to the centralised structure. It also had the attractive feature of being possible to terminate the MPC algorithm before convergence (of iterates) and still guarantee stability making it possible to obtain acceptable results by using just a single iteration.

However, non iterative schemes provide the additional benefit of reduced communication requirements. The authors in [172] were able to formulate a non iterative communication based distributed MPLFC (coordination exists between subsystems) that included both input set point constraint (i.e load reference setpoint) and generation rate constraint in a multi-area system. Robustness against parameter uncertainties was also achieved with reduced computational burden when compared to the centralised

and decentralised formulations. A mix of different types generating units within each local control area was considered in [173] for robust DMPC based on linear matrix inequalities (LMIs) with GRC and valve position limits for a four area interconnected power system. Robustness against parameter uncertainty, load changes and unit failure were achieved with stability and convergence guarantees by applying a time varying state feedback local controller for each area. The LMIs were used in defining an upper bound on the objective function somewhat improving conservativeness. A novel DMPC scheme with guaranteed stability, feasibility and constraint satisfaction was implemented in [174]. This was achieved without the need for supervision or iterations between controllers. Here controller parameters used were calculated via an offline algorithm and was an application of the DMPC approach proposed in [175]. For a four area system, a three term control law was applied to each area and the proposed approach met the objectives of AGC with similar complexity to conventional MPC. Distributed MPC applications in the deregulated setting can be found in [176, 177]. These schemes were also of the non iterative, partially connected configuration with information exchanged only once between local controllers while consideration bilateral contractual agreements between GENCOs and DISCOs with input and generation rate constraints in multi area power systems.

## Discussion

The use of model predictive control for load frequency control in power systems has been extensively covered so far. Applications cover as wide a range from isolated single area systems to interconnected networks. Initially centralised techniques were applied in both single and multi-area systems. But with the evident limitations of centralised algorithms; increase in computational, communications, and non intervention requirements of LFC there was a shift towards non-centralised applications. Within the non-centralised framework, decentralised and distributed MPC were utilised. With the increasingly generic application of MPC, several algorithms included constraints such as GRC and set point references. With the use of constraints, pricing and other dynamic market considerations were also included in later formulations through the use of, for example DPM. However, the decision of which architecture to use is also dependent on the nature of the problem to be solved. For example in [160] a centralised formulation was deemed suitable due to the "small" size of the power network under consideration where only negligible gains might be accrued from a non-centralised approach having smaller optimisations problems and communication times. However, non-centralised frameworks are increasingly the norm. Decentralised MPC currently outperforms

conventional AGC and where suitable can be successfully utilised. They also offer lower complexity compared to distributed schemes [178]. Where the physical couplings between the subsystems are weak or where for the purposes of coordination the dynamic interaction between subsystems can be considered in the design of the control systems [52], this can be applied. On the other hand if distributed MPC algorithms are to achieve global optimal performances similar to centralised architectures, it would require extensive communications of global state and information objectives probably in a fully connected and cooperative algorithm. With the current advances in communications technology achieving this objective could be getting closer. More accurate predictions and closed loop performance can be achieved in such a situation. Similarly hierarchical architectures with information exchange often outperform distributed approaches. These "classical" MPLFC schemes considered thus far are designed by decomposing the control problem based on the context of power system *i.e* on an area by area basis. New generation technologies were not integrated into the centralised models and did not contribute to frequency control. However, for other controllable generation sources or loads to effectively take part in LFC based on local frequency measurements non-centralised approaches are increasingly required for their coordination with conventional generators. A control approach for the decomposition of the model for a single area based on its structural properties and the problem to be solved is then required in order to solve the LFC problem. New control approaches that accommodate the characteristics of the future grid are thus desirable.

## 2.6 Model Predictive Control in Future Power Grids

The review of model predictive load frequency control in Section 2.5 focused on applications that did not include the new technologies and strategies which typically define the framework and characteristics of the future grid although it did include works based on the deregulated framework. This section gives a review of work done in the literature with regards to the use of MPC within this context where new low carbon technologies and new approaches to power system operations are implemented.

### 2.6.1 MPC Application in Future Power Systems

The future grid is envisioned to cover a wide spectrum of the power system ranging from communications to sensors and devices. Different areas of focus include demand response, economic dispatch, wide area monitoring, with technologies such as energy

storage, plugin hybrid electric vehicles (PHEVs), thermostatically controlled loads, renewable technologies, microgrids and much more. Model predictive control has been applied to several of these focus areas with the use of different new technologies.

#### 2.6.1.1 Centralised

Centralised MPC has been applied in systems characterised by only conventional and wind generation. For example, an analysis of the performance of nonlinear MPC (NMPC) in the presence of wind energy was done in [38]. Wind output was treated as the main system disturbance based on a positive worst case scenario. The responses of MPC were better than the standard PI controller while improving coordination between primary, secondary and tertiary frequency in relation to optimal operation that leads to a minimum cost. This implementation was for a single area power system with explicit generation capacity and rate constraints accounted for in the MPC algorithm. Also in [179] imbalance uncertainty for the Nordic network was considered to be as a result of wind farms located within a single area with the uncertainty in load assumed to be dominated by an intermittent wind farm output. For the worst case deviation scenario in wind-power production, a robust non linear MPC (RNMPC) was able to satisfy system constraints where the nominal NMPC could not. Here, centralised MPC was considered suitable for the size and topography of the network. Additionally tie line constraints created by decomposing the single area model were satisfied but a trade off between system performance and robustness which would still be needed when compared to NNMPC. An extension of [38] to a three area system having three disturbance scenarios was implemented in [180] via robustified nonlinear MPC (RNMPC). For the three area system considered, in the presence of severe disturbances, RNMPC met system constraints when both PI and nominal NMPC (NNMPC) could not. However, for less severe disturbances where tie-line constraints are not violated, NNMPC outperformed RNMPC due to the less conservative nature of NNMPC when compared to RNMPC. Maintenance of frequency deviation within the acceptable range as well as frequency restoration in the presence of varying wind output was achieved. However, wind was considered as a negative load playing no part in frequency control. In these early applications the wind resource did not contribute to LFC. No new technologies responded to local frequency measurements and thus no model or optimal decomposition methods were required.

### 2.6.1.2 Distributed

For the centralised MPC no decomposition techniques were implemented and in most instances did not even contribute to LFC. However, when new technologies such as BESS are required to take part in balancing the flow of power in the network methods which are able to decompose the optimisation problem into smaller sub problems are often needed. As noted in 2.4 decomposition methods are adopted in this scenario. In addition, they facilitate the integration of new energy sources into the grid. These methods can be combined with MPC. For example in [181] MPC was used as the look ahead algorithm with multi-step optimisation. The problem was decomposed using an optimality decomposition and approximate newton method allowing parallel computations of sub problems while the unlimited point algorithm was used in solving the constrained optimisation problem. In the presence of renewable energy variation and storage, co-ordination was achieved with inexpensive computation and fast convergence in a decomposed two area network with solutions of the distributed algorithm similar to the centralised result. However, the benefit of fast convergence is dependent on the length of the prediction horizon *i.e* the convergence times increases with increasing horizon length. Distributed MPC is also used for solving the distributed optimal power flow problem in [182]. The aim was to achieve coordination between storage and renewable generation across areas in a two area power system. By decomposing the problem into sub problems and applying an extension of the approximate Newton Directions method for non-linear optimisation decomposition, the amount of information areas need to exchange to achieve centralised convergence is reduced with the additional benefit of faster convergence rates. However, these convergence rates still depended on the chosen method and horizon length but the methodology showed applicability for the efficient utilisation of energy resources across different areas.

Distributed optimisation techniques based on primal-dual decomposition via sub-gradient iterations have increasingly being applied to smart grid applications using MPC. For example in [183] distributed MPC based on the use of dual decomposition was used to achieve a power balance between households having micro-CHP units (prosumers) using a price mechanism. Dual decomposition and sub-gradient iterations were applied in the DMPC with each end user able to share imbalance information with its immediate neighbours via Lagrangian multipliers such that convergence of network demand and supply of power is achieved. Both the QP and MIQP approaches were applied with fast, convex and slow, non-convex but better performance respectively achieved for each. The combination of embedded micro CHPs and distributed MPC information sharing model in the power network was able to achieve power balance

and the network was also scalable. In [184] the same work was approached from a different perspective. This time rather than considering power balance only, heat balance between end users was also considered. That is the microCHP and distributed control algorithm were designed to also follow heat demands rather than only power demands. This was achieved by adding heat storage to the network and including the heat convergence problem as a constraint in the power control problem. A MIQP formulation was used and information is shared only with immediate neighbours as in [183] meaning only local information used. There are several points worth noting in these applications: They are mainly focused on the optimal power flow problem and not LFC. Hence no local frequency measurements take place and as a result the fast convergence requirements are relaxed. Loads do not actively take part in LFC.

### 2.6.1.3 Hierarchical

One early application of hierarchical MPC related to smart grids was implemented in [185] for intelligent consumers with a high level MPC controller managing external power inputs and MPC aggregator-like controllers at the lower level managing smart consumers. Flexibility, scalability, the possibility of time scale separation and plug and play capabilities without the need for controller redesign was achieved by using properly defined cost functions at both levels with communication between both controllers. Hierarchical MPC was applied in [186] to control a set of intelligent and regular consumers with power supplied from a wind farm and a power plant. The Minkowski sum method was used to find the individual and combined constraints (resource polytopes) for a set of consumers by using their vertex representations and summing vertex by vertex. This made it possible to calculate exact constraints on the power and energy capabilities of consumers, achieving greater efficiency in the use of the flexibility intelligent consumers. Variations in load *i.e* natural consumption and varying production from wind farms were well accommodated.

In future power networks hierarchical MPC is mainly applied in microgrids. In [187] hierarchical MPC was implemented for LFC, unit commitment and economic dispatch. Following systematic modelling of the electric vehicles and the microgrid; on a longer time scale MPC was implemented at the higher level for economic dispatch, while the lower level was used to achieve frequency control with good coordination between electric vehicles and the micro-grid. Renewable generation is modelled as a disturbance. Mixed integer linear programming (MILP) was used for generator scheduling and electric vehicles were optimally integrated without any effect on their mobility demands and contributed to improved power balance within the micro-grid. It is worth noting

that state of charge control of the electric vehicles is achieved by the higher level controller. A similar modelling approach was adopted by the authors in [188] when designing an energy management system in a smart grid with fluctuating renewable generation and electric vehicles. However, in this case, secondary control is used at the top layer to generate reference trajectories for the lower layer controller where primary control of frequency and tie-line is achieved within a single area. In [189, 190], MPC is applied to an experimental microgrid for the optimisation of distributed generators and renewable energy resources. A modelling methodology involving the use of a mixed integer linear framework is used to formulate a more general and flexible optimisation of the microgrid taking into account economic dispatch of generation, curtailment schedule, energy storage, grid interaction and unit commitment at the higher level controller. MPCs prediction capabilities were applied to compensate for forecast errors. Hence an MPC-MILP control scheme that was able to economically optimise the operation of the microgrid in the presence of operational constraints was achieved. This was considered on a small plant generation scale and the lower level controller was used for frequency, voltage and phase/power quality control by fast responding electrical devices. A two layer multi timescale hierarchical control for a grid connected microgrid containing a PV panel, battery, microturbine, input from the power network and a partially non predictable load was designed in [191]. The higher level computes optimal economic references for components of the microgrid over a long time interval while the lower layer formulated with a stochastic MPC tracks these references by employing a shrinking horizon strategy while ensuring probabilistic constraint satisfaction. Most of these schemes were able to achieve frequency control based on a long time optimisation problem at the higher level.

Distributed optimisation/splitting algorithms have also equally being applied to the hierarchical control of smart grids. A control strategy to minimise the imbalance between the forecasted and actual demand and supply of electricity and hence avoid network congestion was proposed in [192] based on the universal smart energy framework. Distributed model predictive control in a hierarchical structure is used to optimise the combined flexibility of households (prosumers). Building on [184, 183], households having heat pumps are treated as flexible prosumers of heat. A cooperative formulation was implemented via dual decomposition and Lagrangian relaxation; prosumer coupling constraint and the central coordinator constraint are the dual variables. In this way information is shared between prosumers and congestion was avoided using the developed algorithm. A two layer hierarchical MPC for a power plant portfolio of conventional and renewable energy was implemented in [193]. Danzig Wolfe

decomposition approach was used in defining the underlying optimisation problem yielding a hierarchical structure which provided better scalability and flexibility when compared to a centralised solution. An MPC like aggregation is used to solve the optimisation problem of a large number of flexible consumers in [194]. The aggregator is the central coordinator while the Douglas-Rachford splitting method is used to split the large problem into smaller problems solved in parallel locally by each flexible consumer in order to follow a consumption profile. The aggregator solves an economic global objective and communication is between units and the aggregator which coordinates the entire set-up. An analytical comparison of the centralised, decentralised and distributed MPC algorithms for residential energy systems incorporating battery storages was done in [195]. However, the distributed MPC was based on a hierarchical design using a market maker as the central coordinator that manages an iterative price negotiation process to flatten the aggregate power usage in the network. Here, the limitation of centralised MPC with respect to large optimisation problems was highlighted (for a large number of residential customers) while the decentralised and distributed hierarchical control benefited by being scalable and flexible. Interestingly while these applications equally share the energy balance problem among users they are not combined with LFC. In addition they are also greater communication requirements as a result of the decomposition algorithms used in integrating the loads.

In this section a review of the applications of model predictive control in future grids has been given. Several observations can be highlighted:(i)The integration of BESS into the grid for LFC without causing issues of stability is important in future grids.(ii) MPC with its multi input multi output property can easily be used as a central controller in integrating BESS into the power system model where they can participate LFC with conventional generators (iii) Decentralised control of frequency responsive devices integrated into the grid is highly desirable for systems resilience, privacy and fault tolerance in the future grid and has been a subject of research (iv) This has been implemented using problem decomposition techniques linked to optimal control. The stability guarantees are dependent on the system the quick convergence of the algorithms which might not be possible due to consensus and sharing requirements. In addition constraint satisfaction is only at steady state. Therefore MPC which can satisfy transient constraints provides a more reliable control technique. In order to decompose the model however without adopting splitting algorithms which still ensuring BESS systems are frequency responsive the method of overlapping model decomposition is adopted.(v) However, the stability and robustness of this method to uncertainties caused by ignored dynamics in the decentralised models has not been

analysed. In addition the analysis would focus on the transmission system where in most cases these algorithms are analysed at distribution level particularly in hierarchical applications which focus mainly on microgrids.

## 2.7 Conclusion

This chapter has covered a significant amount of information related to the research carried out in this thesis. First of all a background on the subject of load frequency control was given. A complete mathematical model development procedure for the implementation of LFC studies was enumerated. The three control loops that make up frequency control within the VIU framework were explained. These were all covered in Section 2.1 concluding with an example simulation of LFC in a two area system. In Section 2.2 a centralised formulation of the MPC algorithm was given with a review of the different architectures of MPC in the literature; decentralised, distributed and hierarchical configurations. A main takeaway from this section is that MPC offers a wide variety of formulations and flexibility in controller design that makes it suitable for use in large scale networked systems such as the smart grid.

A detailed discussion of BESS was given in Section 2.3. The advantages of using BESS when compared to other components of a future power network were enumerated. In addition the some control techniques used in integrating BESS into the grid was given. In Section 2.4, the decomposition methods used in the integration of BESS into the grid for frequency control was highlighted. For implementation using MPC the overlapping decomposition techniques was explained and the requirements for stable control design highlighted. Following this, in Section 2.5, MPLFC in the power system was focused on the standard traditional structure and on the gradual development of MPC applications for LFC using centralised, decentralised and distributed control architectures. Also shown was how different system constraints such as generation rate, deadband and power constraints were introduced over the years. Furthermore, deregulated market structures and economic considerations were also accounted for in several MPC formulations. Clearly MPC offers an advanced control algorithm for LFC applications. In Section 2.6 different architectures of MPC in future power systems were reviewed. It was shown that MPC design can be used in future power networks to achieve set control and optimisation objectives.

From this review several observations emerge. The design of MPC controllers for the use of BESS in LFC are in the first instance required for the integration of BESS into the power grid. Frequency should be accepted as an input to the BESS

---

to create an independent control action or response of the BESS. In addition unlike conventional systems where tie-lines define locations of system decomposition for autonomous control design, in future power systems the splitting of a system composed of a BESS and conventional generators which allow the BESS to local receive a feedback of frequency requires decomposition methods. This makes the design of decentralised MPC controllers supporting local control more challenging. In addition, the notions of stability of decentralised controllers using MPC is not easily shown in such a situation. The different response speed of BESS and generators also make direct application of MPC controllers which are sampled at a single base rate in the system difficult. These issues are interesting research areas that would be addressed in the remainder of this thesis within the context of LFC in future power networks.



# Chapter 3

## Load Frequency Control with Battery Energy Storage

### 3.1 Introduction

This chapter focuses on the development of a model predictive load frequency control model considering the deregulated power system structure integrated with battery energy storage systems. In Section 1.1 the fundamental reasons behind the transition to the smart grid system were enumerated. There an overview of the deregulated power system and how this new market structure facilitates the move to a smarter grid was explained. From there some of the basic components that make up the smart grid were introduced including battery energy storage systems.

The relevant equations relating to the main components that make up a model predictive controller were developed in Section 2.2 of Chapter 2. The choice of MPC makes it possible to take advantage of some characteristics inherent in its formulation. In this chapter, we will see how in particular the multi-input multi-output characteristic is used for the integration of BESS into the power system in such way that power and energy constraints on the BESS are explicitly accounted for while simultaneously achieving energy recovery without the need to design a separate control layer specifically for this purpose which is not usually considered in most applications.

A BESS can serve multiple purposes when connected to the power grid as was noted in Section 2.3 of Chapter 2. Historically, when used in LFC the focus is usually on providing BESS power output in support of generators such as in [196, 121]. However, since BESS operation is also constrained by their energy capacity it is beneficial to factor this in when considering their participation in LFC. One approach is to reduce

the BESS output power the closer it gets its energy limits. That is, the BESS power output is a function of its energy level see [197–199] where this was achieved via a droop control design. However, energy recovery is not explicitly handled using this approach. In microgrid systems renewable generation such as wind and solar panels are coordinated with BESS for meeting load demand. In larger power networks, a similar approach is taken where large wind turbines are coordinated with BESS in order to increase the dispatchability of wind farms. The interactions between BESS and conventional generators including their subsequent impact on system operation is not obvious since the BESS operate decoupled from the dynamic model of the system. BESS is modelled as an additional disturbance input to the system (see [124]) separate from the model representing the power system.

As noted in Section 1.3 new strategies that account for the inter-temporal dependencies, including power and energy constraints of BESS coordinated with bulk generation are of increasing importance. Hence for integration into the power system, models that enables the BESS to participate in frequency regulation while also improving the dynamic behaviour of the power system are desirable. Ideally a model with minimal complexity, that is of a similar order as the models of components parts the existing power system and comparatively responds within a similar or of the same time scale of operation in order to retain good stability and improve the performance of the grid is preferable. In addition, at the same time, algorithms that can systematically meet the operational requirements of the integrated models are also required.

This chapter therefore develops a new integrated model of the deregulated system with battery energy storage. Furthermore an MPC controller is designed to function as a TSO for the implementation of load frequency control. The controller is of the centralised variation. The BESS is considered as a direct and controllable addition to the legacy power system, (*i.e.*, similar to a generation asset); the MPC-based LFC scheme incorporates a BESS model, and ensures offset-free frequency regulation under contracted and uncontracted demand changes while meeting system constraints (including battery capacity). The MPC-controlled BESS is able to support the LFC function of a deregulated power system, improving the transient response, with the added benefit that there is no need to design filters for handling how transients are handled by traditional plant and BESS. Hence the following contributions are made in this chapter:

- A CMPC scheme is proposed for the LFC problem for a two area deregulated power system integrated with battery energy storage systems in both areas which

support generators in handling planned(contracted) and unplanned (uncontracted) load disturbances in each area.

- Energy recovery is accounted for in the algorithmic design process in addition to input and GRC constraints on both the generators and battery systems.

In the rest of this chapter Section 3.2 gives an explanation of the BESS model and its state space derivation. In Section 3.3 a complete formulation of the deregulated model integrated with the derived BESS model is presented. Section 3.4 develops the centralised model predictive controller while Section 3.5 uses numerical simulations to show the effectiveness of the approach including a discussion of the results. In Section 3.6 the impact of energy recovery on the system is discussed while Section 3.7 is used for concluding remarks.

## 3.2 Development of BESS Model Supporting Load Frequency Control

In Section 2.1 the dynamic models of the components that make up the power system model used for LFC studies were developed. A noticeable feature of these models is their reduced complexity which is able to capture the main dynamic behaviour of the power system. They models have proven to be effective for load frequency control analysis. In this section different BESS LFC models are examined and a model similar in complexity to the standard governor turbine models used for LFC is developed.

Within the optimisation literature a common model used (e.g for planning) is the simplified general energy storage model represented by the state of charge with charging and discharging power over a specified time interval. This model also accounts for charging and discharging efficiencies. In order words the primary focus when applying this model is mainly for the determination of optimal inputs using preview information (forecasts) such as for slow changing loads or renewable generation which allows for economic and reliable operation with conventional generators. These models tend to be of the form

$$E_{k+1}^s = E_k^s + \eta_c P_k T_s - \frac{1}{\eta_d} P_k T_s \quad (3.1)$$

where  $P_k$  is the power flow in or out of the BESS and  $\eta_c$  and  $\eta_d$  represents respectively charging and discharging efficiency,  $T_s$  the sampling time and  $E^s$  the energy level. For this model to be used for LFC studies it would have to be based on deviations from an

equilibrium (incremental approach) similar to modelling in 2.1. In control applications, different dynamic BESS models have been applied. Nominally a BESS consists of a battery bank and a converter which acts as the link between the BESS and power grid. The converter links the BESS to the grid via a transformer arrangement depending on the configuration of the bridge circuit i.e number of pulses (six,twelve) and the type of bridge circuit; such as three phase or two way bridge. The different variations and configurations can be found in [200]. However for modern multi-terminal direct current grids (MTDC) grids, voltage source converters (VSC) effectively perform the same function. A description of various configurations of VSCs and their applications for DC/AC interfacing can be found in [201].

In modelling the BESS, different parameters can be taken into consideration. Some of basic ones include temperature, battery capacity, ageing and economic viability. Not all of these parameters are dynamic, and when this is taken into consideration simplified models capturing the important parameters can be derived. In general, despite the different modelling approaches no single model design is able to accurately capture all the required parameters for a complete dynamical analysis of the BESS and therefore the decision on what model to use would depend on the what is considered sufficient on a case by case basis [202]. Naturally the higher model fidelity the better the expected performance when applied to control problems.

In LFC, circuit models combining resistors, capacitors and diodes were some of the first models used in modelling BESS. These include the simple Thevenin circuit having a voltage source in series with a parallel RC circuit. This model is characterised by RC values which are dependent on other battery parameters. Several other equivalent circuit models include those developed by using data from the manufacturers' specifications in combination with experiments which also consider environmental temperature, self discharge, capacity overvoltage and internal resistance [203]. An early model developed in [196] proved to be suitable for dynamic stability analysis in power systems. This model consisting of a battery module and a converter represented by several transfer function blocks was successfully used for frequency suppression following a load disturbance within a single area. In this model an RC combination is used to determine the time constants for the BESS which makes them suitable for use in combination with the governor-turbine time constant based models formulated in Section 2.1. Similarly an incremental BESS model having a converter and battery was used developed in [204]. This circuit model was combined in a state space model also for a single area. These models however, did not explicitly account for state of charge. Non linear models have

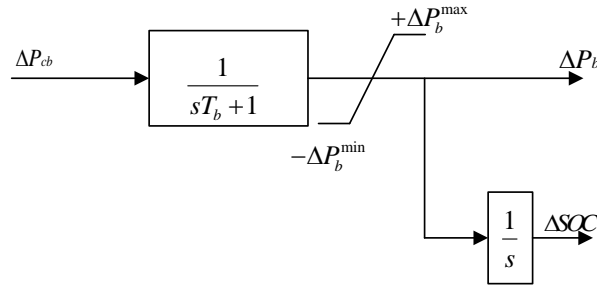


Fig. 3.1 Battery model

also been developed which can capture chemical and temperature related characteristics of BESSs and can represent different types of BESS.

However, not every BESS parameter is needed for LFC. That is, the model does not need to incorporate every model and parameter influencing the BESS operation. In most cases designs that account for the power and state of charge have proven to be sufficient for LFC studies in the power system. A simplified circuit based dynamic model was developed in [205]. This model with three states was further simplified in [114] and when compared to the more detailed non linear models showed closely similar and acceptable dynamical behaviour. One of the main drawbacks of these models is that for the purpose of application the values of the circuit components would need to be at hand.

A modification of the first order model in [119] to account BESS power and state of energy is the first order lag model with state of charge. A simple single integrator (*i.e.*, first-order) is used for the state of charge, with saturation limits on power output. A representation of this model is shown in Figure 3.1.

The battery output power,  $\Delta P_b$ , depends on the reference output power  $\Delta P_{cb}$  as

$$\Delta P_b = \frac{1}{sT_b + 1} \Delta P_{cb} \quad (3.2)$$

when expressed dynamically (converting from Laplace to time domain) is

$$\Delta \dot{P}_b = \frac{1}{T_b} (\Delta P_{cb} - \Delta P_b) \quad (3.3)$$

where

$$\Delta P_b^{\min} \leq \Delta P_b \leq \Delta P_b^{\max}.$$

Though the dynamical model is linear, the output depends nonlinearly on the reference input owing to the output constraint, thus is challenging to control with classical methods (*e.g.* PI control).

The state of charge is calculated by integrating the output power of the BESS, albeit considering capacity constraints:

$$\Delta \dot{SOC} = \frac{1}{B_c} \Delta P_b, \quad (3.4)$$

with

$$SOC^{\min} \leq SOC \leq SOC^{\max}.$$

The upper and lower limits can be configured, for example, to correspond to the battery being empty or fully charged; the particular choice of limits depends on the nominal operating point. A more detailed explanation of these constraints is given in Section 3.4.3.

### 3.2.0.1 State Space representation

The development the complete state space representation of the model that captures the interaction between a change in both power and energy output of the battery can now be given as:

$$\begin{bmatrix} \Delta \dot{P}_b \\ \Delta \dot{SOC}_b \end{bmatrix} = \begin{bmatrix} \frac{-1}{T_b} & 0 \\ 1 & 0 \end{bmatrix} \begin{bmatrix} \Delta P_b \\ \Delta SOC_b \end{bmatrix} + \begin{bmatrix} \frac{1}{T_b} \\ 0 \end{bmatrix} [\Delta P_{cb}] \quad (3.5)$$

In this way model sufficient for LFC applications has been developed and represented in state space form. This model has a feature that the output power remains constant during operation and is not a function of the level of the state of charge of the BESS. The model is also expressed in terms of deviation from a nominal operating point (incremental in nature) and also has the flexibility that reasonable power and energy capacity in MW/MWh are the only parameters required for integration into the grid for LFC studies. Note that in this model the BESS responds to changes in frequency which is either a positive or a negative change. It's power output either decreases or increases corresponding to discharging or charging. Therefore it is unnecessary to consider simultaneous charging and discharging since realistically LFC is not implemented for simultaneous occurrences of an increase and decrease in system frequency.

### 3.3 Deregulated power system with BESS

In this section we develop the model used for LFC within the deregulated framework with contribution from the BESS. This final model would accurately represent the BESS integrated into the deregulated power system model and capture all dynamic interactions between all subsystems enabling contributing to LFC. The overall performance of the power system is improved with a positive contribution from the BESS. To simplify this exposition the parameters and variables used in the model are listed in Table 3.1.

The model is based on a two-area deregulated power system made up of two generation companies in each area. These are the GENCOS. Similarly, there are four distribution companies in the model which are being supplied by the GENCOS. These are the DISCOs with a similar split in the numbers of DISCOs per area as with the GENCOS. Note that the deregulated modelling approach is not restricted to these number of GENCOS, DISCOs and areas including the integrated number of BESS. The BESS model developed in Section 3.2 is used to include the participation of battery storage facilities within each area under the assumption that this represents an aggregation of several small single dynamic models within each area. However, for the current area capacity it is also possible to consider this as a single installed battery system—one BESS plant per area consistent with BESS capacities indicated in Section 2.3. These single large capacity plants are what is adopted in this thesis. The two areas are connected by a tie-line and both are managed by a single TSO responsible for providing the LFC control signals to the generating units. Figure 3.2 is a single line representation of the two area system showing the GENCOS, DISCOs and BESS per area. A more detailed transfer function model is shown in Figure 3.3 representing a schematic diagram for the two-area system under consideration showing the GENCOS, DISCOs and BESS within each area.

In the remainder of this section, we develop the complete dynamical model of the system based on the components within each control area and the inter-area interconnection between them. In the sequel, the parameters indicated in Table 3.1 of the power system variables are prefixed with  $\Delta$  to denote that they are deviations from their values at a nominal operating point. Also for the two area system using Table 3.1,  $i \in \{1, 2\}$ ,  $k \in \{1, \dots, 4\}$ ,  $l \in \{1, \dots, 4\}$  and  $b \in \{1, 2\}$ . Scheduled (contracted) demands are denoted by an overbar, while unscheduled (uncontracted) demands are marked with a tilde.

Parameter	Description
$i$	index representing a control area
$k$	index of generators (GENCOs)
$l$	index of DISCOs
$b, i$	index of BESS in area $i$
$\Delta P_{bi}$	change in BESS $b$ 's power output in area $i$ (p.u)
$\Delta SOC_i$	state of charge of battery $b$ in area $i$
$B_{c,i}$	capacity of battery $b$ in area $i$
$\Delta P_{cb,i}$	input reference of battery $b$ in area $i$
$\mathcal{D}_i$	DISCOs in area $i$
$\mathcal{G}_i^e$	GENCOs in area $i$
$\Delta P_{Mi,k}$	change in mechanical output power of generator $k$ in area $i$ (p.u)
$\Delta P_{Mi}$	total variation power output of generators in area $i$ (p.u)
$\Delta P_{vi,k}$	change in governor output of generator $k$ in area $i$ (p.u)
$\Delta P_{vi}$	change in governor output of generators in area $i$ (p.u)
$R_{i,k}$	droop characteristics of generators $k$ in area $i$ (Hz/p.u)
$T_{gi,k}$	governor time constant of generators $k$ in area $i$ (s)
$T_{Ti,k}$	turbine time constant of generator $k$ in area $i$ (s)
$\Delta P_{ci,k}$	input reference of generator $k$ in area $i$
$\Delta \bar{P}_{Li,l}$	total scheduled load demand in area $i$ by DISCO $l$ (p.u)
$\Delta \tilde{P}_{Li,l}$	total unscheduled load demand in area $i$ by DISCO $l$ (p.u)
$\Delta P_{tie,i}$	total change in tie-line energy flow of area $i$
$\Delta P_{tie,i}^{sch}$	scheduled tie-line flow of area $i$
$\Delta f_i$	change in frequency of area $i$ Hz
$D_i$	equivalent damping coefficient of area $i$ (p.u/Hz)
$H_i$	equivalent inertia of area $i$ (p.u s)
$ACE_i$	area control error for area $i$
$\beta_i$	frequency bias setting for area $i$ (p.u/Hz)
$\tau_{i,k}$	ACE participation factors for generator $k$ in area $i$
$\chi_{k,l}$	contract participation factor of generator $k$ with DISCO $l$
$P_{ri}$	capacity rating of area $a$ MW
$C_{i,k}$	contracted power supplied by generator $k$ in area $i$

Table 3.1 Nomenclature of Parameters

### 3.3.1 Interconnection of GENCOs and DISCOs

In the restructured environment GENCOs and DISCOs can freely engage in contracts with each other within and across different areas at favourable rates. As a result of this new arrangement different contractual combinations can exist between GENCOs and DISCOs. These contracts are represented within this current setting using the concept

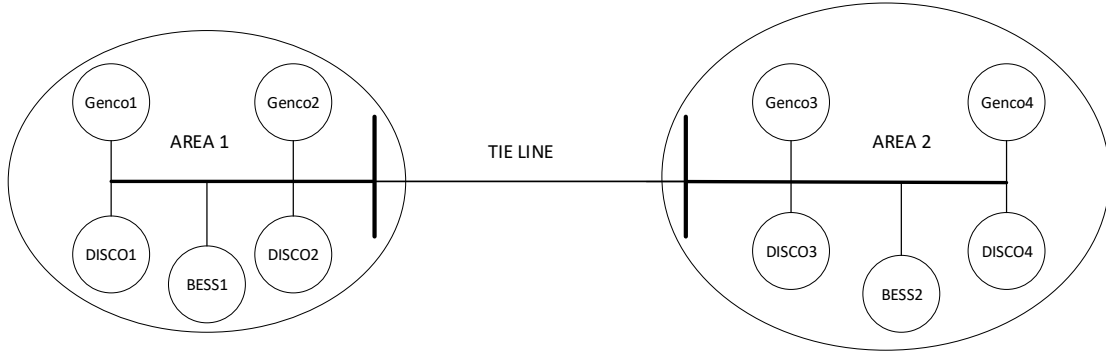


Fig. 3.2 Single line diagram of a two-area deregulated power system comprising conventional thermal generators and battery energy storage in each area. The MW capacity of area 2 is larger than that of area 1

of a DISCO participation matrix (DPM) [5]. Using the DPM creates a convenient way to visualise all contractual agreements between GENCOS and DISCOs in the network .

$$DPM = \begin{bmatrix} \chi_{1,1} & \chi_{1,2} & \chi_{1,3} & \chi_{1,4} \\ \chi_{2,1} & \chi_{2,2} & \chi_{2,3} & \chi_{2,4} \\ \chi_{3,1} & \chi_{3,2} & \chi_{3,3} & \chi_{3,4} \\ \chi_{4,1} & \chi_{4,2} & \chi_{4,3} & \chi_{4,4} \end{bmatrix} \quad (3.6)$$

For the two area model with four GENCOS and four DISCOs the *DPM* matrix is a four by four matrix. The individual elements of the matrix represent the contracted agreements between a GENCO and a DISCO. These are referred to as contract participation factors (cpf) as shown in Figure 3.3 and quantify the part of the total load required by DISCO  $l$  contracted to be supplied by GENCO  $k$ —here represented by  $\chi$ . Each row of the matrix represents a GENCO and each column a DISCO. When the elements of a column are added together their total should always be equal to 1 i.e  $\sum_{k=1}^4 \chi_{k,l} = 1$ . When the *DPM* is square, this is a left stochastic matrix and represents the condition that the entire load demand for each DISCO has been satisfied because all the contracted amounts with each GENCO has been supplied by them. This condition does not necessarily need to hold for the rows, otherwise the *DPM* would be a double stochastic matrix.

From the structure of the *DPM* it is also possible to identify local and inter area demands using the block diagonal and off diagonal blocks of matrix respectively. Hence the *DPM* contains all contracted load demands within the deregulated model. Uncontracted load demands occur as unscheduled disturbances due to unexpected

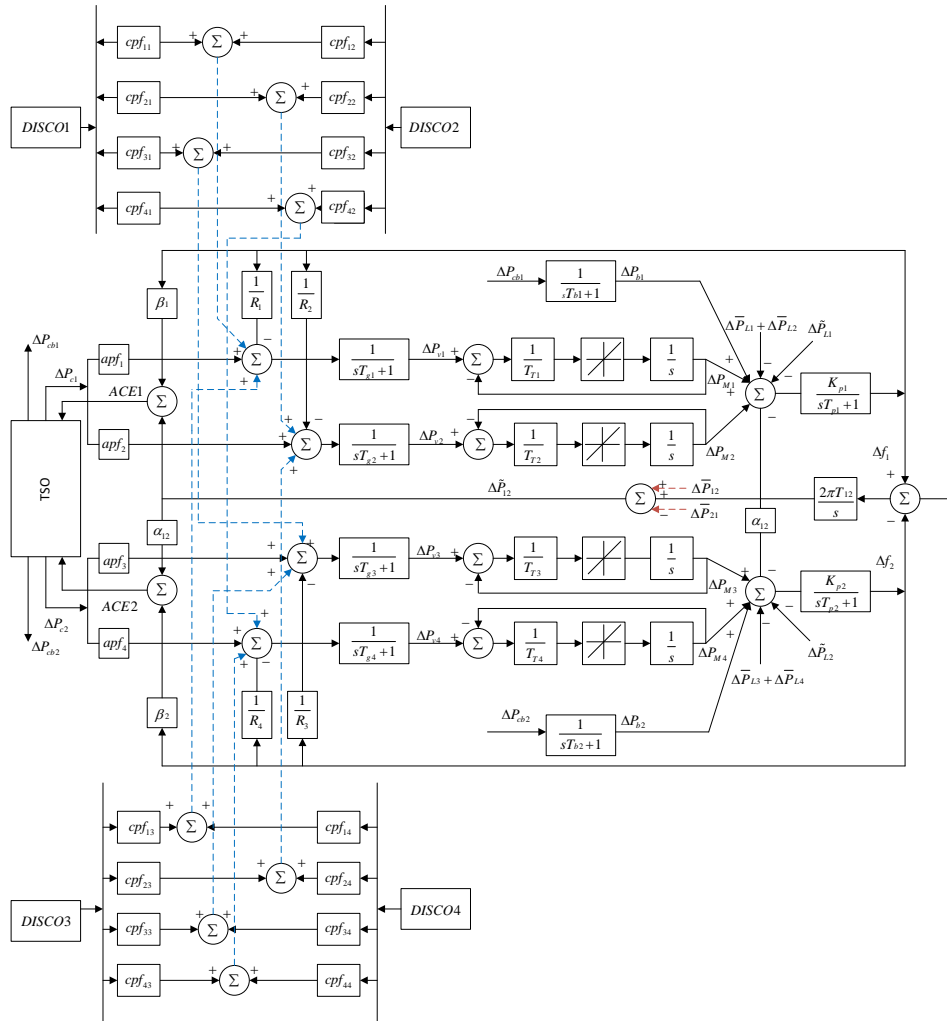


Fig. 3.3 The power system with GENCOs, DISCOs and BESS in each area based on the deregulated framework.

requests for additional power from DISCOs. Hence the total demand from a DISCO is the combination of its contracted and uncontracted load demands.

The *DPM* is applied in the following sense. Denoting the total contracted load from DISCO  $l$  as  $\Delta\bar{P}_{Ll}$ , the total power contracted for supply by GENCO  $k$  is

$$C_{i,k} = DPM_k \begin{bmatrix} \Delta\bar{P}_{L1} \\ \Delta\bar{P}_{L2} \\ \Delta\bar{P}_{L3} \\ \Delta\bar{P}_{L4} \end{bmatrix} = \sum_{l=1}^4 \chi_{k,l} \Delta\bar{P}_{Ll}, \quad (3.7)$$

where  $DPM_k$  denotes the  $k$ th row of  $DPM$  and  $C_{i,k}$  the contracted power of GENCO  $k$  in area  $i$  represented by the blues lines in Figure 3.3.

The uncontracted load-generation balance is dealt with in a similar way, albeit with a key difference. As previously highlighted the uncontracted load arises where unexpected demands for additional power (unscheduled disturbances) are made by a DISCO. The burden of supplying this unscheduled load is shared among the GENCOs taking part in LFC in the area where the additional demand falls, according to further participation factors termed *area participation factors*, and arranged in an *area participation matrix* (apf) in Figure 3.3 here represented by  $\tau$ ,

$$APM = \begin{bmatrix} \tau_{1,1} & 0 \\ \tau_{1,2} & 0 \\ 0 & \tau_{2,3} \\ 0 & \tau_{2,4} \end{bmatrix}, \quad (3.8)$$

since area 1 comprises GENCOs 1 and 2, and area 2 GENCOs 3 and 4. The sum of the participation factors of all generators in an area must be equal to 1. That is

$$\tau_{1,1} + \tau_{1,2} = 1, \quad \tau_{2,3} + \tau_{2,4} = 1 \quad (3.9)$$

Denoting the uncontracted load demand in area  $i$  as  $\Delta\tilde{P}_L$ , the total load demanded in an area is given by

$$\Delta\tilde{P}_{Li} = \sum_{l \in \mathcal{D}_i} \Delta\bar{P}_{Ll} + \sum_{l \in \mathcal{D}_i} \Delta\tilde{P}_{Ll}. \quad (3.10)$$

where for example in area 1,  $\sum_{l=1}^2 \Delta\tilde{P}_{Ll}$  has been lumped into  $\Delta\tilde{P}_{Ll}$  in Figure 3.3 and henceforth is simply  $\Delta\tilde{P}_{Li}$ . Hence, the total power to be supplied by GENCO  $k$  (including contracted and uncontracted) is

$$\sum_{l=1}^4 (\chi_{k,l} \Delta\bar{P}_{Ll}) + \tau_{i,k} \Delta\tilde{P}_{Li} = C_{i,k} + \tau_{i,k} \Delta\tilde{P}_{Li}. \quad (3.11)$$

### 3.3.2 GENCO dynamic model

For the basic GENCO dynamic model, as noted in Section 3.3 there are two GENCOs per area. Each of these GENCOs represents a power generation facility whose aggregate dynamics are adequately captured using the standard non-reheat thermal plant consisting of a governor and turbine. This output power from a GENCO is

represented by  $\Delta P_{Mi,k}$ . This turbine model for the GENCOS under the deregulated framework is similar to the one in Section 2.1. For the purposes of providing clarity on the generation rate constraint the power is initially represented as  $\Delta P_{ti,k}$ . Hence the mechanical power output for each of the GENCOS can be represented by;

$$\Delta \dot{P}_{ti,k} = \frac{1}{T_{Ti,k}} (\Delta P_{vi,k} - \Delta P_{Mi,k}) \quad (3.12)$$

$$|\Delta \dot{P}_{ti,k}| \leq GRC \quad (3.13)$$

$$\Delta P_{Mi,k} = \Delta P_{ti,k}, \quad (3.14)$$

where  $GRC$  is the generation rate constraint. In the absence of this limit, the model simplifies to

$$\Delta \dot{P}_{Mi,k} = \frac{1}{T_{Ti,k}} (-\Delta P_{Mi,k} + \Delta P_{vi,k}). \quad (3.15)$$

Henceforth  $\Delta P_{Mi,k}$  is assumed to include GRC unless otherwise stated. As noted earlier generators under LFC track a reference power. This is the input to the governor of GENCO  $k$  in area  $i$ . Denoting this as  $\Delta P_{refi,k}$ , it is the net sum of (derived from the summing block each blue dotted lines connects to) the contracted portion of this load demand by DISCOs, the regulated frequency error and the GENCO's proportion  $\tau_{i,k}$  of the control signal  $\Delta P_{ci}$  for area  $i$  from the TSO:

$$\Delta P_{refi,k} = -\frac{\Delta f_{i,k}}{R_{i,k}} + \tau_{i,k} \Delta P_{ci} + \sum_{l=1}^4 (\chi_{k,l} \Delta \bar{P}_{Ll}). \quad (3.16)$$

A GENCOs governor dynamics can thus be written as

$$\Delta \dot{P}_{vi,k} = \frac{1}{T_{gi,k}} (-\Delta P_{vi,k} + \Delta P_{refi,k}). \quad (3.17)$$

The description of all the parameters in (3.16) and (3.17) are given in Table 3.1. The governor model therefore includes the contracted and uncontracted load to be met by a GENCO.  $\Delta P_{ci}$  is the reference change in the general output when uncontracted load demands occur which is split among the generators using the area participation factors  $\tau_{i,k}$ . This value is zero in the absence of uncontracted load changes since all generators meet their contracted load demands. Therefore no further output adjustments is required by them.

### 3.3.3 Scheduled inter-area transfers and tie-line dynamics

The scheduling of supply–demand contracts between GENCOs and DISCOs in different areas also requires, for any set of contracts across the system, a scheduled value of inter-area power transfer. Indeed, this is the net imbalance between contracted supply and demand in each area—more precisely, the demand of DISCOs in area 2 from GENCOs in area 1 minus the demand of DISCOs in area 1 from GENCOs in area 2—and is expressed as

$$\Delta\bar{P}_{12} = \sum_{k=1}^2 \sum_{l=3}^4 \chi_{k,l} \Delta\bar{P}_{Ll} - \sum_{k=3}^4 \sum_{l=1}^2 \chi_{k,l} \Delta\bar{P}_{Ll} \quad (3.18)$$

where the convention is that  $\Delta\bar{P}_{12} > 0$  implies net transfer from area 1 to area 2. Conversely from the perspective of area two this is given as

$$\Delta\bar{P}_{21} = \sum_{k=3}^4 \sum_{l=1}^2 \chi_{kl} \Delta\bar{P}_{Ll} - \sum_{k=1}^2 \sum_{l=3}^4 \chi_{kl} \Delta\bar{P}_{Ll} \quad (3.19)$$

Irrespective of the scheduled transfer, a tie-line power flow is induced by frequency imbalance across the two areas. In particular, the dynamics of the tie-line power flow from area 1 to area 2 are

$$\Delta\dot{P}_{12} = 2\pi T_{12}(\Delta f_1 - \Delta f_2), \quad (3.20)$$

where  $\Delta f_i$  is the frequency deviation in area  $i$  and  $T_{12}$  is the line synchronizing coefficient. This allows us to define an unscheduled tie-line flow as the error between the actual flow  $\Delta P_{12}$  and the scheduled flow  $\Delta\bar{P}_{12}$ :

$$\Delta\tilde{P}_{12} = \Delta P_{12} - \Delta\bar{P}_{12}. \quad (3.21)$$

Note that in (3.20) and (3.21) the areas are assumed to be of equal area capacities, Hence  $\alpha_{12}$  which represents the area capacity ratios is equal to 1 and  $\Delta\dot{P}_{21} = -\Delta\dot{P}_{12}$ . Also  $\Delta\bar{P}_{12} = -\Delta\bar{P}_{21}$ .

### 3.3.4 Area frequency dynamics and control error

The overall frequency dynamics in each area are finally defined according to the balance between total generation (including battery output) and total load (including

contracted and uncontracted loads, plus any battery consumption). The deviation in the area 1 frequency from its nominal value is governed by the dynamics

$$\frac{T_{p1}\Delta\dot{f}_1 + \Delta f_1}{K_{p1}} = \Delta P_{b1} - \Delta P_{12} + \sum_{k=1}^2 \left[ \Delta P_{Mi} - \sum_{l=1}^4 (\chi_{kl}\Delta\bar{P}_{Ll}) - \tau_i\Delta\tilde{P}_{Ll} \right] \quad (3.22)$$

where  $K_{p1}$  and  $T_{p1}$  are the gain and time constant respectively for area 1 of the power system with a similar expression for area 2<sup>1</sup>. The difference between (3.22) and (2.16) is the inclusion of contracted loads associated with the deregulated framework. The *area control errors* are

$$ACE_1 = \beta_1\Delta f_1 + \Delta\tilde{P}_{12} \quad (3.23)$$

$$ACE_2 = \beta_2\Delta f_2 + \alpha_{12}\Delta\tilde{P}_{12} \quad (3.24)$$

where  $\alpha_{12}$  is the ratio of the rated powers, and allows different base quantities in each area.

The control objective is to regulate  $ACE$  in each area to zero. Achievement of this renders  $\Delta f_1 \rightarrow 0$  and  $\tilde{P}_{12} \rightarrow \bar{P}_{12}$ , *i.e.*, nominal frequency is achieved, tie-line flows are at scheduled levels, and—if the battery power output is also regulated to zero in steady-state—each GENCO meets its contractual obligations:

$$\Delta P_{Mi,k} \rightarrow \sum_{l=1}^4 (\chi_{k,l}\Delta\bar{P}_{Ll}) + \tau_{i,k}\Delta\tilde{P}_{Li} \quad (3.25)$$

To this end, therefore, the proposed AGC, which is centralized, provides the following as control inputs to the GENCOs and battery systems within each area: the reference power to the conventional generating units and the reference power to the battery storage system, *i.e.*,  $\Delta P_{ci}$  and  $\Delta P_{cbi}$ , respectively, in area  $i$ . The area control error of each area must be equal to zero. For this to be achieved (3.21) must be equal to zero at steady state. That is there are no unscheduled tie-line flows between each area since in keeping with standard LFC practice only generators in an area are supposed to meet any uncontracted load demand at steady state in that area. Inter-area power flows for unplanned loads is only provided during transient to support system stability.

---

<sup>1</sup> $K_{p1}$  and  $T_{p1}$  are derived from the damping and inertia constants used in the swing dynamics of 2.14 and 2.16 using the following relationship:  $Kp = \frac{1}{D}\text{Hz/puMW}$  and  $Tp = \frac{2H}{fD}\text{s}$ . See [39, 15] for details

### 3.3.5 Different area capacities

In real power systems the capacities of various individual control areas are different. This is for example indicated in Figure 3.2 where area 2 is larger than area 1. This difference is not geographical but based on rated power generation capacity. Taking the difference in area capacities into consideration requires some modifications to the equations affected by the capacity factor  $\alpha$  which is no longer equal to 1. This changes the equations for total supplied generator power, inter-area transfers and tie-line given in (3.11),(3.18),(3.19) and (3.20) respectively. The convention adopted is power flow out of an area is positive while into an area is negative and the factor  $\alpha_{ji}$  multiplies all power flows from area  $i$  into area  $j$ . For example in the total contracted power flow *i.e* (3.7)  $C_{1,1}$  of GENCO 1, supply to  $\bar{P}_{L3}$  and  $\bar{P}_{L4}$  in area 2 are multiplied by capacity ratio  $\alpha_{21}$  in the direction of power flow. The same changes are applied to the inter-area transfers and the *DPM*. To this end the contracted power (3.7),scheduled line transfer 3.18 is rewritten explicitly as

#### Contracted Power of GENCOs

$$C_{1,1} = \chi_{1,1}\Delta\bar{P}_{L1} + \chi_{1,2}\Delta\bar{P}_{L2} + \alpha_{21}\chi_{1,3}\bar{P}_{L3} + \alpha_{21}\chi_{1,4}\Delta\bar{P}_{L4} + \tau_{1,1}\Delta\tilde{P}_{L1} \quad (3.26)$$

$$C_{1,2} = \chi_{2,1}\Delta\bar{P}_{L1} + \chi_{2,2}\Delta\bar{P}_{L2} + \alpha_{21}\chi_{2,3}\bar{P}_{L3} + \alpha_{21}\chi_{2,4}\Delta\bar{P}_{L4} + \tau_{1,2}\Delta\tilde{P}_{L1} \quad (3.27)$$

$$C_{2,3} = \alpha_{12}\chi_{3,1}\Delta\bar{P}_{L1} + \alpha_{12}\chi_{3,2}\Delta\bar{P}_{L2} + \chi_{3,3}\bar{P}_{L3} + \chi_{3,4}\Delta\bar{P}_{L4} + \tau_{2,3}\Delta\tilde{P}_{L2} \quad (3.28)$$

$$C_{2,4} = \alpha_{12}\chi_{4,1}\Delta\bar{P}_{L1} + \alpha_{12}\chi_{4,2}\Delta\bar{P}_{L2} + \chi_{4,3}\bar{P}_{L3} + \chi_{4,4}\Delta\bar{P}_{L4} + \tau_{2,4}\Delta\tilde{P}_{L2} \quad (3.29)$$

#### Scheduled inter-area transfer

$$\begin{aligned} \Delta P_{tie,1}^{sch} = \Delta\bar{P}_{12} &= \alpha_{21}[(\chi_{1,3} + \chi_{2,3})\Delta\bar{P}_{L3} + (\chi_{1,4} + \chi_{2,4})\Delta\bar{P}_{L4}] \\ &\quad - [(\chi_{3,1} + \chi_{4,1})\Delta\bar{P}_{L1} + (\chi_{3,2} + \chi_{4,2})\Delta\bar{P}_{L2}] \end{aligned} \quad (3.30)$$

$$\begin{aligned} \Delta P_{tie,2}^{sch} = \Delta\bar{P}_{21} &= \alpha_{12}[(\chi_{3,1} + \chi_{4,1})\Delta\bar{P}_{L1} + (\chi_{3,2} + \chi_{4,2})\Delta\bar{P}_{L2}] \\ &\quad - [(\chi_{1,3} + \chi_{2,3})\Delta\bar{P}_{L3} + (\chi_{1,4} + \chi_{2,4})\Delta\bar{P}_{L4}] \end{aligned} \quad (3.31)$$

For the tie-line flow, the general equation is  $\Delta P_{tie,j} = -\alpha_{ij}\Delta P_{tie,i}$ .

#### Tie-line

$$\Delta\dot{P}_{12} = 2\pi T_{12}(\Delta f_1 - \Delta f_2) \quad (3.32)$$

$$\Delta\dot{P}_{21} = -\alpha_{12}2\pi T_{12}(\Delta f_1 - \Delta f_2), \quad (3.33)$$

### 3.3.6 State-space model and discrete-time prediction model

Following the development of this power system model, the new combined system is then used to yield a continuous time linear time -invariant model for the complete two area power system. This is represented by

$$\dot{x} = A^c x + B^c u + \bar{B}^c \bar{P}_L + \tilde{B}^c \tilde{P}_L \quad (3.34)$$

$$y = C^c x + D^c \bar{P}_L \quad (3.35)$$

The complete matrices are given in the appendix.

The control inputs for the combined models of the system contains reference powers for both the conventional plant and the BESS:

$$u = [\Delta P_{c1} \quad \Delta P_{cb1} \quad \Delta P_{c2} \quad \Delta P_{cb2}]^\top,$$

and  $\bar{P}_L$  and  $\tilde{P}_L$  denote, respectively, the stacked vectors of contracted and uncontracted loads. The state vector

$$x = [x_i \quad P_{tiei} \quad x_j]^\top,$$

where

$$x_i = [\Delta f_i \quad \Delta P_{Mi,k} \quad \Delta P_{vi,k} \quad \Delta P_{bi} \quad \Delta SOC_i \quad \Delta P_{tiei}]^\top,$$

$$x_j = [\Delta f_j \quad \Delta P_{Mj,k} \quad \Delta P_{vj,k} \quad \Delta P_{bj} \quad \Delta SOC_j]^\top,$$

contains the individual states within each area plus the tie-line power. Also the output is a vector of the individual area control errors and the desired reference state of charge to be tracked for the BESS

$$y = [\Delta ACE_1 \quad \Delta SOC_1 \quad \Delta ACE_2 \quad \Delta SOC_2]^\top,$$

This model is discretized, yielding

$$x^+ = Ax + Bu + \bar{B}\bar{P}_L + \tilde{B}\tilde{P}_L \quad (3.36)$$

where  $x^+$  is the discrete-time successor state to  $x$ . Note that, in order to be useful as a prediction model, measurements or estimates of all states, the contracted load *and* the uncontracted load must be available. The MPC controller formulated here

in the next section assumes the availability of all data, in order to retain simplicity and enable a clear exposition. Therefore henceforth for the rest of this thesis unless otherwise stated this is the assumption under which all simulations are implemented.

### 3.4 MPC formulation for LFC

In this section a centralised MPC controller is designed based on the model developed in Sections 3.2 and 3.3. The proposed MPC controller performs the load–frequency control function of the TSO in order to ensure that both scheduled and unscheduled disturbances are handled without excessive (*i.e.* constraint violating) disruption to system frequency and scheduled power transfers. The controller should also optimally utilize the BESS for frequency support which should improve the performance of LFC when compared with what is attainable using only the conventional generation. At the same time, the controller aims to ensure the battery operates within its limits, avoiding deep charging/discharging in order to prolong life.

To this end, the centralised finite-horizon optimal control using model predictive control problem is formulated as follows:

#### 3.4.1 Prediction equations

Following the discretisation of the continuous time model and the subsequent derivation of the discrete model, a suitable prediction model is required for the prediction of the system behaviour in order to generate the required optimal inputs. However, since the key requirement in LFC is the response to changes in load demand; contracted and uncontracted, the design model should account for these disturbances if offset free tracking is to be achieved at steady state. In the context of LFC this means the steady state value of the frequency and ACE should be zero.

Therefore in this problem, in order to achieve offset free tracking the prediction model employs deviation variables,  $\bar{x} \triangleq x - x_{ss}$  and  $\bar{u} \triangleq u - u_{ss}$ ; the pair  $(x_{ss}, u_{ss})$  is a (non-zero) steady-state equilibrium pair associated with the measured disturbance  $\bar{B}\bar{P}_L + \tilde{B}\tilde{P}_L$ . This is derived by defining the system model in steady state terms

$$x_{ss} = Ax_{ss} + Bu_{ss} + \bar{B}\bar{P}_{Lss} + \tilde{B}\tilde{P}_{Lss} \quad (3.37)$$

subtracting (3.37) from (3.36)

$$\bar{x}^+ = A\bar{x} + B\bar{u} \quad (3.38)$$

This prediction model therefore explicitly handles (provided  $x_{ss}, u_{ss}$  can be accurately computed) disturbance rejection in order to achieve LFC objective of regulation. The state space prediction is thus given by

$$\bar{\mathbf{x}}^+ = F\bar{\mathbf{x}} + G\bar{\mathbf{u}} \quad (3.39)$$

where all the variables represented in (3.39) are as previously derived in Section 2.2 where  $\bar{\mathbf{x}}$  and  $\bar{\mathbf{u}}$  are stacked vectors of  $x$  and  $u$ .

The decision variable obtained from the prediction is the sequence of controls,  $\bar{\mathbf{u}} = \{\bar{u}_0, \dots, \bar{u}_{N-1}\}$ ,  $\bar{x}$  is the current state measurement, and the state and input constraints include, *inter alia*, state-of-charge constraints, power output constraints, and any frequency deviation bounds, all adjusted to account for the change of variables from  $(x, u)$  to  $(\bar{x}, \bar{u})$ .

### 3.4.2 Controller Objective Function

The objective function for which the prediction equation is applied is

$$V_N^0(\bar{x}) = \min_{\bar{\mathbf{u}}} V_N(\bar{x}, \bar{\mathbf{u}}) \quad (3.40)$$

subject to, for  $k = 0, \dots, N-1$ ,

$$\bar{x}(k+1) = A\bar{x}(k) + B\bar{u}(k)$$

$$\bar{x}_0 = \bar{x}$$

$$\bar{u}^{\min} \leq \bar{u}(k) \leq \bar{u}^{\max}$$

$$\bar{x}^{\min} \leq \bar{x}(k) \leq \bar{x}^{\max}.$$

which is explicitly defined as

$$V_N(\bar{x}, \bar{\mathbf{u}}) = \sum_{k=0}^{N-1} (\bar{x}^\top(k)Q\bar{x}(k) + \bar{u}^\top(k)R\bar{u}(k) + \bar{x}_N^\top P\bar{x}_N) \quad (3.41)$$

where  $Q, R, P$  are positive definite matrices. This objective function yields the following desired steady-state property:

$$V_N(\bar{x}, \bar{\mathbf{u}}) = 0 \iff ACE_i = 0, \Delta SOC_n = 0 \text{ for } i = 1, 2.$$

That is, at the minimum of the objective function, the  $ACE$  is zeroed, and both BESS maintain their charge (emphasizing that it is  $\Delta SOC_i = 0$  and not  $SOC_i = 0$ ). In other words, the BESS here do not take part in the market operation of the system, *e.g.* in day-ahead balancing, but operate as an ancillary service supporting LFC. Their contribution to the frequency support is tuned via the matrices  $Q$  and  $R$ . One benefit of applying MPC is the use of the weighting matrices which provides a means of controlling the behaviour and contribution of the battery. In Section 3.6 a further explanation and investigation of the impact of these weights as they relate to the systematic tuning for the energy recovery phase of the BESS state of charge is given.

### 3.4.3 System Constraints

In the operation of physical systems, various components are subjected to constraints i.e physical limits. In the case of power systems with thermal plants using steam driven turbines, the output power can only increase at a specified maximum rate. However, in most cases economic operation is synonymous with operating close to or around the physical limits of the system. These limits could be related to the states or the input of the system and could be on the rate of change or on the absolute magnitude of the variable being constrained. Such limits are usually imposed for quality control purposes and for the safety of operating equipment. For the deregulated power system with BESS the following system constraints were considered.

#### 3.4.3.1 Battery Constraints

The main state constraints on the BESS which directly affect it's dynamical behaviour based on the model developed in Section 3.2 are constraints on the power and state of charge.

#### Power Constraints

The BESS is limited by its maximum power capacity. This create a bound on the power capacity of the BESS. When in operation the power output determines the depth charge/discharge which directly impacts the degradation/safety of the BESS, hence it might be safe to operate at a lower power capacity with other economic considerations such as operational longevity. The equation representing this constraint is already given in Section 3.2 but is repeated here for completeness:

$$\Delta P_b^{\min} \leq \Delta P_b \leq \Delta P_b^{\max}.$$

### State of Charge Constraint

In order to keep the BESS operating within acceptable regions the state of charge of the BESS can be constrained. This not only helps to keep the BESS within safe working limits particularly for lead acid or lithium ion BESS where deep discharge could lead to permanent damage, it could also provide a means to prolong the life of BESS by using the systematic constraint handling machinery of MPC. In this thesis the focus is preventing deep discharge or overcharge of the BESS. In applications, the most common operating regions are the ranges between 20% – 80% and 30% – 70%. This ensures a certain level of operational safety and flexibility when using the BESS.

When the BESS is fully charged the state of charge is 100%. When fully discharged it is 0%. The aim is to maintain the SOC around the mid operating region of 30% which is 50% of battery capacity. In BESS degradation modelling the state of charge and the depth of discharge can be expressed in quadratic terms to represent battery degradation and this is captured by the model developed and included in the MPC cost function. Another benefit is that depending on BESS technology, safe operation within a specified range could prevent the BESS from entering the regions where degradation behaviour becomes highly exponential. The state of charge at the next time step can be represented as

$$\Delta SOC_{k+1} = \Delta SOC_k \pm T_s \Delta P_{bk}.$$

The actual value of the depth of discharge can be obtained by subtracting the value of the state of charge from 1.

$$\Delta DOD = 1 - \Delta SOC.$$

The state of charge constraint can then be stated as in equation 3.7 which is also repeated here for completeness

$$\Delta SOC_i^{\min} \leq \Delta SOC_i \leq \Delta SOC_i^{\max}.$$

#### 3.4.3.2 Generation Constraints

Generation rate constraints limit the rate of change of the output power from generating units. This occurs as a result of physical limits on the thermal and mechanical movements associated with generators [16]. In the absence of these limits it is possible for the system to chase large disturbances which could lead to undue wear and tear

on generators [39]. These rates have an impact on the area control errors which could deviate further leading to an increased dependence on inter-area tie-line flow to reduce the ACE to zero. This constraint is given as

$$T_s \Delta P_{Mi,k}^{\min} \leq \Delta \bar{P}_{Mi,k} \leq T_s \Delta P_{Mi,k}^{\max} \quad (3.42)$$

where  $\Delta \bar{P}_{Mi,k} = (\Delta P_{Mi,k+1} - \Delta P_{Mss}) - (\Delta P_{Mi} - \Delta P_{Mss})$ .

The combined matrix of state constraints is given by

$$\underbrace{\begin{bmatrix} \Delta \bar{P}_{M1,1}^{\min} \\ \Delta \bar{P}_{M1,2}^{\min} \\ \Delta \bar{P}_{B,1}^{\min} \\ \Delta \bar{S\bar{O}C}_1^{\min} \\ \Delta \bar{P}_{M2,3}^{\min} \\ \Delta \bar{P}_{M2,4}^{\min} \\ \Delta \bar{P}_{B,2}^{\min} \\ \Delta \bar{S\bar{O}C}_2^{\min} \end{bmatrix}}_{\mathbf{x}^{\min}} \leq \underbrace{\begin{bmatrix} \Delta \bar{P}_{M1,1} \\ \Delta \bar{P}_{M1,2} \\ \Delta \bar{P}_{B,1} \\ \Delta \bar{S\bar{O}C}_1 \\ \Delta \bar{P}_{M2,3} \\ \Delta \bar{P}_{M2,4} \\ \Delta \bar{P}_{B,2} \\ \Delta \bar{S\bar{O}C}_2 \end{bmatrix}}_{\mathbf{x}_k} \leq \underbrace{\begin{bmatrix} \Delta \bar{P}_{M1,1}^{\max} \\ \Delta \bar{P}_{M1,2}^{\max} \\ \Delta \bar{P}_{B,1}^{\max} \\ \Delta \bar{S\bar{O}C}_1^{\max} \\ \Delta \bar{P}_{M2,3}^{\max} \\ \Delta \bar{P}_{M2,4}^{\max} \\ \Delta \bar{P}_{B,2}^{\max} \\ \Delta \bar{S\bar{O}C}_2^{\max} \end{bmatrix}}_{\mathbf{x}^{\max}} \quad (3.43)$$

Where the overbar indicates the deviations from the steady state targets. The generation rate constraints have been transformed into equivalent state constraints using (3.42) and are combined with the state constraints on the BESS as shown in (3.43). These constraints are obtained by extracting the lines of the state transition matrix representing the given state. Note that this proposed approach is also able to handle other operational constraints such as limits tie-line flows.

### 3.4.3.3 Input Constraints

The inputs constraints indicate physical limits that cannot be exceeded in the operation of the system. Here they are used to indicate limits on the maximum input capacity of the generators and BESS.

$$\underbrace{\begin{bmatrix} \Delta P_{c1}^{\min} \\ \Delta P_{cb1}^{\min} \\ \Delta P_{c2}^{\min} \\ \Delta P_{cb2}^{\min} \end{bmatrix}}_{\mathbf{u}^{\min}} \leq \underbrace{\begin{bmatrix} \Delta P_{c1} \\ \Delta P_{cb1} \\ \Delta P_{c2} \\ \Delta P_{cb2} \end{bmatrix}}_{\mathbf{u}_k} \leq \underbrace{\begin{bmatrix} \Delta P_{c2}^{\max} \\ \Delta P_{cb2}^{\max} \\ \Delta P_{c2}^{\max} \\ \Delta P_{cb2}^{\max} \end{bmatrix}}_{\mathbf{u}^{\max}} \quad (3.44)$$

Which when combined are represented by the constraints developed in Section 2.2.

$$\Delta P_{ci}^{\min} \leq \Delta P_{ci} \leq \Delta P_{ci}^{\max}.$$

### 3.4.4 Centralised Solution

The centralised MPC solution that is used to solve the LFC problem is thus as follows:

$$\min_{\mathbf{u}} = \frac{1}{2} \mathbf{u}_k^\top H \mathbf{u}_k + f^\top \mathbf{u}_k \quad (3.45)$$

subject to

$$P_c \mathbf{u}_k \leq q_c + S_c x_k \quad (3.46)$$

and where  $f$  is as defined in (2.48). The solution to this problem solved at each sampling time instant determines the inputs to the GENCOS and the BESS within each area, subject to the defined constraints.

## 3.5 Numerical simulation and discussion

In this section a number of simulations are performed to demonstrate the effectiveness of the centralised MPC formulation when BESS participate in LFC in the deregulated environment. The parameters used for the simulations in this chapter and the rest of this thesis were selected using values from [127, 16, 121, 164] as reference guides. All simulations were implemented in Matlab. The values used in this chapter are given in table 3.2

	GENCO1	GENCO2	GENCO3	GENCO4
$T_{Gi}(s)$	0.085	0.088	0.095	0.08
$T_{Ti}(s)$	0.350	0.30	0.295	0.320
$R_i(\text{Hz/pu})$	2.4	2.4	2.4	2.4
$\alpha_i$	0.55	0.45	0.50	0.50
	Area 1		Area 2	
$T_b(s)$	0.2		0.2	
$D(\text{pu/Hz})$	0.0833		0.0833	
$2H(\text{pu.s})$	0.1667		0.1667	
$\beta(\text{pu/Hz})$	0.425		0.425	

Table 3.2 Parameters of the two area deregulated model

The BESS in both areas are of different capacities with the battery in area 1 having a maximum power capacity of 10MW, which is assumed for both discharging and charging, while the state of charge is constrained between 20 and 80% of the full capacity of 20MWh. For area 2, the BESS maximum power capacity is 20MW, and its full energy capacity 40MWh with the state of charge constrained in the same range as that of the battery in area 1. For the MPC design, the dynamics were discretized with a sampling time of 0.1s and the horizon was set to 50 steps (*i.e.*, 5s). The cost matrices were chosen as  $Q = 100I_x$  and  $R = I_u$ , which achieved a satisfactory balance between frequency and BESS state of charge restoration and where  $I_x$  and  $I_u$  are of the appropriate dimensions. The terminal cost matrix  $P$  was determined as the solution to the discrete-time Lyapunov equation associated with  $(A, B, Q, R)$  and a stabilizing control law  $u = Kx$ ; while this  $P$  guarantees closed-loop stability in the absence of constraints the choice of the horizon adopted more or less guarantees stability.

Both input and state constraints are considered with the generation rate constraint of 0.0010pu/s which is assumed to be the same for all GENCOs. An input constraint of 0.02pu is imposed on the GENCOs for each area. The value of the input and maximum power constraint on the BESS 1 is set at 0.0083pu (*i.e.*, the assumption is that both the inverter and BESS maximum power capacities are equal for area 1) and 0.01 in area 2.

Note that in the implementation of LFC, for any number of areas which make up a power system, if the number of areas is equal to  $n$  *i.e.*,  $i \in [1, \dots, n]$ , the corresponding number of controllable tie lines power flows is given by  $n - 1$ . This is because should the number of independent tie-line power flows in the model be equal to the total number of areas which make up the model, controllability issues could occur [206]. Hence in the model developed, during simulation only the tie-line for area 1 *i.e.*  $\Delta P_{tie1}$  is included in the model.  $\Delta P_{tie2}$  is automatically controlled in this way.

Also since the different capacities of the area are taken into consideration,  $\alpha_{12}$  is not equal to 1 but is instead determined by the ratio of the area capacities (*i.e.*,  $\alpha_{12} = \frac{P_{r1}}{P_{r2}} \neq 1$ ). The area capacities are  $P_{r1}, P_{r2} = 1200, 2000$ . The tie line synchronising coefficient is 0.0707 puHz. Area two is larger than area one and this is illustrated in Figure 3.2. Two scenarios are investigated during simulations with the first one being a situation where there are no uncontracted load demands occurring in the power system. This is the scenario where only agreed contractual agreements are been met. In the second scenario additional uncontracted load demands occur which place an extra load requirement on both the generators and additional response on the batteries within each area of the power system.

### 3.5.1 Case I—No uncontracted load demands

The first case considered in the simulation is the one where there are no unscheduled load demands in the network. In this case DISCOs do not exceed the contractual agreements they have made with GENCOs both within and outside their area of operation. Therefore the output of each generator is expected to be equal to the total amount of power procured by all the DISCOs with each GENCO. On the other hand as the generators change their outputs to meet contracted demands, the BESS is expected to improve the response of the system during transients while also satisfying any capacity related constraints limiting its operation.

The  $DPM$  used in this scenario is as follows:

$$DPM = \begin{bmatrix} 0.3 & 0.25 & 0.1 & 0.25 \\ 0.1 & 0.25 & 0.2 & 0.2 \\ 0.2 & 0.25 & 0.5 & 0.25 \\ 0.4 & 0.25 & 0.2 & 0.3 \end{bmatrix}.$$

For the case of contracted demands, the load requirement made by each DISCO in area 1 is  $0.0035 pu$  while the demand by each DISCO in area 2 is  $0.002 pu$ . Since all the DISCOs keep their contractual agreements, the participation factors have no influence on the generator outputs at steady state at this stage.

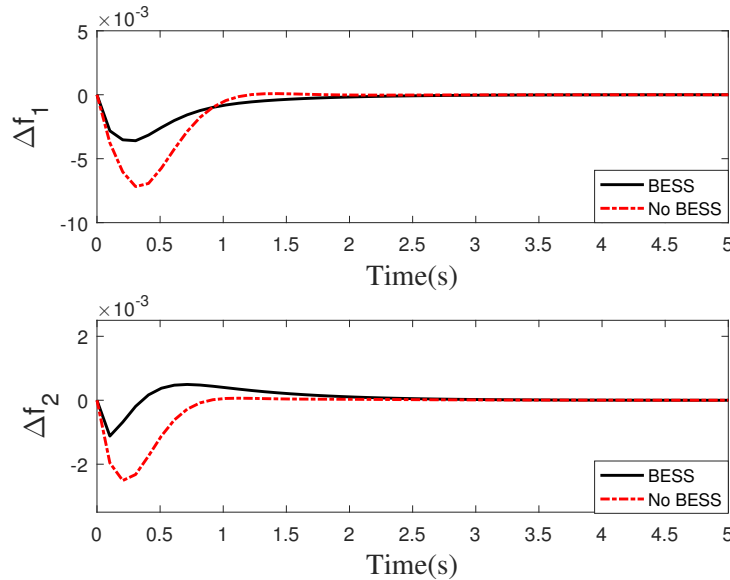


Fig. 3.4 Frequency deviations for areas 1 and 2, case 1

From Figures 3.4 and 3.5 it is seen that the requirements of LFC for both the frequency and  $ACE$  to be regulated to zero are met. This is the expected outcome since generators were able to generate the required outputs which meet the contractual agreements with DISCOs while the DISCOs in turn made demands equal to the agreements made with GENCOs. Importantly the figures compare the output for the situation with and without a BESS and a smoother LFC performance is achieved with the BESS. This shows with the design coordination was achieved between the BESS and GENCOs with significant improvement in LFC dynamic performance during transients when the BESS is operational.

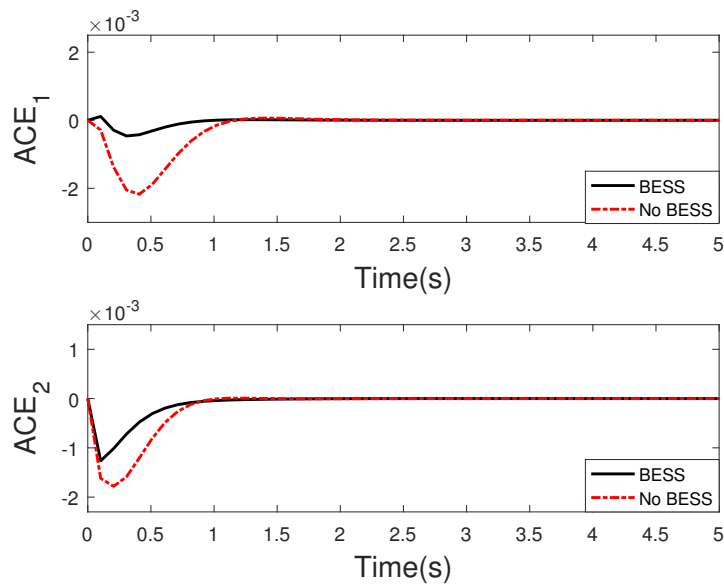


Fig. 3.5 Area control error for areas 1 and 2, case 1

In Figure 3.6 the output response of each GENCOs is depicted. The values of the output power of each GENCO is calculated using (3.11) minus the uncontracted loads. These values are represented by the dotted lines in Figure 3.3. From the plots it can be seen that each GENCO adjusts its output to meet the required contracted demand. Also, similar to the case of frequency and  $ACE$  outputs, the generators have a smoother response with BESS and show lower peaks when compared to the situation without BESS. Note that at steady state when  $ACE_i$  and  $\Delta SOC_i$  are regulated to zero, based on the parameters selected for simulation the GENCOs meet their expected power outputs as indicated by the dotted lines in Figure 3.6

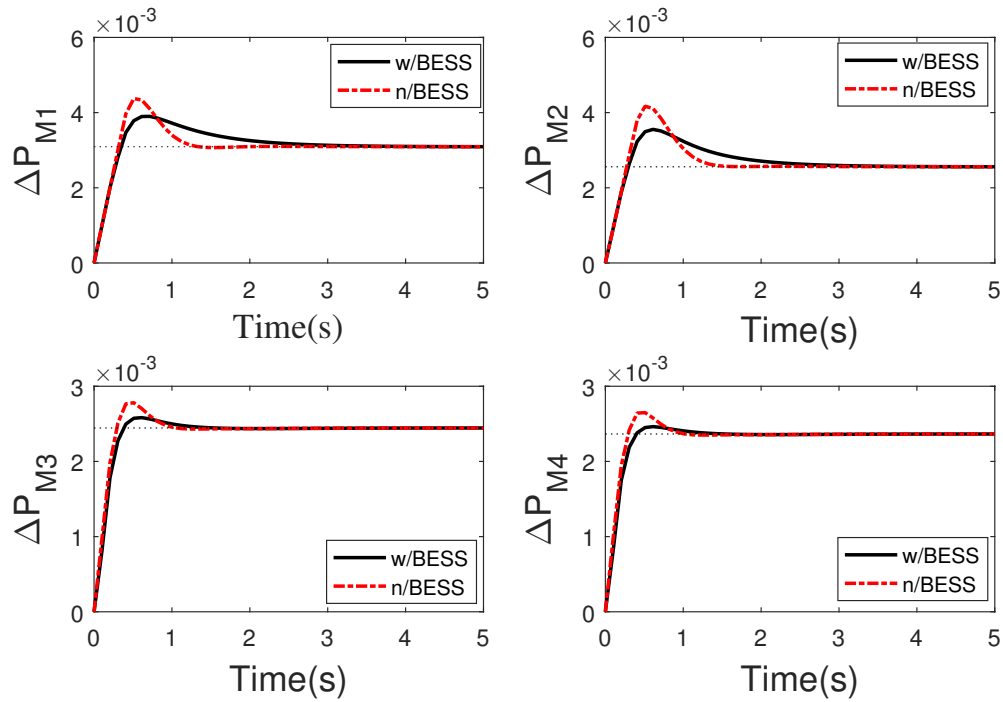


Fig. 3.6 Output power of all generators both areas, Case 1

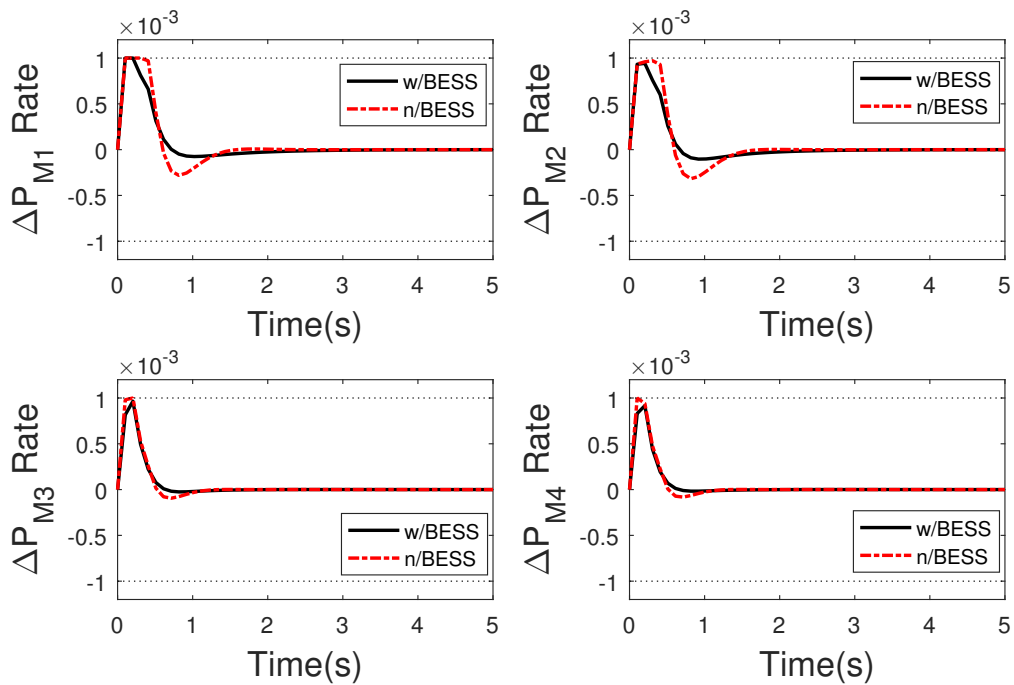


Fig. 3.7 Generation rate constraint of all generators in area 1 and 2, Case 1

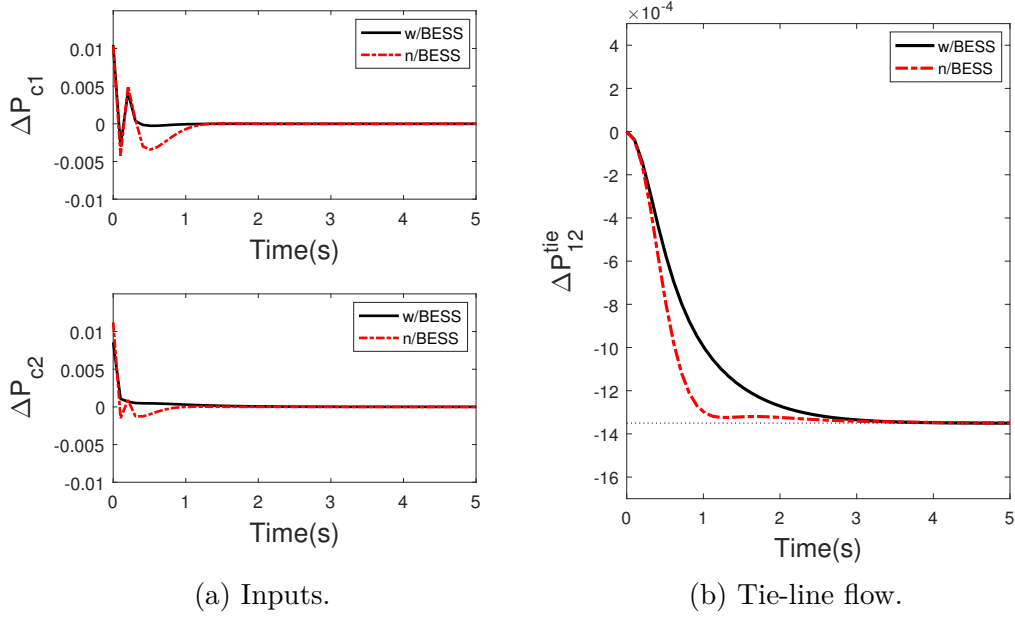


Fig. 3.8 Inputs to areas 1 and 2, and tie-line flow case 1

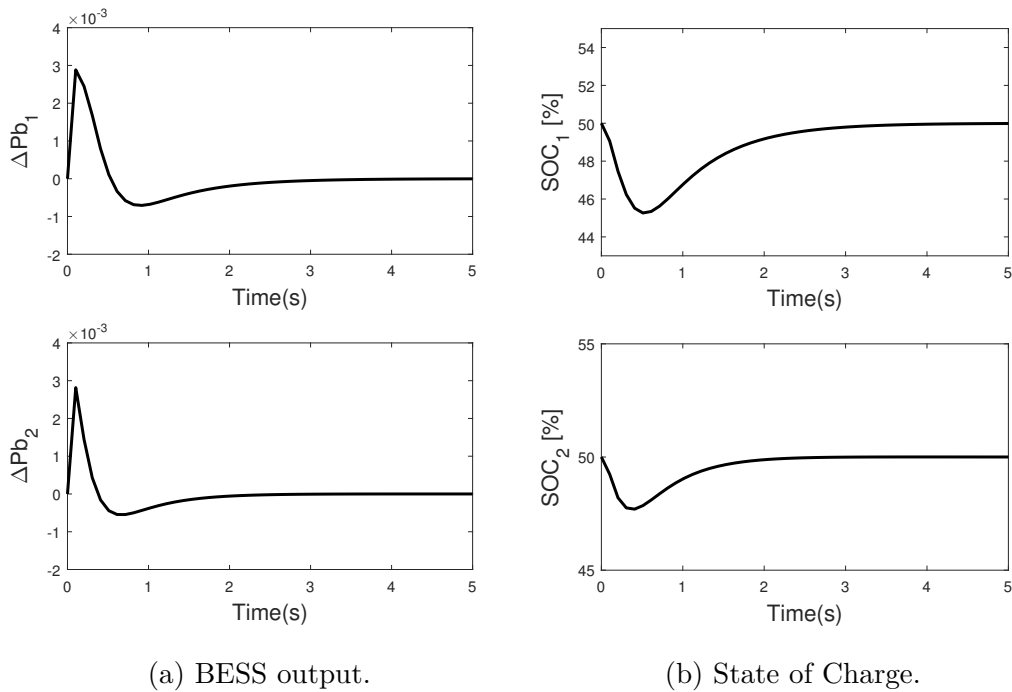


Fig. 3.9 BESS output power and State of Charge in percentages in areas 1 and 2, case 1

The generation rate constraint is given in Figure 3.7 which shows the rate of change of the generator outputs with the limits imposed by GRC also shown. The dotted lines indicate the maximum and minimum values of the constraints. Based on the selected values of the DISCOs load requirements these constraints are satisfied and show an improved performance in the presence of a BESS. Significantly generators need not ramp very quickly reducing the impact of wear and tear on them.

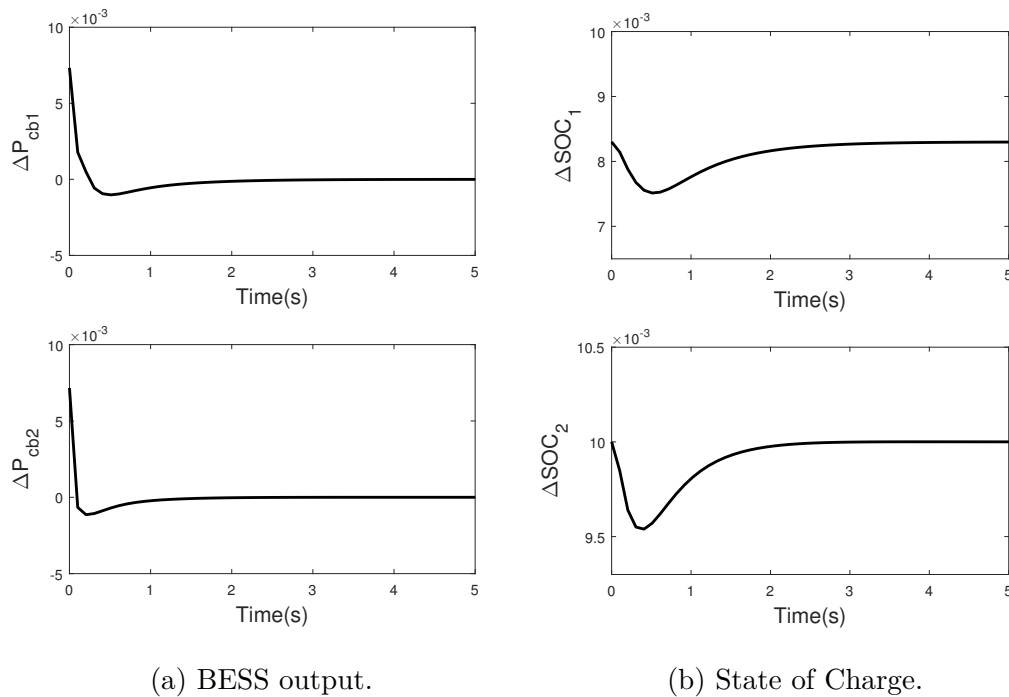


Fig. 3.10 BES inputs and State of Charge(pu) areas 1 and 2, case 1

The inputs of each of the generators converges to zero indicating that all contractual agreements have been met and in the absence of uncontracted load changes GENCOs do not adjust their reference outputs. This can be seen in Figure 3.8 Here we also observe an improvement in the transient behaviour with a BESS when compared to the case without one. The tie-line outputs are also indicated in Figure 3.8. In the deregulated power system this value should be equal to the scheduled tie-line flow between both areas which in this instance is equal to  $-0.0013pu$  and in both cases this value is tracked. Based on the convention for tie-line flows adopted in this thesis the negative indicates that area 1 being supplied by power from area 2.

The change BESS power outputs and state of charge are given in figure 3.9. The convention adopted in this thesis is an increase in the power output represents a discharge while a decrease in output means a charge. The input and state of charge

in per unit to the BESS is shown in Figure 3.10. As noted the overall change in the BESS power output is expected to be zero and the state of charge should return to its nominal value in section. As expected the battery output is positive during the transients, indicating discharge, and the state of charge tracks back to the nominal position (*i.e.*,  $\Delta SOC_n = 0$ ) at steady state.

### 3.5.2 Case II—Uncontracted load demands

In this section a second scenario where uncontracted load demands occur in the deregulated power system is investigated. This is the situation where DISCOs make more demands for power in addition to the contracted power already being supplied by GENCOs. Based on LFC this additional demand must only be met by GENCOs in the area where they occur and is shared between them according their predetermined participation factors.

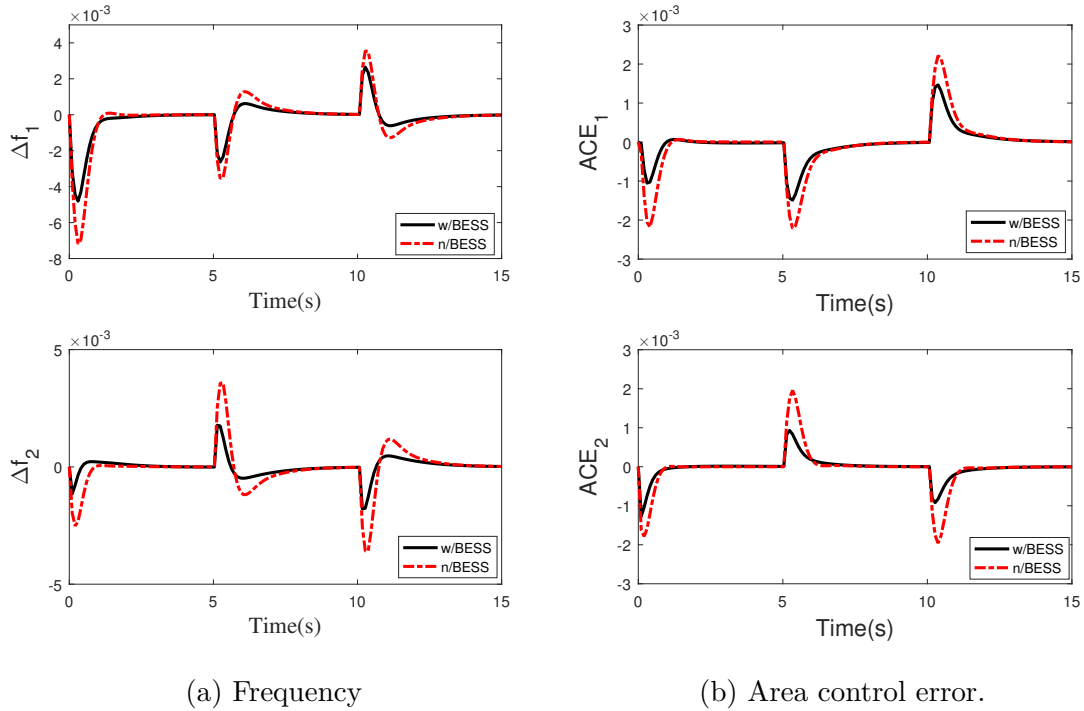


Fig. 3.11 Frequency and ACE in areas 1 and 2, case 2

The outputs of each GENCO is calculated using the total GENCO power flow equations such as 3.26 for GENCO 1 whenever an unscheduled load demands occurs. In this scenario at the times this additional request for power happen, the inputs of

each GENCO is modified and converges to a value representative of its portion of the additional demand it is supposed to supply based on its participation factor.

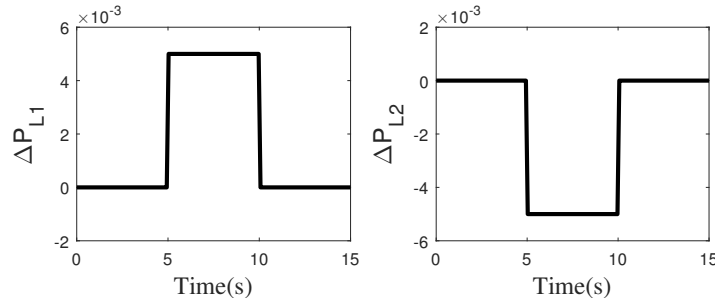


Fig. 3.12 Unscheduled load changes in areas 1 and 2, Case 2

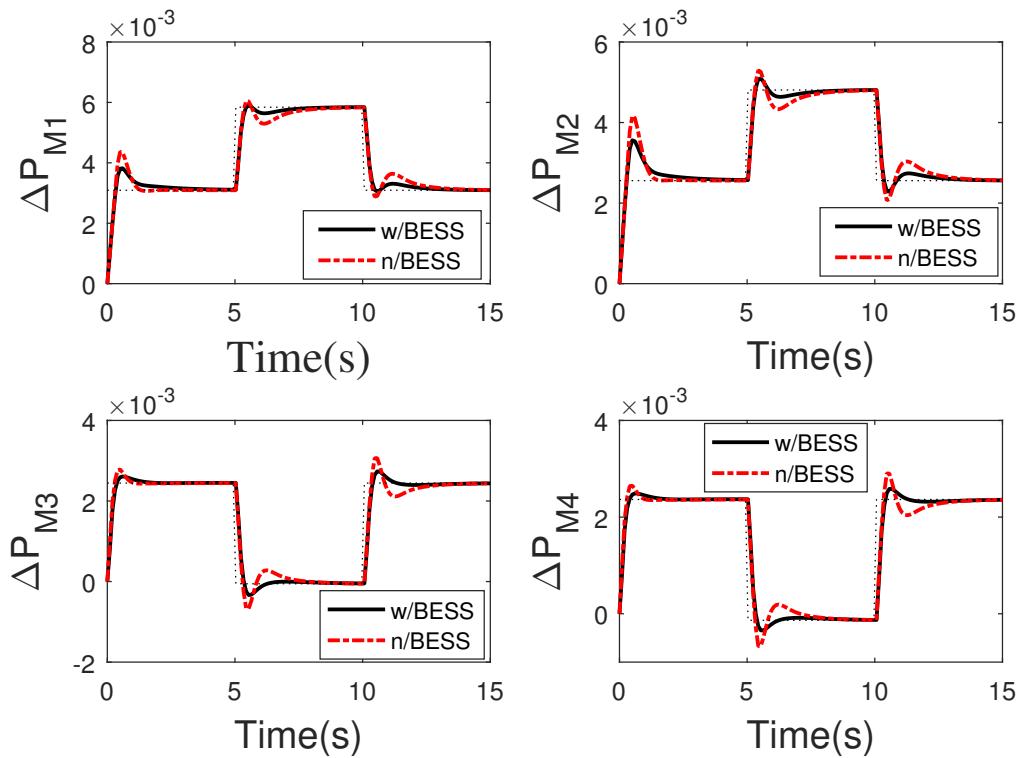


Fig. 3.13 Output powers of all generators in both areas, Case 2

An unscheduled load of 0.005 occurs in both area at 5s and 10s during the simulation. This uncontracted load change is shown in Figure 3.12 which is a positive load change for area 1 and a negative load change in area 2. Similar to case 1 since generators are supposed to cater for load disturbances in their areas, the tie-line flow changes only

change during the transients and settles to the same steady state value of scheduled tie-line flow of  $0.0013 pu$  as in case 1.

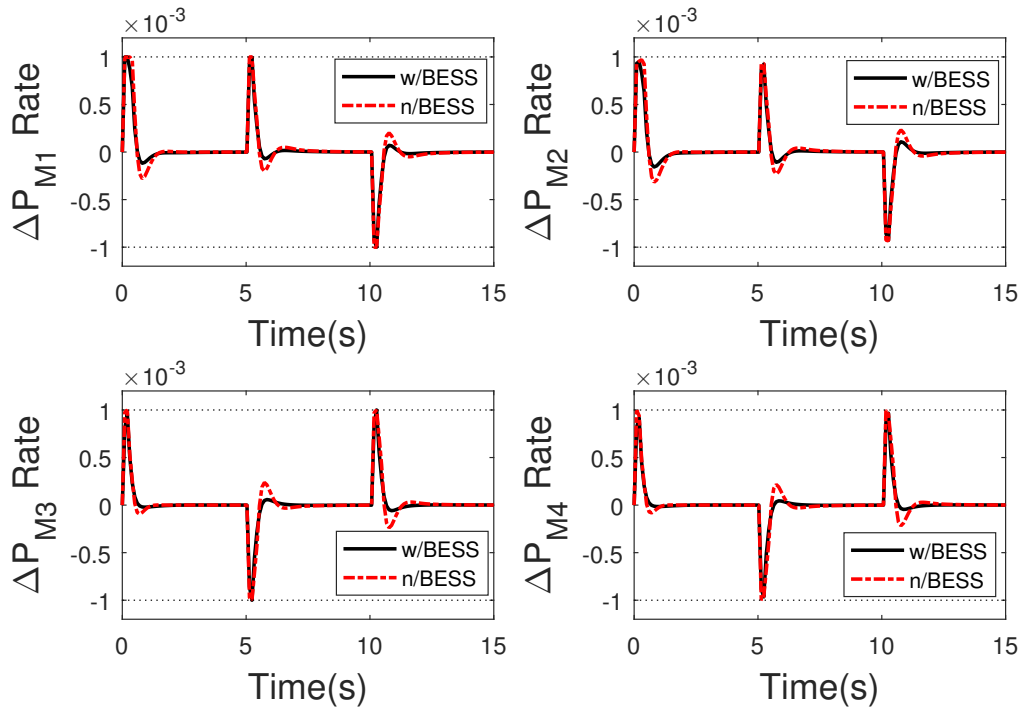


Fig. 3.14 Generation rate constraint of all generators in area 1 and 2, Case 2

The BESS behaviour remains unchanged in terms of the final steady state values, however they are expected to respond each time an unscheduled load change is added or deducted by a DISCO. This means that the BESS improves the transients performances each time an unscheduled change in load occurs but returns its nominal operating point after this disturbance has been cleared by the GENCOs.

Therefore, having described the expected behaviour of the system in the presence of unscheduled load changes, the figures following show the results of the simulation. From Figure 3.11 the change in both the frequency and ACE is zero whenever there is a change in demand indicating that all scheduled and unscheduled demands have been met by the generators.

For the generators as expected their outputs change to match the new level of power requested by DISCOs as these requests occur. This is shown by the dotted lines in Figure 3.13. It can be seen that when the unscheduled load changes occur, the generators change their outputs to meet the portion of the new demand they are expected to match. The corresponding generation rate plots are given in Figure 3.14 also occurring at the times when changes in demand occur

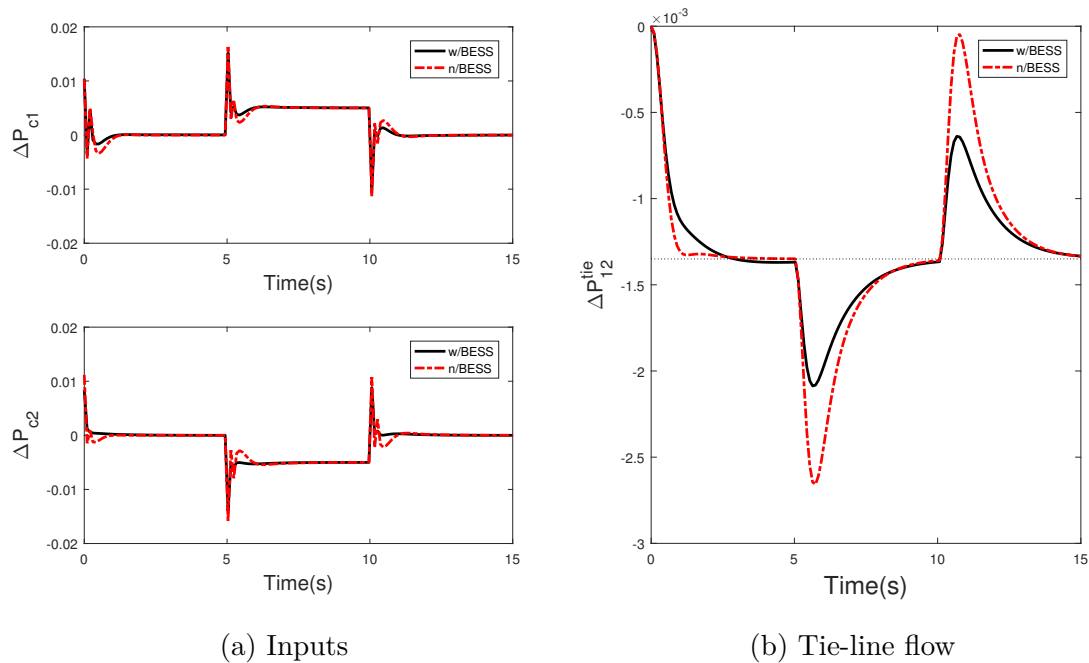


Fig. 3.15 Inputs to areas 1 and 2 and tie-line flow case 2

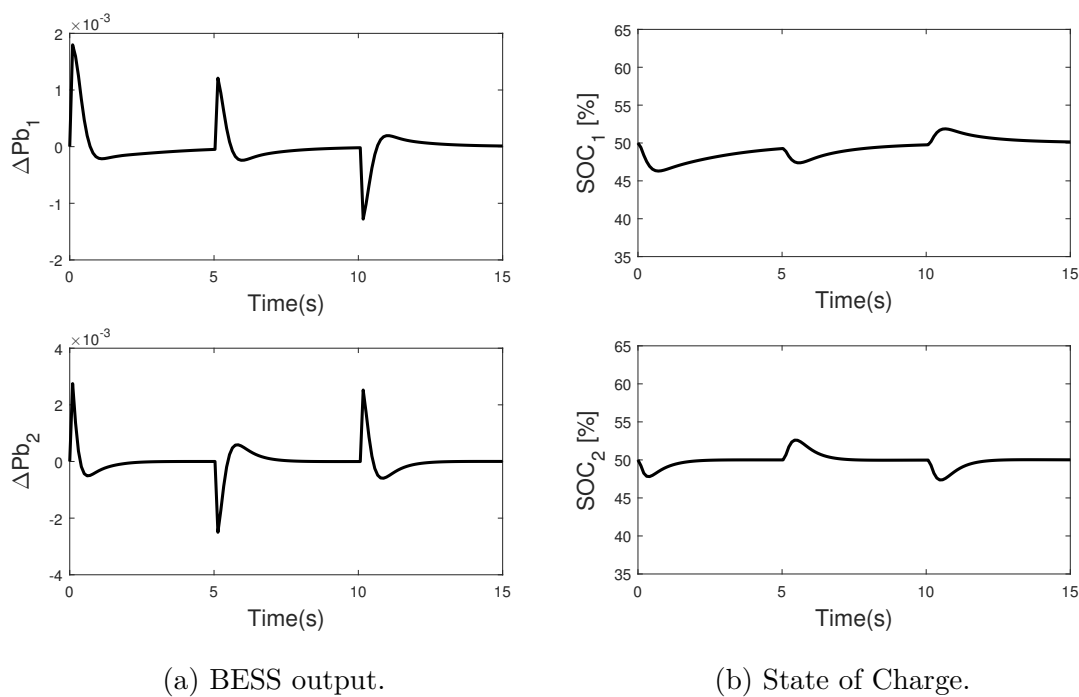


Fig. 3.16 BESS output power and state of charge in percentages in areas 1 and 2, case 2

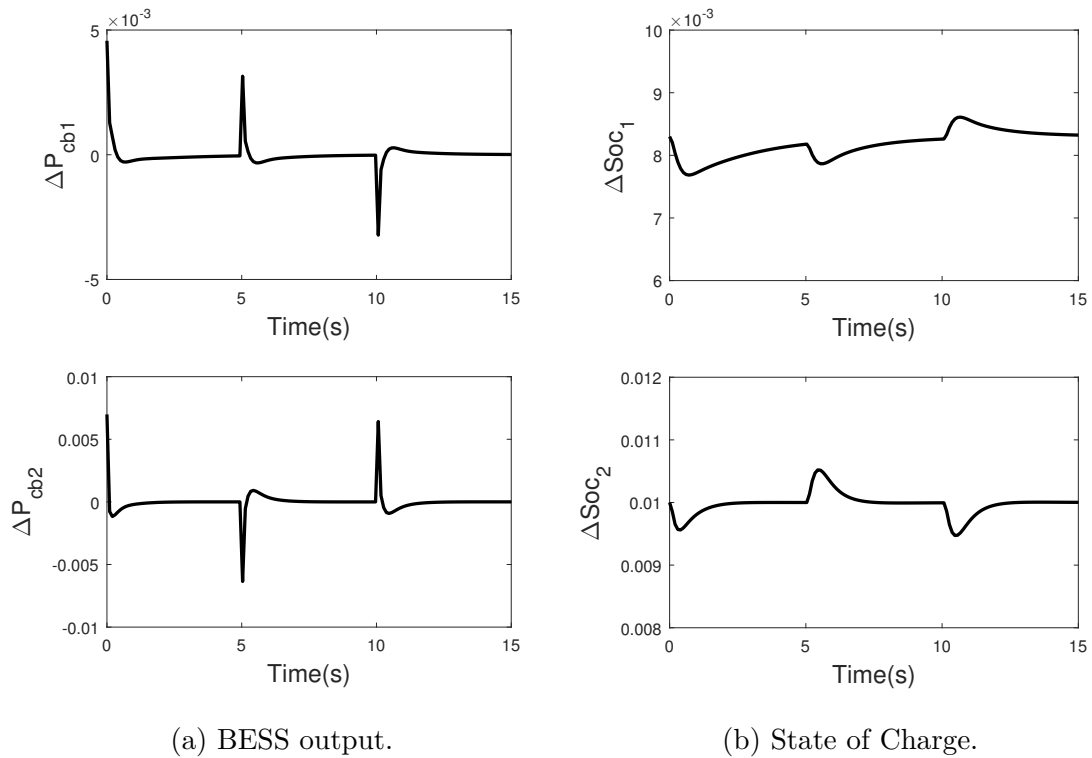


Fig. 3.17 BES inputs and State of Charge(pu) areas 1 and 2, case 2

The inputs to generators in each area is shown in Figure 3.15 and expectedly converge to the values which are indicative of their contribution to meeting this additional load demand based on their participation factors. In the absence of these load changes they return to zero. Also the tie-line displays expected behaviour since irrespective of the changes in load the scheduled tie-line flow is always attained at steady states.

The BESS response is given in Figure 3.16. It can be seen that at each times a change occurs, the BESS power output also changes. Note that here since a decrease in load occur in area 2 the output power of the bess reduced indicating a charge, This can also be seen in the behaviour of the state of charge which also increases. However, since the requirement is to maintain the state of charge at the optimal value of 50 percent the controller drive it to this reference. The input and state of charge in per unit to the BESS is shown in Figure 3.17. From all the figures, similar to the results obtained in case one, the BESS improves the transient performance of the deregulated power system.

### 3.6 Net Energy Neutrality and Energy Recovery

In the previous sections we have assumed that there is a requirement for the state of charge of the BESS is returned to its nominal value after the handling any load changes. By using the constraint ability of MPC maximum and minimum bounds on the energy consumption and generation of the BESS can be maintained during operation. When BESS are primarily for optimisation using models such as in (3.1) the dynamics mainly evolve over a slow timescale sometimes up to hours. For frequency control the timescale of operation is in seconds.

The model adopted in this thesis is applicable for use within the short timescales for LFC. Also by using MPC, with a quadratic cost function, the state of charge could be used in defining a suitable degradation cost function for the BESS similar to [95]. This means that the BESS is both frequency sensitive and cost accommodating while also allowing for energy recovery. This need to maintain a net neutral energy level immediately after every operation is similar to demand response schemes such as in electric vehicles which must be at a certain level of charge after a specific time [207] or in thermostatically controlled loads which must also maintain a certain temperature at a specified time.<sup>2</sup>

One benefit of this approach is that the BESS is able to recover its state of charge to a proper level before the next frequency excursion event and possibly avoid an inability to support frequency regulation. This is possible because the BESS works in two phases: a frequency regulation phase and an energy recovery phase. In the frequency regulation phase BESS charges or discharges and once the disturbance had been cleared by generators and frequency has been restored to the nominal operating point the BESS are then in the energy recovery phase for state of charge restoration to its optimal point.

The requirement could have an impact on the generator behaviour depending on the area capacity and the size of the BESS. It could also lead to unnecessary manoeuvring of the generators and increase in costs. Hence it might be beneficial to relax this constraint. With MPC this can be achieved by varying the weights on the state of charge.

---

<sup>2</sup>The phrase net energy neutrality here is related to BESS energy capacity and not to the signal sent by the ISO to the BESS. For example the ReGD signal for fast BESS response is zero mean but is not net energy neutral meaning losses due to charge and discharge are not accommodated in the signal. In this situation it is possible for any offsets to be handled internally by the storage device

### 3.6.1 Impact of energy recovery

In this section the relaxing and varying the requirement for energy recovery is investigated. To this end simulation was carried out with manually selected (heuristically) values of the tuning parameter  $Q$  in the case when an uncontracted load change occurs (similar to case 2) but right at the beginning of the simulation. Large values of  $Q$  when compared to  $R$  means the priority is to drive the states to equilibrium at the expense of large control actions [51]. All the other parameters are the same as those used in Section 3.5. However, the generation rate constraint was set to 0.0014 and the maximum power of the BESS in area 1 was set to 3MW.

The impact of varying the weights is shown in Figure 3.18. Varying the weight from the maximum to the minimum value corresponds to relaxing the requirement to quickly drive the state of charge to its equilibrium; in this instance net energy neutrality. Hence, what  $Q$  does is to affect the rate of recharge, which when the system is asymptotically stable means  $\Delta SOC \rightarrow 0$  in all cases is possible. The relaxation of this constraints can be interpreted as an energy deferment on the part of the BESS. In the context of LFC a simplifying assumption can be made that the BESS is not required to recharge until when it is idle or can be recharged at time of minimal demand such as at night.

An important consideration in LFC is the cost of regulation. The impact of varying the weights on the cost of regulation when considering only frequency and tie-lines (Regulation) and the total costs of the system entire i.e including GENCOS and BESS (Full System) is given in Table 3.3. It is obvious that by relaxing this constraint the cost of regulation reduces and remains cheaper for the case with BESS when compared to the case without BESS. These costs have been calculated using

$Q_{SOC}$	With BESS		No BESS	
	Regulation	Full System	Regulation	Full system
0.01	0.0390	0.0745	0.1062	0.1833
10	0.0388	0.1412	0.1062	0.1833
100	0.0387	0.8135	0.1062	0.1833
500	0.0396	3.9824	0.1062	0.1833
1000	0.0480	8.0069	0.1062	0.1833

Table 3.3 Weights and the corresponding costs for the case of BESS and no BESS. Regulations refers to the costs of regulation only *i.e* frequency and ACE while full systems refers to total system costs.

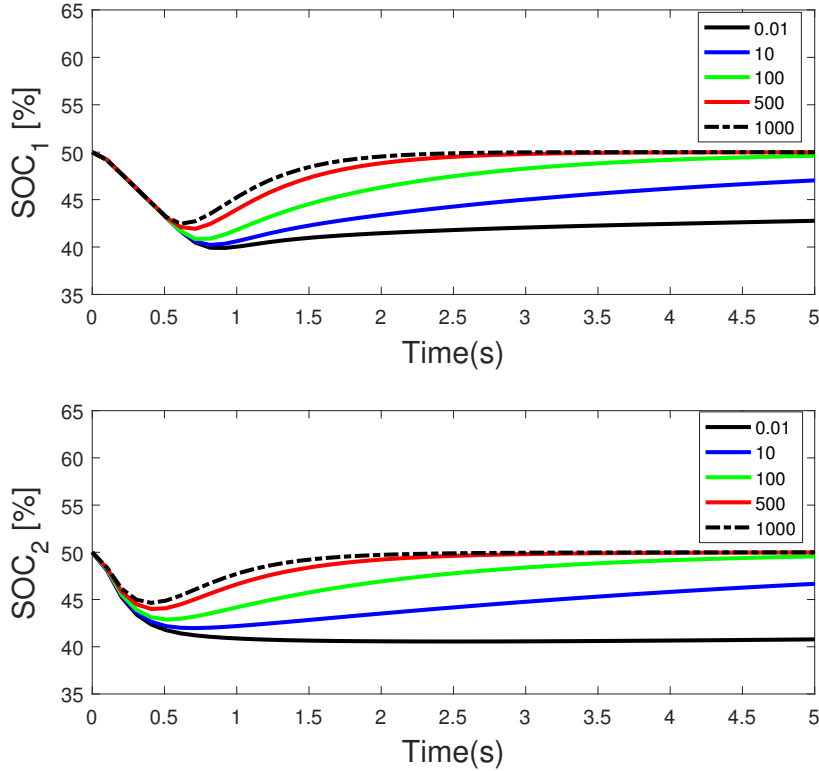


Fig. 3.18 Change in the energy recovery time of the BESS as a result of weight adjustments indicated by the coloured lines: black (0.01), blue(10), green(100), red(500) and black dash line(1000) in the legend for areas 1 and 2

$$J_c = \sum_{t=1}^{Ls} (\bar{x}_k^T Q \bar{x}_k + \bar{u}_k^T R \bar{u}_k) \quad (3.47)$$

where  $Ls$  is the simulation length. However, the total cost of regulation increases up to a certain threshold above which the cost of the entire process begins to exceed the cost of regulation without BESS, even though the cost of regulation still remains lower with BESS. This can be seen in Figure 3.19 where only the case of  $Q_{soc} = 0.01$  and  $Q_{soc} = 1000$  corresponding to a case of no requirement for energy recovery and a strict requirements for one. The frequency dynamic is improved and the tie-line still tracks the scheduled values despite the large variation in the values of  $Q$ . Interestingly comparing the costs in Table 3.3 and Figure 3.18 there is a parallel relationship between the minimum threshold weight required for energy recovery and the point at which the costs of running the full system with BESS starts to exceed that of a situation without BESS. This threshold is somewhere within the range  $Q_{soc} = 10 - 100$ .

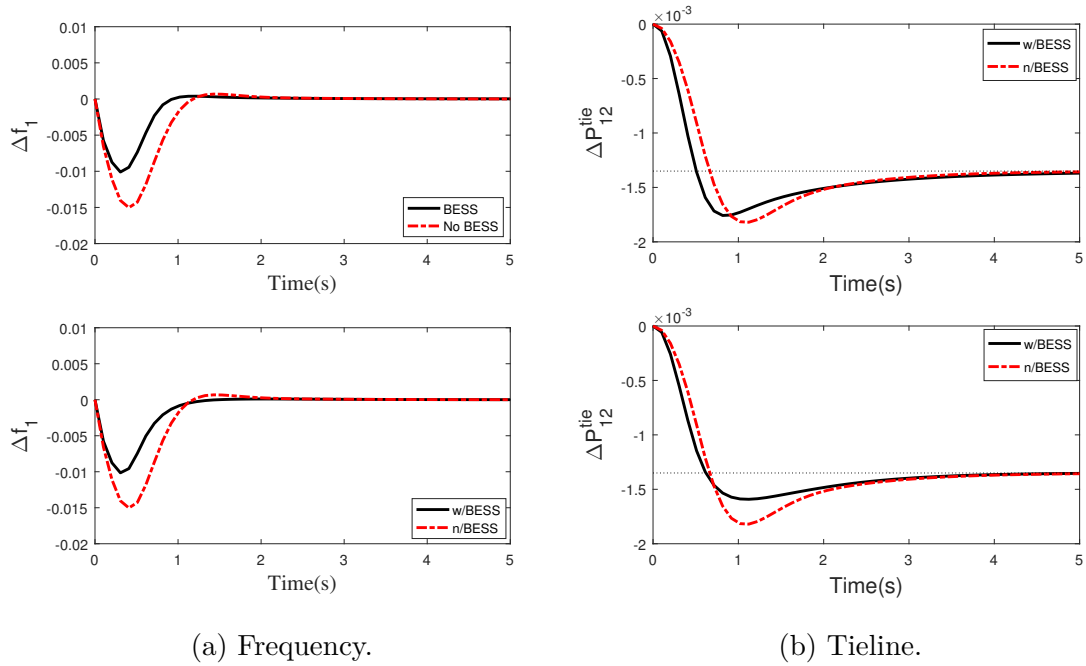


Fig. 3.19 Frequency deviation in area 1 and Tie-line in area one and two for different weights on  $Q_{soc}$ . Top:  $Q_{soc} = 0.01$ . Bottom:  $Q_{soc} = 1000$ .

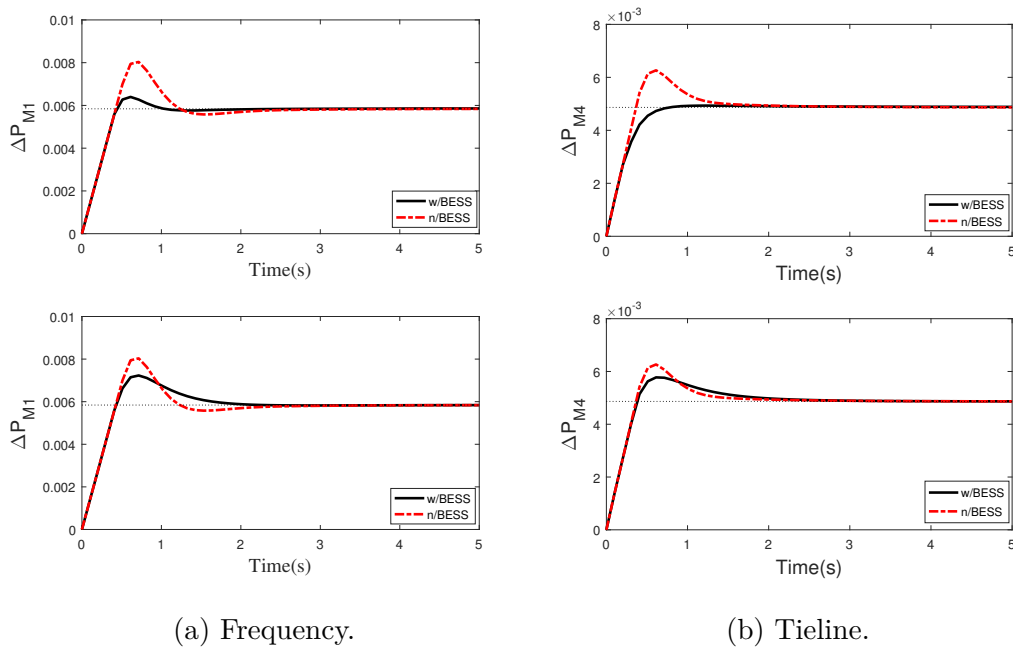


Fig. 3.20 Output power deviation of GENCOs 1 and 4 for different weights on  $Q_{soc}$ . Top:  $Q_{soc} = 0.01$ . Bottom:  $Q_{soc} = 1000$ .

In Figure 3.20 the effect on GENCOs 1 and 4 is shown with the changes in generator behaviour clearly seen; the GENCOs needing less manoeuvring in their transients with lower weights. The impact on frequency is not as obvious since energy recovery occurs after frequency restoration even though this also affects generator settling time. There is also a dependence on the capacity of the BESS and its energy recovery effect on system dynamics which increases with increasing BESS capacity as a ratio of total area capacity. An additional benefit of varying weights is that it provides flexibility in a situation where it may be beneficial for a BESS to be charged beyond the reference of fifty percent particularly when this may prove to be of operational value such as in excess renewable energy storage. Note that this point is assumed to be the optimal operating point of all BESS in this thesis.

### 3.7 Conclusion

In the future power system the issue of load frequency control is likely to become more challenging considering the highly heterogeneous nature of the grid. New modelling and control methods that offer flexibility and performance guarantees are increasingly required to meet this requirement. One critical aspect is on the development of models that explicitly account for the impact of some of the new devices that are being connected to the grid. Taking advantage of the opportunities for improved grid performance that some of these devices offer is important if the benefits of a smart grid are to be obtained.

In this chapter a two area model with a BESS installed in each area has been developed. This has been done within the context of a smart deregulated power system where the interaction between GENCOs and DISCOs is modelled. Frequency control is achieved using MPC. A simplified BESS model suitable for integration into this system was developed. The multivariable nature and systematic constraint capability of MPC was used to coordinate the BESS system and the GENCOs to achieve improved LFC performance compared to the case here no BESS was installed in the deregulated model. All load matching requirements were satisfied and the performance of the BESS in demand scenario produced the expected results of net power and energy following the clearance of the load demand by the GENCOs.

Furthermore an investigation was carried out on the possibility of managing the BESS by relaxing the strict requirement for energy recovery. It was seen that it is possible to reduce system cost and the manoeuvring of generators by varying this weight. This investigation provided an interesting insight on the probable use of this weight for

---

providing smarter energy management for the BESS at lower costs and with less wear and degradation on both the BESS and generators. Suggestions on how to achieve this dynamically and smartly are given in Chapter 6. The model is also suitable for application without the deregulated structure and examples of these are given in the subsequent chapters.



# Chapter 4

## Decentralised Predictive Load Frequency Control with Battery Energy Storage

### 4.1 Introduction

In Chapter 3 a model of the power system was derived and a centralised model predictive controller was designed in order to tackle the problem of load frequency control. In the context of the future power grid the battery energy storage system, integrated into the legacy power grid was able to successfully support conventional generators in improving the frequency dynamics of the system while also improving the transient performance of the conventional generators. The BESS model developed was of a level of complexity that met the requirements for LFC design. The modelling structure however increased the level of heterogeneity of power sources in the grid; but by employing the multi input output properties of MPC frequency regulation in the power system was obtained despite the additional model complexity created by the deregulated framework.

With this modelling approach one of the long standing issues in regards to the integration of distributed energy resources (DERS) in the legacy system was addressed; how to model, integrate and operate the future grid from the perspective of LFC with these devices [208]. The dynamic model of the BESS developed in Section 3.2 was integrated into the power system model in such a way that the BESS showed a similar dynamic response to frequency changes like conventional generators. This reflected

in the simulations in Section 3.5 where the BESS responded to changes in frequency induced by the scheduled and unscheduled load demands made by DISCOs.

The derivation of models that capture the dynamic interactions between subsystems with the objective of obtaining minimal coordination architectures between them which is necessary for the control of power in order to maintain frequency stability has been highlighted as an important aspect of smart grid design [28]. This makes it possible to decouple such models in such a way that shared interactions are available to each subsystem. In Section 2.4 decomposition techniques that make this possible were given. Designing local controls for each subsystem in smart networks is therefore critical. As noted in Section 2.2, decentralised designs offer the benefits of scalability, fault resilience and reduced communication requirements. In an early study in [119] the ability of BESS to support LFC was investigated. The system was monolithic; a single lumped model. While this simplifies centralised control design, it is challenging for decentralised architectures. Other modelling approaches have been used such as for example in [124] where the BESS is not explicitly included in the central model even though the controller design is decentralised. Commonly when coordinated control of BESS and conventional generation is analysed, the dynamic effects of BESS in relation to the LFC problem is not considered. Rather in most cases the focus is on the use of BESS for renewable output smoothing [114, 100, 98] or for operational support of wind power [115, 117]. In this thesis we have an explicit model of a smart grid made up of two subsystems that together provide frequency regulation services. The model consists of two interacting subsystems. Where the subsystems in this case are the BESS and generators. In view of the benefits of decentralised control, in this chapter local predictive controllers are designed for these two subsystems that make up the centralised model. Since the model structure already captures the dynamic interactions between subsystems, this would be exploited in independent controller synthesis. To this end, the aim is to achieve the following objectives:

- decompose the centralised model into submodels in a way that each subsystem is compatible with LFC design
- design stabilising decentralised controllers for each subsystem and achieve co-ordinated operation between the generator and BESS subsystems leading to satisfactory LFC performance.

In order to fully capture the impact of the interactions and to aid exposition, henceforth a single area system is considered. This is as a result of the decentralised design approach. In a multi-area interconnected system decentralised design would

require either a distributed inter-area controller for good dynamic response due to the tie-line dynamics or a single TSO coordinated with decentralised local BESS controllers per area which is beyond the scope of work considered here. This chapter probes into decentralised control in an area which is hardly analysed and shows via proofs that stability is guaranteed even with decentralised control. Hence the rest of this chapter is as follows; Section 4.2 describing the power system model with BESS. Section 4.3 explains the process of model decomposition. Section 4.4 covers the decentralised MPC design while Section 4.5 is used for stability analysis. In Section 4.6 the decentralised controller is described and Section 4.7 outlines the simulations carried out with a discussion of the subsequent results. The final section is used for concluding remarks.

## 4.2 Centralised Model Development

The focus of this section is the development of the centralised power system model which would serve as the starting point for the design of decentralised model predictive load frequency controllers. The power system under consideration in this case is an isolated one and the dynamic equations comprising the model are similar to the ones developed for the generators in Section 2.1. This model also includes the BESS represented by the model developed in Section 3.2. However, for this analysis the deregulated modelling structure used in 3.3 is omitted from the centralised model. For the purpose of controller design the same assumptions made in the LFC design of Section 2.1 also apply *i.e.*, the generators all swing with a common frequency as a result of the negligible electrical distance between them. The BESS which responds to this swing in frequency is modelled as a single storage unit. This aggregation of the conventional and BESS represents single area system analysed in this chapter.

### 4.2.1 Model Dynamics

The dynamics of the aggregated conventional generation consists of governor and turbine dynamics. The equations representing this combined dynamic are the same as (2.10) and (2.12) which are repeated here for readability. The speed governor dynamic equation is given by;

$$\Delta \dot{P}_V = \frac{1}{T_G} (\Delta P_C - \Delta P_V - \frac{1}{R} \Delta \omega) \quad (4.1)$$

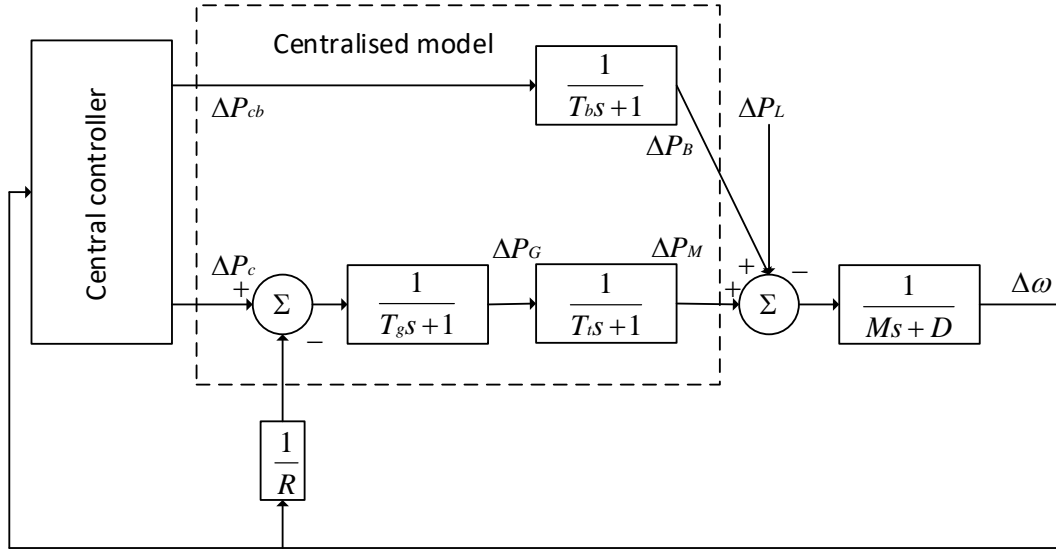


Fig. 4.1 The centralised model power system consisting of BESS and generators. Local control is achieved by a centralised controller in response to a common frequency represented by  $\Delta\omega$ .

While the turbine dynamic equation is given by;

$$\Delta\dot{P}_M = \frac{1}{T_T}(\Delta P_V - \Delta P_M) \quad (4.2)$$

The BESS dynamical equations based on the same simplified model developed in Section 3.2 are the BESS output power and state of charge given in (4.3) and (4.4) respectively.

$$\Delta\dot{P}_b = \frac{1}{T_b}(\Delta P_{cb} - \Delta P_b) \quad (4.3)$$

$$\Delta S\dot{O}C = \frac{1}{B_c}\Delta P_b, \quad (4.4)$$

Similar to the convention in Chapter 2 the response of the BESS is an increase in power *i.e* a positive  $\Delta P_B$  indicates BESS discharging and a negative  $\Delta P_B$  charging. The trajectory of the state of charge is in the opposite direction to that of the BESS power and rises or falls if the power flow is negative or positive respectively. The BESS responds to the variations in frequency of the isolated power system caused by the power network responding to a load change. Hence the equation of swing dynamic is

as given in (4.5) under the assumption of deviations from the nominal are caused by small perturbations:

$$\dot{\Delta\omega} = \frac{1}{2H}(\Delta P_M + \Delta P_B - \Delta P_L + D\Delta\omega) \quad (4.5)$$

With the difference from (2.14) being the inclusion of the BESS power output into the power system. This centralised model can be represented as shown in Figure 4.1.

### 4.2.2 The Control problem

The control objective is to provide secondary-level frequency regulation in order to maintain frequency deviations,  $\Delta\omega$ , close to zero despite load deviations  $\Delta P_L$ . This is achieved by setting reference signals—the control inputs to the system— $\Delta P_c$  and  $\Delta P_{cb}$  to appropriate values given the state of the system and current load deviation. At the same time, the BESS state of charge should be maintained close to a desired nominal level,  $\overline{SOC}_B$ . As this point a remark is in order

**Remark 1.** *In practice the reference signals  $\Delta P_c$  and  $\Delta P_{cb}$  need to be disaggregated to provide meaningful control signals to the physical plant and BESS that comprise the system. Moreover, the interface between these reference signals and the actuation of these systems will be managed by lower-level control. These higher-fidelity details are beyond the scope of this thesis and as noted previously the model adopted is sufficient for LFC studies.*

Note that if  $\Delta\omega$  is regulated to zero, then

$$(\Delta\omega, \Delta P_M, \Delta P_G, \Delta P_B) = (0, \Delta P_L, \Delta P_L, 0)$$

is an equilibrium for the system under the inputs  $\Delta P_c = \Delta P_L$  and  $\Delta P_{cb} = 0$ , the latter meaning  $SOC$  is constant. In other words, the BESS does not contribute power to the system in steady state and serves to provide support for the transient stability of the power system as has already been demonstrated in Chapter 3.

Additionally in achievement of this objective, all system constraints must be satisfied. These include not just the hard limits on  $SOC$ , but also any operational or physical constraints on the system, including frequency limits and generation rate constraint. These constraints can be represented using the formulation in Section 2.2.1; in the case of generation rate constraints, the same approach used in Section 3.4 is also applied here. All constraints are captured by linear inequalities of the form.

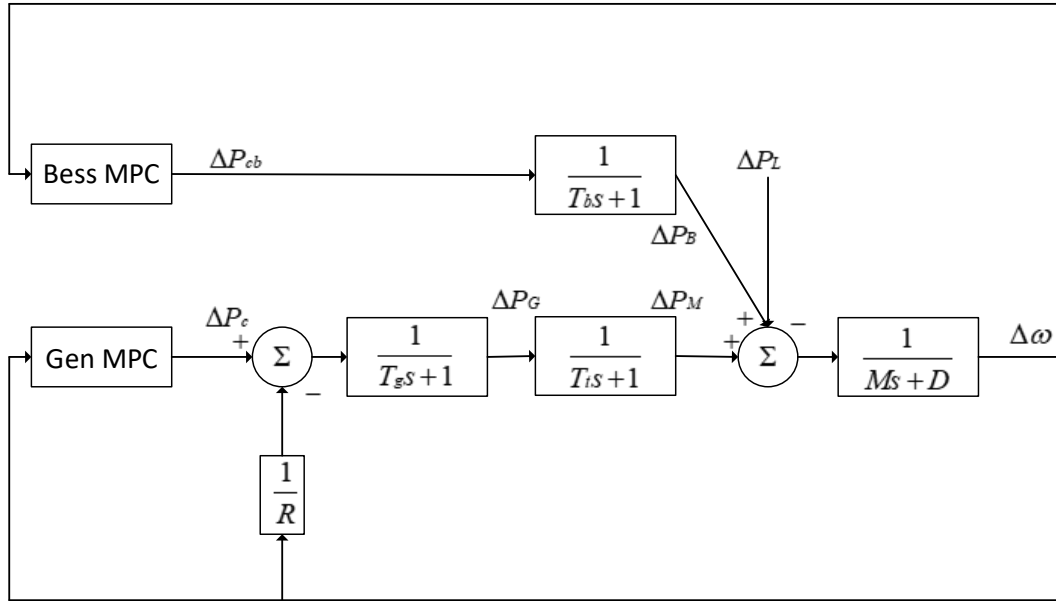


Fig. 4.2 Model with decentralised controllers

$$\tilde{\mathbf{P}}_{\mathbf{x}}x \leq \mathbf{q}_x \quad \text{and} \quad \tilde{\mathbf{P}}_{\mathbf{u}}u \leq \mathbf{q}_u \quad (4.6)$$

where  $x \in \mathbb{R}^n$  and  $u \in \mathbb{R}^m$  are, respectively, the state vector and control input vector, defined as

$$x = [\Delta\omega \quad \Delta P_G \quad \Delta P_M \quad \Delta P_B \quad SOC]^\top,$$

$$u = [\Delta P_c \quad \Delta P_{cb}]^\top.$$

The inputs are applied to the centralised model developed in Section 4.2.1 to control both subsystems. This is possible due to the multi input output capability of MPC. Automatic coordinated action between the two control inputs for each subsystem is handled by the central controller and any interactions are explicitly accounted for and the objectives for control are readily achieved.

However, a non-centralised approach to the control problem provides several advantages such as in the case of fault resilience and reduced communication requirements. Depending on the size of the power system, available physical communication structure and bandwidth requirements a centralised design could pose significant challenges both technically and economically [178]. A centralised modelling approach integrating the BESS followed by a suitable decomposition of the centralised system provides a means

for local controller design and introduces not only fault tolerance but also improves operational flexibility.

Therefore in order to solve this control problem a decentralized control architecture is designed that comprises independent, conventional model predictive controllers for the conventional plant and the BESS—see Fig. 4.2. The conventional plant controller measures the (aggregated) states of the generator— $\Delta P_M$ ,  $\Delta P_G$ —plus the system frequency  $\Delta\omega$ , and manipulates the reference input  $\Delta P_c$ . The BESS controller measures the states of the battery— $\Delta P_B$ ,  $SOC_B$ —plus the system frequency, and manipulates the reference input to the BESS,  $\Delta P_{cb}$ .

The use of a decentralised control architecture could however lead to changes in the prediction models used for each subsystem as a result of the loss of information regarding subsystem interactions. This could create operational issues relating the coordination between both subsystems. Notwithstanding, a main challenge that arises, as will be made clear in subsequent sections, is that prediction errors are inevitable in such a scheme because the behaviour of each subsystem (power outputs of generators and BESS) in the system are not modelled in the decentralized prediction models. This removes any guarantees of constraint satisfaction, recursive feasibility and stability that conventional MPC would endow under mild design conditions; guarantees in nominal MPC are indeed nominal, and are predicated on accuracy of the prediction model. While this may be addressed by using robust-by-design MPC, such approaches induce significant conservatism. This issue would also be addressed in this chapter by an analysis of the stability and feasibility of the proposed decentralised scheme, with the development of conditions under which these can be ensured.

### 4.3 Model Decomposition Methodology

In this section the centralised model developed in Section 4.2 is decomposed in order to create the decentralised structure that provides a convenient way to design individual controllers for each subsystem. The structure of this model is manipulated to suit the control design objectives and the technical challenges relating to subsystem model selection, the identification of interactions and coordination are treated.

### 4.3.1 Structured system model

The composite model can be written in the following form, using the provided definitions of  $x$  and  $u$ , in the form

$$\dot{x} = A^c x + B^c u + E^c \Delta P_L \quad (4.7)$$

When LFC is implemented in this model both the generators and BESS respond to changes in frequency. However, the frequency of the system is as a result of the synchronous operation (synchronised rotational speed) of the generators with variations caused by small perturbations in load around its nominal value. The BESS respond to these variations leading to a change in its output power.

The implication of these dynamical responses of both subsystems is that the swing equation is the coupling dynamic between the two subsystems. In the standard LFC model, the order of the states is as given previously with  $\Delta\omega$  the first state. For the purpose of decentralised controller design the states are reordered so that the common state is between —interfaces— the states of the subsystems it connects. To this end the state and corresponding input vectors are now;

$$x = [\Delta P_G \quad \Delta P_M \quad \Delta\omega \quad \Delta P_B \quad SOC_B]^\top,$$

$$u = [\Delta P_c \quad \Delta P_{cb}]^\top.$$

Note that the reordering of the states means there is a change in the position of each state within the state transition, input and disturbance matrices creating a model structure that conveniently places the common state as the central link between subsystems. Hence, (4.7) now has the following explicit form.

$$A^c = \begin{bmatrix} -1/T_g & 0 & -1/(T_g R) & 0 & 0 \\ 1/T_t & -1/T_t & 0 & 0 & 0 \\ 0 & 1/M & -D/M & 1/M & 0 \\ 0 & 0 & 0 & -1/T_b & 0 \\ 0 & 0 & 0 & 1 & 0 \end{bmatrix}$$

$$B^c = \begin{bmatrix} 1/T_g & 0 & 0 & 0 & 0 \\ 0 & 0 & 0 & 1/T_b & 0 \end{bmatrix}^\top$$

$$\tilde{B}^c = \begin{bmatrix} 0 & 0 & -1/M & 0 & 0 \end{bmatrix}^\top.$$

Which can be written compactly in this form

$$\begin{bmatrix} \dot{x}_g \\ \dot{x}_s \\ \dot{x}_b \end{bmatrix} = \begin{bmatrix} A_g^c & A_{gs}^c & 0 \\ A_{sg}^c & A_s^c & A_{sb}^c \\ 0 & 0 & A_b^c \end{bmatrix} \begin{bmatrix} x_g \\ x_s \\ x_b \end{bmatrix} + \begin{bmatrix} B_g^c & 0 \\ 0 & 0 \\ 0 & B_b^c \end{bmatrix} \begin{bmatrix} u_g \\ u_b \end{bmatrix} + E^c \Delta P_L \quad (4.8)$$

where  $x_g$ ,  $x_b$  denote the states local to the generator and battery, respectively,  $x_s$  is a *shared* state—frequency—and  $u_g$  ( $\Delta P_c$ ),  $u_b$  ( $\Delta P_{cb}$ ) are the control (reference) inputs to the generator and battery. From this it is clear to observe that the system has a partially decentralized structure, with the dynamics of generator and battery coupled via the frequency. This means that obtaining prediction models for use in the independent generation and battery controllers is not straightforward.

Note as remarked earlier that the form of (4.8) can naturally handle higher fidelity models of battery, generator and power system dynamics than considered in this formulation, via different choices of states and block matrices. Meaning this approach is generalised and therefore the MPC formulation that is developed is independent of the models used. The analysis to be provided later on would however sharpen theoretical results by referring to the simple models presented in the previous section.

### 4.3.2 Discretisation

In the design of the discrete MPC controller the continuous time model with form (4.8) is discretised in order to derive prediction models compatible with the formulation. However, the use of some of the more popular discretisation methods; in particular the zero order hold commonly used for MPC leads to a loss of the block structure of (4.8), instead creating dense matrices that (i) are not so amenable to the decomposition of the model that is necessary for decentralized control, and (ii) do not preserve the transparent link between physical system parameters and discrete-time model matrix elements.

Two methods that do preserve the block structure are the *Forward Euler* method, where the discrete-time model is, for a sampling period of  $\Delta t$ ,

$$x^+ = (I + \Delta t A^c)x + (\Delta t B^c)u + (\Delta t E^c)\Delta P_L,$$

and the, higher-accuracy *Mixed Euler–ZOH* method [209], for which

$$x^+ = (I + D_d(\Delta t)A^c)x + (D_d(\Delta t)B^c)u + (D_d(\Delta t)E^c)\Delta P_L$$

with

$$D_d(\Delta t) = \text{diag} \left( \int_0^{\Delta t} e^{A_{ii}^c t} dt, \dots, \int_0^{\Delta t} e^{A_{MM}^c t} dt \right)$$

For a system decomposed into  $M$  subsystems. Both result in a discrete-time model with a block structure identical to the one in (4.8):

$$\begin{bmatrix} x_g \\ x_s \\ x_b \end{bmatrix}^+ = \begin{bmatrix} A_g & A_{gs} & 0 \\ A_{sg} & A_s & A_{sb} \\ 0 & 0 & A_b \end{bmatrix} \begin{bmatrix} x_g \\ x_s \\ x_b \end{bmatrix} + \begin{bmatrix} B_g & 0 \\ 0 & 0 \\ 0 & B_b \end{bmatrix} \begin{bmatrix} u_g \\ u_b \end{bmatrix} + \begin{bmatrix} 0 \\ E_s \\ 0 \end{bmatrix} \Delta P_L. \quad (4.9)$$

### 4.3.3 Model Expansion and Decomposition

In (4.9) we now have a model where the coupling between the two subsystems is via the common state which is *frequency*. This shared state is critical for the decentralised control design since it has a strong influence on the both subsystems.

A direct decomposition of the centralised model based on the block structure does not achieve this objective because the shared state would only then be available to one submodel. In terms of LFC what this implies is that if controllers are designed based on such a decomposed system the BESS would not take part in LFC because that frequency measurements would not be possible since the dynamic is absent from it's model. This implies that the shared state creates an overlap of the two subsystems. In large scale power networks the physical areas create a natural decomposition into sub-networks interlinked by tie-lines. However, this is not evident in all systems such as the smart grid and decomposition algorithms are required which split the network into subsystems. Localised controllers using only the local states can then be designed for each subsystem.

Thus, for a more accurate decomposition the model (4.9) may therefore be decomposed into two *overlapping* submodels pertaining to the generator system and BESS by using the technique of overlapping decompositions [150]. This method allows to decompose a large scale system by decoupling the state variables into independent subsystems. Local controllers can then be designed for each subsystem and the control input applied to the original system is determined independently for each subsystem.

The is particularly useful if the coupling between subsystems in large-scale systems are strong and cannot be ignored in the design of local controllers.

The concept of overlapping decomposition was introduced in 2.4. There we saw that it is based on the mathematical framework known as the inclusion. In addition it was observed that while the method of overlapping decomposition allows for the expansion of a large scale network into a higher order system of decoupled systems, the inclusion principle provides the theoretical framework that guarantees the properties of the expanded system include those of the original system. Hence design in the expanded state space can be contracted for application in the original state space of the network.

More formally, consider the discrete system

$$S : \begin{cases} x_{k+1} &= Ax_k + Bu_k \\ y_k &= Cx_k \end{cases} \quad (4.10)$$

where  $x \in R^n$ ,  $u \in R^m$  and  $y \in R^p$  are, respectively, the state input and output vectors. Following expansion the system can be represented as

$$\tilde{S} : \begin{cases} \tilde{x}_{k+1} &= \tilde{A}\tilde{x}_k + \tilde{B}\tilde{u}_k \\ \tilde{y}_k &= \tilde{C}\tilde{x}_k \end{cases} \quad (4.11)$$

where  $\tilde{x} \in R^{\tilde{n}}$ ,  $\tilde{u} \in R^{\tilde{m}}$  and  $\tilde{y} \in R^{\tilde{p}}$  are, respectively, the state input and output vectors of the expanded system. The systems  $S$  and  $\tilde{S}$  are represented by the triplets  $(A, B, C)$  and  $(\tilde{A}, \tilde{B}, \tilde{C})$  respectively. Also it is assumed that  $n \leq \tilde{n}$ ,  $m \leq \tilde{m}$  and  $p \leq \tilde{p}$ . Thus for the expanded system, subsystem  $i$  can be written as

$$\tilde{S}_i : \begin{cases} \tilde{x}_{ik+1} &= \tilde{A}_i\tilde{x}_{ik} + \tilde{B}_i\tilde{u}_{ik} \\ \tilde{y}_{ik} &= \tilde{C}_i\tilde{x}_{ik} \end{cases} \quad (4.12)$$

for  $i = 1 \dots M$ . The state of the original and expanded systems are related by the linear transformation

$$\tilde{x} = Vx$$

**Definition 1.** *The system  $\tilde{S}$  includes the system  $S$  if there exists the ordered pair of matrices  $(U, V)$  with  $UV = I$  such that for an initial state  $x_o \in S$  and a fixed input  $u_k$ , the following solution is obtained [150]*

$$\begin{aligned}\tilde{x}(k; x_o, u) &= Ux(k; x_o, u) \\ yx_k &= y\tilde{x}_k \quad \forall k \geq 0\end{aligned}\tag{4.13}$$

Also assuming for an initial state  $x_o \in S$ , and a fixed input  $u = u_k$  if

$$\begin{aligned}\tilde{x}(k; Vx_o, u) &= Vx(k; x_o, u) \\ yx_k &= y\tilde{x}_k \quad \forall k \geq 0\end{aligned}\tag{4.14}$$

holds, then  $\tilde{S}$  is an expansion of  $S$  i.e.  $\tilde{S} \supset S$ . Where  $yx_k$  and  $y\tilde{x}_k$  are output the solutions for  $x_o \in S$  and a fixed input  $u_k$  and  $\tilde{x}_o \in \tilde{S}$  with a fixed input  $u_k$ .

Generally, (4.14) is a special case of inclusion - restriction/expansion - and in order for the original system  $S$  to be a restriction of the expanded system  $\tilde{S}$  the following algebraic relations apply;  $\tilde{A}V = V$ ,  $\tilde{B} = VB$ ,  $\tilde{C}V = C$  or  $MV = 0$ ,  $N = 0$  and  $LV = 0$ . The matrices  $M$ ,  $N$ , and  $L$  are complementary matrices and their explicit expressions can be found in the appendix. These matrices can be used to derive explicit relations between  $S$  and  $\tilde{S}$

$$\tilde{A} = VAU + M, \quad \tilde{B} = VB + N, \quad \tilde{C} = CU + M.$$

The selection of the value of the elements of the complementary matrices can be used as a tuning tool to determine the degree and strength of coupling between subsystems. A selection that leads to a sparse matrices is therefore thus desirable for weak couplings to be obtained.

Therefore without loss of generality, for a two subsystem network, if the model is assumed to have three states  $(x_1^T, x_2^T, x_3^T)^T$  with  $x_2$  the common/shared state, then 4.10 can be written as.

$$S: \begin{bmatrix} x_1 \\ x_2 \\ x_3 \end{bmatrix}^+ = \begin{bmatrix} A_{11} & A_{12} & A_{13} \\ A_{21} & A_{22} & A_{23} \\ A_{31} & A_{32} & A_{33} \end{bmatrix} \begin{bmatrix} x_1 \\ x_2 \\ x_3 \end{bmatrix} + \begin{bmatrix} B_{11} & B_{12} \\ B_{21} & B_{22} \\ B_{31} & B_{32} \end{bmatrix} \begin{bmatrix} u_1 \\ u_2 \end{bmatrix}\tag{4.15}$$

The shared subsystem dynamic (state or matrix depending on application) is  $A_{22}$ . Applying the transformation matrices, the two subsystems can be grouped into  $S_1$  with states  $z_1 = (x_1^T, x_2^T)^T$  and  $S_2$  having the states  $z_2 = (x_2^T, x_3^T)^T$ . This new expanded system can be written as follows

$$\tilde{S} : \begin{bmatrix} z_1 \\ z_2 \end{bmatrix}^+ = \begin{bmatrix} A_{11} & A_{12} & 0 & A_{13} \\ A_{21} & A_{22} & 0 & A_{23} \\ A_{21} & 0 & A_{22} & A_{23} \\ A_{31} & 0 & A_{32} & A_{33} \end{bmatrix} \begin{bmatrix} z_1 \\ z_2 \end{bmatrix} + \begin{bmatrix} B_{11} & B_{12} \\ B_{21} & B_{22} \\ B_{21} & B_{22} \\ B_{31} & B_{32} \end{bmatrix} \begin{bmatrix} u_1 \\ u_2 \end{bmatrix} \quad (4.16)$$

In (4.16) the dashed lines indicate the subsystems which are now clearly separated into two disjoint models with the state appearing in both subsystems. Definition 1 establishes zero state equivalence between both  $S$  and  $\tilde{S}$  which means the behaviour of each subsystems is preserved in the expanded system [150]. The individual models of each subsystem are now determined explicitly and can be represented by

$$\begin{aligned} \tilde{S}_1 : z_1 &= \underbrace{\tilde{A}_1 z_1 + \tilde{B}_1 u_1}_{\text{subsystem 1}} + \underbrace{\tilde{A}_{12} z_2 + \tilde{B}_{12} u_2}_{\text{coupling}} \\ \tilde{S}_2 : z_2 &= \underbrace{\tilde{A}_2 z_2 + \tilde{B}_2 u_2}_{\text{subsystem 2}} + \underbrace{\tilde{A}_{21} z_1 + \tilde{B}_{21} u_1}_{\text{coupling}} \end{aligned} \quad (4.17)$$

**Remark 2.** *This state decomposition is suitable for the control objective because each subsystem now contains frequency. The BESS supports LFC by improving the transient stability of the system i.e at steady state it's output power is zero while for the generator it is equal to the load demand. Also, for the model developed in section 4.2 the system is already input decentralised which simplifies the analysis. Further insights are given in section 4.3.4.*

#### 4.3.4 Decomposition of Power System Model

This design approach is applied to the model given by equation 4.8. This leads to the creation of the following models

$$\begin{aligned} \begin{bmatrix} x_g \\ x_s \end{bmatrix}^+ &= \begin{bmatrix} A_g & A_{gs} \\ A_{sg} & A_s \end{bmatrix} \begin{bmatrix} x_g \\ x_s \end{bmatrix} + \begin{bmatrix} B_g \\ 0 \end{bmatrix} u_g + \begin{bmatrix} 0 \\ E_s \end{bmatrix} \Delta P_L + \begin{bmatrix} 0 \\ A_{sb} \end{bmatrix} x_b \\ \begin{bmatrix} x_s \\ x_b \end{bmatrix}^+ &= \begin{bmatrix} A_s & A_{sb} \\ 0 & A_b \end{bmatrix} \begin{bmatrix} x_s \\ x_b \end{bmatrix} + \begin{bmatrix} 0 \\ B_b \end{bmatrix} u_b + \begin{bmatrix} E_s \\ 0 \end{bmatrix} \Delta P_L + \begin{bmatrix} A_{sg} \\ 0 \end{bmatrix} x_g \end{aligned}$$

Let  $z_g = (x_g, x_s)$  and  $z_b = (x_s, x_b)$ . The models can be written in the following compact forms:

$$z_g^+ = \tilde{A}_g z_g + \tilde{B}_g u_g + \tilde{E}_g \Delta P_L + \tilde{A}_{gb} z_b \quad (4.18a)$$

$$z_b^+ = \tilde{A}_b z_b + \tilde{B}_b u_b + \tilde{E}_b \Delta P_L + \tilde{A}_{bg} z_g \quad (4.18b)$$

A close observation of this reveals the fact that there is no loss of accuracy: model (4.18) gives correct values for  $z_g^+$  and  $z_b^+$  given  $z_g$ ,  $z_b$ ,  $u_g$ ,  $u_b$ ,  $P_L$ . In other words, each model independently gives correct predictions of the one-step ahead of its local state ( $x_g$  or  $x_b$ ) and the shared state  $x_s = \Delta\omega$  *provided that* a measurement of the other subsystem's state ( $x_b$  or  $x_g$ ) is available. However, meeting the latter requirement is quite problematic in an MPC framework, where  $N$ -step ahead predictions are utilized for control.

This is because it implies that in order to get accurate  $N$ -step ahead predictions of the local states of each sub-model represented by  $x_g$  (or  $x_b$ ), each local controller would require a knowledge of the future trajectory of its corresponding neighbouring subsystem state  $x_b$  (or  $x_g$ ). The non-causality created by this requirement motivates the use of a simpler, decentralized model for prediction in the generator and battery controllers which can be represented by the following equations:

$$\bar{z}_g^+ = \tilde{A}_g \bar{z}_g + \tilde{B}_g u_g + \tilde{E}_g \Delta P_L \quad (4.19a)$$

$$\bar{z}_b^+ = \tilde{A}_b \bar{z}_b + \tilde{B}_b u_b + \tilde{E}_b \Delta P_L. \quad (4.19b)$$

The use of the models in the forms of (4.19) handles the issue of non causality in the prediction models, however this leads to another issue—loss of accuracy. This is because given  $\bar{z}_g = z_g$ , the application of  $u_g$  and  $P_L$  to (4.19) generally results in  $\bar{z}_g^+ \neq z_g^+$ . Moreover, a more subtle issue arises, motivating the one further change to the models used for prediction.

**Lemma 1.** *The desired steady state*

$$(\Delta\omega, \Delta P_M, \Delta P_G, \Delta P_B, SOC_B) = (0, \Delta P_L, \Delta P_L, 0, \overline{SOC_B})$$

is, for all  $\Delta P_L$ , not an equilibrium of the model (4.19). It is, however, an equilibrium of the model

$$\bar{z}_g^+ = \tilde{A}_g \bar{z}_g + \tilde{B}_g u_g + \tilde{E}_g \Delta P_L \quad (4.20a)$$

$$\bar{z}_b^+ = \tilde{A}_b \bar{z}_b + \tilde{B}_b u_b. \quad (4.20b)$$

Denoting the state–input pair consistent with achieving equilibrium at the desired setpoint characterized in Lemma 1 as  $(\bar{z}_{i,ss}, u_{i,ss})$ , for  $i \in \{g, b\}$ , noting that if  $(\bar{z}_i, u_i) = (\bar{z}_{i,ss}, u_{i,ss})$  then

$$\begin{aligned} \bar{z}_{g,ss} &= \tilde{A}_g \bar{z}_{g,ss} + \tilde{B}_g u_{g,ss} + \tilde{E}_g \Delta P_L \text{ and } \Delta \omega_{ss} = C_g \bar{z}_{g,ss} = 0 \\ \bar{z}_{b,ss} &= \tilde{A}_b \bar{z}_{b,ss} + \tilde{B}_b u_{b,ss} \text{ and } SOC_{B,ss} = C_b \bar{z}_{b,ss} = \overline{SOC}_B. \end{aligned}$$

Note that  $\bar{z}_{b,ss}$  is invariant to  $\Delta P_L$  but  $\bar{z}_{g,ss}$  has to be recomputed each time the latter changes. Therefore, we make the following assumption about the information that will be available to the battery and generator controllers.

**Assumption 1** (Availability of measurements). *The state relating to the generators subsystem is available to it i.e  $z_g = (x_g, x_s) = (\Delta P_G, \Delta P_M, \Delta \omega)$ , plus the load disturbance  $\Delta P_L$ , is known to the generator controller at each sampling instant. The state  $z_b = (x_s, x_b) = (\Delta \omega, \Delta P_B, SOC_B)$  is known to the BESS controller at each sampling instant.*

It is worth remarking that in the model (4.20) the battery dynamics omit the load disturbance. This reinforces the notion that, in the proposed secondary frequency control, the BESS does not contribute to the steady-state power balance. This is consistent with the explanation given in Remark 2 which also indicates that the BESS contributes to transient stability enhancement improving dynamic performance while the generator meets the desired load demand.

Finally, the suitability of the model (4.20) in a predictive controller is reinforced by the following results; reachability is a sufficient condition for the successful design of certain parameters within the predictive controllers [51].

**Lemma 2** (Reachability of the prediction models). *If all system parameters in  $A^c$ ,  $B^c$  are non-zero then the pairs  $(\tilde{A}_g, \tilde{B}_g)$  and  $(\tilde{A}_b, \tilde{B}_b)$  are reachable.*

## 4.4 Decentralized MPC formulation

In Section 4.3 models suitable for prediction using MPC have been developed. Following this development in this section, independent MPC formulations for generator and BESS using the decentralized models (4.20) for prediction would be presented. Since the decentralised models ignore interactions between the subsystems, there is a level of uncertainty in the predictions derived from the decentralised model formulations. Hence, an analysis of the effect of the uncertainty induced by the prediction errors is carried out with the aim to show that stability and recursive feasibility can still be achieved despite the presence of this uncertainty.

The model predictive load frequency control problem can now be solved independently using only the plant dynamics related to the BESS and generator subsystems. In keeping with the general performance of MPC algorithms, each controller now uses a prediction of its corresponding plant dynamics to determine the sequence of future actions that, together with the associated state predictions, optimizes a performance index while satisfying any constraints. The control inputs of the optimal sequence from each controller is applied to power system plant in order to achieve the objective of frequency control and state of charge restoration.

Hence for the load–frequency problem, the independent optimal control problems for generator and BESS, is termed problem  $\mathbb{P}_i(z_i)$  for  $i \in \{g, b\}$  and current state  $z_i$ , is defined by

$$\min_{\mathbf{u}_i} V_{N,i}(z_i, \mathbf{u}_i) \quad (4.21)$$

subject to, for  $k = 0, \dots, N - 1$ ,

$$\begin{aligned} \bar{z}_i(0) &= z_i \\ \bar{z}_i(k+1) &= f_i(\bar{z}_i(k), u_i(k)) \\ G_i \bar{z}_i(k) &\leq g_i \\ H_i u_i(k) &\leq h_i \\ G_{f,i}(\bar{z}_i(k+N) - \bar{z}_{i,ss}) &\leq g_{f,i}, \end{aligned}$$

where

$$f_i(\bar{z}_i(k), u_i(k)) = \begin{cases} \tilde{A}_g \bar{z}_g(k) + \tilde{B}_g u_g(k) + \tilde{E}_g \Delta P_L & i = g \\ \tilde{A}_b \bar{z}_b(k) + \tilde{B}_b u_b(k) & i = b. \end{cases}$$

In determining the optimal solution to the problem of equation (4.21) each subsystem controller (*i.e.* generator and BESS) solves this problem at each sampling instant,

given the latest measurements of the state and other parameters. There is no communication between controllers as determined by the independent operation of each controller. The decision variable in the problem is  $\mathbf{u}_i$ , the sequence of  $N$  future control inputs:

$$\mathbf{u}_i := \{u_i(0), u_i(1), \dots, u_i(N-1)\}.$$

This sequence is chosen to minimize the quadratic performance index  $V_{N,i}(\bar{z}_i, \mathbf{u}_i)$ , which penalizes deviations from the desired steady-state pairs  $(\bar{z}_{i,ss}, u_{i,ss})$  over the duration of the  $N$ -step prediction horizon:

$$V_{N,i}(\bar{z}_i, \mathbf{u}_i) := V_{f,i}(\bar{z}_i(N) - \bar{z}_{i,ss}) + \sum_{k=0}^{N-1} \ell_i(\bar{z}_i(k) - \bar{z}_{i,ss}, u_i(k) - u_{i,ss})$$

where

$$\begin{aligned} V_{f,i}(z_i) &:= z_i^\top P_i z_i \\ \ell_i(z_i, u_i) &:= z_i^\top Q_i z_i + u_i^\top R_i u_i \end{aligned}$$

and where the matrices  $Q_i$ ,  $R_i$  and  $P_i$  satisfy the following assumptions.

**Assumption 2** (Cost function matrices). *For  $i \in \{g, b\}$ ,  $Q_i$  and  $R_i$  are positive definite matrices.*

**Assumption 3** (Terminal cost matrices). *For  $i \in \{g, b\}$ ,  $P_i$  is the solution to the algebraic Riccati equation*

$$P_i = Q_i + \tilde{A}_i^\top P_i \tilde{A}_i - \tilde{A}_i^\top P_i \tilde{B}_i (R_i + \tilde{B}_i^\top P_i \tilde{B}_i)^{-1} \tilde{B}_i^\top P_i \tilde{A}_i$$

Assumptions 2 and 3 are mild design conditions. Note that because the pairs  $(\tilde{A}_g, \tilde{B}_g)$  and  $(\tilde{A}_b, \tilde{B}_b)$  are reachable, the solution to the Riccati equation exists and is unique for all  $Q_i$  and  $R_i$  satisfying Assumption 2.

The optimal control problems contain constraints on states and inputs of each subsystem and these are obtained from the constraints equations by selecting the rows applicable to the generator and BESS problems respectively, and are based on the following assumption.

**Assumption 4** (Properties of constraint sets). *For  $i \in \{g, b\}$ , the set  $\mathbb{X}_i := \{z_i : G_i z_i \leq g_i\}$  is closed, with  $\bar{z}_{i,ss}$  within its interior for all considered  $\Delta P_L$ . The set*

$\mathbb{U}_i := \{u_i : H_i u_i \leq h_i\}$  is closed and bounded, with  $u_{i,ss}$  within its interior for all considered  $\Delta P_L$ .

Now considering these constraints for each subsystem, this is a mild assumption for the BESS, since the desired steady state  $\bar{z}_{b,ss} = (\Delta\omega_{ss}, \Delta P_{B,ss}, SOC_{B,ss}) = (0, 0, \overline{SOC}_B)$  for all  $\Delta P_L$ , and therefore the condition amounts to ensuring that any limits on these three states are closed, permit zero power flow from the BESS, and specify the desired  $SOC$  to be any state other than fully discharged or fully charged. The assumption is, however, a more demanding requirement on the generation system since the desired steady state  $\bar{z}_{g,ss} = (\Delta P_G, \Delta P_M, \Delta\omega) = (\Delta P_L, \Delta P_L, 0)$  with  $u_{g,ss} = \Delta P_L$  shifts with changing  $\Delta P_L$ . What this condition then amounts to is a limit on the size, relative to the system constraints, of load changes that can be handled by the controller. This limitation can be handled by referring to *admissible*  $\Delta P_L$  which refers to a limit of the size of the disturbance that does not lead to a loss of stability and feasibility.

The final consideration in the formulation is the set of constraints on the terminal state prediction,  $\bar{z}_i(N)$ . These are designed to satisfy the following assumption.

**Assumption 5** (Terminal set invariance and admissibility). *For  $i \in \{g, b\}$ , the terminal constraint set  $\mathbb{X}_{f,i} := \{z_i : G_{f,i}(z_i - z_{i,ss}) \leq g_{f,i}\}$  is an admissible and invariant set; that is,  $\mathbb{X}_{f,i}$  satisfies, for all admissible  $\Delta P_L$ :*

$$z_i - \bar{z}_{i,ss} \in \mathbb{X}_{f,i} \implies \begin{cases} (\tilde{A}_i + B_i K_{\infty,i})(z_i - \bar{z}_{i,ss}) \in \mathbb{X}_{f,i} \\ z_i \in \mathbb{X}_i, \\ u_{i,ss} + K_{\infty,i}(z_i - \bar{z}_{i,ss}) \in \mathbb{U}_i \end{cases}$$

where  $K_{\infty,i}$  is the (infinite-horizon) linear quadratic regulator gain associated with the Riccati equation solved to determine  $P_i$ .

Secondly, the set  $\mathbb{X}_{f,i}$  contains the point  $\bar{z}_{i,ss}$  within its interior, for all admissible  $\Delta P_L$ .

Note that the design ingredients  $P_i$  and  $\mathbb{X}_{f,i}$  are standard in MPC, and can be computed given the system model, cost and constraints [51]. A popular choice of terminal set satisfying by construction the invariance and admissibility conditions given in Assumption 5 is the maximal admissible set, which may be found by solving a sequence of linear programming (LP) problems [210]. Another guide to the construction of this set can be found in [48]. The form of the terminal set  $\mathbb{X}_{f,i}$  depends on the steady-state pair  $(\bar{z}_{i,ss}, u_{i,ss})$ . Since the form depends on the steady value it therefore suggests that it may need to be re-computed every time these desired steady states

change and, by extension, each time the load disturbance changes; however, in the face of such a situation an approach would be to parametrize the set  $\mathbb{X}_f$  in terms of  $(\bar{z}_{i,ss}, u_{i,ss})$ , allowing it to be obtained with elementary operations each time the latter changes [211].

Solving problem  $\mathbb{P}_i(z_i)$  at a state  $z_i$  for each subsystem generates an optimal sequence comprising current and future controls given by

$$\bar{\mathbf{u}}_i^0(z_i) := \{\bar{u}_i^0(0; z_i), \bar{u}_i^0(1; z_i), \dots, \bar{u}_i^0(N-1; z_i)\},$$

The first control in this sequence is applied to the real system, and the process (of solving the problem and applying the first control in the optimized sequence) is repeated at each subsequent state. This induces state feedback of the form

$$u_i = u_{i,ss} + \kappa_{N,i}(z_i) = u_{i,ss} + u_i^0(0; z_i).$$

The solution to the optimisation problem represents the corresponding cost, as a function of  $z_i$ , which is also the *value function* given by:

$$V_{N,i}^0(z_i) := \min_{\mathbf{u}_i} V_{N,i}(z_i, \mathbf{u}_i) = V_{N,i}(z_i, \mathbf{u}_i^0(z_i)).$$

The domain of the value function is the set of states for which the optimisation problem for each subsystem  $\mathbb{P}_{N,i}(z_i)$  has a solution:

$$\mathcal{Z}_{N,i} := \{z_i : \mathbb{P}_{N,i} \text{ is feasible}\}.$$

The value function has some interesting properties that are used to establish stability in the design of MPC controllers. In the case of stability of the origin, the standard approach is to use the value function of the infinite horizon optimal control problem as a Lyapunov function. This means the solution of the optimal control problem used in the derivation of the MPC controller under mild assumptions on the stage cost and terminal costs can be used as a Lyapunov function. The satisfaction of the conditions for stability enabling the use of the value function as Lyapunov function in the case of a finite horizon control problem is dependent of the establishment of appropriate upper and lower bounds on the value function which are in turn dependent on the appropriate selection of the stage, terminal costs and the terminal region [51]. For the purposes of control design in this thesis two properties are of particular interest:

**Lemma 3** (Value function properties - Regulation). *The value function decreases monotonically as the time to go  $k$  increases. This establishes the descent property of the optimal cost computed by the controller and can be, under suitable assumptions stated as*

$$V_{N,i}^0(f(z_i, \kappa_{N,i}(z_i))) \leq V_{N,i}^0(z_i) - l(\kappa_{N,i}(z_i))$$

*The existence of positive constants  $c_i$ ,  $d_i$  and  $a$  all  $> 0$  such that the value function has the following properties;*

$$\begin{aligned} V_{N,i}^0(f(z_i, \kappa_{N,i}(z_i))) &\geq c_i |z_i|^a \quad \forall z_i \in \mathcal{Z}_{N,i} \\ V_{N,i}^0(f(z_i, \kappa_{N,i}(z_i))) &\leq d_i |z_i|^a \quad \forall z_i \in \mathbb{X}_{f,i} \\ V_{N,i}^0(f(z_i, \kappa_{N,i}(z_i))) &\leq V_{N,i}^0(z_i) - c_i |z_i|^a \quad \forall z_i \in \mathcal{Z}_{N,i} \end{aligned}$$

The first item establishes the continuous decrease of the value function which makes it suitable to be used as a Lyapunov function to establish stability. The second item defines bounds on the stage and terminal cost. Operation within the limits of these bounds guarantees stability of the designed controller. The relevant assumptions on which these equations are based can be found in [51], with a detailed explanation on the derivations of this lemma. Lemma 3 is for the case of regulation. In particular here, for the case of tracking, the value function enjoys the following properties under the assumptions and design conditions defined thus far in this section.

**Lemma 4** (Value function properties - Tracking). *Suppose Assumptions 1–5 hold, and that  $\Delta P_L$  is constant. The value function satisfies*

$$\begin{aligned} c_i \|z_i - \bar{z}_{i,ss}\|^2 &\leq V_{N,i}^0(z_i) \leq d_i \|z_i - \bar{z}_{i,ss}\|^2 \\ V_{N,i}^0(\bar{z}_i^0(1; z_i)) &\leq V_{N,i}^0(z_i) - c_i \|z_i - \bar{z}_{i,ss}\|^2 \end{aligned}$$

*for all  $z_i \in \mathcal{Z}_{N,i}$ , where  $\bar{z}_i^0(1; z_i)$  is the optimal one-step ahead state prediction obtained by applying the first optimal control  $u_i^0(0; z_i)$  to the prediction model (4.20) starting from  $\bar{z}_i(0) = z_i$ , and  $d_i > c_i > 0$  are constants. Moreover,*

$$V_{N,i}^0(z_i^0(1)) \leq \gamma_i V_{N,i}^0(z_i) \quad \text{where } \gamma_i := (1 - c_i/d_i) \in (0, 1). \quad (4.22)$$

Due to the coordinate shift created by  $\bar{z}_{i,ss}$  for non-zero steady state targets the constant  $d_i$  is not necessarily the same as in 3. The value function represented by  $V_{N,i}^0(\cdot)$  is not generally known in closed-form, but is evaluated at a given  $z_i$  by solving problem  $\mathbb{P}_i(z_i)$ . The constant  $\gamma_i$  bounds the rate of decrease of this function;  $\gamma_i$  is not usually

known, but may be (perhaps conservatively) estimated from the choices of tuning parameters in the MPC problem.

Were the true dynamics of the generator and BESS given by the models used for prediction, the system would enjoy closed-loop stability as a consequence of this result, since the value function satisfies the condition of a Lyapunov function along trajectories of the system; in particular, it decreases monotonically. In reality, however, these prediction models are inaccurate, neglecting interactions between generator and BESS via the power system, so closed-loop stability can not be inferred from Lemma 4. The stability analysis in the next section is carried out in order to provide a solution to this problem.

## 4.5 Stability analysis

In order to obtain suitable prediction models for each subsystem a formal decomposition and model selection procedure was applied. In this way independent models that do not rely on any interconnection variables which are not known prior to prediction into the future were obtained. These models then represented dynamical systems useful for decentralised prediction. However, the standard lyapunov stability analysis based on using the properties of the value function could no longer be applied directly in the determination of stability.

The main issue that prevents properties of the value function from being sufficient to ensure closed-loop stability is the inaccuracy of the prediction models: given some initial state  $z_i$ , for  $i = g$  or  $b$ , the real subsystem evolves, under the optimal input  $u_i^0(0)$ , to  $z_i^+ = \tilde{A}_i z_i + \tilde{B}_i u_i^0(0) + E_i \Delta P_L + \tilde{A}_{ij} z_j$  representing the true system dynamics (where  $j = b$  if  $i = g$ , and vice versa) and *not* the value  $z_i^0(1)$  predicted by the model. This raises at a minimum two relevant questions: does the value function satisfy the conditions of a Lyapunov function along the *true* system trajectories? More fundamentally, is the optimal control problem even feasible at the next state? In this section an analysis of this situation is carried out in order to provide answers to these questions. The results obtained draw on the *robustness* inherent to model predictive controllers, which itself is a consequence of the value function being a continuous function of the state  $z_i$ ;[51] they show that, even though no non-deterministic uncertainty is present in this setting, the errors induced by omitting cross-coupling terms in the dynamics may be bounded and exploited to establish stability of the closed loop.

In the remainder of this section, it is assumed that Assumptions 1–5 hold, and also that  $\Delta P_L$  is constant; the latter allows a nominal form of stability to be established,

which is a necessary and fundamental step towards achieving stability in the face of time-varying load disturbances.

**Lemma 5** (Lipschitz continuity of the value function). *For each  $i \in \{b, g\}$ , the value function  $V_{N,i}^0(z_i)$  satisfies*

$$\|V_{N,i}^0(z_i^1) - V_{N,i}^0(z_i^2)\| \leq L_i \|z_i^1 - z_i^2\|$$

for all  $(z_i^1, z_i^2) \in \mathcal{Z}_{N,i} \times \mathcal{Z}_{N,i}$  and some  $L_i > 0$ . If  $z_i^1 - z_i^2$  corresponds to a change in only  $x_s$ , with  $x_g^1 = x_g^2$  and  $x_b^1 = x_b^2$ , then

$$\|V_{N,i}^0(z_i^1) - V_{N,i}^0(z_i^2)\| \leq L_i^s \|z_i^1 - z_i^2\|$$

where  $L_i^s \leq L_i$ .

The key point is that small deviations in state cause small deviations in value function. This now makes it possible to establish conditions under which the value function satisfies the monotonic decrease condition along trajectories of the real system. This is done by considering sublevel sets of the value function:

$$\Omega_i(r) := \{z_i : V_{N,i}^0(z_i) \leq r\} \text{ for } r > 0.$$

Denote the largest sublevel set contained in  $\mathcal{Z}_{N,i}$  as  $\Omega_i(R_i)$ .

**Theorem 1.** *If there exist scalars  $r_i \in (0, R_i]$ , for  $i \in \{g, b\}$ , such that for all admissible  $x_b$ ,  $x_g$  and  $\Delta P_L$*

$$\|A_{sb}x_b\| < W_g r_g \tag{4.23a}$$

$$\|A_{sg}x_g + E_s \Delta P_L\| < W_b r_b \tag{4.23b}$$

where

$$W_i := \frac{1 - \gamma_i}{L_i^s} \text{ for } i \in \{g, b\},$$

then, starting from any  $z_i(0) \in \mathcal{Z}_{N,i}$ ,  $i \in \{g, b\}$ : (i) problem  $\mathbb{P}_i(z_i)$  is recursively feasible; (ii) all constraints are satisfied; (iii) the states  $z_i$  remain within  $\Omega_i(R_i)$  for all time, and enter and remain within a set  $\Omega_i(r_i) \subseteq \Omega_i(R_i)$  after some finite time; (iv) the real states  $x$  converge to a neighbourhood of the desired steady-state values.

This result establishes stability of the controlled system under the condition that the errors induced by neglectation of cross-coupling terms in the dynamics are suitable

small. The derived conditions are somewhat abstract, however, upper-bounding a non-specific interaction term by a function of dependent parameters of the controller. This can be improved upon, however, and provide more insight to the power system problem by considering the particular kind of discretization employed.

**Corollary 1.** *Suppose the discretization of the system is performed using the Mixed Euler–ZOH method, with a sampling time of  $\Delta t$ . Then the bounds in (4.23) are*

$$|\Delta P_B| < \frac{D}{1 - e^{-(D/M)\Delta t}} W_g r_g \quad (4.24a)$$

$$|\Delta P_M - \Delta P_L| < \frac{D}{1 - e^{-(D/M)\Delta t}} W_b r_b, \quad (4.24b)$$

where  $M$  is the mechanical starting time and  $D$  is the frequency-dependent load coefficient. If forward Euler discretization is used, then the corresponding bounds are

$$|\Delta P_B| < \frac{M}{\Delta t} W_g r_g \quad (4.25a)$$

$$|\Delta P_M - \Delta P_L| < \frac{M}{\Delta t} W_b r_b. \quad (4.25b)$$

The result states that if the BESS power output and the difference between the generator output power and the load demand—the power imbalance—are kept small, then feasibility and stability of the decentrally controlled system hold. This supports intuition about how the system will respond to load disturbances when controlled in this way: the battery and generator both respond to frequency deviations, but only the generator supports the load in steady-state. It follows that (i) the prediction accuracy of the generator’s model diminishes, risking feasibility and stability, whenever the battery is active (non-zero  $\Delta P_B$ ); on the other hand, the prediction accuracy of the battery’s model decreases when the generator is not supporting the load ( $\Delta P_M \neq \Delta P_L$ ).

To further interpret this result, note that we desire the right-hand sides to be large because this then allows more flexibility in the outputs of the BESS and generators. At the same time, however, we desire  $r_b$  and  $r_g$  to be small, because these tell us about the “size” of the neighbourhood that the system provably converges to around the desired steady state. We therefore may infer the following:

- $W_i$ , which depends only on  $\gamma_i$  and  $L_i$ , is a property of the controller; it will change depending on the choices of tuning parameters—for example, controllers with

$|Q_i| \gg |R_i|$  tend to have smaller  $\gamma_i$ —but not in a way that can be characterized readily. In fact, these parameters are difficult even to estimate, and for the purpose of this analysis and discussion,  $W_i$  can be considered constant and unknown.

- The bound increases sharply as  $e^{-(D/M)\Delta t} \rightarrow 1$ . This happens predominantly as a consequence of (i) increasing  $M$ , mechanical starting time (which is twice the system inertia constant) and (ii) decreasing  $\Delta t$ . The implication of the former is that the derived bounds are more readily met in systems with large inertia, which is in agreement with what is known about system frequency stability and inertia. With a shorter sampling period, the errors caused by omission of terms in the dynamic model have a shorter time to accumulate; thus, the predictions are more accurate.
- There is a positive dependence on  $D$ , in that systems with larger values tend to produce larger bounds and be more stable, albeit this is weak; this is demonstrated in Figure 4.3 and is also evident from the fact that  $D$  is absent from the bounds corresponding to forward Euler discretization. The same also shows that the dependence on  $M$  is approximately linear.

The final part of this section concludes the analysis by addressing the apparent discrepancy between the fact that no non-deterministic uncertainty is present in our problem yet the stability result achieves convergence only to a neighbourhood around the desired steady states.

**Assumption 6** (Stabilizability via decentralized linear control). *The system  $x^+ = Ax + Bu$  is stabilized by the control law*

$$u = \begin{bmatrix} u_g \\ u_b \end{bmatrix} = \begin{bmatrix} \tilde{K}_g & 0 \\ 0 & \tilde{K}_b \end{bmatrix} x.$$

where  $\tilde{K}_g, \tilde{K}_b$  are the unconstrained optimal state-feedback control laws

$$u_g = \tilde{K}_g z_g = \begin{bmatrix} K_{gg} & K_{gs} \end{bmatrix} \begin{bmatrix} x_g \\ x_s \end{bmatrix}$$

$$u_b = \tilde{K}_b z_b = \begin{bmatrix} K_{bs} & K_{bb} \end{bmatrix} \begin{bmatrix} x_s \\ x_b \end{bmatrix}.$$

associated with the generator and battery optimal control problems (with  $\Delta P_L = 0$ ).

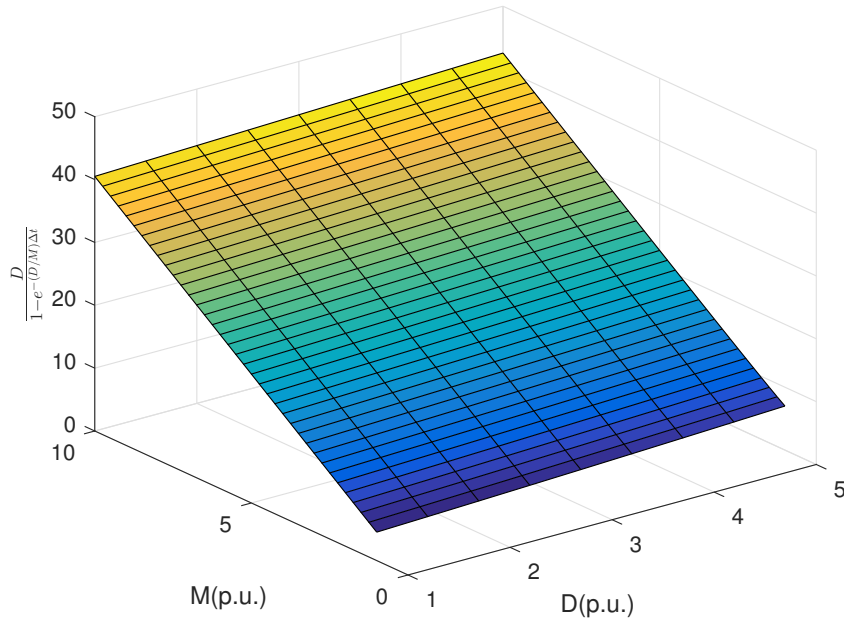


Fig. 4.3 Surface plot showing the dependence on mechanical starting time  $M$  and system damping  $D$

**Theorem 2.** *Suppose Assumption 6 holds. If the  $r_b$  and  $r_g$  meeting (4.23) are sufficiently small, then for any  $z_i(0) \in \mathcal{Z}_{N,i}$ ,  $i \in \{b, g\}$ , the real states  $x(k)$  and inputs  $u(k)$  converge to desired steady-state values asymptotically.*

## 4.6 Decentralised MPC scheme LFC in Smart Power System

In this section we propose decentralised MPLFC scheme for a smart power system consisting of generator and a BESS. Starting from the centralised power system model (4.7) is discretised adopting a sparsity preserving discretisation method. The decomposition procedure in Section 4.3.3 is then used in the derivation of decentralised models for each subsystem represented by (4.19). Following the determination of steady state targets, see Section 4.6.1,  $z_{i,ss}$  is supplied using the target calculator and the optimal input to each system  $u_i$  is obtained by solving the optimisation problem in (4.21) for  $k = 1 \dots N - 1$  time steps. The local cost function of each subsystem can be expressed explicitly as:

$$V_{N,i}(\bar{z}_i, \mathbf{u}_i) = z_i^\top P_i z_i + \sum_{k=0}^{N-1} z_i^\top Q_i z_i + u_i^\top R_i u_i \quad (4.26)$$

The matrices  $Q_i$  and  $R_i$  are tuning parameters that can be used to achieve a desired performance while the matrix  $P_i$  is determined as described in assumption 3. After applying the input, the system dynamic is updated and the process repeated at the next time step.

#### 4.6.1 Tracking Targets

In order to define the parameters used in the design procedure in terms of deviation variables steady state targets are calculated. The desired targets refer to state  $x_{ss}$  input  $u_{ss}$  and  $y_{ss}$ . These targets are determined at each time instant and the output  $y_{ss}$  which is assumed to be available/known is used in determine the state and input targets at each time instant. The use of deviation variables also enables offset free tracking to achieved using MPC.

For the purposes LFC this means the objective is to drive the output  $y$  to the desired  $y_{ss}$  which for the single area is the frequency. In this instance there is also the requirement (which can be relaxed) to achieve energy neutrality on the BESS following LFC action. The translates to the system being at equilibrium when the states and inputs  $z_i$  and  $u_i$  are driven to the desired  $z_{i,ss}$  and  $u_{i,ss}$  that ensure the desired outputs  $y_{i,ss}$  are attained. From lemma 1 we established that achieving equilibrium at the desired setpoints, was based on model 4.20. The final steady state value of the BESS is invariant to the load disturbance. This is supports intuition regarding the operation of the grid as highlighted previously. Since the BESS only responds to frequency it means the final value of its states is independent of the load when compared to the generators. In a sense this means the BESS does not require information on steady target targets computed by the generator; the values of  $z_{g,ss}$ ,  $z_{b,ss}$ ,  $u_{g,ss}$ , and  $u_{b,ss}$  are not dependent on any information sharing. This makes it possible to solve two different consistency equations; one for each subsystem.

$$\begin{bmatrix} I - \tilde{A}_i & \tilde{B}_i \\ \tilde{C}_i & 0 \end{bmatrix} \begin{bmatrix} z_{i,ss} \\ u_{i,ss} \end{bmatrix} = \begin{bmatrix} \tilde{E}_i P_{L,ss} \\ y_{i,ss} \end{bmatrix} \quad (4.27)$$

## 4.7 Simulations and Discussion

In this section numerical simulations are carried out to demonstrate the effectiveness of the proposed approach in achieving load frequency control in an isolated power system. Two scenarios are considered; the first scenario is based on the design of decentralised MPC controllers based on sub-models derived from the discretisation of the centralised model of Section 4.3.1 using the forward Euler method. The results are presented in Section 4.7.1. In the second scenario a comparison is made between the use of three discretisation methods in the design of decentralised MPC controllers for each subsystem. In each scenario, centralised MPC design is also implemented and is serves as the benchmark control scheme alongside the decentralised MPCs discretised using different discretisation methods. The results are given in Section 4.7.2

### 4.7.1 Scenario 1 - Decentralised Forward Euler

The isolated system on which the simulations are based is given in figure 4.1 and consists of the BESS and a set of lumped generators which together make up the two subsystems of the model. This centralised model is discretised using the Euler method with a sampling time of 0.1s seconds. The sparse centralised model is then decomposed using the procedure outlined in Section 4.3.3. The subsequent decentralised models are then used on the design of decentralised controllers.

The prediction horizon  $N$  is set to 50 time steps *i.e.* 5s and is used for the  $i$ th controller. The rated capacity of the area is  $Pr = 2000$  MW on a 2000 MVA base. The capacity of the BESS is 10 MW/40 MWh. The tunable parameters  $Q$  and  $R$  used in determining the weights for the states in the centralised model were selected to be  $Q = \text{diag}[10, 0.01, 10, 0.01, 50]$  and  $R = I_u$  where  $u$  is equal to the total number of subsystems in the model *i.e.*,  $u = 2$ . In the case of the decentralised controllers, the weights used for each model is given by;  $Q_g = \text{diag}[0.01, 0.01, 5]$  while  $Q_b = \text{diag}[50, 0.01, 250]$ . These values were selected as a compromise between the best frequency performance possible and with respect to the BESS getting the right balance between the requirements of frequency response and state of charge restoration. The values of  $R$  were  $R_g = I_{ug}$  and  $R_b = I_{ub}$  where  $I_{ui}$  for  $i = g, b$  are identity matrices of appropriate sizes. The values of the gains for both the centralised and decentralised controllers are obtained as noted in assumptions 3 and 5.

The BESS power output is constrained to its maximum rated value of 0.005pu while the state of charge is constrained between 20% – 80% of the BESS capacity.

$D$ (pu/Hz)	$2H$ (pu s)	$R$ (Hz/pu)	$T_G$ (s)	$T_T$ (s)	$Tb$ (s)
0.0059	0.199	2.22	0.1	0.35	0.3

Table 4.1 The power systems parameters

Generation rate constraint is considered and this is set at 10% (*i.e.*,  $0.0017MW/s$ ) for the generator with an input constraint of  $0.02pu$ . The model parameters used for the simulation are given in table 4.1. The value of the load disturbance *i.e.*  $\Delta P_L = 0.004pu$  and is set to occur at 0.5s into the simulation.

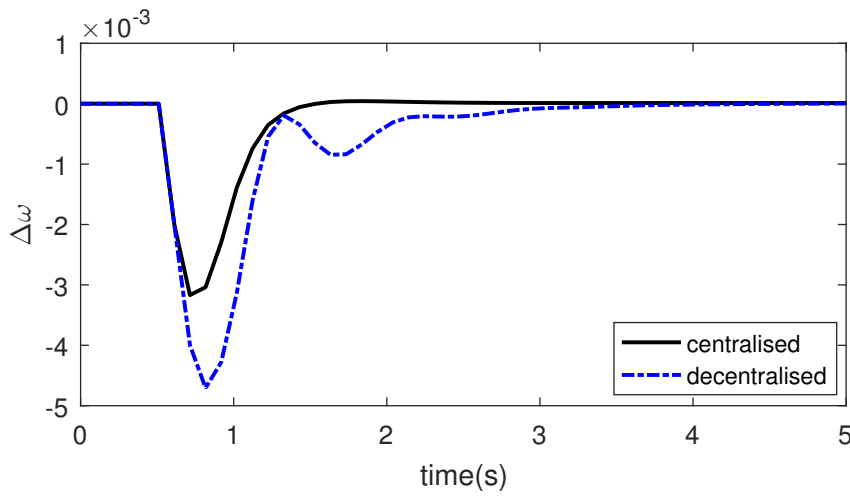


Fig. 4.4 Frequency deviation in response to a load disturbance

The result for the frequency deviation is shown in Figure 4.4. It can be seen that in both the centralised and decentralised cases the frequency is restored to its nominal value following the occurrence of the load disturbance at 0.5s. From an LFC perspective the main objective is to drive the deviation in frequency to zero in the presence of a change in load demand. In addition to this being achieved, it can also be seen that the performance obtained when using decentralised MPCs is acceptable when compared to the centralised MPC. However, as a result of model inaccuracy due to the ignored cross coupling terms in the prediction model, there is as expected some degradation in performance when compared to the fully connected centralised MPC. This is because the centralised controller has full knowledge of interactions between the generators and BESS subsystems enabling better coordinated action during operation. Noticeably, there is no undesirable loss of coordination between the two systems which could have created issues of instability.

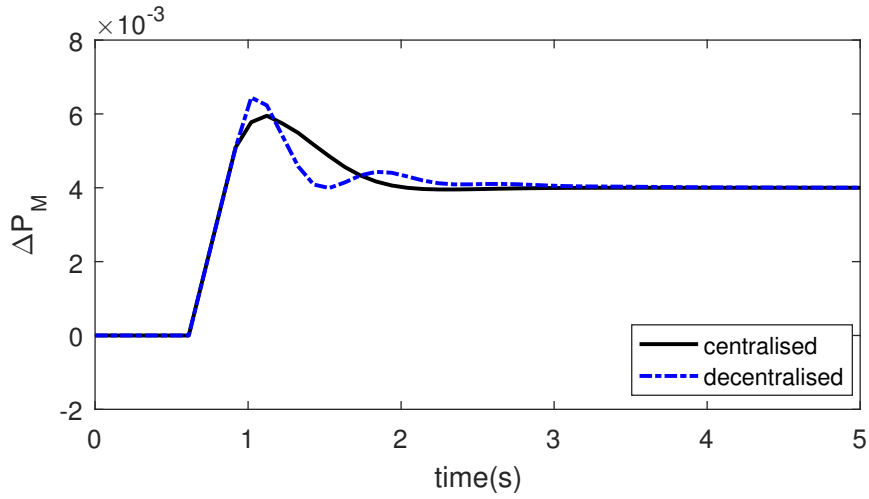


Fig. 4.5 Generator power outputs

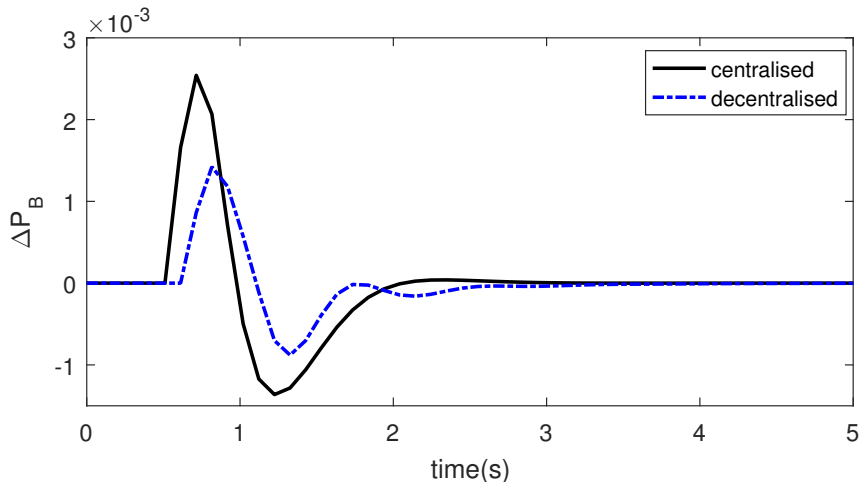


Fig. 4.6 Battery power outputs

Figure 4.5 shows the generator power outputs for each control design approach. The generator is able to track the load, with  $\Delta P_M = \Delta P_L$  in both cases with almost the same settling time. The dynamical behaviour of centralised and decentralised approach do not differ significantly in this case. This could possibly be due to the fact that the generator is the primary subsystem, directly coupled to the system frequency. So independent of the knowledge of any other subsystem behaviour the dynamical responses do not differ significantly. For the BESS, both its power output and state of charge are driven to their nominal values using a decentralised MPC *i.e.*  $(P_{B,ss}, SOC_{B,ss}) = (0, \overline{SOC}_B)$ . This can be seen in Figures 4.6 and 4.7 respectively. Figure 4.8 is the state of charge in per unit values. However, in this case the impact on performance is greater than for the case of the generator. In a way this supports

intuition; the BESS model has been integrated into the synchronised power system model. BESS do not contribute to or determine the synchronous speed of the system, *i.e.*, they do not swing but only respond to changes in frequency. As a result their performance is more impacted when any interactions or cross couplings are ignored in the process of designing controllers for them.

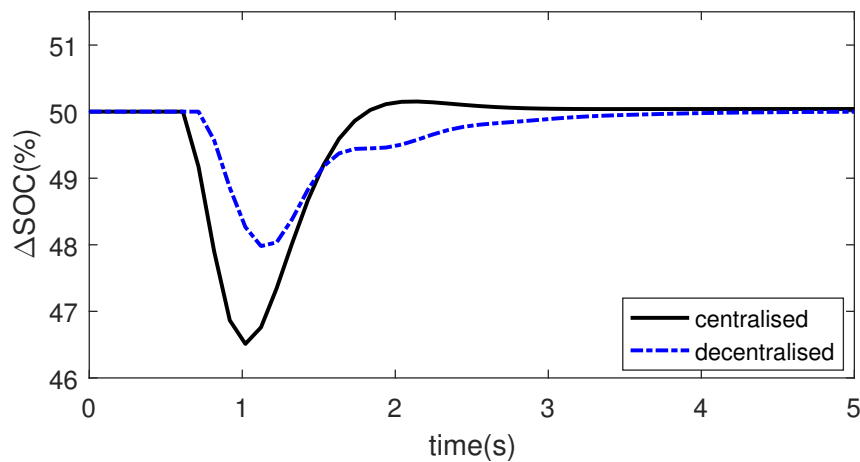


Fig. 4.7 Battery state of charge outputs

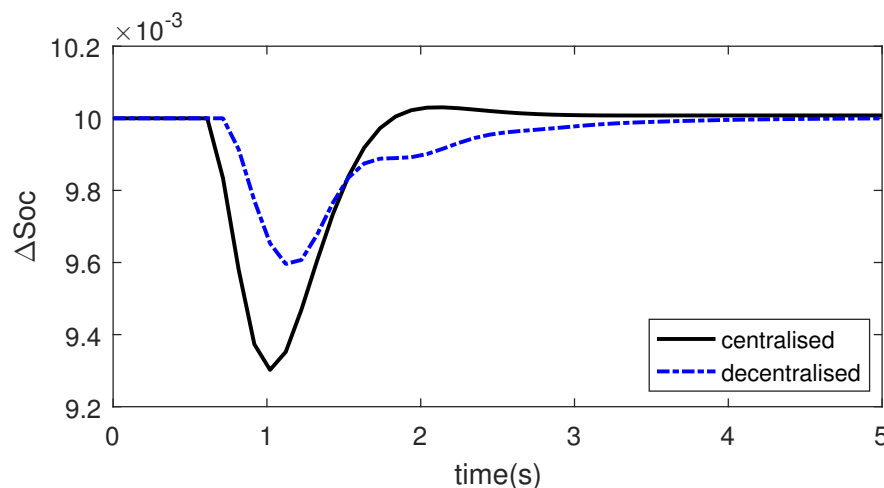


Fig. 4.8 Battery state of charge outputs in pu

Figures 4.9 and 4.10 show the controllable inputs to the subsystems and indicate that for both control approaches the inputs are driven to the desired steady states. The BESS power is driven by its local controller to zero while the generator settles at the reference set point. The same arguments regarding the dynamical performances are also applicable in this situation. Figure 4.11 shows the generation rate with the

red dotted lines indicating the rate constraint. The constraint is active in both cases with the decentralised case showing a slightly oscillatory pattern after the exiting the constraint region in keeping with the generator behaviour shown in figure 4.5.

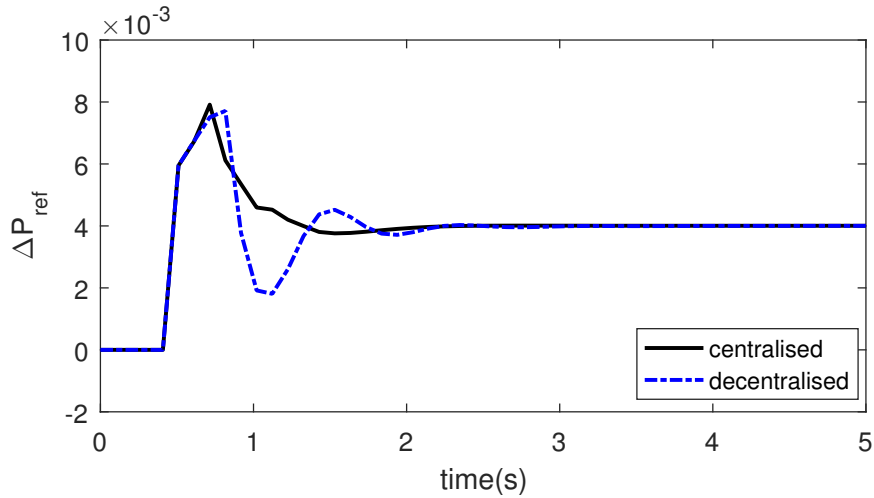


Fig. 4.9 Generator reference inputs

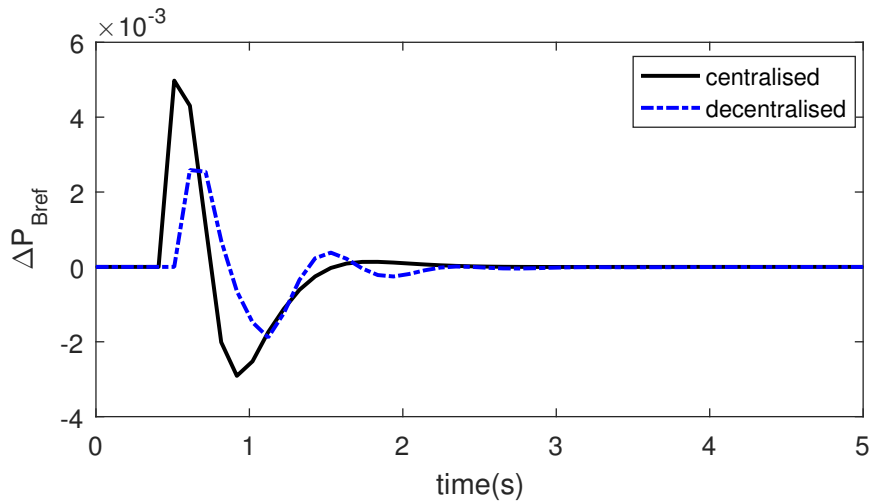


Fig. 4.10 Battery control inputs.

From the preceding results, it can be seen that despite the use of inaccurate prediction models in the design of local controllers for each subsystem, the desired equilibrium point of  $(\Delta\omega, \Delta P_M, \Delta P_G, \Delta P_B, SOC_B) = (0, \Delta P_L, \Delta P_L, 0, \overline{SOC}_B)$  at steady state is attained with acceptable performance. More importantly this signifies that following the proposed design approach, the application of the optimal inputs from both decentralised controllers at each time step in the presence of model inaccuracy and the specified load  $\Delta P_L$  did not drive the system to instability. The conditions

guaranteeing stability of the decentralised design using the robustness inherent in MPC were satisfied and good outputs were obtained in the absence of any communication between controllers. Figure 4.12 is a plot of the bounds in (4.25) for both subsystems.

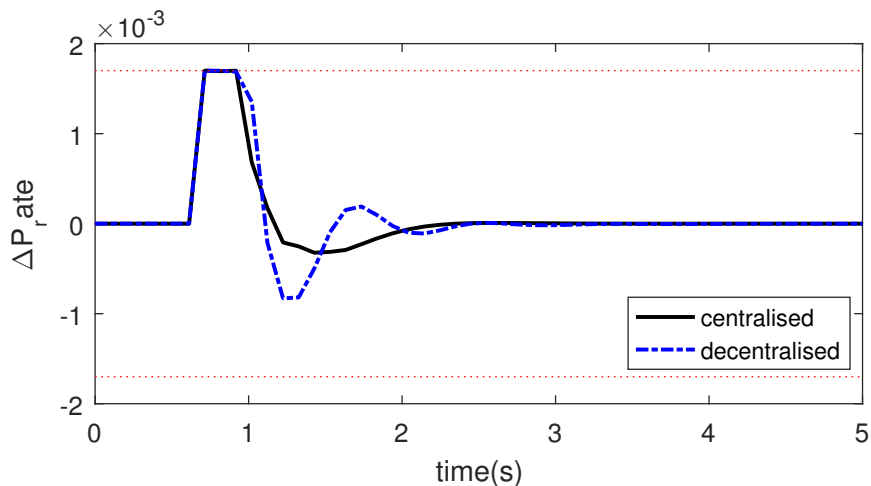


Fig. 4.11 generation rate constraints.

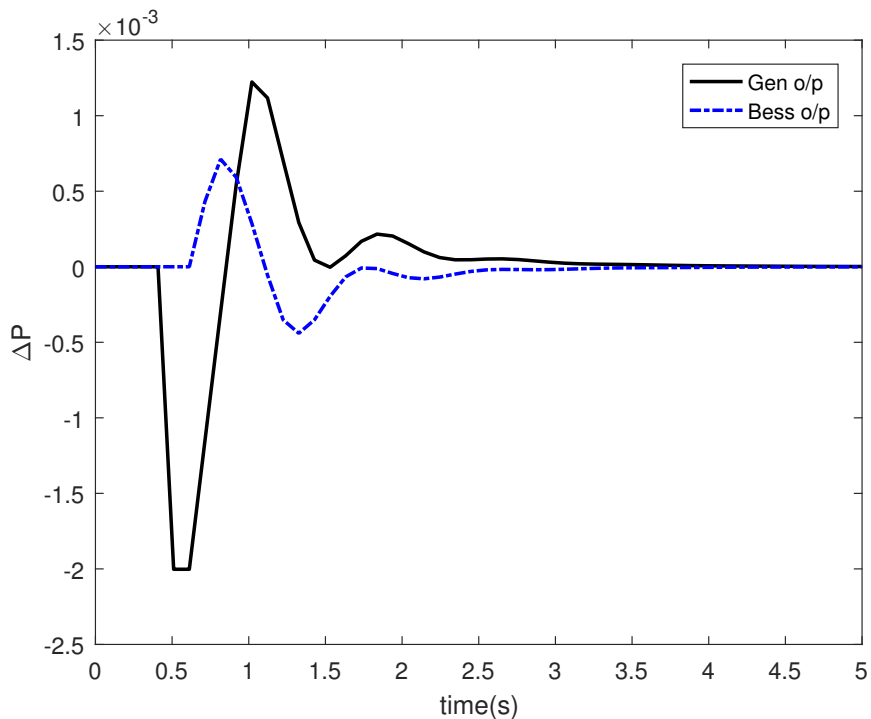


Fig. 4.12 Sample of bounds for both the generator and BESS.

### 4.7.2 Scenario 2 - ceMPC, eDMPC, meDMPC and zDMPC LFC

In this scenario, the centralised model is discretised using the zero order hold leading to an exact model representation. Decentralised models are then developed using Euler, mixed Euler and zero order hold approaches. The zero order hold is an exact match for the system making it convenient for MPC synthesis. However, applying this method induces artificial interactions between subsystems. Designing decentralised controllers in this way would produce dynamical performances closer in performance to the centralised case. The forward euler and mixed euler methods retain the sparse structure of the system with the mixed euler being more accurate. For easy referencing in this section the centralised MPC would be referred to as cMPC, while the based on method used in obtaining the discrete model before decomposition three decentralised MPC (DMPC) schemes are defined; Euler MPC (eDMPC), mixed Euler (meDMPC) and the zero order hold (zDMPC).

The centralised model discretised using the zero order hold is the benchmark used for comparative purposes. To obtain the mixed euler, the centralised model in continuous time is first of all decomposed to obtain the BESS and generator sub-models. At this stage the approach adopted is that since the generators are responsible for the system speed, the frequency dynamic is attached to the generator subsystem.

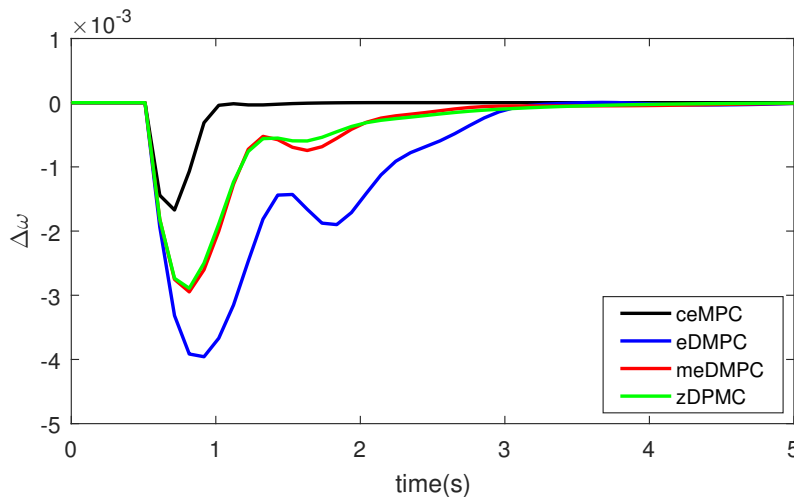


Fig. 4.13 Frequency deviation in response to a load disturbance

The prediction horizon used in this scenario is also set to 50 time steps *i.e.*, 5s and this is used for the *i*th controller. The rated capacities of the isolated area and BESS are the same as in scenario one. The tunable parameters  $Q$  and  $R$  used in the centralised

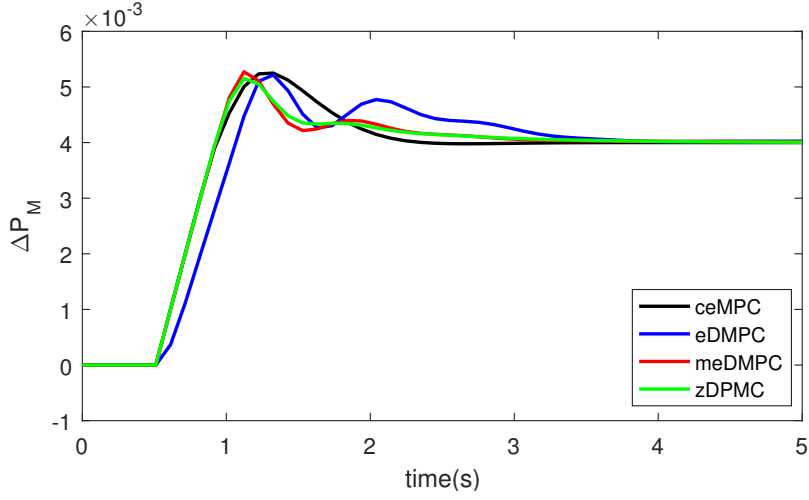


Fig. 4.14 Generator power outputs

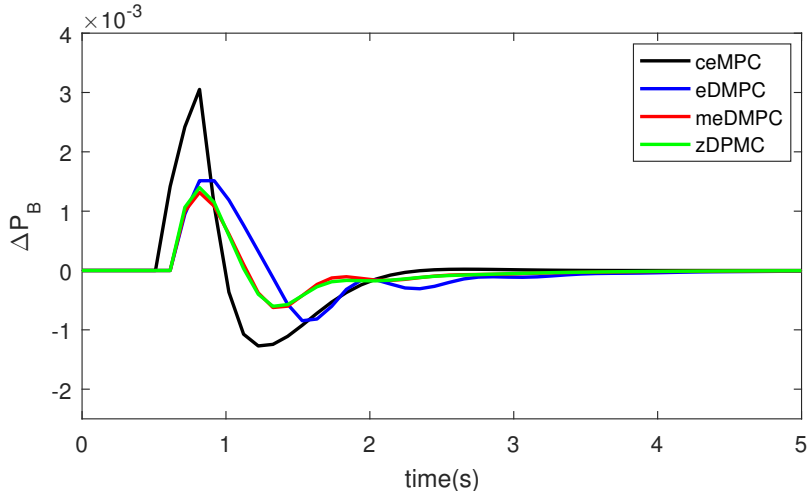


Fig. 4.15 Battery power outputs

controller design in this case are  $Q = \text{diag}[100, 0.01, 10, 0.01, 50]$  and  $R = I_u$  where  $u$  is equal to the total number of subsystems *i.e.*,  $u = 2$ . For the decentralised MPCs  $Q_i$  and  $R_i$  for each controller were  $Q_g = \text{diag}[0.01, 0.01, 10]$  while  $Q_b = \text{diag}[50, 0.01, 150]$ . These values were also selected after tuning in order to obtain the desired LFC performances. Similar to scenario one, in the case of the BESS subsystem, the tuning parameters were selected to achieve an acceptable balance between frequency and state of charge restoration. The values of  $R_i$  were  $R_g = I_{u_g}$  and  $R_b = I_{u_b}$  where  $I_{u_i}$  are identity matrices of appropriate dimensions. The values of the gains were selected based on assumption 3 and 5 for both the centralised and decentralised models.

The results for frequency response is given in Figure 4.13. Here it can be seen that all controllers still achieve the objective of LFC; regulation of the frequency to its nominal value. Also since the meDMPC and zDMPC are more accurate they give better performance than the eDMPC.

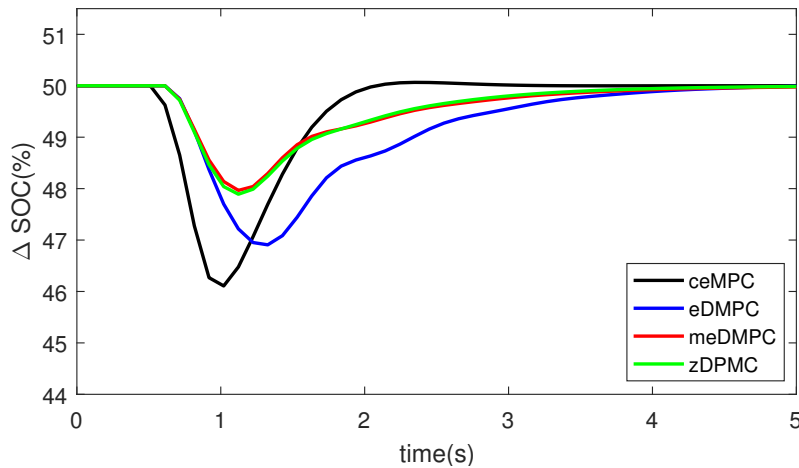


Fig. 4.16 Battery state of charge outputs

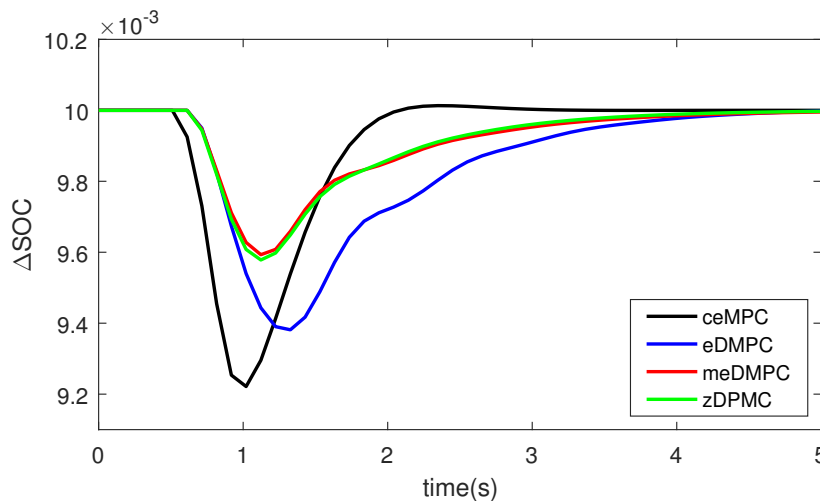


Fig. 4.17 Battery state of charge outputs in pu

The generator and BESS power outputs are shown in Figures 4.14 and 4.15 respectively. The plots show that for every design approach the generators track the desired load demand- $\Delta P_M = \Delta P_L$ . The dynamic responses in this case are similar in every instance. However, the meDMPC and zDMPC show closer dynamic responses when compared to the eDMPC. Similar conclusions can be drawn from the response plots

of the BESS power output. The same impact on the BESS performance caused by the neglected cross couplings in the design process are also observed in this scenario. Furthermore, the results of eDMPC slightly differs from those of the meDMPC and zDMPC. This could be because since the eDMPC is less accurate, the BESS designed with this approach responds more independently trying to support system frequency by supplying more power when compared to the meDMPC and zDMPC where the generator behaviour is more accurate leading to less BESS power outputs. This is also reflected in results for the state of charge shown in Figures 4.16 and 4.17 in percentages and per unit respectively.

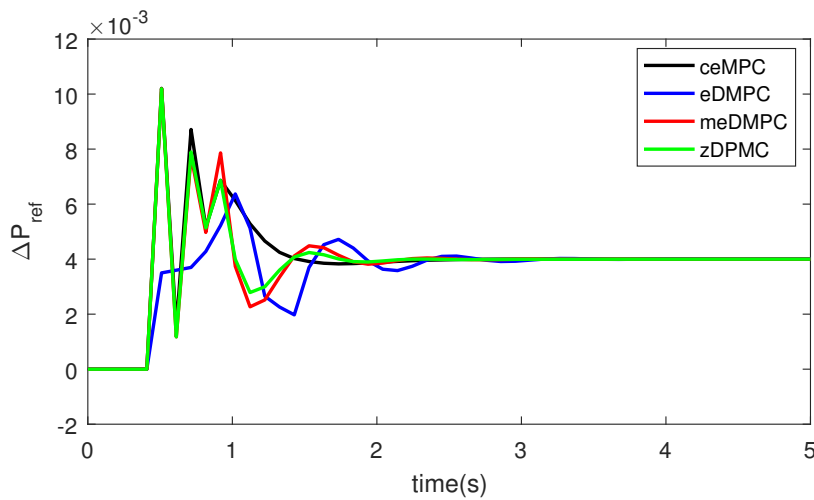


Fig. 4.18 Generator reference inputs

The generator input is shown in Figure 4.18. The inputs designed using all formulations track the required load demand. A closer look at the inputs also display a similar trend with the generator power output. The ceMPC, eDMPC and meDMPC have similar transient performance while the eDMPC follows a different pattern. For the BESS, the inputs also display a similar trend to what was obtainable in the power inputs with the ceMPC output much higher than the DMPC inputs. This is shown in Figure 4.19. The generation rate constraint is shown in Figure 4.20 where only the eDMPC did not reach the constraint bounds. From these simulations we that performances of the generator is similar for the ceDMPC, meDMPC and the zDMPC but differs slightly for the eDMPC. This is because in the first three instances we have a model match which is not the case for the eDMPC.

A comparison of the average computation times and associated costs of each MPC formulations is given in Table 4.2. The values of the computations times were calculated as the average of the time required to solve the optimisation problem over entire time

Algorithm	Subsystem	Av Comp Time (s)	Cost
CeMPC		0.025	$9.4 \times 10^{-4}$
zDMPC	Gen	0.0087	$4.07 \times 10^{-4}$
	Bess	0.019	0.0018
meDMPC	Gen	0.0012	$4.77 \times 10^{-4}$
	Bess	0.010	0.0021
eDMPC	Gen	0.0007	0.0014
	Bess	0.0008	0.0072

Table 4.2 Comparison of the average computation times and cost for the centralised, decentralised zero order hold, decentralised mixed Euler and decentralised Euler MPC controllers

steps of the prediction horizon. This time is smaller than what was obtainable in the centralised case for each of the individual subsystems for all the decentralised MPC approaches. Since the non centralised problems would be solved in parallel, use of the decentralised approach would be faster than the centralised approach. However, the total computational cost associated with each decentralised method is higher than for the centralised case. This is not unexpected since more controllers are in use. This could possible change depending on the size and spread of the system. Also, computational costs of the eDMPC method is much higher than the other methods and it's speed of computation faster. This is likely due to the higher degree of mismatch and reduced accuracy of the Euler method.

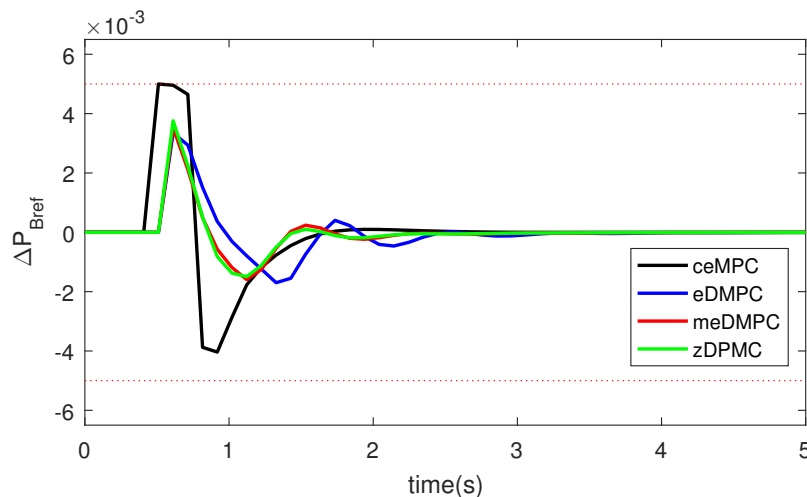


Fig. 4.19 Battery control inputs.

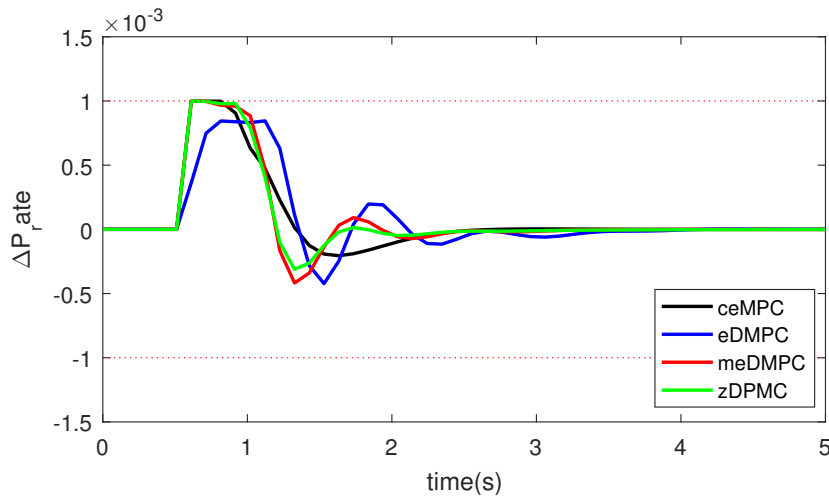


Fig. 4.20 generation rate constraints.

## 4.8 Conclusion

The future grid is one that would increasingly involve the integration and operation of new technologies such as battery energy systems. This might require the redesign of power systems models in order to achieve the requirements of load frequency control. These systems would also need advanced control strategies that can accommodate the different dynamic characteristic of all devices that make up of the future grid. However, such a system introduces new interactions hitherto not present in the legacy grid which may not be explicitly defined or clearly identifiable. This creates new design challenges in frequency control management.

Centralised MPC provides a readily available solution that can be used in the design of controllers in the future smart grid. However, new devices integrated into the grid to support LFC often require independent control design. To this end decentralised control design was proposed and implemented in this chapter. In the first instance a procedure for the decomposition of the centralised model which makes the coupling dynamic available to both subsystems was implemented. The concept behind this approach is any strong coupling required for local control design is available to both subsystems. In the approach adopted in this chapter model decomposition helps to define the true subsystem dynamics and make the coupling dynamic available to both subsystems which in this case was the swing equation. However, only frequency measurements are made locally available to both controllers. The other interactions represented by the power outputs from both subsystems are not explicitly included in the controller design.

Ignoring these interaction led to a loss of accuracy in predictions and the nominal guarantees of stability and recursive feasibility of MPC were no more certain. Using the analytical approach presented in this chapter it was shown that such guarantees are obtainable even with the decentralised design approach. Following this, in a first scenario eDMPC was implemented successfully with the objectives of load frequency control achieved. No communication was needed between local controllers and the system was stable in the presence of a fixed load disturbance.

Several observations can be made from an LFC perspective

- The interaction, coordination and communication between different sources of generation has an appreciable impact on LFC performance. ceMPC accounts for all couplings and interactions. For the decentralised controllers to achieve comparable performances some level of communication would be required. However, with decentralised control parallel and faster computation is achieved. The means devices supporting LFC respond quicker to exogenous disturbances.
- The swing equation is a coupling dynamic for all devices that impact this state. In addition, it can be used in representing interactions (power influences) between subsystems. Decomposition methods that account for this coupling between all the subsystems in future power grids could facilitate the design of local decentralised controllers.
- The discretisation method employed when using MPC also has an impact on LFC performance as was seen in the final simulations with performances varying between the eDMPC, meDMPC and zDMPC. .

In conclusion decentralised controllers have been designed for coupled generating subsystems in a power grid. The control of power imbalance required for acceptable frequency response was obtained. Most importantly, an approach that can be used in the design of decentralised controllers based on subsystem models suitable for decentralised prediction was successfully presented. The challenge of uncertainty and dynamic mismatch caused by decentralised prediction errors was handled via an in depth stability analysis. It was demonstrated that stability and even feasibility can still be achieved despite the presence of this uncertainty. In addition in terms of computation times the decentralised methods are faster. When used for load frequency control successful decentralised controllers for future power grids can be implemented with the proposed method.

## 4.9 Proofs

To complete this chapter the relevant proofs are given in this section. First, to aid the exposition, we recall the explicit form of the power system model and the mixed euler ZOH method.

### Continuous-time dynamics

$$\frac{dx}{dt} = A^c x + B^c u + E^c \Delta P_L$$

where the compact form representing the complete expressions for each term are given in (4.8)

#### 4.9.1 Mixed Euler–ZOH discretization

$$x^+ = (I + D_d(\Delta t)A^c)x + (D_d(\Delta t)B^c)u + (D_d(\Delta t)E^c)\Delta P_L$$

with (d = discrete)

$$D_d(\Delta t) = \text{diag} \left( \int_0^{\Delta t} e^{A_{ii}^c t} dt, \dots, \int_0^{\Delta t} e^{A_{MM}^c t} dt \right)$$

#### 4.9.2 Deriving a discrete-time model

Here we consider discretizing (using ZOH) the generator, frequency and battery dynamics separately, and handling the interactions with forward Euler. So the overall approach is the mixed Euler–ZOH one.

$$\frac{d}{dt} \begin{bmatrix} x_g \\ x_s \\ x_b \end{bmatrix} = \begin{bmatrix} A_g^c & A_{gs}^c & 0 \\ A_{sg}^c & A_s^c & A_{sb}^c \\ 0 & 0 & A_b^c \end{bmatrix} \begin{bmatrix} x_g \\ x_s \\ x_b \end{bmatrix} + \begin{bmatrix} B_g^c & 0 \\ 0 & 0 \\ 0 & B_b^c \end{bmatrix} \begin{bmatrix} u_g \\ u_b \end{bmatrix} + \begin{bmatrix} 0 \\ E_s^c \\ 0 \end{bmatrix} \Delta P_L$$

This is acceptable since we don't mind if the individual matrices that make up this system 'go dense' with discretization, but we want to retain the basic structure of the model.

From [209] the discretization can be written as

$$x_g^+ = e^{A_g^c \Delta t} x_g + D_g(\Delta t) (B_g^c u_g + A_{gs}^c x_s) \quad (4.28a)$$

$$x_s^+ = e^{A_s^c \Delta t} x_s + D_s(\Delta t) (A_{sg}^c x_g + A_{sb}^c x_b + E_s^c \Delta P_L) \quad (4.28b)$$

$$x_b^+ = e^{A_b^c \Delta t} x_b + D_b(\Delta t) (B_b^c u_b) \quad (4.28c)$$

where

$$D_g(\Delta t) = \int_0^{\Delta t} e^{A_g^c t} dt \quad (4.29a)$$

$$D_s(\Delta t) = \int_0^{\Delta t} e^{A_s^c t} dt \quad (4.29b)$$

$$D_b(\Delta t) = \int_0^{\Delta t} e^{A_b^c t} dt. \quad (4.29c)$$

Evaluating these three integrals of matrix exponentials:

$$D_g(\Delta t) = \begin{bmatrix} -T_g (e^{-(1/T_g)\Delta t} - 1) & 0 \\ \star & -T_t (e^{-(1/T_t)\Delta t} - 1) \end{bmatrix}$$

$$D_s(\Delta t) = -(M/D) (e^{-(D/M)\Delta t} - 1)$$

$$D_b(\Delta t) = \begin{bmatrix} -T_b (e^{-(1/T_b)\Delta t} - 1) & 0 \\ \dagger & \Delta T \end{bmatrix}.$$

where  $\star$  and  $\dagger$  are more complicated expressions containing second-order terms.

It is now possible to evaluate any of the matrices in the discrete-time model. For example,

$$A_{gs} = D_g(\Delta t) A_{gs}^c = \begin{bmatrix} -T_g (e^{-(1/T_g)\Delta t} - 1) & 0 \\ \star & -T_t (e^{-(1/T_t)\Delta t} - 1) \end{bmatrix} \begin{bmatrix} -1/(T_g R) \\ 0 \end{bmatrix}.$$

### 4.9.3 Lemma 1

It is easiest to prove all of the results in this Chapter by considering the continuous-time, rather than discretized, subsystem dynamics; the basic properties of a continuous-time system are preserved with discretization under mild conditions. However, initially we consider the discretized models for this first result. Before proving lemma 1, note that

by comparing (4.19),(4.20) and (4.28), we have:

$$\begin{aligned} \tilde{A}_g &:= \begin{bmatrix} A_g^d & D_g(\Delta t)A_{gs}^c \\ D_s(\Delta t)A_{sg}^c & A_s^d \end{bmatrix} & \tilde{B}_g &:= \begin{bmatrix} D_g(\Delta t)B_g^c \\ 0 \end{bmatrix} & \tilde{E}_g &:= \begin{bmatrix} 0 \\ D_s(\Delta t)E_s^c \end{bmatrix} \\ \tilde{A}_b &:= \begin{bmatrix} A_s^d & D_s(\Delta t)A_{sb}^c \\ 0 & A_b^d \end{bmatrix} & \tilde{B}_b &:= \begin{bmatrix} 0 \\ D_b(\Delta t)B_b^c \end{bmatrix} & \tilde{E}_b &:= \begin{bmatrix} D_s(\Delta t)E_s^c \\ 0 \end{bmatrix} \end{aligned}$$

where, for  $i \in \{g, s, b\}$ ,

$$A_i^d = \begin{cases} e^{A_i^c \Delta t} & \text{if mixed Euler-ZOH} \\ I + A_i^c \Delta t & \text{if forward Euler} \end{cases}$$

and

$$D_i(\Delta t) = \begin{cases} \int_0^{\Delta t} e^{A_i^c t} dt & \text{if mixed Euler-ZOH} \\ \Delta t & \text{if forward Euler} \end{cases}$$

*Proof.* Consider the steady states of (4.19a) and (4.20):

$$\begin{aligned} \bar{z}_g &= \tilde{A}_g \bar{z}_g + \tilde{B}_g u_g + \tilde{E}_g \Delta P_L \\ \bar{z}_b &= \tilde{A}_b \bar{z}_b + \tilde{B}_b u_b + \lambda \tilde{E}_b \Delta P_L. \end{aligned}$$

where either model is recovered by appropriate specification of  $\lambda$ . Rewriting,

$$\begin{aligned} 0 &= (\tilde{A}_g - I) \bar{z}_g + \tilde{B}_g u_g + \tilde{E}_g \Delta P_L \\ 0 &= (\tilde{A}_b - I) \bar{z}_b + \tilde{B}_b u_b + \lambda \tilde{E}_b \Delta P_L. \end{aligned}$$

Thence, using the definitions of system matrices,

$$0 = \begin{bmatrix} A_g^d - I & D_g(\Delta t)A_{gs}^c \\ D_s(\Delta t)A_{sg}^c & A_s^d - I \end{bmatrix} \bar{z}_g + \begin{bmatrix} D_g(\Delta t)B_g^c \\ 0 \end{bmatrix} u_g + \begin{bmatrix} 0 \\ D_s(\Delta t)E_s^c \end{bmatrix} \Delta P_L \quad (4.30a)$$

$$0 = \begin{bmatrix} A_s^d - I & D_s(\Delta t)A_{sb}^c \\ 0 & A_b^d - I \end{bmatrix} \bar{z}_b + \begin{bmatrix} 0 \\ D_b(\Delta t)B_b^c \end{bmatrix} u_b + \lambda \begin{bmatrix} D_s(\Delta t)E_s^c \\ 0 \end{bmatrix} \Delta P_L. \quad (4.30b)$$

Now, considering that  $\bar{z}_g = \begin{bmatrix} x_g \\ x_s \end{bmatrix}$  and  $u_g = \Delta P_c$ , and working on (4.30a),

$$0 = \begin{bmatrix} A_g^d - I & D_g(\Delta t)A_{gs}^c \\ D_s(\Delta t)A_{sg}^c & A_s^c - I \end{bmatrix} \begin{bmatrix} x_g \\ x_s \end{bmatrix} + \begin{bmatrix} D_g(\Delta t)B_g^c \\ 0 \end{bmatrix} \Delta P_c + \begin{bmatrix} 0 \\ D_s(\Delta t)E_s^c \end{bmatrix} \Delta P_L.$$

Substituting in the steady-state  $x_g = \begin{bmatrix} \Delta P_G \\ \Delta P_M \end{bmatrix} = \begin{bmatrix} \Delta P_L \\ \Delta P_L \end{bmatrix}$  and  $u_g = \Delta P_c = \Delta P_L$ , we get

$$\begin{aligned} 0 &= (A_g^d - I) \begin{bmatrix} \Delta P_L \\ \Delta P_L \end{bmatrix} + D_g(\Delta t)B_g^c \Delta P_L \\ 0 &= D_s(\Delta t)A_{sg}^c \begin{bmatrix} \Delta P_L \\ \Delta P_L \end{bmatrix} + D_s(\Delta t)E_s^c \Delta P_L. \end{aligned}$$

If forward Euler discretization is employed, these equations become

$$\begin{aligned} 0 &= \Delta t A_g^c \begin{bmatrix} \Delta P_L \\ \Delta P_L \end{bmatrix} + \Delta t B_g^c \Delta P_L \\ 0 &= \Delta t A_{sg}^c \begin{bmatrix} \Delta P_L \\ \Delta P_L \end{bmatrix} + \Delta t E_s^c \Delta P_L, \end{aligned}$$

which for  $\Delta t > 0$  become independent of the sampling time  $\Delta t$ :

$$\begin{aligned} 0 &= A_g^c \begin{bmatrix} \Delta P_L \\ \Delta P_L \end{bmatrix} + B_g^c \Delta P_L \\ 0 &= A_{sg}^c \begin{bmatrix} \Delta P_L \\ \Delta P_L \end{bmatrix} + E_s^c \Delta P_L, \end{aligned}$$

(The same result would arise with the mixed Euler–ZOH discretization.)

Verification that the right-hand sides are equal to zero follows immediately by insertion of the continuous-time matrices:

$$\begin{aligned} \begin{bmatrix} -1/T_g & 0 \\ 1/T_t & -1/T_t \end{bmatrix} \begin{bmatrix} \Delta P_L \\ \Delta P_L \end{bmatrix} + \begin{bmatrix} 1/T_g \\ 0 \end{bmatrix} \Delta P_L &= 0 \\ \begin{bmatrix} 0 & 1/M \end{bmatrix} \begin{bmatrix} \Delta P_L \\ \Delta P_L \end{bmatrix} + \begin{bmatrix} -1/M \end{bmatrix} \Delta P_L &= 0. \end{aligned}$$

This establishes that  $(\Delta P_G, \Delta P_M, \Delta \omega) = (\Delta P_L, \Delta P_L, 0)$  is an equilibrium of (4.19a) and (4.20a). What remains to be shown is that  $(\Delta \omega, \Delta P_B, SOC_B) = (0, 0, \overline{SOC}_B)$  is *not* an equilibrium of (4.19)b but it is an equilibrium of (4.20)b.

Starting from (4.30b), and considering that  $\bar{z}_b = \begin{bmatrix} x_s \\ x_b \end{bmatrix}$  and  $u_b = \Delta P_{cb}$ , we substitute in the steady-state values  $x_b = \begin{bmatrix} \Delta P_B \\ SOC_B \end{bmatrix} = \begin{bmatrix} 0 \\ \overline{SOC}_B \end{bmatrix}$ ,  $x_s = \Delta \omega = 0$  and  $u_b = \Delta P_{cb} = 0$ :

$$0 = \begin{bmatrix} A_s^d - I & D_s(\Delta t)A_{sb}^c \\ 0 & A_b^d - I \end{bmatrix} \begin{bmatrix} 0 \\ 0 \\ \overline{SOC}_B \end{bmatrix} + \begin{bmatrix} 0 \\ D_b(\Delta t)B_b^c \end{bmatrix} 0 + \lambda \begin{bmatrix} D_s(\Delta t)E_s^c \\ 0 \end{bmatrix} \Delta P_L$$

which implies

$$\begin{aligned} 0 &= D_s(\Delta t)A_{sb}^c \begin{bmatrix} 0 \\ \overline{SOC}_B \end{bmatrix} + \lambda D_s(\Delta t)E_s^c \Delta P_L \\ 0 &= (A_b^d - I) \begin{bmatrix} 0 \\ \overline{SOC}_B \end{bmatrix}. \end{aligned}$$

This time assuming mixed Euler–ZOH discretization—although the result is independent of the discretization scheme—we get, for the right-hand side expressions,

$$-(M/D) \left( e^{-(D/M)\Delta t} - 1 \right) \begin{bmatrix} 1/M & 0 \end{bmatrix} \begin{bmatrix} 0 \\ \overline{SOC}_B \end{bmatrix} + \lambda(M/D) \left( e^{-(D/M)\Delta t} - 1 \right) (1/M) \Delta P_L$$

and

$$\begin{bmatrix} e^{-(1/T_b)\Delta t} - 1 & 0 \\ T_b(1 - e^{-(1/T_b)\Delta t}) & 0 \end{bmatrix} \begin{bmatrix} 0 \\ \overline{SOC}_B \end{bmatrix}.$$

It is easily verified that the latter expression is identically zero, and the former expression is zero if and only if  $\lambda \Delta P_L = 0$ ; that is, if and only if  $\lambda = 0$  when  $\Delta P_L \neq 0$ .  $\square$

#### 4.9.4 Lemma 2

*Proof.* The simplest way to proceed in lemma 2 is to consider the continuous-time subsystems and establish reachability of these; reachability of their discretized counterparts then readily follows<sup>1</sup>.

Consider first the pair  $(\tilde{A}_g^c, \tilde{B}_g^c)$ :

$$\tilde{A}_g^c = \begin{bmatrix} A_g^c & A_{gs}^c \\ A_{sg}^c & A_s^c \end{bmatrix} \quad \text{and} \quad \tilde{B}_g^c = \begin{bmatrix} B_g^c \\ 0 \end{bmatrix}$$

The order of  $\tilde{A}_g^c$  is three; therefore, we need to check the rank of the matrix

$$\mathcal{R}_g = \begin{bmatrix} \tilde{B}_g^c & \tilde{A}_g^c \tilde{B}_g^c & \tilde{A}_g^c \tilde{A}_g^c \tilde{B}_g^c \end{bmatrix}.$$

Then

$$\mathcal{R}_g = \begin{bmatrix} 1/T_g & -1/T_g^2 & 1/T_g^3 \\ 0 & 1/(T_g T_t) & -1/(T_g T_t^2) - 1/(T_g^2 T_t) \\ 0 & 0 & 1/(M T_g T_t) \end{bmatrix},$$

the determinant of which is

$$\det \mathcal{R}_g = \frac{1}{M T_g^3 T_t^2}.$$

This is non-zero for all finite  $M, T_g, T_t$  and hence the pair  $(\tilde{A}_g^c, \tilde{B}_g^c)$  is reachable for all practical systems.

A similar analysis applied to the pair  $(\tilde{A}_b^c, \tilde{B}_b^c)$  establishes the same outcome. This time,

$$\mathcal{R}_b = \begin{bmatrix} 0 & 1/(M T_b) & -D/(M^2 T_b) - 1/(M T_b^2) \\ 1/T_b & -1/T_b^2 & 1/T_b^3 \\ 0 & 1/T_b & -1/T_b^2 \end{bmatrix}$$

and the determinant of this is

$$\det \mathcal{R}_b = \frac{1}{M^2 T_b^3}.$$

This is also non-zero for all practical parameter values. □

For Lemmas 3 and 4 the proofs as in [51] where the complete detailed solutions can be derived from the text therein.

---

<sup>1</sup>see e.g. T. Hagiwara, "Preservation of reachability and observability under sampling with a first-order hold," in *IEEE Transactions on Automatic Control*, vol. 40, no. 1, pp. 104–107, Jan. 1995

### 4.9.5 Lemma 5

*Proof.* The first part of Lemma 5 is established in [51]; it is proved that a conventional linear–quadratic optimal control problem subject to polyhedral constraints has a Lipschitz-continuous value function.

In the second part, suppose  $z_i^1 \neq z_i^2$  but  $x_g^1 = x_g^2$  and  $x_b^1 = x_b^2$ ; therefore, only  $x_s^1 \neq x_s^2$  accounts for the difference between  $z_i^1$  and  $z_i^2$ . The stated bound must therefore hold, with  $L_i^s$  no greater than  $L_i$ ; if  $L_i^s$  were greater than  $L_i$  then the first inequality could not hold for all  $(z_i^1, z_i^2) \in \mathcal{Z}_{N,i} \times \mathcal{Z}_{N,i}$ .  $\square$

The upshot of this result is that if we consider the variation in  $z_i^1, z_i^2$  to arise only from a difference in frequency, a smaller Lipschitz constant may apply. This would lead to less conservative results.

### 4.9.6 Theorem 1

The proof of theorem 1 is as follows:

*Proof.* Consider some  $z_i \in \Omega_i(\bar{r}_i)$ . We have  $V_{N,i}^0((z_i^0(1))) \leq \gamma_i V_{N,i}^0(z_i) \leq \gamma_i \bar{r}_i$ . By Lipschitz continuity,

$$V_{N,i}^0(f(z_i, \kappa_{N,i}(z_i))) \leq V_{N,i}^0((z_i^0(1))) + L_i \|z_i^0(1) - f(z_i, \kappa_{N,i}(z_i))\|$$

Now consider the difference  $z_i^0(1) - f(z_i, \kappa_{N,i}(z_i))$ . The optimal one-step ahead prediction is

$$\begin{aligned} z_g^0(1) &= \tilde{A}_g z_g + \tilde{B}_g u_g^0(0) + \tilde{E}_g \Delta P_L \\ z_b^0(1) &= \tilde{A}_b z_g + \tilde{B}_b u_b^0(0), \end{aligned}$$

while the true successor states are

$$\begin{aligned} z_g^+ &= \tilde{A}_g z_g + \tilde{B}_g u_g^0(0) + \tilde{E}_g \Delta P_L + \begin{bmatrix} 0 \\ A_{sb} x_b \end{bmatrix} \\ z_b^+ &= \tilde{A}_b z_g + \tilde{B}_b u_b^0(0) + \begin{bmatrix} A_{sg} x_g \\ 0 \end{bmatrix} + \begin{bmatrix} E_s \Delta P_L \\ 0 \end{bmatrix}. \end{aligned}$$

Therefore,

$$\|z_i^0(1) - f(z_i, \kappa_{N,i}(z_i))\| = \begin{cases} \|A_{sb} x_b\| & i = g \\ \|A_{sg} x_g + E_s \Delta P_L\| & i = b \end{cases}$$

and, moreover, the difference is only in the state  $x_s$ , meaning the previous bound can be sharpened via Lemma 5 to

$$V_{N,i}^0(f(z_i, \kappa_{N,i}(z_i))) \leq \begin{cases} V_{N,g}^0((z_g^0(1)) + L_g^s \|A_{sb}x_b\| & i = g \\ V_{N,b}^0((z_b^0(1)) + L_b^s \|A_{sg}x_g + E_s \Delta P_L\| & i = b \end{cases}.$$

Now, considering that  $V_{N,i}^0((z_i^0(1))) \leq \gamma_i \bar{r}_i$ , if for some  $r_i \in (0, \bar{r}_i]$

$$L_g^s \|A_{sb}x_b\| < (1 - \gamma_g)r_g$$

and

$$L_b^s \|A_{sg}x_g + E_s \Delta P_L\| < (1 - \gamma_b)r_b$$

for all admissible  $x_b$ ,  $x_g$  and  $\Delta P_L$ , then

$$V_{N,i}^0(f(z_i, \kappa_{N,i}(z_i))) \leq \gamma_i \bar{r}_i + (1 - \gamma_i)r_b < \bar{r}_i$$

and so  $f(z_i, \kappa_{N,i}(z_i)) \in \Omega_i(\bar{r}_i)$ ; this establishes part (i).

Part (ii) is established by noting that if  $z_i(0) \in \Omega_i(\bar{r}_i) \subset \mathcal{Z}_{N,i}$  then all constraints are satisfied; the recursively feasibility result further implies that all constraints are satisfied for all time.

For part (iii), consider a  $z_i(0) \in \Omega_i(\bar{r}_i) \setminus \Omega_i(r_i)$ . Then

$$V_{N,i}^0(z_i(1)) \leq \gamma_i V_{N,i}^0(z_i(1)) + (\rho_i - \gamma_i) V_{N,i}^0(z_i(1))$$

where  $\rho_i$  is some value in  $(\gamma_i, 1)$ . Then

$$V_{N,i}^0(z_i(k)) \leq \rho_i^k \bar{r}_i$$

from which it follows that  $V_{N,i}^0(z_i(k)) \leq \bar{r}_i$  after some finite  $k'$ , and at this point the state has entered  $\Omega_i(r_i)$ .

Finally, part (iv): if each  $z_i(k) \rightarrow \Omega_i(r_i)$  then  $x = S_g z_g + S_b z_b$  converges to, and remains within, a set  $S_g \Omega_g(r_g) + S_b \Omega_b(r_b)$ .

□

### 4.9.7 Corollary 1

The proof relating to Corollary 1 is given next. These established bounds are concerned with the following off-diagonal terms.

$$A_{sb}x_b \quad \text{and} \quad A_{sg}x_g + E_s\Delta P_L$$

Expressing each of these in terms of the sampling time and system parameters:

$$\begin{aligned} A_{sb}x_b &= D_s(\Delta t)A_{sb}^c x_b \\ &= -(M/D) \left( e^{-(D/M)\Delta t} - 1 \right) \begin{bmatrix} 1/M & 0 \end{bmatrix} \begin{bmatrix} \Delta P_B \\ SOC_B \end{bmatrix} \\ &= \frac{1 - e^{-(D/M)\Delta t}}{D} \Delta P_b \end{aligned}$$

Then the bound

$$\|A_{sb}x_b\| < W_g r_g$$

becomes

$$\left\| \frac{1 - e^{-(D/M)\Delta t}}{D} \Delta P_B \right\| < W_g r_g$$

this can be reworked into the inequality in corollary 1 by noting that  $M > 0$ ,  $D > 0$ ,  $\Delta t > 0$  and so

$$\left\| \frac{1 - e^{-(D/M)\Delta t}}{D} \Delta P_B \right\| = \frac{1 - e^{-(D/M)\Delta t}}{D} \|\Delta P_B\|.$$

The forward Euler bounds follow by noting that, in that case,  $D_d(\Delta t)$  is just replaced everywhere by  $\Delta t$ . That gives  $A_{sb} = \Delta t A_{sb}^c$  and so

$$\left\| \frac{\Delta t}{M} \Delta P_B \right\| < W_g r_g$$

A similar process applied to the term  $A_{sg}x_g + E_s\Delta P_L$  results in the correct bound.

### 4.9.8 Theorem 2

*Proof.* For some  $z_i \in \Omega_i(\delta_i)$ ,  $\delta_i > 0$  sufficiently small, the optimal solution to the constrained optimal control problem is equal to that of the corresponding unconstrained problem. Thus, if  $r_i \leq \delta_i$ , for  $i \in \{b, g\}$ , the system is after some finite time controlled by linear state feedback. If Assumption 6 holds, the overall system is stable and the states converge to the target equilibrium values.  $\square$

# Chapter 5

## Hierarchical Predictive Load Frequency Control with Battery Energy Storage

### 5.1 Introduction

Future power systems are expected to be made up of both conventional and new generation technologies. The legacy grid without the presence of new sources of power generation was already a large scale complex system albeit homogeneous in nature consisting of mainly conventional generators. The integration of new power generating technologies would lead to an increase in the level of heterogeneity in the power grid. This level of diversity in power sources in the grid create changes in not only the spatial but also temporal nature of the grid. As seen in Chapter 4, in the context of load frequency control, the design of local controllers for the subsystems requires an alternative approach for independent design considering only local dynamics where the common dynamic of concern *i.e.* the frequency is made available in each local controller to ensure responsiveness of the battery system to changes in frequency. A decomposition methodology was required in this instance due to the absence of a clear system structure for model partitioning such as control areas which could then be used for local controller design.

Thus far, the centralised and decentralised architectures of MPC controllers have been used in achieving load frequency in future power systems. For non centralised control architectures distributed approaches provide optimal performances closer to the centralised performance and are therefore commonly used in the design of distributed

controllers for a systems with subsystems. Communication between controllers make it possible for them to take into account the predicted actions of their neighbours before determining their own action. The decomposition of the system is done based on spatial groupings of subsystems.

The spatial problem based decomposition however, does do not take into account what would be a temporal decomposition in future power grids. For example, in LFC when a new reference is sent to conventional generators of the thermal type, additional steam is driven into the steam chest which leads to the movement of valves controlling steam flow leading to governor action. This steam is then passed through the turbine blades at high speed leading to the rotation of the shaft attached to the turbine which then drives the generator generating electrical power. There is therefore a time constant associated with both the governor and turbine which can be seen as one timescale of operation. BESS with no rotating parts respond at faster rates than generators and therefore operate at a different timescale. A system of integrated generators and BESS can therefore be treated as a multi time-scale dynamical system having subsystems that respond at different rates.

This difference in the response speeds of generators and BESS is already changing the way LFC is implemented in certain markets. For example, in some scenarios attempts are being made to provide fast LFC signals specifically for fast responding devices see Section 1.5. Beyond this, the benefits of fast acting BESS was seen in the United Kingdom when aggregated BESS contributed to the restoration of power and the recovery of frequency [212, 213]. This was following the trip of both a wind farm and a thermal power station.

In such a multi-timescale dynamical system setting therefore an inherent feature of the state space model is that it is characterised by states that evolve at different rates. Hence states could be grouped in slow and fast states. But this means within LFC it now possible to have two timescales. The issue that arises in the application of MPC to such a system is in the selection of a single suitable sampling time for discretisation. The approaches adopted in solving circumventing this issue include adjusting the time constants of the subsystems such as in [124] or ignoring fast time constants totally [127, 131]. Hierarchical MPC accommodates multiple sampling and in this chapter hierachical multi-timescale LFC in future power grids would be addressed.

## 5.2 Hierarchical Model Predictive Control

In the design of model predictive controllers a sampling time is selected in accordance with the responsiveness of the systems dynamics. This single sampling time corresponds to an update rate linked to system behaviour. However, many industrial processes are dynamic systems which consist of multiple timescales. This can be seen in systems with slow and fast responsive states. Examples can be found in aircraft [214, 79], microgrids [78] and vehicles [80]. When such multirate systems that have been combined into a single model are sampled at a single centralised rate - usually the fastest rate, the computational burden required to solve the problem might be prohibitive.

A way this can be addressed is to adopt one sampling rate in the slow timescale with a suitable horizon which accounts for the slow states. However, if this same horizon is used for the fast states it could lead to an increase in the computational burden which might be unnecessary since the system dynamics may have settled quickly enough making the excess information redundant. In addition, the update rates of the controller is much slower than the input rate that matches the fast dynamic behaviour. Conversely, if a fast sampling rate is adopted, this could lead to degradation in the performance of the slow states due to oversampling and poor dynamic response. In addition, the mismatch relating to the update rate required for the slow states compared to that of the fast sampled system could impact performance. Adjusting the horizon to a range suitable to the long horizon leads to increased computational complexity and cost in the fast timescale. These issues relating to matching horizons and updates for multi timescale systems can be suitably handled by adopting multirate hierarchical control. This framework allows design at different sampling rates facilitating implementation based on separate horizons and update rates that match the different dynamical behaviours since now separate sampling times can be adopted creating slow and fast update models of the system.

In the context of LFC this means the fast and slow sampling can be done to match the behaviour of the BESS and generator respectively. LFC in this instance can be seen as multi timescale with the single model now sampled into slow and fast update models. The approach commonly adopted in the literature is one where the slow system at the higher level is based on economic or static optimisation problems of several minutes or hours outside the timescale of LFC [188, 187, 191].

In addition, several industrial process also display separable dynamical behaviour. A common approach adopted in solving these class of systems is the singular perturbation theory since the fast and slow dynamics are clearly separable supporting

decentralised dynamic behaviour [215–217]. Furthermore, rather than applying the singular perturbation there are hierarchical formulations that instead leverage the separable dynamic characteristic in multirate hierarchical design. Here, at the upper layer, a centralised controller working at a slower rate and based on a reduced order model of aggregated subsystems generate references for lower controllers designed for each independent subsystem sampled at a faster sampling rate [77, 82]. The key here is that the subsystems are independent and where interconnections exist they are assumed to be weak supporting decentralised approach [85]. However, for systems with non separable dynamics further considerations are required. Here the couplings between subsystems are not weak such as in thermal-electric vehicle or aircraft systems having highly coupled dynamics [218, 219]. For the case of LFC design using BESS and generators their dynamics are not directly coupled in open loop. When taking part in LFC they are linked by the system frequency. This was clearly highlighted in Chapter 4 for the design of decentralised controllers where a model decomposition methodology made it possible for the frequency dynamic to be present in both subsystem models. This overlapping decentralised lower layer control structure where the systems are linked by a common variable has not been covered in the literature.

Hence we have a system with multiple timescales in a single centralised model having subsystems that are strongly coupled. In other words, the centralised model is made up of two linear independent models which would otherwise operate independently where they not coupled by the swing equation of the area under control. Though similar applications where independent linear systems together contribute power to meet a common goal exist in industry such as in a wind farm made up of an ensemble of wind turbine generators, in this situations there is no common dynamic. In Chapter 4 this sparse structure of the power system model was exploited in the design of decentralised controllers. The pure DMPC design was implemented without any information sharing or knowledge of predicted behaviour of each subsystem. Distributed MPC can potentially be used to provide similar dynamic performance to the centralised MPC but requires communication between controllers at each time step. All these considerations lead to the contributions of this chapter:

1. propose a hierarchical LFC algorithm that for two timescale design having low and fast update models for LFC in future power grids.
2. extend the proposed hierarchical two timescale formulation to case of lower level controllers for linear subsystems linked by a common dynamic state

### 5.3 Two Layer Hierarchical LFC Structure

In this section the two layer hierarchical control structure is developed. To this end the centralised model can be represented by a linear discrete time invariant system given by:

$$\begin{aligned} x^+ &= Ax + Bu + B\tilde{P}_L \quad i.e \\ x^+ &= Ax + Bu + E^s \Delta P_L \end{aligned} \quad (5.1)$$

Which is the same centralised model used in Chapter 4. Hence the same dynamical equations for the generator turbine and governor, BESS output power and state of charge and frequency are applicable in this Chapter i.e equations (4.1), (4.2), (4.3), (4.4) and (4.5) respectively. Hence similarly  $x \in \mathbb{R}^n$  and  $u \in \mathbb{R}^m$  are, respectively, the state vector and control input vector, defined as

$$\begin{aligned} x &= [\Delta\omega \quad \Delta P_G \quad \Delta P_M \quad \Delta P_B \quad SOC]^\top, \\ u &= [\Delta P_c \quad \Delta P_{cb}]^\top. \end{aligned}$$

The following notations are used in this Chapter for ease of exposition. The nominal sampling time given by  $T$  refers to rate at which the centralised model in (5.1) is sampled and this is coincident with the fast sampling rate. The discrete time index at the nominal sampling time is  $k$ . For the model sampled at the slower sampling rate the sampling time is  $T_s$  while the corresponding discrete time index is  $k_s$ . The inputs for the slow update model is  $u^s$  and the corresponding slow update model states are  $x^s$ . The inputs derived in the slow time scale are held constant for  $v$  time steps of the nominal model equal to one sampling interval  $T_s$  of the slow model. The link between sampling intervals and timesteps of the nominal and slow update models are thus  $T_s = Tv$  and  $k = k_s v$  where  $v > 0$ . The lower level optimisation problem is solved at each time instant  $k$  while the upper layer problem is solved at each time instant  $k_s$ . For clarity the range  $\forall k \in [k, kv + v]$  refers to  $k = 0, 1, 2 \dots v$  i.e  $k \bmod v$ . Hence whenever  $k \bmod v$  equals zero corresponding to the end of one long sampling interval  $T_s$  the slow time scale model optimisation problem is solved. Within each long sampling interval  $u_s$  is held constant while  $u = u_s$ .

Following the model development procedure adopted for the integrated future grid consisting of BESS and generator subsystems, the interacting dynamics were accounted for and as result BESS was able to support generators in providing LFC services. As

was shown in Chapter 4 the model was block diagonal with the generator and BESS subsystems making up the diagonal blocks. The coupling dynamic which is the swing equation was the first state in the model corresponding to the first row of the state transition matrix before the order in which the states are arranged in the model is changed. This structure was then used in the model expansion and disaggregation procedure creating two local subsystems with states defined as  $z_g$  and  $z_b$ . These local states explicitly represented the expected dynamic behaviour of each subsystem which now receives a local frequency feedback. Assuming initially, for the purpose of hierarchical control development in this chapter there exists two disaggregated models  $\bar{z}_g$  and  $\bar{z}_b$  which exclude the coupling between both subsystems (ignoring the model disturbance for now). The inputs of these models are  $\bar{u}_g$  and  $\bar{u}_b$ . In light of this the open loop dynamics of the "interacting models" that make up the centralised model such as (5.1) can be defined by:

$$\tilde{z}_g^+ = \tilde{A}_g \tilde{z}_g + \tilde{B}_g \tilde{u}_g + \tilde{A}_{gb} \tilde{z}_b + \tilde{B}_{gb} \tilde{u}_g \quad (5.2a)$$

$$\tilde{z}_b^+ = \tilde{A}_b \tilde{z}_b + \tilde{B}_b \tilde{u}_b + \tilde{A}_{bg} \tilde{z}_g + \tilde{B}_{bg} \tilde{u}_g \quad (5.2b)$$

These decomposed models of (5.3) can be seen as the straightforward individual model of each subsystem. There is no model overlap or overlapping information in the disaggregated models. Hence the subsystems can be seen as similar to the decentralised models in Chapter 4 which when combined form the centralised model of 5.1 but with a key difference. Note the slight abuse of notation of the matrices of (5.3) where the variables all have a tilde above them. Further clarification is provided in Section 5.4.1. The proposed hierarchical structure for LFC of this system is given in Figure 5.1. The upper layer controller at each time step  $k_s$  is solved using the slower update model and the subsequent solution is used to generate references for the lower layer controller developed using the faster update model of the system.

### 5.3.1 Upper Layer Controller Design

The upper layer controller is designed based on a slow time scale model of the centralised system of (5.1). This model is sampled with a sampling rate of  $T_s$  which is equal to  $v$  times of the fast sampling rate. This yields the slow update model given by

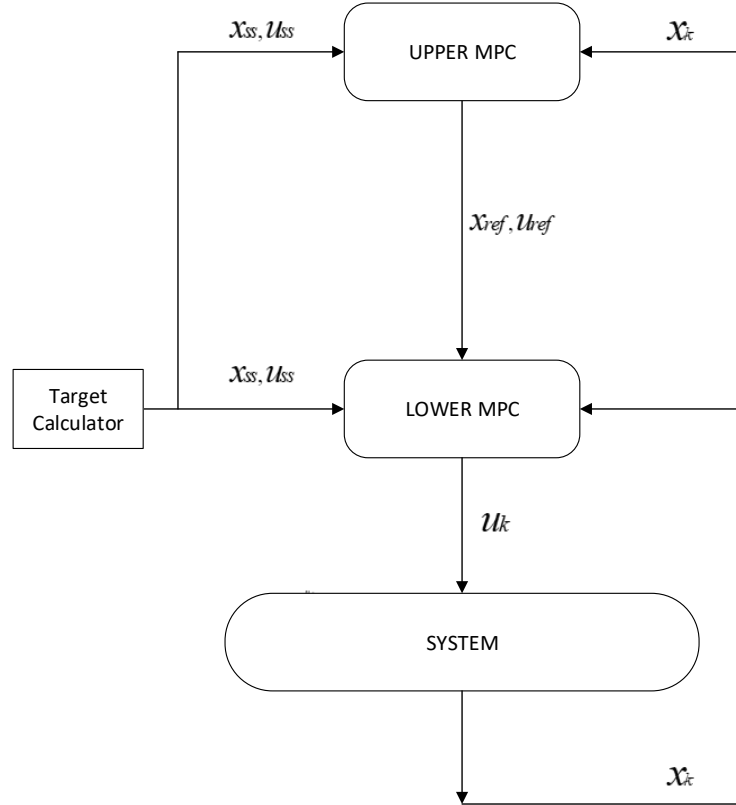


Fig. 5.1 The hierarchical control structure. The upper layer controller generates target references for the lower layer controller

$$\begin{aligned}
 x^s(k_s + 1) &= A_s x^s(k_s) + B_s u^s(k_s) \\
 y^s(k_s) &= C x^s(k_s)
 \end{aligned}
 \tag{5.3}$$

Where  $A_s = A^v$  and  $B_s = \sum_{j=0}^{v-1} A^j B$ . The slow timescale model is hence a derivative of the fast(nominal) model sampled every  $v$  samples or time steps  $k$  of the fast timescale model. This is the model used in the design of the high level controller. The optimal solution of the slow timescale model is then used in the generation of reference trajectories to tracked by the lower layer controller in the fast timescale. Therefore at this layer the system is sampled at a rate to match the slower dynamics of the centralised model and in addition acts as a trajectory planner for the lower layer controller.

This dual purpose of dynamics responsiveness and trajectory planner of the upper layer controller is achieved as follows; once the optimisation problem of the higher level model has been solved, it is now possible to generate reference state and input trajectories that are to be tracked by the lower layer controller designed using the fast update model over a shorter horizon. These references are generated over the entire length of the prediction horizon of the lower layer controller. That is the lower level controller is not required to make predictions that must end at the next update of the upper layer controller.

At the higher lever, the MPC is formulated using the same procedure described in Section 3.4. Hence a steady state target calculator is employed in solving the optimisation problem. This enables the hierarchical approach to achieve the desired steady state value for frequency required in LFC which is zero. Therefore in this problem, in order to achieve offset free tracking the prediction model employs deviation variable;  $\bar{x}^s \triangleq x^s - x_{ss}$  and  $\bar{u}^s \triangleq u^s - u_{ss}$ . The pair  $(x_{ss}, u_{ss})$  is a (non-zero) steady-state equilibrium pair associated with the measured disturbance  $EP_L$ . At this point, the higher level optimisation problem designed for the slow timescale with a horizon  $N$  can be solved. Therefore, at each slow time step  $k_s$  the following problem is solved:

$$J_U^0(\bar{u}^s) = \min_{\bar{\mathbf{u}}^s} V_U(\bar{x}^s, \bar{\mathbf{u}}^s) \quad (5.4)$$

subject to, for  $k = 0, \dots, N - 1$ ,

$$\begin{aligned} \bar{x}^s(k_s + 1) &= A_s \bar{x}^s(k_s) + B_s \bar{u}^s(k_s) \\ \bar{x}^s(0) &= \bar{x}^s(k_s) \\ \bar{u}^{s \min} &\leq \bar{u}^s(k_s) \leq \bar{u}^{s \max} \\ \bar{x}^{s \min} &\leq \bar{x}^s(k_s) \leq \bar{x}^{s \max}. \end{aligned}$$

Explicitly

$$V_N(\bar{x}^s, \bar{\mathbf{u}}^s) = \sum_{i=0}^{N-1} (\bar{x}^{s \top}(k_s + i) Q \bar{x}^s(k_s + i) + \bar{u}^{s \top}(k_s + i) R \bar{u}^s(k_s + i) + \bar{x}_N^{s \top} P \bar{x}_N^s) \quad (5.5)$$

The optimal solution to the optimisation problem of (5.5) is  $\bar{\mathbf{u}}^s$ . At each time step  $k_s$  of the upper layer the input sequence  $\bar{u}_s(k_s/k_s)$  is used in generating the reference input and state trajectories for the lower layer controller. Following this the optimisation problem is then solved again at the next time step  $k_s + 1$  equivalent to  $v$  timesteps of the lower layer controller.

### 5.3.2 Lower layer Controller Design

The lower level controllers are designed to track the references trajectories generated by the upper layer controller and are derived based on the fast update. The sampling time selected at this level is used to ensure the use of faster updates and shorter horizons corresponding to the fast system states. This sampling time is selected to coincide with the sampling time used for the nominal system model and to which the inputs generated at this level are applied. The model used for the controller at this level in the centralised case is

$$x(k+1) = Ax(k) + Bu(k) \quad (5.6)$$

Whenever the high level controller solves the slow update model problem at each time  $k_s$  the higher level input sequence  $\bar{\mathbf{u}}_s$  is available. The reference states and input over the horizon of fast update model are then generated using this sequence. Note that each input  $u_{k_s/k_s}^s$  is held constant over the long sampling interval corresponding to  $v$  time steps of the lower input. That is for the range  $k \in [k, k+v)$ . This ensures coordinated control actions between the upper and lower layers of the hierarchical structure. Without this reference generation and tracking coordination would be lost between both layers and the structure becomes decentralised.

A common approach adopted for the lower layer control in hierarchical MPC structures is for the lower layer controller to be designed using a shrinking horizon where the length of the prediction decreases as the time step of the lower layer increases. In such applications the length of the lower horizon is equal to  $v$  time steps *i.e* one sampling time  $T_s$  of the slow update model. This is the approach adopted in [85, 77, 82]. However, this means that there is an assumption that the system dynamics must have settled within the single sampling interval of the slow time scale model. Such an approach could for example be useful for mission critical based applications such as in [79]. However, this induces conservativeness and possibly rigorous control if the states are far from their target. This is because for coordination between both layers the state of the fast update model must terminate at  $x_{k_s+1/k_s}^s$  the next update of the upper layer controller. While it is possible to reduce this conservativeness by selecting a higher value of  $v$  this is highly dependent on practical considerations relating to the actual slow and fast models/states. Hence, in this approach the horizon of the lower layer  $N > v$ . Therefore  $N$  can be selected to have the same number of time steps for both layers after discretisation.

The references generated by application of the upper layer inputs to the fast update model over the short horizon can be fixed. However, since they are generated by applying the upper layer input sequence  $\bar{\mathbf{u}}^s$  this means the references shift with the input applied at each time  $k$  of the lower layer within one sampling interval  $T_s$  of the slower update model. This means that the references shift forward a step for each application of the upper layer input used in deriving references for the lower layer controller. Recall that  $u_{k+i} = \bar{u}_{k_s}^s \forall k = k_s v, \forall i \in [1, v-1]$  and that at the lower layer  $N > v$ . This means at each time over this range after applying the input at step  $k$ , at timestep  $k+1$  the generated references are shifted one step ahead to  $N+1$ . This shifting process continues until  $v-1$  within the long sampling interval while range of the reference moves to  $N+v-1$ . To accommodate this shifting for each fixed input of  $\bar{u}_{k_s}^s$  entire reference ranges of the states and inputs vectors to be tracked at the lower layer are  $(N+n)v$  and  $(N+m)v$  respectively. This provides references relating to the system behaviour at each sampling time of the applied input  $\forall i \in [1, v-1]$  over each long sampling time interval rather than this ranges being fixed.

Hence the optimisation problem at lower level over a horizon  $N$  is then given by

$$J_L^0(\bar{u}) = \min_{\bar{\mathbf{u}}} V_L(\bar{x}, \bar{\mathbf{u}}) \quad (5.7)$$

subject to, for  $k = 0, \dots, N-1$ ,

$$\begin{aligned} \bar{x}(k+1) &= A\bar{x}(k) + B\bar{u}(k) \\ \bar{x}(0) &= \bar{x}k \\ \bar{u}^{\min} &\leq \bar{u}(k) \leq \bar{u}^{\max} \\ \bar{x}^{\min} &\leq \bar{x}(k) \leq \bar{x}^{\max}. \end{aligned}$$

Explicitly

$$V_L(\bar{x}, \bar{\mathbf{u}}) = \sum_{i=0}^{N-1} (\bar{x}^\top(k+i)Q\bar{x}_{k+i} + \bar{u}^\top(k+i)R\bar{u}(k+i)) + \bar{x}_N^\top P\bar{x}_N \quad (5.8)$$

The multirate hierarchical procedure is given in Algorithm 5.1. There are several ways of ensuring coordination between the upper and lower layers in any hierarchical MPC formulation. For example, an economic optimisation problem could be solved at the higher level in the slow time scale to generate the tracking references for the lower level [77, 187]. In other cases a combination of the inputs from both layers is applied directly to the system. Output references are then derived by applying the

---

**Algorithm 1** Algorithm 5.1 Hierarchical MPC Procedure for multirate System
 

---

1. **Parameters:**  $k, k_s, k_{s1}, n \in \mathbb{N}$ .
  2. **Initialisation:** Initialise both controllers  $k, k_s = 0; x^s(k_s/k_s), x(k/k) = x(0)$ . Initialise inner loop counters  $k_{s1} = k_s$ , the lower count update and set  $n = 1$  which selects  $u^s(k_s/k_s)$
  3. **Steady State Target Calculation:** Solve the steady state equations to obtain  $x_{ss}, u_{ss}$ . The values obtained are used at both levels of the hierarchical structure ensuring consistency.
  4. **Higher layer Control Problem:** At time  $k$  equal to 1, set  $k_s$  equal to 1 and solve the optimisation problem (5.4) to obtain the sequence  $\bar{u}^s \forall i \in [0, N - 1]$  of the higher layer control output over the long horizon.
  5. **Reference Trajectory Generation:** Generate the references trajectories to be tracked by the lower layer controller.
    - (a) For all  $i \in [1, v]$  apply  $u_{k_s}^s$  to (5.1), generating state and input references for one sampling interval  $T_s$  incrementing  $k_{s1}$  at each time  $i$ .
    - (b) If  $k_{s1} > v$  reset  $k_{s1}$  to 1 and increment  $n$  by 1 to select  $u_{k_s+1}^s$
    - (c) Repeat procedure to generate references  $x_{ref}, u_{ref}$  of length  $(N + v)n$  and  $(N + v)m$  for the states and inputs respectively. This process generates additional lengths of  $nv$  and  $mv$  to support range shifting for each sampling interval  $T_s$ .
  6. **Reference Selection:** Extract references  $x_{ref}, u_{ref}$  at time  $k$  corresponding to the length  $Nn$  and  $Nm$ . Increase  $k_s$  by 1.
  7. **Communication of References:** Communicate the  $x_{ref}$  with range  $x_{ref} \in k, k + 1, \dots, N$  and  $u_{ref} \in k, k + 1, \dots, N - 1$  to the lower controller.
  8. **Lower Level Controller Problem:** Solve the lower level optimisation (5.4) at time  $k, \forall k \in [k, \dots, k + N - 1]$  and apply  $u_{k/k}$  to the system.
  9. **System Update:** Update  $x_{k+1}$  and set  $k = k + 1$  i.e  $k \leftarrow k + 1$
  10. **Repeat Lower Control Problem:** Repeat the lower control problem incrementing  $k_s, k_{s+1}, \dots \forall i \in [k, \dots, kv]$ . At each time  $k$  shifting the reference ranges for both the states and inputs at time  $k, k + 1, \dots, v$  by  $n, 2n, \dots, vn$  and  $m, 2m, \dots, vm$  respectively.
  11. **Reset Upper Counter:** If  $k_s > v$  reset  $k_s$  to 1 and repeat steps 2, 3, 4, 5, 6, 7, 8, 9.
-

slow update inputs to the fast update model [85, 82]. Depending on the application a suitable coordination strategy can be adopted. What is important in implementation is that there should be a way to achieve coordination between both levels otherwise the problem reduces to decentralised or distributed control in the absence of coordination between layers.

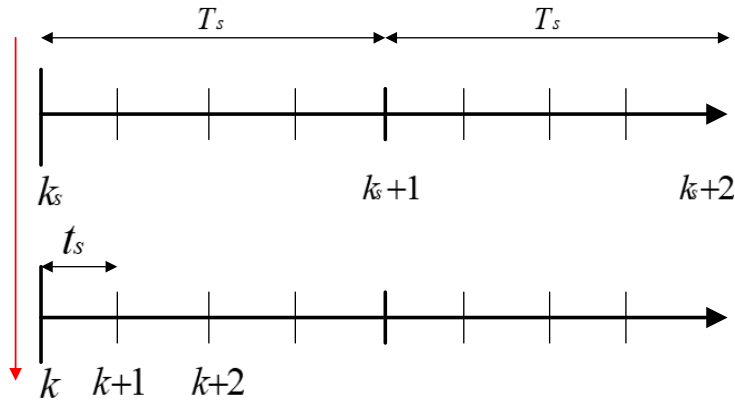


Fig. 5.2 Depiction of the connection between both timescales. The slow timescale is  $k_s$  with sampling interval  $T_s$  for the upper layer while the fast timescale coincident with that of the nominal model is  $k$  with sampling interval  $T$ . Hence  $T_s = Tv$  and  $k = k_s v$ . Red lines indicate the direction of information flow.

In the case of Algorithm 5.1 the approach adopted is similar to reference tracking. However, there is some subtlety required as a result of the multirate nature of the system. In order to ensure consistency on account of the different sampling times used for both control layers there is an inherent input connection accounted for applying a zero order hold for each sampling interval of the slow time scale and using this to generate lower layer tracking references over  $v$  sampling times of the lower layer. This is similar to the methodology used in [85]. This process enables can be referred to as resampling with a difference that here only the lower layer inputs are applied to the system. In this way despite the differences in horizon lengths, consistency between both layers is therefore maintained by tracking the input references at the lower layer. In this way the multirate dynamic behaviour of the system states is consistently accounted for including any interactions between these subsystems is handled. This means systems with clearly separable dynamics can also be handled while accounting for any common dynamic that serves as a link between slow and fast states. From the schematic diagram of the hierarchical structure shown in Figure 5.1 it can be seen

that the optimal inputs generated at the lower levels are applied directly to the system under control.

In terms of communication the method adopted here is a top down design approach which means the successful implementation of the algorithm is dependent on the ability of the upper layer controller to correctly produce feasible trajectories for the lower layer to follow. Hence communication is one way and there is no flow of information from the lower to the upper layer controller. In future power grids where it is envisaged there would be large data flows which could improve controller decision making the ability to provide only key required data could free up bandwidth for other critical control functions.

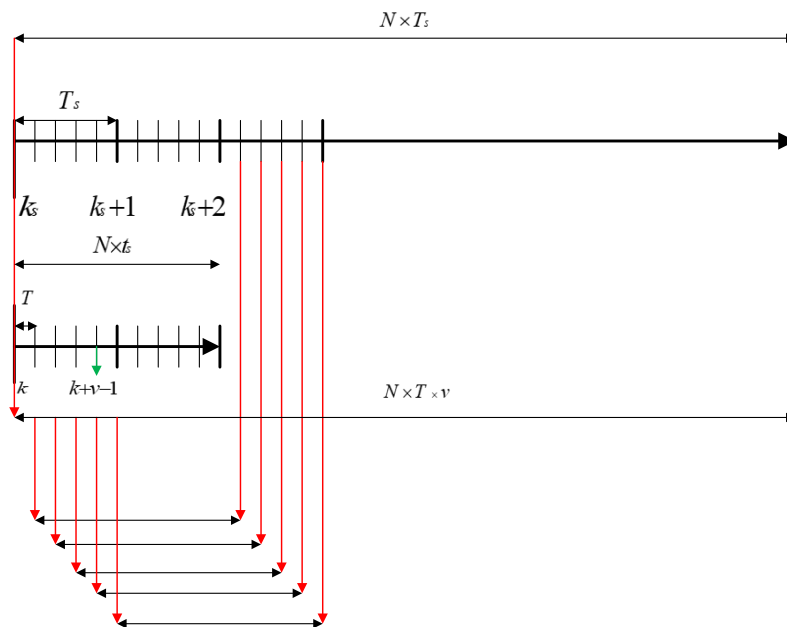


Fig. 5.3 The shifting procedure used to calculate the references for each hold of the upper layer input for  $v$  number of time steps of the lower layer input

In addition it is worth noting some specific features of the current algorithm relating to how the disturbance is accounted for in the control structure. From Figure 5.1 the steady state target values are available to both the upper and lower layer controllers. Therefore at both levels the MPC is designed using deviation variables similar to the approach adopted in this thesis as indicated in Chapter 3. However, the solution to optimal upper level input used in generating the references for the lower layer controller is not  $u_k^s$  but  $\bar{u}_k^s$ . Since the solution to the optimisation problem at the lower layer is also in deviation variables *i.e.*  $\bar{u}_k = u_k - u_{ss}$  and  $\bar{x}_k = x_k - x_{ss}$  the

references coming from the upper controller should also be in deviation variables. Hence  $\bar{u}_{ref,k} = u_k - u_{ss}$  and  $\bar{x}_{ref,k} = x_k - x_{ss}$ . Therefore at the lower level let  $\tilde{u}_k = \bar{u}_k - \bar{u}_{ref,k}$  and  $\tilde{x}_k = \bar{x}_k - \bar{x}_{ref,k}$ . This means the deviation variables at the lower level can be expressed instead as  $\tilde{u}_k = u_k - u_{ss}$  and  $\tilde{x}_k = x_k - x_{ss}$  where  $\bar{u}_k$  and  $\bar{x}_k$  have been replaced by  $\tilde{u}_k$  and  $\tilde{x}_k$  respectively. Which can also be interpreted as  $\bar{u}_k - \bar{u}_{ref,k} = u_k - u_{ss}$  and  $\bar{x}_k - \bar{x}_{ref,k} = x_k - x_{ss}$  at each time  $k$ . Note that  $\bar{x}_{ref}$  and  $\bar{u}_{ref}$  are vectors.

A further remark is appropriate at this stage regarding the trajectories tracked by the lower level controller explaining shifting. From Algorithm 5.1 the references are not fixed as explained previously but are shifted at each time step  $k$  when the lower layer optimisation problem is solved. The references are calculated using  $\bar{u}_k^s$  over  $i \in [k, \dots, k + Nv]$ , where  $Nv = (N + n)v$  which uses information available over an additional horizon corresponding to one sampling interval  $T_s$  of the slow timescale. This process is depicted in Figure 5.3 and shows how by shifting the reference information generated at time  $k, k + 1, \dots, k + v$  changes for each time step as calculations progress forward in the horizon.

### 5.3.3 Clarification of Open Loop Dynamic Behaviour

In Chapter 4 decentralised controllers were designed following the model disaggregation process which created subsystems representative of the true dynamic of both BESS and generators. However, both subsystems were connected by a common state; the frequency dynamic. For the power system model if the process of disaggregation does not include the common state the interaction is lost. To gain further insight the disaggregated model structure is used to provide clarification. Earlier on (5.2) repeated here for readability defined the disaggregated submodels without swing dynamics as (now expressed in decentralised prediction form)

$$\tilde{z}_g^+ = \tilde{A}_g \tilde{z}_g + \tilde{B}_g \tilde{u}_g \quad (5.9a)$$

$$\tilde{z}_b^+ = \tilde{A}_b \tilde{z}_b + \tilde{B}_b \tilde{u}_b \quad (5.9b)$$

The models in Chapter 4 were (also in the decentralised prediction form)

$$z_g^+ = \tilde{A}_g z_g + \tilde{B}_g u_g \quad (5.10a)$$

$$z_b^+ = \tilde{A}_b z_b + \tilde{B}_b u_b \quad (5.10b)$$

In these models while equation (5.9) contains the common state,(5.10) does not. If there was no swing dynamic each system would act independently in supplying power. Therefore we that the dynamics of both subsystems are linked by the common frequency dynamic and because of this they become exhibit coupled behaviour. This implies that without the frequency both systems are essentially decoupled but since they connected and synchronised (BESS respond to frequency changes) with the grid they are coupled. By extension if the BESS power is excluded from the frequency dynamic both systems become entirely decoupled and the generators alone would be responsible for LFC. BESS become uncontrollable loads. To demonstrate the effect of the swing coupling an open loop step response of the power system has been simulated and the results are shown in Figure 5.4. The parameters are similar to those used in Section 4.7.

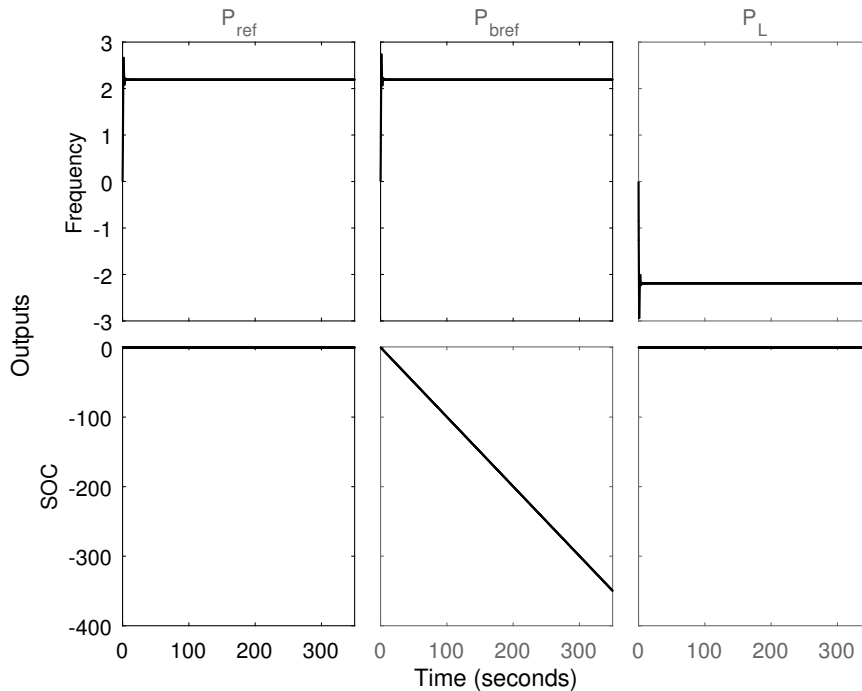


Fig. 5.4 Open loop step response of the power system dynamic to a load disturbance

In Figure 5.4  $P_{ref}$ ,  $P_{bref}$  and  $P_L$  are the generator, BESS and disturbance inputs respectively. The outputs are frequency and state of charge. The generator input has no effect on the BESS state of charge. However both inputs affect frequency indicating they are coupled by this dynamic. The effect of  $P_L$  leads to a drop in frequency. Both subsystems generate inputs that in open loop respond equally to compensate for this drop in frequency.

## 5.4 Numerical Simulations

In this section numerical simulations are carried out to demonstrate the proposed algorithm and its suitability for use in a power systems consisting of states which can be categories into slow and fast states. This is something that has rarely been considered in the literature. For most applications of MPC with a BESS integrated into the grid, the requirements for different sampling rates is simplified by either selecting the sampling time in such a way that the faster dynamics are ignored or by assuming BESS time constants which put their timescale close to the that of generators. The proposed multirate hierarchical structure is used in simulating a power system using time constants for the BESS and generators that clearly differ in magnitude. The LFC problem is thus tackled in this setting.

### 5.4.1 Impact of Shifting and Multirate sampling

First of all the effect of shifting is demonstrated. The parameters used for the simulation are given in Table 5.1

$D$ (pu/Hz)	$2H$ (pu s)	$R$ (Hz/pu)	$T_G$ (s)	$T_T$ (s)	$Tb$ (s)
0.083	0.17	2.22	0.2	2.00	0.15

Table 5.1 Parameters of the power system

The output power of both subsystems constitute their interactions and are captured in the frequency dynamic. The rated capacity of the simulated power system is  $Pr = 2000\text{MW}$  on a  $2000\text{MVA}$  base. The capacity of the BESS is  $10\text{MW}/40\text{MWh}$  large enough to affect the system frequency when charging or discharging and actively affecting LFC performance.

The sampling time of the slow time scale model used in the design of the upper layer controller is  $0.7\text{s}$  with a horizon of 50. A sampling rate of  $0.07\text{s}$  was selected for the nominal model. Hence  $v$  is equal to 10. The values used for  $Q$  and  $R$  were the same at both levels with  $Q = \text{diag}[10, 0.01, 10, 0.01, 10]$  and  $R = \text{dia}[1, 1]$ .

From Figure 5.5 the application of shifting increased speed of the frequency dynamic hence LFC is significantly improved with a faster response without compromising the performance of generator and BESS subsystems which can be seen in Figures 5.6 and 5.7 respectively. The BESS dynamics are also improved as compared to the when fixed references are used. The rippling effect on both the frequency and BESS dynamics do not appear with shifting and the state of charge shows less of an overshoot.

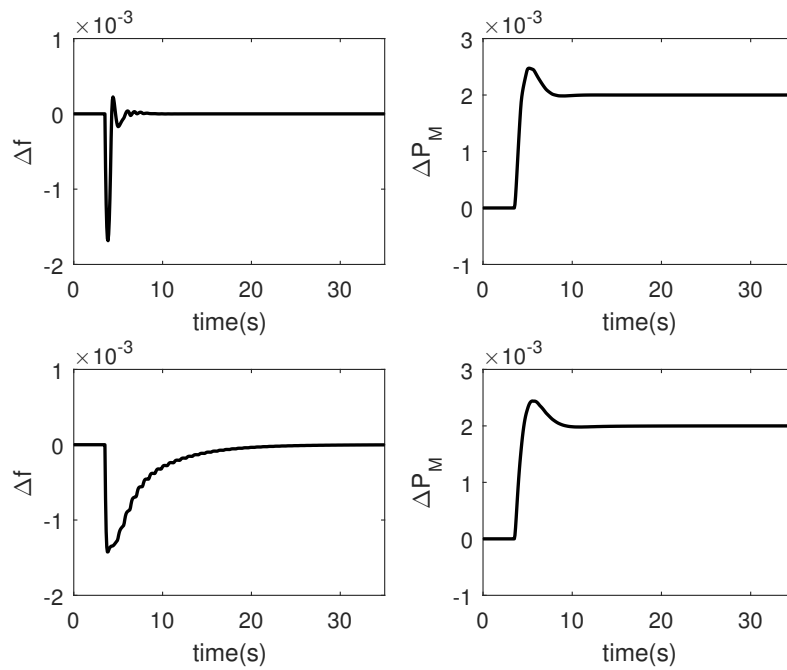


Fig. 5.5 The effect of shifting on the frequency and generator output. Top shifting, bottom no shifting.

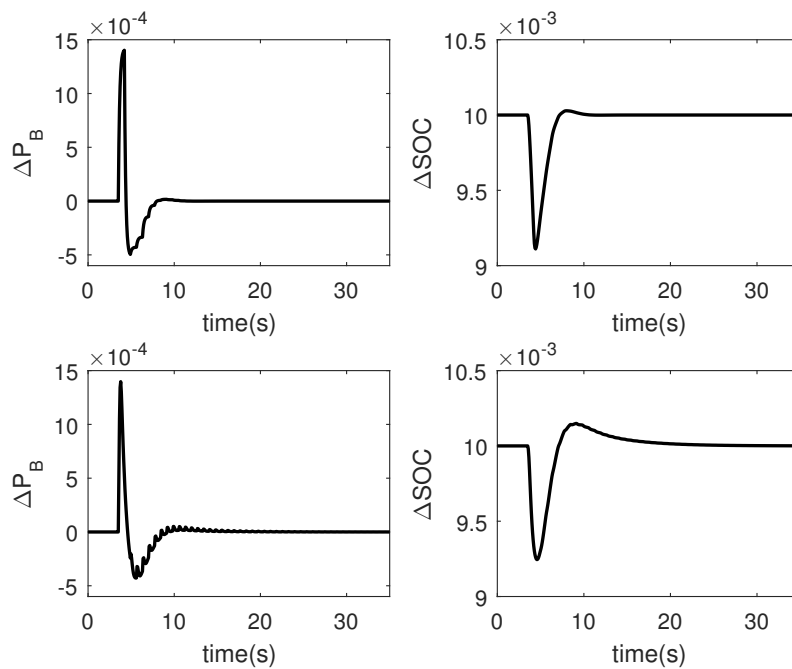


Fig. 5.6 The effect of shifting on battery performance. Top shifting, bottom no shifting.

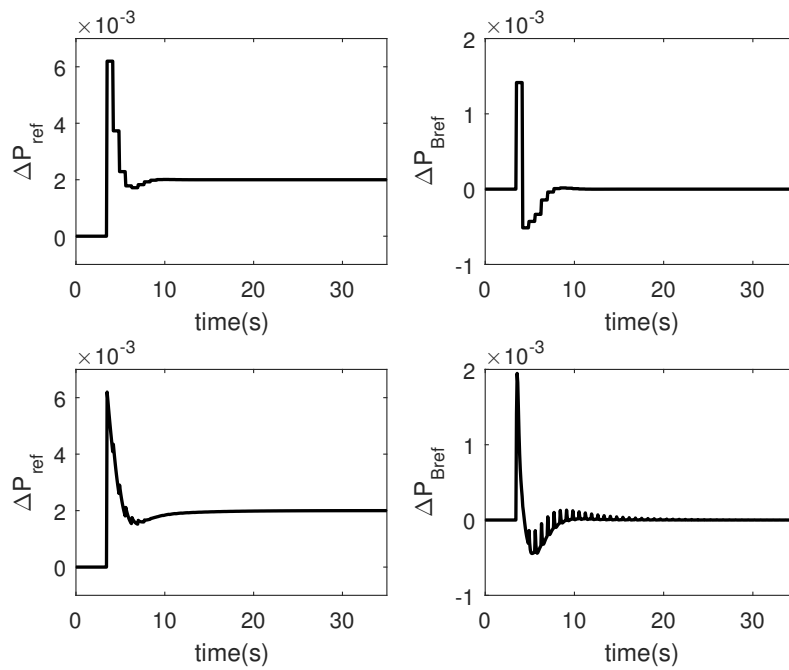


Fig. 5.7 The effect of shifting on system inputs. Top with shifting, bottom no shifting.

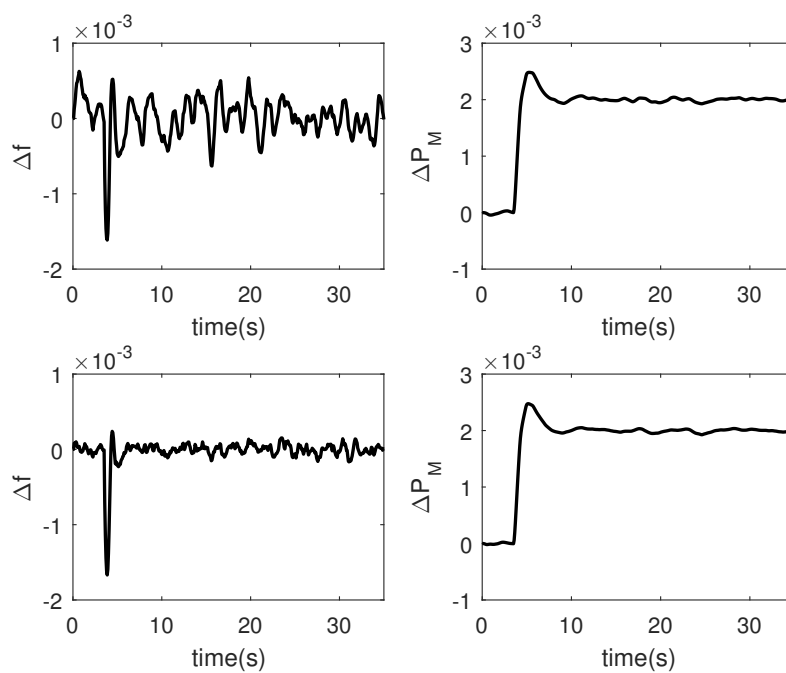


Fig. 5.8 The effect of noise on BESS system on frequency and generator output. Top: high level input only. Bottom: hierarchical input

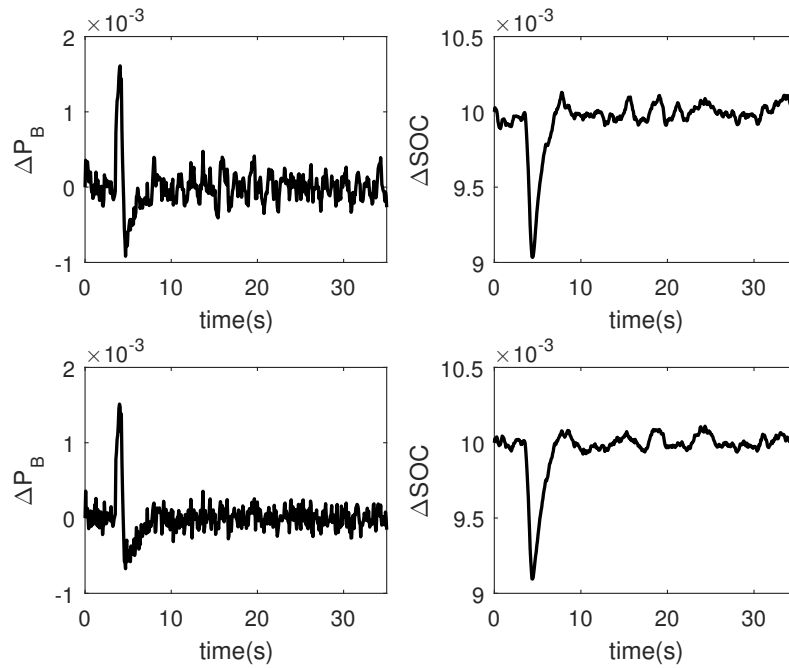


Fig. 5.9 The effect of noise on BESS systems. Top: high level input only, bottom: hierarchical input

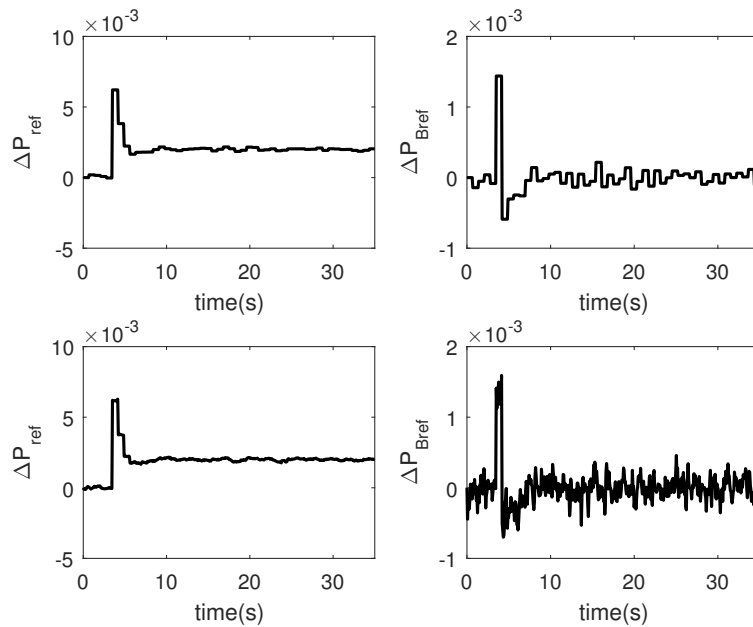


Fig. 5.10 The effect noise on the BESS system on both its and the generators inputs. Top: high level input only. Bottom: hierarchical input.

In addition, in order to show the impact of variable rate sampling a simulation is carried out comparing the dynamical response of the system when the BESS is subjected to a normal randomly distributed noise. The results show the system dynamics when only the higher level input and when the hierarchical inputs are applied to the system.

Figure 5.8 shows that when only the high level input is applied to the system, the frequency is more susceptible to the high frequency noise while the response obtained using the hierarchical control input shows better handling of the unmeasured high frequency noise. For the BESS responses due to the higher sampling the high frequency noise impact is now more visible which can be seen in Figures 5.9 and 5.10 respectively.

### 5.4.2 Hierarchical Load Frequency Control

In this section the effectiveness of the proposed hierarchical approach is compared against a centralised control design subject to slow and fast sampling rates corresponding to the response speed of the slow and fast states. For the purposes of this simulation the same area and BESS capacities including the horizons of section 5.4.1 are used.

In the design of the hierarchical controller the slow time scale sampling time 0.25s. The value used in the design of the lower layer controller is 0.05s. Hence  $v$  is equal to 5. The values used for  $Q$  and  $R$  in both control structures *i.e* centralised and hierarchical were the same. This was also the case at both levels of the hierarchical controllers with  $Q = \text{diag}[100, 0.01, 0.01, 0.01, 100]$  and  $R = \text{diag}[1, 1]$ . The parameters used for the simulation are given in Table 5.2.

$D$ (pu/Hz)	$2H$ (pu s)	$R$ (Hz/pu)	$T_G$ (s)	$T_T$ (s)	$Tb$ (s)
0.083	1.34	2.22	0.1	0.55	0.1

Table 5.2 Parameters of the power system

The disturbance sequence used in the simulation is given in Figure 5.11. An values of the input constraints of the generator and BESS were set to  $0.0045pu$  and  $0.002pu$  respectively. The BESS power is constrained between  $0.005pu$  and  $-0.005pu$  while for the state of charge it is between  $0.004pu$  and  $0.016pu$  corresponding to a range of 20% – 80% percent. The results compare the performance of centralised sampled at the  $0.7s$ (slow), centralised sampled at  $0.07s$ (fast) and the hierarchical MPC labelled as CMPC, FCMPC and HMPC respectively. A prediction horizon of 50 times steps is used in all instances. The frequency deviation and generator output plots are shown in Figure 5.12. Here we see that the trajectories of both the CMPC and HMPC are similar. However, the FCMPC does not track as well as the other MPCs due to

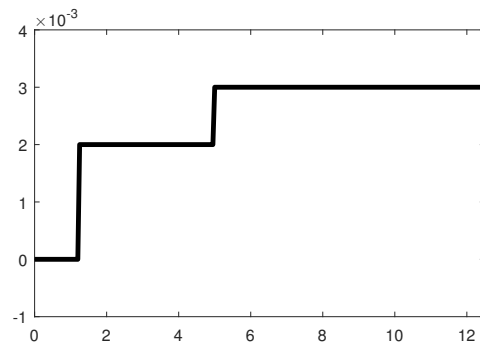


Fig. 5.11 The disturbance sequence

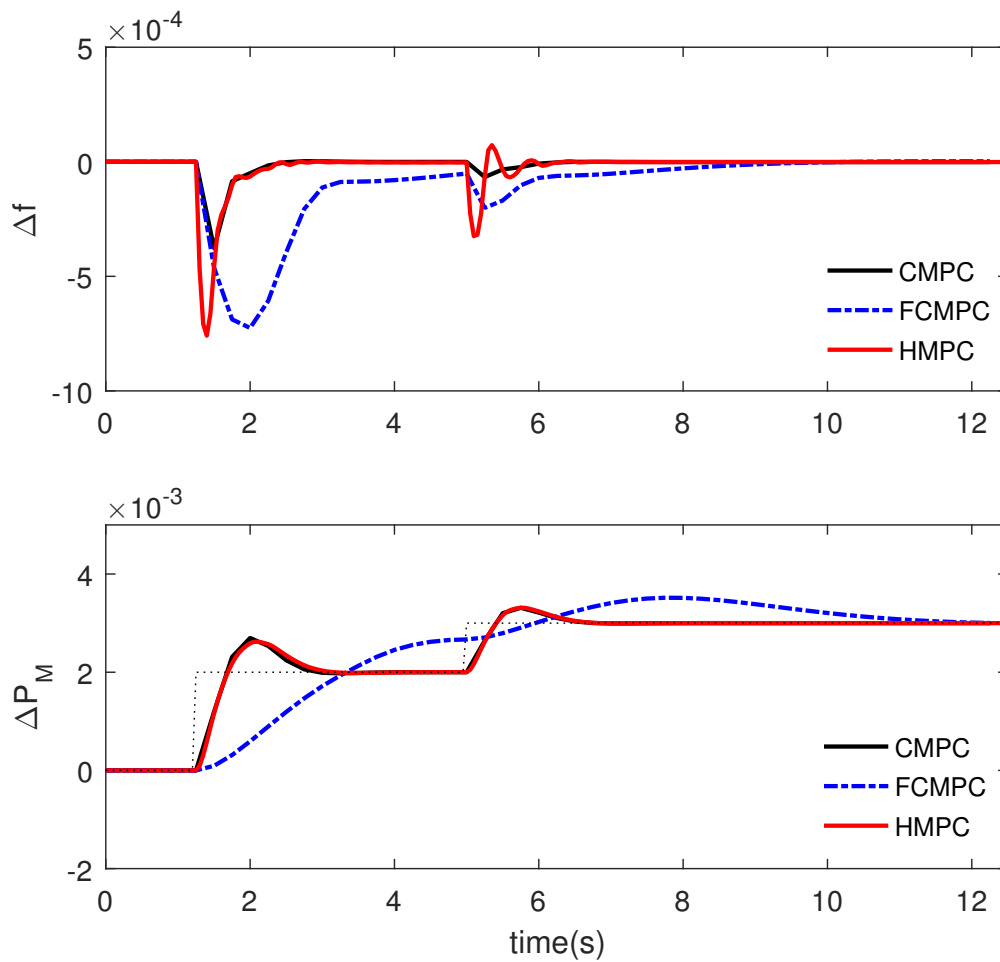


Fig. 5.12 Frequency deviation and generator outputs comparing centralised and hierarchical control

the sampling rate employed. Without a hierarchical controller providing references

using a long horizon at the upper layer, employing a faster sampling rate only to the nominal model reduces prediction horizon affecting dynamic performance. Hence the responsiveness of the generator is reduced and this is reflected in the ability of the controller to reduce the frequency deviation to zero. This match the benchmark performance using FCMPC longer prediction horizons are required. This would increase the computational requirements and cost.

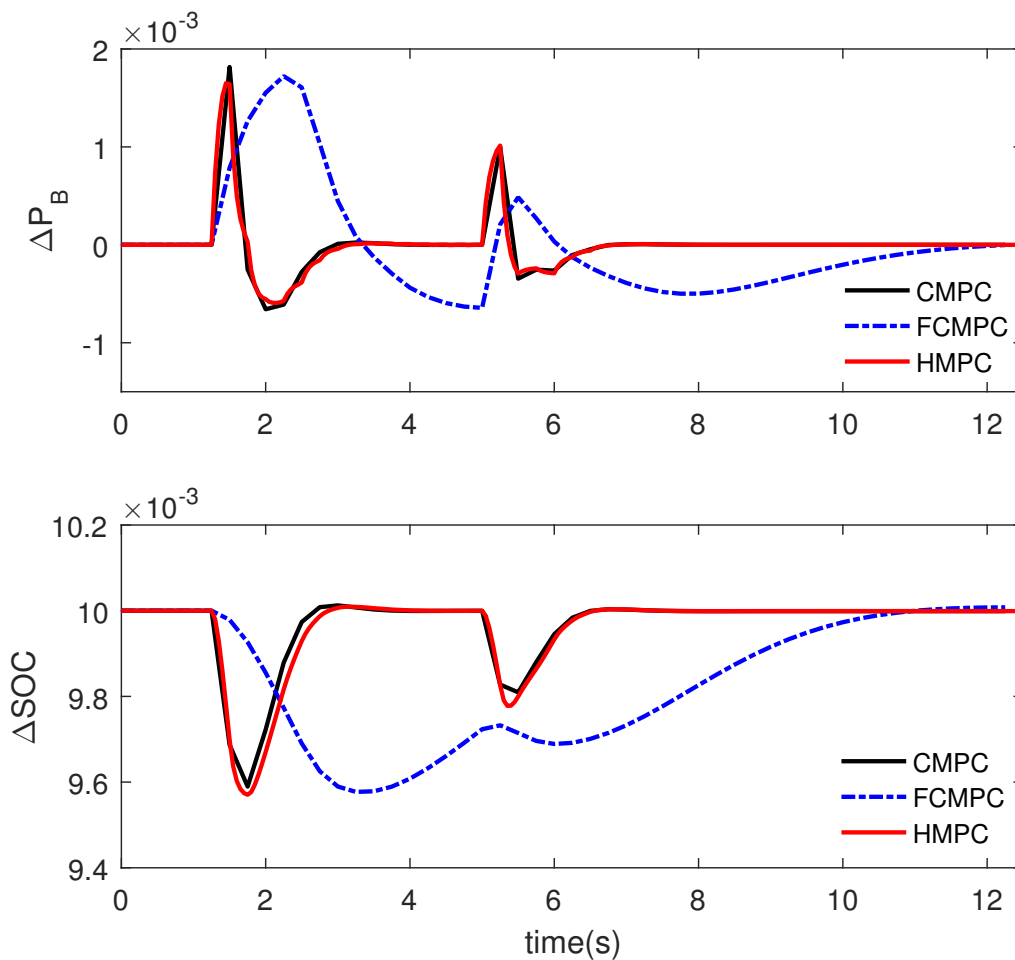


Fig. 5.13 Battery dynamics for centralised and hierarchical control

The performance of the BESS using the different MPC configurations is shown in Figure 5.13. The results in this case also indicate that the performances of the CMPC and HMPC are similar with the HMPC slightly faster than the CMPC. The FCMPC also displays undesirable transient behaviour. Figure 5.14 compares the generator and BESS inputs. Again the responses of both the CMPC and HMPC are similar. The FCMPC dynamic shows a noticeable deviation from the other MPCs and is driven to

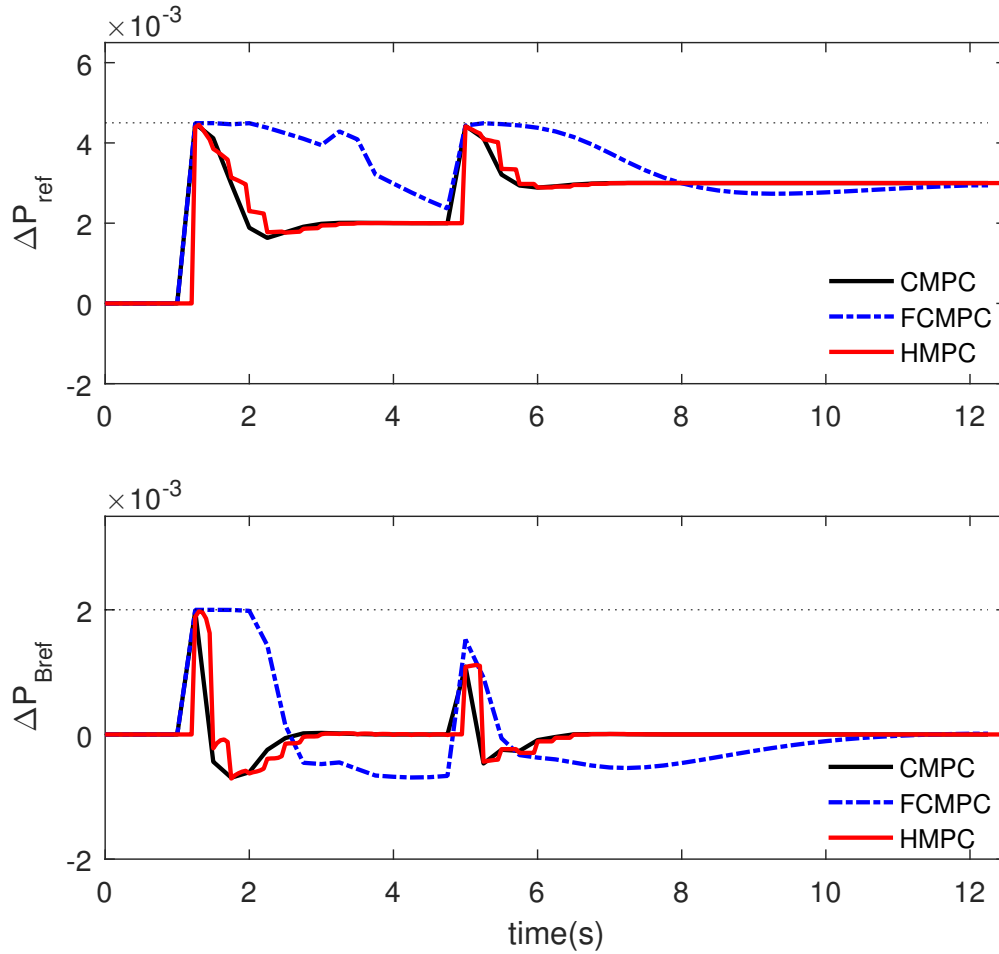


Fig. 5.14 Systems inputs:Generator Top, BESS Bottom. Dotted lines are the input constraints

and remains at the constraints for a longer time when compared to the other MPC formulations. In conclusion the simulation indicate that with the proposed algorithm hierarchical multi timescale control can be applied to the simulated power system while obtaining results similar to the centralised case.

Method	Level	Av Comp Time (s)	Cost
CMPC		$5.1 \times 10^{-4}$	$5.77 \times 10^{-5}$
HMPC	up	$3.71 \times 10^{-4}$	$5.3 \times 10^{-4}$
	low	0.0088	

Table 5.3 Comparison of the average computation times and cost for centralised and hierarchical MPC

A comparison of the average computation times of the optimisation problems over the time steps of the simulation and associated costs are given in Table 5.3. The total average computation time for the HMPC *i.e* is higher than that of the CMPC. However, the computation time at the higher level of the HMPC is less than that of the CMPC. The computation time at the lower level is higher since the number time steps and thus optimisation problems solved is higher. The overall cost of the HMPC is higher since two controllers now contribute to the cost. The values for FCMPC were not included in Table 5.3 since from the previous explanation we know that the computation times and cost are likely to be higher than those of CMPC and HMPC.

## 5.5 The Decentralised Case

In this section, the hierarchical algorithm of Section 5.3 is extended the case of decentralised controllers at the lower level of the control hierarchy for the generator and BESS subsystems. In chapter 4 decentralised controllers were designed with stability proofs for the power system considering the common frequency state. The decentralised model development procedure adopted in that chapter provides a foundation that can be applied for multirate hierarchical control of systems whose interactions are via common dynamical states.

The solution of the high level optimisation problem is used in generating references for the fast update model sampled at the nominal sampling rate. That is

$$x_{k+1} = Ax_k + B\bar{u}_{ks}^s \quad (5.11)$$

This simulation is over the time interval  $\forall i \in [1, (N+n)v]$  for the states and  $\forall i \in [1, (N+m)v]$  for the inputs to enable the use of shifting similar to the centralised case. The steady state targets  $x_{ss}$  and  $u_{ss}$  are available to the high level controller from the steady state target calculator. Recall at this level the optimisation problem is based on deviations variables using steady state target calculations in order to achieve offset free tracking.

The solution of this problem is directly applied to the fast update model without adjusting for the steady state values *i.e*  $\bar{u}_{ks}^s$  is used rather than  $u_{ks}^s = \bar{u}_{ks}^s + u_{ss}$ . In order to solve the particular case of lower interconnected systems linked by a common state, first define the *ith* overlapping lower order system model where  $i \in 1 \dots M$  where  $M$  is the number of subsystems. For the case considered here  $M$  is equals to 2; (i) generator (ii) BESS.

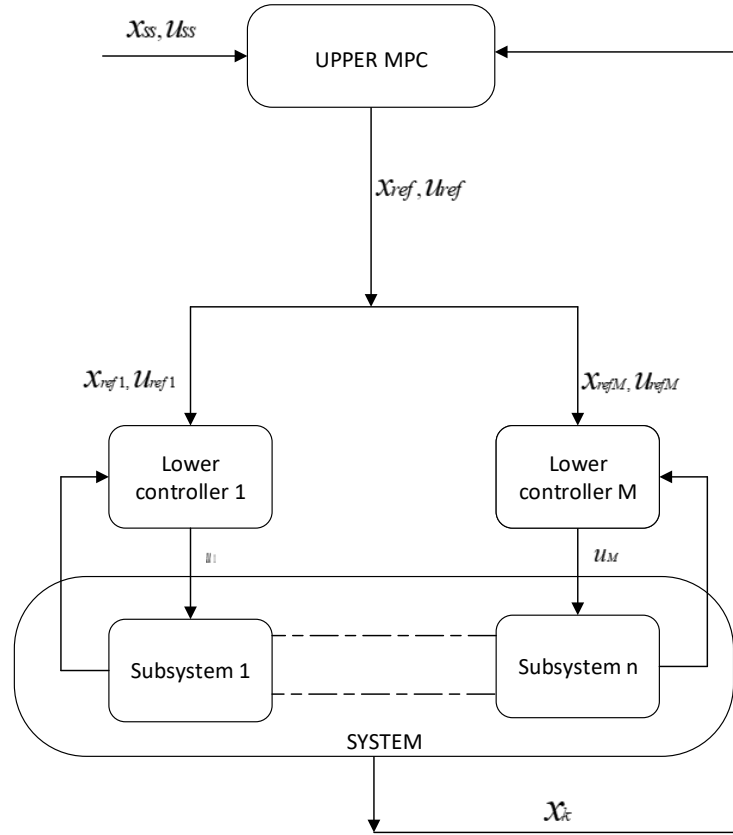


Fig. 5.15 The hierarchical control structure. The upper layer sends reference trajectories to lower layer decentralised controllers designed at the nominal timescale.

Following the procedure for state rearrangement and model decomposition in Section 4.3.3 the decentralised model for each subsystem can be obtained. For the LFC problem under consideration this created two interacting dynamical systems where the  $i$ th subsystem is

$$S_i : \begin{cases} z_i(k+1) &= A^i z_i(k) + B^i v_i(k) + E^i s^i(k) \\ y^i(k) &= C^i z_i(k) \end{cases} \quad (5.12)$$

where  $s_k^i$  represents interactions. Decentralised dynamical models can be derived from equation (5.12) which are suitable for predictions by leaving out the clearly defined interactions. Each subsystem  $S_i$  receives a steady state target pair  $(z_{i,ss}, v_{i,ss})$  in order to solve individual reference tracking problems. The steady state pairs are sent from a centralised target calculator used by the upper layer controller and include the common state.

In addition each lower controller also receives reference trajectories  $z_{i,ref}, v_{i,ref}$  derived from (5.11) which also includes the common state. Each lower level controller tracks the target references via offset free tracking by performing the dual function of disturbance rejection at each time instant  $k$  and trajectory reference tracking over the horizon of the lower control layer.

Hence the individual problem solved by each controller at the lower level in the fast time interval  $k$  and represented  $\mathbb{P}_i(z_i)$  for  $i \in [1, ..M]$  and current state  $z_i$ , is defined by

$$\min_{\mathbf{v}_i} V_{N,i}(z_i, \mathbf{v}_i) \quad (5.13)$$

subject to, for  $k = 0, \dots, N - 1$ ,

$$\begin{aligned} \bar{z}_i(0) &= z_i \\ \bar{x}_i(0) &= x_i \\ \bar{z}_i(k+1) &= f_i(\bar{z}_i(k), v_i(k)) \\ G_i \bar{z}_i(k) &\leq g_i \\ H_i v_i(k) &\leq h_i \end{aligned}$$

where  $x_i$  includes the common state of  $z_i$ .

Since each local controller performs a dual function of steady state and reference tracking the local problems solved by lower controllers has a cost  $V_{N,i}(z^i, \mathbf{v}_i)$  defined by:

$$V_N(\bar{z}_i, \bar{\mathbf{v}}_i) = \sum_{k=0}^{N-1} \bar{z}_i(k)^\top Q^i \bar{z}_i(k) + \bar{v}_i(k)_k^\top R^i \bar{v}_i(k) \quad (5.14)$$

where  $\bar{z}_i, \bar{v}_i$  are deviation variables based on  $z_{i,ss}, v_{i,ss}$ . Note the slight abuse of notation. To accommodate offset free tracking deviations variables given  $\bar{z}_i = z_i(k) - z_{i,ss}$  and  $\bar{v}_i = v_i(k) - v_{i,ss}$  are used in the MPC formulation and predictions are in deviation variables. The references are also in deviation variables *i.e*  $\bar{z}_{i,ref} = z_i(k) - z_{i,ss}$  and  $\bar{v}_{i,ref} = v_i(k) - v_{i,ss}$ . Hence in (5.14)  $\bar{z}_i = \bar{z}_i - \bar{z}_{i,ref}$  and  $\bar{v}_i = \bar{v}_i - \bar{v}_{i,ref}$ .

The approximated prediction models used in the design of each local low level controller contains only the common state. There is no shared information between the local controllers and decision making is entirely decentralised. Each local controller receives a local feedback containing only its local states and does not have any informa-

---

**Algorithm 2** Algorithm 5.2 Hierarchical Decentralised MPC for multirate System
 

---

1. **Parameters:**  $k^i, k_s, k_{s1}^i, n \in \mathbb{N}$ .
  2. **Initialisation:** Initialise both controllers  $k^i, k_s = 0; x^s(k_s/k_s), z_i(k/k) = x(0)$ . Initialise inner loop counters  $k_{s1} = k_s^i$ , the lower count update and set  $n = 1$  which selects  $u^s(k_s/k_s)$
  3. **Steady State Target Calculation:** Calculate the steady state targets  $x_{ss}, u_{ss}$ . The values obtained are used at both levels of the hierarchical structure ensuring consistency.
  4. **Higher layer Control Problem:** At time  $k$  equal to 1, set  $k_s$  equal to 1 and solve (5.4) to obtain the sequence  $\bar{u}^s \forall i \in [0, N-1]$  of the higher layer control output over the long horizon.
  5. **Reference Trajectory Generation:** Generate the references trajectories to be tracked by the lower decentralised controllers.
    - (a) For all  $i \in [1, v]$  apply  $u_{k_s}^s$  to (5.1) generating state and input references for one sampling interval  $T_s$  incrementing  $k_{s1}$  at each time  $i$ .
    - (b) If  $k_{s1} > v$  reset  $k_{s1}$  to 1 and increment  $n$  by 1 to select  $u_{k_s+1}^s$
    - (c) Repeat procedure to generate references  $x_{ref}, u_{ref}$  of length  $(N+v)n$  and  $(N+v)m$  for the states and inputs respectively. This process generates additional lengths of  $nv$  and  $mv$  to support range shifting for  $z_i, v_i$ .
  6. **Reference Selection:** Extract  $z_{i,ref}, v_{i,ref}$  to include the common state in the case of  $z_i$  from  $x_{ref}, u_{ref}$  corresponding to the length  $Nn$  and  $Nm$ . Increase  $k_s$  by 1.
  7. **Communication of References:** Communicate  $z_{i,ref}$  and  $v_{i,ref} \forall k \in [k, k+1, \dots, N]$  and  $u_{ref} \in k, k+1, \dots, N-1$ . At this point also communicate  $z_{i,ss}, v_{i,ss}$  extracted from  $x_{ss}, u_{ss}$  to each local controller.
  8. **Lower Level Controller Problem:** Solve (5.14) at time  $k, \forall k \in [k, \dots, k+N]$ . Combine the inputs  $z_i$  for  $i \in [1, \dots, M]$  to get  $u_k$  at time  $k/k$  and apply it to the system
  9. **System Update:** Update  $x(k+1)$  and set  $k = k+1$  i.e  $k \leftarrow k+1$
  10. **Repeat Lower Control Problem:** Repeat the lower optimisation incrementing  $k_s, k_s+1, \dots \forall i \in [k, \dots, kv]$ . At each time  $k$  shift  $z_{i,ref}, v_{i,ref}$  ranges for both the states and inputs of  $z_i$  and  $v_i$  at time  $k, k+1, \dots, v$  by  $n, 2n, \dots, vn$  and  $m, 2m, \dots, vm$  respectively.
  11. **Reset Upper Counter:** If  $k_s > v$  reset  $k_s$  to 1 and repeat steps 2, 3, 4, 5, 6, 7, 8, 9.
-

tion about the dynamical behaviour of neighbouring subsystems. However, the desired trajectories are generated by central upper controller for the full order system.

With all this in place Algorithm 5.1 can now be extended to the case of decentralised lower level controllers whose references are supplied by a higher controller designed in a slow timescale. Figure 5.15 is a schematic representation of the hierarchical decentralised structure. The design of the upper layer controller remains the same with changes only made to the lower controllers to account for the control of two systems linked by a common state.

## 5.6 Numerical Simulation and Discussion

In this section simulations are implemented to compare the hierarchical control schemes with the centralised approach. Here the area and BESS capacities are the same as those used in section 5.4. The upper layer centralised controller is designed with a sampling time of 0.7s. While for the lower layer controllers the system a sampling time of 0.07s is used. Hence  $v$  is equal to 10. The values used for  $Q$  and  $R$  in the different MPC structures are the same with  $Q = \text{diag}[100, 0.01, 10, 0.01, 100]$  and  $R = \text{diag}[1, 1]$ . The parameters used for the simulation are given in Table 5.4.

Algorithm 5.1 is now extended to the case of decentralised lower level controllers. This process is implemented using algorithm 5.2

$D$ (pu/Hz)	$2H$ (pu s)	$R$ (Hz/pu)	$T_G$ (s)	$T_T$ (s)	$Tb$ (s)
0.083	1.34	2.22	0.1	2.0	0.15

Table 5.4 Parameters of the power system

The prediction horizon used in this scenario is also set to 50 time steps and this is used all controllers including the  $i$ th controller at the lower level. Note that for the decentralised MPCs,  $Q_i$  and  $R_i$  for each controller were  $Q_g = \text{diag}[0.01, 0.01, 100]$  and  $Q_b = \text{diag}[100, 0.01, 100]$ . These values were also selected after tuning in order to obtain the desired LFC performances. The values of each  $R_i$  were:  $R_g = I_{ug}$  and  $R_b = I_{ub}$  where  $I_{ui}$  are identity matrices of appropriate dimensions. The same disturbance sequence used in the centralised case is also applied in this scenario.

The frequency and generator responses are given in Figure 5.16. The three formulations of MPC are labelled CMPC, DHMPC and HMPC for centralised, decentralised hierarchical and hierarchical MPC respectively. The centralised MPC gave the best frequency performance when compared to the DHMPC and HMPC.

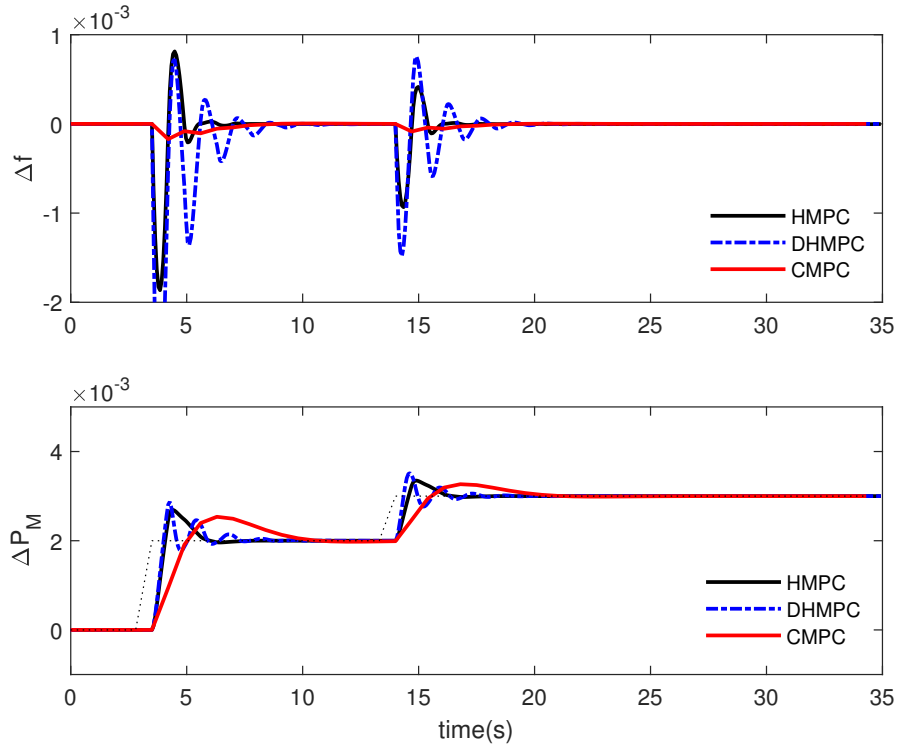


Fig. 5.16 Frequency deviation and generator outputs comparing centralised and hierarchical control

Method	Level	Av Comp Time (s)	Cost
CMPC		0.0013	0.013
HMPC	up	0.0025	0.0039
	low	0.0107	
DHMPC	up	$7.8 \times 10^{-5}$	0.0039
	low Gen	$1.41 \times 10^{-5}$	0.011
	low Bess	$3.88 \times 10^{-5}$	0.001

Table 5.5 Comparison of the average computation times and cost for centralised, centralised hierarchical and decentralised hierarchical MPC

Table 5.5 compares the costs and average computation times of CMPC, HMPC and DHMPC. In the case of DHMPC, at the lower level, the computations times for the BESS and generator is faster than that of CMPC. But this comes at the price of a total cost *i.e* summed across both levels hen compared to CMPC. HMPC also has a higher cost tand computation times across both levels than CMPC. Hence overall the computational time of the HMPC is faster than for both CMPC and HMPC.

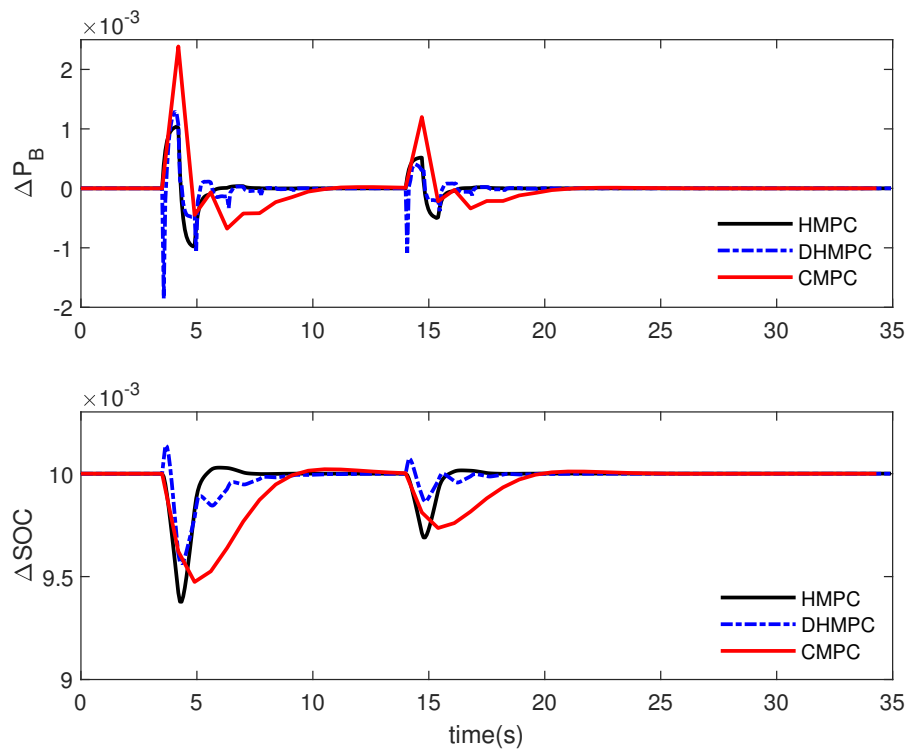


Fig. 5.17 Battery dynamics for centralised and hierarchical control

For the generator output, the performances are similar though the CMPC displayed a longer settling time. This is with no oscillations as is the case with the HMPC. The BESS responses are given in Figure 5.17. Here the HMPC gave a more acceptable performance when compared to the other two formulations. Both its power output and state of charge have better dynamics which are more acceptable. The inputs to the system are given in Figure 5.18. Here the HMPC also gives a more acceptable performance with the DHMPC having the least performance. However, all inputs settle to their expected values thereby ensuring that the LFC objective of regulating the frequency deviation to zero to be achieved.

## 5.7 Conclusion

The ability to achieve load frequency control in a future power system made up of a combination of conventional generating units and a battery storage systems would require new control strategies due to the increasing temporal spatial variability of the grid. There has been significant focus on the spatial and interconnected nature

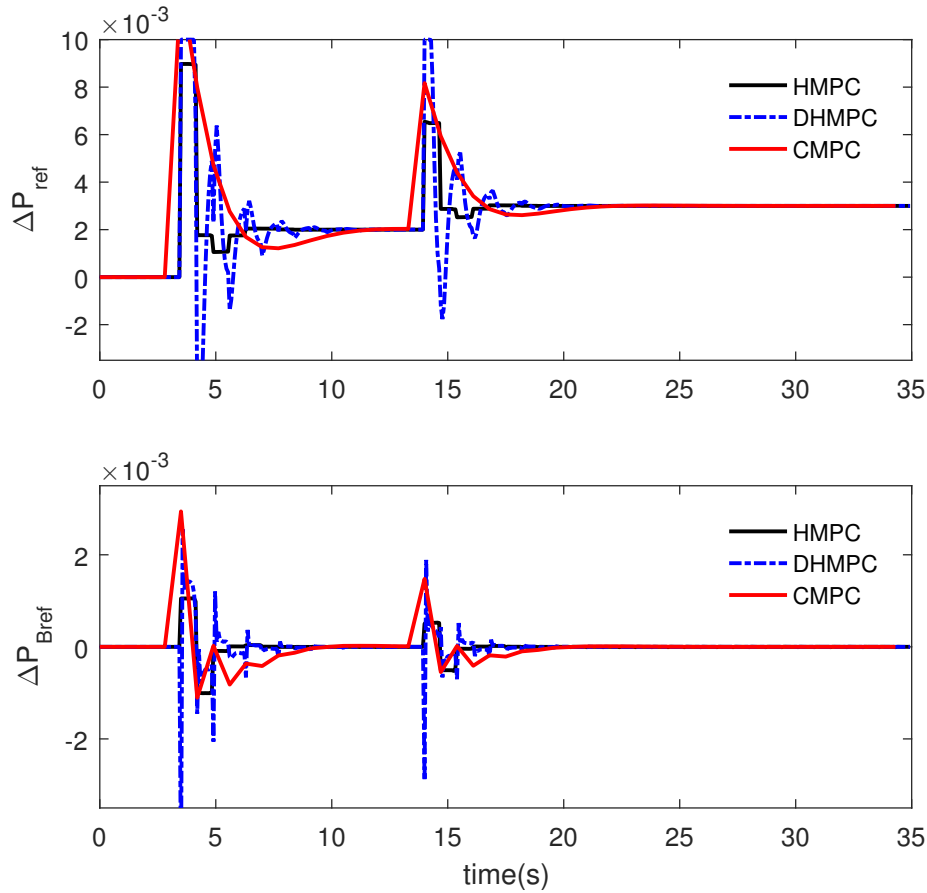


Fig. 5.18 Systems inputs:Generator Top, BESS Bottom.

of a future grid where clear areas of demarcations make the LFC control design problem manageable. However, due to the increase in the use of new generation technologies and the drive for them to participate in LFC alongside conventional generators decomposition techniques are required. In addition the response times of the different generation sources within this new power system systems may vary significantly and the use of a single controller sampled at one rate might lead to situation where the responsiveness of some devices is ignored.

In this chapter a two layer control architecture is developed consisting of systems coupled via the system frequency. The approach adopted is suitable for systems where some of the states can be classed as slow and others as fast. That is, multi timescale systems. The main features are at the higher level a slow timescale model is used to determine the long term behaviour of the system and serves as a trajectory generator.

While at the lower level, the controller is designed in the fast timescale and tracks the reference trajectories from the upper layer controller.

To ensure offset free tracking both layers are designed using deviation variables. Such a multi-timescale hierarchical LFC problem for systems characterised by coupled dynamics of variable temporal response is seldom considered in the literature. Here with little information exchange performances close to the centralised case sampled in the slow timescale were achieved. However, for the decentralised case in particular the impact of significant differences in sampling rates, ignored dynamics and decentralised prediction without information exchange in solving the optimisation problems led to reduced dynamical performances. There are solutions that can be adopted and suggestions on how these be done to improve performance as given in the concluding chapter. However, the main objectives of restoring the frequency to its nominal value was achieved with the participation of BESS and conventional generators.

# Chapter 6

## Conclusion and Future Work

The transition of the power grid from a homogeneous vertically integrated network to a heterogeneous intelligent one —the *smart grid* — continues to provide opportunities for innovative, reliable and cost efficient control applications. A key function for both the traditional and future power systems is load frequency control. Simply put, at any point in time demand must match supply *i.e* all sources of energy be they synchronous machines or distributed generation which take part in load frequency control must respond to this demand. Model predictive control as an advanced control methodology that has the technical attributes of optimality, prediction, variable structure and systematic constraint handling make it a suitable candidate for the load frequency control in future grids. This has been the control method adopted, developed and analysed in this thesis. In this concluding chapter of this thesis a summary of the contributions made and possible future directions than can be taken to extend the work done is therefore presented.

### 6.1 Conclusions and Contributions

This thesis has focused on the development of novel model predictive load frequency control strategies in future power grids. The difference between the conventional approach to load frequency control and that adopted in this thesis is the use of battery energy storage systems to support conventional generators in providing LFC as an ancillary service. This means that the standard models and algorithms needed to be adjusted to accommodate the participation of BESS in LFC without comprising the standards expected in terms of LFC performance. However, for this to be achieved an understanding of the concept of LFC and what it is supposed to achieve, the model predictive control algorithm and its various structures and challenges including the

benefits and drawbacks of each structure and the different approaches in the use of BESS for LFC and some of its wide ranging applications is important. The integration of these three knowledge areas is what provides a good technical background in the development of model predictive load frequency control with BESS in future power grids.

- In Chapter 2 a comprehensive review was given encompassing four main technical areas. The first major section was an overview of the LFC dynamics concluding with an example of LFC application based on integral controllers. The second main section detailed the MPC formulation adopted in this thesis with a technical review of the different MPC structures with a focus on a range of approaches from literature. The third main section focused on the technology of choice in this thesis; BESS. The advantages of using BESS in future grids for providing several ancillary services was given. In light of this potential future applications of BESS in future grids was given with a concluding focus of load frequency control applications. This led the fourth section which compared the recent state of the art in optimal load control to model predictive control from the perspective of model decomposition. Model predictive load frequency control has increasingly become an interesting area of research for load-frequency control and power system applications. Several applications exist in the literature in the conventional sense, i.e outside of what is considered a future grid scenario, and the final main section of this chapter was a review of the literature in this regard. Further to this a review of MPLFC in future grid scenarios is given where the support provided by several new technologies including BESS in achieving MPLFC is treated. The review covered centralised, distributed and hierarchical MPC structures.
- Chapter 3 presented the first technical contribution of this thesis. A centralised LFC scheme for a two area deregulated power system consisting of conventional generators and battery energy storage systems in both areas was proposed. In the first instance in order to ensure effective LFC performance the deregulated model was modified to accommodate a BESS model suitable for LFC analysis. A description of the model development process for the deregulated framework was presented along with the integrated BESS system. Here the modelling of several concepts specific to the deregulated framework were presented; generators referred to as GENCOs, distribution companies referred to as DISCOs and a TSO controller. The mechanism by which the GENCOs and DISCOs interact and its

integration into the LFC problem i.e the DPM was also presented. From here the concept of scheduled and unscheduled load changes was also introduced. The BESS model is then combined with the deregulated framework and unlike what is commonly obtained in the literature the dynamics is integrated into the system model creating dynamic interactive behaviour between the generators and BESS. The model is designed to ensure zero frequency and ACE deviation is achieved while also ensuring the state of charge is returned to a given optimal position making sure the BESS is ready to participate in the next frequency excursion event. Limits on the reference governor setpoint and GRC were considered. For the BESS, limits on the input, BESS power and state of charge were also included in the final design. Simulations with this dynamic model for both planned and unplanned load changes showed how BESS were able to improve the transient dynamics performance of LFC. In conclusion an analysis of the impact of energy recovery on system dynamics and the associated cost effects on the power system via changing the weights on the state matrix was implemented. This indicated an interesting area of future research outlined in Section 6.2. This chapter hence demonstrated the successful modelling and control of a future power grid within the deregulated framework with BESS support using MPC algorithm and parts of this contribution has been published [36].

- In Chapter 4 a non centralised MPLFC algorithm was presented. The decentralised control architecture was adopted for dynamically interacting subsystems subjected to constraints with guarantees for recursive feasibility despite the presence of bounded disturbances created by ignored interacting subsystem dynamics. First of all a decomposition methodology that led to the creation of subsystems with explicit representation of their dynamics was adopted. This principal theoretical assumption in this method is that the expanded state space created by the use of transformation matrices contains the dynamic behaviour of the nominal state space. From this expanded space, subsystems models that approximate the dynamical behaviour in the nominal state space were extracted. This created subsystems similar to the case of interconnected areas but with the disaggregated models created within an area. Models suitable for decentralised prediction were then available for the design of predictive controllers for the generator and BESS subsystems. Importantly, this procedure made the common frequency state available to both subsystems ensuring responsiveness to changes in frequency. The attainment of the objectives of LFC via the generator and BESS systems was thus guaranteed. However, this created a case of errors in

the prediction model induced by the ignored interactions used in the prediction equations in the design of the controllers. Following this an analysis of the stability and recursive feasibility of the controllers was carried out based on the inherent robustness properties of MPC. Here the descent properties of the value function which is used to represent a Lyapunov function in MPC is used to prove stability and feasibility. Suitable bounds were established within which the stability of the controllers is guaranteed provided the perturbations caused by the system dynamics remain within these scalars. A key contribution in regard to the LFC problem however was the link of these bounds to the accuracy of the method of discretisation adopted in the calculation of the discrete prediction models. Performance accuracy was then showed to be linked to the accuracy of the adopted method of discretisation via the mechanical starting time and time dependent load constant. Simulations demonstrated the success of the adopted approach in solving the LFC problem with generation rate, BESS power, energy and input constraints.

- In Chapter 5 a hierarchical multirate model predictive controller was designed for load frequency control in the setting of a future power grid with slow and fast dynamic states. This is a consideration that is rarely taken into account in the design of LFC controllers in future power systems. The spatial nature of the grid has led to the development of non centralised controllers suitable for addressing the spatial issue. Here the temporal nature of the future grid is also considered in the controller design. Hence in this chapter a investigation was carried on the use of multi rate control to in the design of MPLFC. The simplifying assumption of similar BESS and generator time constants adopted in most works that makes it easier for the sampling time to be selected that ensures responsiveness of both subsystems was not adopted. Rather the case of disparate time constants more in keeping with the dynamic responses of both systems where a central sampling time leads to undesirable dynamic response for the system whose responsiveness is adversely affected was analysed. An algorithm that solves the multirate issue while also addressing the LFC problem in the presence of state and input constraints including the management of BESS state of charge was developed and implemented. The desired equilibrium positions for the BESS, conventional generators and frequency following a disturbance to the system was achieved. The algorithm was then extended to the case of decentralised lower controllers designed at the lower level for systems coupled via an common interacting state which is the frequency. Suitable tracking performance was

also achieved for a bigger difference in the sampling times of the slow and fast update models. However, there is scope for improved dynamic performance. The actions of the lower decentralised regulators designed in the expanded space affect the dynamic behaviour of the system possibly due to neglected interactions at this level or a mismatch between the slow update controller designed in the nominal state space and the decentralised regulators designed in the expanded space. Since in this thesis inherent robustness is assumed robust by designs which could possibly provide further insights is not applied. This presents interesting future considerations. A combination of robust techniques and communication of planned trajectories across the levels of the control structure is likely to improve performance significantly. However, when compared to the literature where the lower controllers are designed for non overlapping interconnected lower level models here the case is for overlapping subsystems disaggregated within a control area. These considerations have seldom being considered in literature for load frequency control and were successfully implemented in this chapter.

## 6.2 Future Research Directions

The research carried out in this thesis could be extended in several useful technical directions:

- In the final section of Chapter 3 simulations were carried out which demonstrated the impact of varying the weights on the state of charge on system dynamics as well as regulation costs. The focus was on a potential procedure for state of charge management which is crucial in BESS operations. A fixed equilibrium point for the state of charge has been adopted in this thesis. However, this requirement can be relaxed. Several approaches can be adopted. The model can be redesigned so that the state of charge is no longer a target reference in the power system but rather can be fixed as an additional optimisation variable and its final position tracked. Alternatively, with the modelling approach adopted in this thesis the MPC algorithm can be adjusted to accommodate dynamic weights on the BESS state of charge which would be recalculated each time a disturbance occurs and beyond set thresholds the weight on the state of charge varied. This would induce a dynamic state of charge management capability on the BESS system since the weights determine how quickly the BESS recharges. Additionally, rather than recharging via the conventional generators renewable generation could be included in the model with the BESS recharging using

the energy from renewable generation. This might however require scheduling approaches combining optimisation via optimal power flows (OPF) and control. The combination of LFC and OPF is a research area that is also recently gaining traction in the literature. Extensions to handling uncertainty such as renewable generation and other services relating to the distribution network can also be considered.

- The work carried out in Chapter 4 can be extended to the case of distributed overlapping controllers for subsystems connected via a common state. The assumptions on the system relating to the Lyapunov properties of the value function and inherent robustness can then be extended to the distributed case rather than also resorting to robust by design. Stability could be guaranteed by adopting the use of LMIs to calculate stabilising gains and terminal costs for the decentralised systems under the assumption that stability of the controllers designed in the expanded space guarantees stability of the nominal system in its original state space. This can be inferred by the inclusion principle. In addition, due to model decomposition based on device groupings and the distributed decentralised requirements for LFC design in a multi area setting the work carried out focused on a single area system. This could be extended to multi area models with the decentralised behaviour between controllers located within an area while the behaviour of inter area controllers is distributed allowing for information exchange of predicted generators state and inputs. Several non centralised configurations can be adopted with extensions to include the deregulated framework.
- In Chapter 5 the hierarchical controllers have been designed for a two layer scheme. A future research direction that can be adopted for the work done in this case is an extension to a generic  $N$  number of layers. In the LFC case studied in this thesis  $N$  would be equal to three with the top most layer designed for the system time constant while the subsequent lower layers are designed for the generator and BESS systems respectively. Hence each lower layer would be in charge of one timescale with a unique dynamic response defined for one sampling time. This change would also prove useful in the decentralised case by enabling resampling at the lower levels at the rate of the different dynamics occurring at these levels. In addition, the focus was mainly on the temporal dynamic separation within a single control area. The algorithm could be extended to a distributed setting in a multi-area system within the deregulated model framework. In such a setting the

value of  $v$  is highly critical and off-line optimal values which ensure feasibility and stability are not compromised a priori would prove helpful. These values of  $v$  need not be a whole numbers also. A natural extension of the hierarchical framework in this thesis would be the use of economic MPC at the higher layer. A pricing scheme at this layer could consider the costs of conventional generators and BESS with the optimal input weighed using participation factors to determine the best economical usage of generators and BESS. In this scenario, the centralised model could be modified so that BESS have participation factors and the optimal economic input to the BESS is determined by information on pricing and current state of charge to ensure the BESS has sufficient capacity to contribute to LFC when required.



# References

- [1] J. Machowski, J. W. Bialek, and J. R. Bumby, *Power system dynamics: stability and control*. John Wiley & Sons, 2011.
- [2] J. Momoh, *Smart grid: fundamentals of design and analysis*, vol. 63. John Wiley & Sons, 2012.
- [3] S. Borlase, *Smart Grids: Infrastructure, Technology, and Solutions*. CRC press, 2016.
- [4] S. M. Amin, “Smart grid: Overview, issues and opportunities. advances and challenges in sensing, modeling, simulation, optimization and control,” *European Journal of Control*, vol. 17, no. 5-6, pp. 547–567, 2011.
- [5] V. Donde, M. Pai, and I. A. Hiskens, “Simulation and optimization in an agc system after deregulation,” *IEEE transactions on power systems*, vol. 16, no. 3, pp. 481–489, 2001.
- [6] P. Federal Energy Regulatory Commission, IEA, “Technology roadmap - smart grids.” <https://webstore.iea.org/technology-roadmap-smart-grids>.
- [7] F. Li, W. Qiao, H. Sun, H. Wan, J. Wang, Y. Xia, Z. Xu, and P. Zhang, “Smart transmission grid: Vision and framework,” *IEEE transactions on Smart Grid*, vol. 1, no. 2, pp. 168–177, 2010.
- [8] J. Gao, Y. Xiao, J. Liu, W. Liang, and C. P. Chen, “A survey of communication/networking in smart grids,” *Future generation computer systems*, vol. 28, no. 2, pp. 391–404, 2012.
- [9] J. B. Ekanayake, N. Jenkins, K. Liyanage, J. Wu, and A. Yokoyama, *Smart grid: technology and applications*. John Wiley & Sons, 2012.
- [10] P. Kundur, J. Paserba, V. Ajjarapu, G. Andersson, A. Bose, C. Canizares, N. Hatziargyriou, D. Hill, A. Stankovic, C. Taylor, *et al.*, “Definition and classification of power system stability ieeecigre joint task force on stability terms and definitions,” *IEEE transactions on Power Systems*, vol. 19, no. 3, pp. 1387–1401, 2004.
- [11] L. L. Grigsby *et al.*, *The electric power engineering handbook*. CRC press Boca Raton, 2001.

- [12] D. P. Kothari, "Power system optimization," in *2012 2nd National Conference on Computational Intelligence and Signal Processing (CISP)*, pp. 18–21, IEEE, 2012.
- [13] J. Zhu, *Optimization of power system operation*. John Wiley & Sons, 2015.
- [14] A. J. Wood and B. F. Wollenberg, *Power generation, operation, and control*. John Wiley & Sons, 2012.
- [15] P. Kundur, N. J. Balu, and M. G. Lauby, *Power system stability and control*, vol. 7. McGraw-hill New York, 1994.
- [16] H. Bevrani, *Robust power system frequency control*, vol. 85. Springer, 2009.
- [17] R. D. Christie and A. Bose, "Load frequency control issues in power system operations after deregulation," *IEEE Transactions on Power systems*, vol. 11, no. 3, pp. 1191–1200, 1996.
- [18] J. Kumar, K.-H. Ng, and G. Sheble, "Agc simulator for price-based operation. i. a model," *IEEE Transactions on Power Systems*, vol. 12, no. 2, pp. 527–532, 1997.
- [19] H. L. Willis and L. Philipson, *Understanding electric utilities and de-regulation*, vol. 27. CRC Press, 2018.
- [20] R. Sioshansi, P. Denholm, T. Jenkin, and J. Weiss, "Estimating the value of electricity storage in pjm: Arbitrage and some welfare effects," *Energy economics*, vol. 31, no. 2, pp. 269–277, 2009.
- [21] P. Maloney, "Ferc order 845 opens door a little wider for energy storage." <https://www.utilitydive.com/news/ferc-order-845-opens-door-a-little-wider-for-energy-storage/521992>.
- [22] Ofgem, "Upgrading our energy system: smart systems and flexibility plan." <https://www.gov.uk/government/publications/upgrading-our-energy-system-smart-systems-and-flexibility-plan>, 2017.
- [23] BATSTORM, "Battery storage system to drive power system transition." [https://ec.europa.eu/energy/sites/ener/files/report-\\_battery\\_storage\\_to\\_drive\\_the\\_power\\_system\\_transition.pdf](https://ec.europa.eu/energy/sites/ener/files/report-_battery_storage_to_drive_the_power_system_transition.pdf).
- [24] B. Xu, Y. Dvorkin, D. S. Kirschen, C. A. Silva-Monroy, and J.-P. Watson, "A comparison of policies on the participation of storage in us frequency regulation markets," in *Power and Energy Society General Meeting (PESGM), 2016*, pp. 1–5, IEEE, 2016.
- [25] C. Menictas, M. Skyllas-Kazacos, and T. M. Lim, *Advances in batteries for medium and large-scale energy storage: types and applications*. Elsevier, 2014.
- [26] M. Kintner-Meyer, "Regulatory policy and markets for energy storage in north america," *Proceedings of the IEEE*, vol. 102, no. 7, pp. 1065–1072, 2014.

- [27] A. Berrada, K. Loudiyi, and I. Zorkani, "Valuation of energy storage in energy and regulation markets," *Energy*, vol. 115, pp. 1109–1118, 2016.
- [28] A. Chakraborty and M. D. Ilić, *Control and optimization methods for electric smart grids*, vol. 3. Springer, 2011.
- [29] B. P. Roberts and C. Sandberg, "The role of energy storage in development of smart grids," *Proceedings of the IEEE*, vol. 99, no. 6, pp. 1139–1144, 2011.
- [30] A. Mohd, E. Ortjohann, A. Schmelter, N. Hamsic, and D. Morton, "Challenges in integrating distributed energy storage systems into future smart grid," in *2008 IEEE international symposium on industrial electronics*, pp. 1627–1632, IEEE, 2008.
- [31] G. Carpinelli, G. Celli, S. Mocci, F. Mottola, F. Pilo, and D. Proto, "Optimal integration of distributed energy storage devices in smart grids," *IEEE Transactions on smart grid*, vol. 4, no. 2, pp. 985–995, 2013.
- [32] V. C. Gungor, D. Sahin, T. Kocak, S. Ergut, C. Buccella, C. Cecati, and G. P. Hancke, "A survey on smart grid potential applications and communication requirements," *IEEE Transactions on industrial informatics*, vol. 9, no. 1, pp. 28–42, 2012.
- [33] L. M. Camarinha-Matos, "Collaborative smart grids—a survey on trends," *Renewable and Sustainable Energy Reviews*, vol. 65, pp. 283–294, 2016.
- [34] N. Motee and B. Sayyar-Rodsari, "Optimal partitioning in distributed model predictive control," in *Proceedings of the 2003 American Control Conference, 2003.*, vol. 6, pp. 5300–5305, IEEE, 2003.
- [35] D. Wang, M. Glavic, and L. Wehenkel, "Comparison of centralized, distributed and hierarchical model predictive control schemes for electromechanical oscillations damping in large-scale power systems," *International Journal of Electrical Power & Energy Systems*, vol. 58, pp. 32–41, 2014.
- [36] A. Ajiborisha and P. Trodden, "Model predictive load frequency control of a deregulated power system with battery energy storage," in *2019 IEEE Conference on Control Technology and Applications (CCTA)*, pp. 196–202, IEEE, 2019.
- [37] E. N. of Transmission System Operators for Electricity, "P1 load frequency control and reserves." <https://www.entsoe.eu/publications/system-operations-reports/>.
- [38] A. M. Ersdal, I. M. Cecilio, D. Fabozzi, L. Imsland, and T. Nina F, "Applying model predictive control to power system frequency control," in *Innovative Smart Grid Technologies Europe (ISGT EUROPE), 2013 4th IEEE/PES*, pp. 1–5, IEEE, 2013.
- [39] P. Murty, *Operation and control in power systems*. BS Publ., 2008.
- [40] N. Jaleeli, L. S. VanSlyck, D. N. Ewart, L. H. Fink, and A. G. Hoffmann, "Understanding automatic generation control," *IEEE transactions on power systems*, vol. 7, no. 3, pp. 1106–1122, 1992.

- [41] H. Saadat, *Power system analysis*. McGraw-Hill, 1999.
- [42] O. I. Elgerd, “Electric energy systems theory: an introduction,” 1982.
- [43] B. H. Bakken and O. S. Grande, “Automatic generation control in a deregulated power system,” *IEEE Transactions on Power Systems*, vol. 13, no. 4, pp. 1401–1406, 1998.
- [44] S. J. Qin and T. A. Badgwell, “A survey of industrial model predictive control technology,” *Control engineering practice*, vol. 11, no. 7, pp. 733–764, 2003.
- [45] S. J. Qin and T. A. Badgwell, “An overview of nonlinear model predictive control applications,” in *Nonlinear model predictive control*, pp. 369–392, Springer, 2000.
- [46] M. Morari and J. H. Lee, “Model predictive control: past, present and future,” *Computers & Chemical Engineering*, vol. 23, no. 4, pp. 667–682, 1999.
- [47] D. Q. Mayne, J. B. Rawlings, C. V. Rao, and P. O. Scokaert, “Constrained model predictive control: Stability and optimality,” *Automatica*, vol. 36, no. 6, pp. 789–814, 2000.
- [48] J. Rossiter, *A First Course in Predictive Control*. CRC Press, 2018.
- [49] L. Wang, *Model predictive control system design and implementation using MATLAB®*. Springer Science & Business Media, 2009.
- [50] E. F. Camacho and C. Bordons, *Model predictive control: Classical, robust and stochastic*. Springer International Publishing, 2016.
- [51] J. B. Rawlings and D. Q. Mayne, *Model predictive control: Theory and design*. Nob Hill Pub., 2009.
- [52] P. D. Christofides, R. Scattolini, D. M. de la Pena, and J. Liu, “Distributed model predictive control: A tutorial review and future research directions,” *Computers & Chemical Engineering*, vol. 51, pp. 21–41, 2013.
- [53] R. R. Negenborn and J. Maestre, “Distributed model predictive control: An overview and roadmap of future research opportunities,” *IEEE Control Systems Magazine*, vol. 34, no. 4, pp. 87–97, 2014.
- [54] J. A. Momoh, “Smart grid design for efficient and flexible power networks operation and control,” in *2009 IEEE/PES Power Systems Conference and Exposition*, pp. 1–8, IEEE, 2009.
- [55] S.-H. Wang and E. Davison, “On the stabilization of decentralized control systems,” *IEEE Transactions on Automatic Control*, vol. 18, no. 5, pp. 473–478, 1973.
- [56] R. Scattolini, “Architectures for distributed and hierarchical model predictive control—a review,” *Journal of process control*, vol. 19, no. 5, pp. 723–731, 2009.
- [57] L. Magni and R. Scattolini, “Stabilizing decentralized model predictive control of nonlinear systems,” *Automatica*, vol. 42, no. 7, pp. 1231–1236, 2006.

- [58] S. Rivero, M. Farina, and G. Ferrari-Trecate, "Plug-and-play decentralized model predictive control for linear systems," *IEEE Transactions on Automatic Control*, vol. 58, no. 10, pp. 2608–2614, 2013.
- [59] A. Alessio, D. Barcelli, and A. Bemporad, "Decentralized model predictive control of dynamically coupled linear systems," *Journal of Process Control*, vol. 21, no. 5, pp. 705–714, 2011.
- [60] E. Camponogara, D. Jia, B. H. Krogh, and S. Talukdar, "Distributed model predictive control," *IEEE Control Systems*, vol. 22, no. 1, pp. 44–52, 2002.
- [61] D. Q. Mayne, M. M. Seron, and S. Raković, "Robust model predictive control of constrained linear systems with bounded disturbances," *Automatica*, vol. 41, no. 2, pp. 219–224, 2005.
- [62] M. Farina and R. Scattolini, "Distributed predictive control: A non-cooperative algorithm with neighbor-to-neighbor communication for linear systems," *Automatica*, vol. 48, no. 6, pp. 1088–1096, 2012.
- [63] P. Trodden and A. Richards, "Distributed model predictive control of linear systems with persistent disturbances," *International Journal of Control*, vol. 83, no. 8, pp. 1653–1663, 2010.
- [64] B. T. Stewart, A. N. Venkat, J. B. Rawlings, S. J. Wright, and G. Pannocchia, "Cooperative distributed model predictive control," *Systems & Control Letters*, vol. 59, no. 8, pp. 460–469, 2010.
- [65] P. Giselsson and A. Rantzer, "Distributed model predictive control with suboptimality and stability guarantees," in *49th IEEE Conference on Decision and Control (CDC)*, pp. 7272–7277, IEEE, 2010.
- [66] P. Giselsson and A. Rantzer, "On feasibility, stability and performance in distributed model predictive control," *IEEE Transactions on Automatic Control*, vol. 59, no. 4, pp. 1031–1036, 2013.
- [67] P. Giselsson, M. D. Doan, T. Keviczky, B. De Schutter, and A. Rantzer, "Accelerated gradient methods and dual decomposition in distributed model predictive control," *Automatica*, vol. 49, no. 3, pp. 829–833, 2013.
- [68] F. Farokhi, I. Shames, and K. H. Johansson, "Distributed mpc via dual decomposition and alternative direction method of multipliers," in *Distributed model predictive control made easy*, pp. 115–131, Springer, 2014.
- [69] Z. Wang and C. J. Ong, "Distributed model predictive control of linear discrete-time systems with local and global constraints," *Automatica*, vol. 81, pp. 184–195, 2017.
- [70] C. Conte, M. N. Zeilinger, M. Morari, and C. N. Jones, "Robust distributed model predictive control of linear systems," in *2013 European Control Conference (ECC)*, pp. 2764–2769, IEEE, 2013.

- [71] S. Li and Y. Zheng, *Distributed model predictive control for plant-wide systems*. John Wiley & Sons, 2016.
- [72] J. Stoustrup, “Plug & play control: Control technology towards new challenges,” *European Journal of Control*, vol. 15, no. 3-4, pp. 311–330, 2009.
- [73] A. Ulbig, M. Arnold, S. Chatzivasileiadis, and G. Andersson, “Framework for multiple time-scale cascaded mpc application in power systems,” *IFAC Proceedings Volumes*, vol. 44, no. 1, pp. 10472–10480, 2011.
- [74] P. Tatjewski, “Advanced control and on-line process optimization in multilayer structures,” *Annual Reviews in Control*, vol. 32, no. 1, pp. 71–85, 2008.
- [75] M. Shiroei and A. Ranjbar, “Supervisory predictive control of power system load frequency control,” *International Journal of Electrical Power & Energy Systems*, vol. 61, pp. 70–80, 2014.
- [76] P. Marusak, P. Tatjewski, *et al.*, “Multilayer and integrated structures for predictive control and economic optimisation,” *IFAC Proceedings Volumes*, vol. 40, no. 9, pp. 198–205, 2007.
- [77] B. Picasso, X. Zhang, and R. Scattolini, “Hierarchical model predictive control of independent systems with joint constraints,” *Automatica*, vol. 74, pp. 99–106, 2016.
- [78] W. C. Clarke, C. Manzie, and M. J. Brear, “Hierarchical economic mpc for systems with storage states,” *Automatica*, vol. 94, pp. 138–150, 2018.
- [79] J. P. Koeln and A. G. Alleyne, “Two-level hierarchical mission-based model predictive control,” in *2018 Annual American Control Conference (ACC)*, pp. 2332–2337, IEEE, 2018.
- [80] M. R. Amini, I. Kolmanovsky, and J. Sun, “Robust hierarchical mpc for handling long horizon demand forecast uncertainty with application to automotive thermal management,” in *2019 IEEE 58th Conference on Decision and Control (CDC)*, pp. 6694–6699, IEEE, 2019.
- [81] P. Falcone, F. Borrelli, H. E. Tseng, J. Asgari, and D. Hrovat, “A hierarchical model predictive control framework for autonomous ground vehicles,” in *2008 American Control Conference*, pp. 3719–3724, IEEE, 2008.
- [82] F. Petzke, M. Farina, and S. Streif, “A multirate hierarchical mpc scheme for ensemble systems,” in *2018 IEEE Conference on Decision and Control (CDC)*, pp. 5874–5879, IEEE, 2018.
- [83] M. Farina, A. Perizzato, and R. Scattolini, “Application of distributed predictive control to motion and coordination problems for unicycle autonomous robots,” *Robotics and Autonomous Systems*, vol. 72, pp. 248–260, 2015.
- [84] B. Picasso, D. De Vito, R. Scattolini, and P. Colaneri, “An mpc approach to the design of two-layer hierarchical control systems,” *Automatica*, vol. 46, no. 5, pp. 823–831, 2010.

- [85] M. Farina, X. Zhang, and R. Scattolini, “A hierarchical multi-rate mpc scheme for interconnected systems,” *Automatica*, vol. 90, pp. 38–46, 2018.
- [86] M. Jilg and O. Stursberg, “Hierarchical distributed control for interconnected systems,” *IFAC Proceedings Volumes*, vol. 46, no. 13, pp. 419–425, 2013.
- [87] M. D. Doan, T. Keviczky, and B. De Schutter, “A distributed optimization-based approach for hierarchical mpc of large-scale systems with coupled dynamics and constraints,” in *2011 50th IEEE Conference on Decision and Control and European Control Conference*, pp. 5236–5241, IEEE, 2011.
- [88] P. Braun, T. Faulwasser, L. Grüne, C. M. Kellett, S. R. Weller, and K. Worthmann, “Hierarchical distributed admn for predictive control with applications in power networks,” *IFAC Journal of Systems and Control*, vol. 3, pp. 10–22, 2018.
- [89] C. A. Hans, P. Braun, J. Raisch, L. Grüne, and C. Reincke-Collon, “Hierarchical distributed model predictive control of interconnected microgrids,” *IEEE Transactions on Sustainable Energy*, vol. 10, no. 1, pp. 407–416, 2018.
- [90] M. G. Forbes, R. S. Patwardhan, H. Hamadah, and R. B. Gopaluni, “Model predictive control in industry: Challenges and opportunities,” *IFAC-PapersOnLine*, vol. 48, no. 8, pp. 531–538, 2015.
- [91] F. Díaz-González, A. Sumper, and O. Gomis-Bellmunt, *Energy storage in power systems*. John Wiley & Sons, 2016.
- [92] H.-J. Kunisch, K. Kramer, and H. Dominik, “Battery energy storage another option for load-frequency-control and instantaneous reserve,” *IEEE Transactions on Energy Conversion*, no. 3, pp. 41–46, 1986.
- [93] H. power reserve, “Hornsdale power reserve.” <http://hornsdalepowerreserve.com.au>, 2020.
- [94] I. R. E. Agency, “Innovation landscape brief: Utility-scale batteries.” [https://www.irena.org/-/media/Files/IRENA/Agency/Publication/2019/Sep/IRENA\\_Utility-scale-batteries\\_2019.pdf](https://www.irena.org/-/media/Files/IRENA/Agency/Publication/2019/Sep/IRENA_Utility-scale-batteries_2019.pdf), 2020.
- [95] M. Koller, T. Borsche, A. Ulbig, and G. Andersson, “Defining a degradation cost function for optimal control of a battery energy storage system,” in *2013 IEEE Grenoble Conference*, pp. 1–6, IEEE, 2013.
- [96] D. Dongol, T. Feldmann, M. Schmidt, and E. Bollin, “A model predictive control based peak shaving application of battery for a household with photovoltaic system in a rural distribution grid,” *Sustainable Energy, Grids and Networks*, vol. 16, pp. 1–13, 2018.
- [97] D. T. Vedullapalli, R. Hadidi, B. Schroeder, and R. Baumgartner, “Adaptive scheduling of the battery for peak shaving using model predictive control,” in *2018 IEEE Electronic Power Grid (eGrid)*, pp. 1–5, IEEE, 2018.

- [98] H. H. Abdeltawab and Y. A.-R. I. Mohamed, "Market-oriented energy management of a hybrid wind-battery energy storage system via model predictive control with constraint optimizer," *IEEE Transactions on Industrial Electronics*, vol. 62, no. 11, pp. 6658–6670, 2015.
- [99] M. U. Hashmi, L. Pereira, and A. Bušić, "Energy storage in madeira, portugal: Co-optimizing for arbitrage, self-sufficiency, peak shaving and energy backup," in *2019 IEEE Milan PowerTech*, pp. 1–6, IEEE, 2019.
- [100] M. Khalid and A. Savkin, "An optimal operation of wind energy storage system for frequency control based on model predictive control," *Renewable Energy*, vol. 48, pp. 127–132, 2012.
- [101] M. Koller, T. Borsche, A. Ulbig, and G. Andersson, "Review of grid applications with the zurich 1 mw battery energy storage system," *Electric Power Systems Research*, vol. 120, pp. 128–135, 2015.
- [102] W. Liu, L. Sun, Z. Lin, F. Wen, and Y. Xue, "Multi-objective restoration optimisation of power systems with battery energy storage systems," *IET Generation, Transmission & Distribution*, vol. 10, no. 7, pp. 1749–1757, 2016.
- [103] B. Zhang, P. Dehghanian, and M. Kezunovic, "Optimal allocation of pv generation and battery storage for enhanced resilience," *IEEE Transactions on Smart Grid*, vol. 10, no. 1, pp. 535–545, 2017.
- [104] J. Krata and T. K. Saha, "Real-time coordinated voltage support with battery energy storage in a distribution grid equipped with medium-scale pv generation," *IEEE Transactions on Smart Grid*, vol. 10, no. 3, pp. 3486–3497, 2018.
- [105] Y. Guo, Q. Wu, H. Gao, X. Chen, J. Østergaard, and H. Xin, "Mpc-based coordinated voltage regulation for distribution networks with distributed generation and energy storage system," *IEEE Transactions on Sustainable Energy*, vol. 10, no. 4, pp. 1731–1739, 2018.
- [106] Y. Li, L. Li, C. Peng, and J. Zou, "An mpc based optimized control approach for ev-based voltage regulation in distribution grid," *Electric Power Systems Research*, vol. 172, pp. 152–160, 2019.
- [107] B. Banfield, D. Robinson, and A. P. Agalgaonkar, "Distributed mpc of residential energy storage for voltage regulation and peak shaving along radial distribution feeders," *IEEE Transactions on Energy Conversion*, 2020.
- [108] M. U. Hashmi, D. Deka, A. Bušić, L. Pereira, and S. Backhaus, "Co-optimizing energy storage for prosumers using convex relaxations," in *2019 20th International Conference on Intelligent System Application to Power Systems (ISAP)*, pp. 1–7, IEEE, 2019.
- [109] M. Khalid and A. V. Savkin, "Model predictive control based efficient operation of battery energy storage system for primary frequency control," in *2010 11th International Conference on Control Automation Robotics & Vision*, pp. 2248–2252, IEEE, 2010.

- 
- [110] C. Goebel, H. Hesse, M. Schimpe, A. Jossen, and H.-A. Jacobsen, “Model-based dispatch strategies for lithium-ion battery energy storage applied to pay-as-bid markets for secondary reserve,” *IEEE Transactions on Power Systems*, vol. 32, no. 4, pp. 2724–2734, 2016.
- [111] M. Petrollese, L. Valverde, D. Cocco, G. Cau, and J. Guerra, “Real-time integration of optimal generation scheduling with mpc for the energy management of a renewable hydrogen-based microgrid,” *Applied Energy*, vol. 166, pp. 96–106, 2016.
- [112] M. R. Almassalkhi and I. A. Hiskens, “Model-predictive cascade mitigation in electric power systems with storage and renewables—part i: Theory and implementation,” *IEEE Transactions on Power Systems*, vol. 30, no. 1, pp. 67–77, 2015.
- [113] M. R. Almassalkhi and I. A. Hiskens, “Model-predictive cascade mitigation in electric power systems with storage and renewables—part ii: Case-study,” *IEEE Transactions on Power Systems*, vol. 30, no. 1, pp. 78–87, 2015.
- [114] S. Teleke, M. E. Baran, S. Bhattacharya, and A. Q. Huang, “Optimal control of battery energy storage for wind farm dispatching,” *IEEE Transactions on Energy Conversion*, vol. 25, no. 3, pp. 787–794, 2010.
- [115] L. Xie, Y. Gu, A. Eskandari, and M. Ehsani, “Fast mpc-based coordination of wind power and battery energy storage systems,” *Journal of Energy Engineering*, vol. 138, no. 2, pp. 43–53, 2012.
- [116] F. Sossan, E. Namor, R. Cherkaoui, and M. Paolone, “Achieving the dispatchability of distribution feeders through prosumers data driven forecasting and model predictive control of electrochemical storage,” *IEEE Transactions on Sustainable Energy*, vol. 7, no. 4, pp. 1762–1777, 2016.
- [117] A. V. Savkin, M. Khalid, and V. G. Agelidis, “A constrained monotonic charging/discharging strategy for optimal capacity of battery energy storage supporting wind farms,” *IEEE Transactions on Sustainable Energy*, vol. 7, no. 3, pp. 1224–1231, 2016.
- [118] A. Oudalov, D. Chartouni, C. Ohler, and G. Linhofer, “Value analysis of battery energy storage applications in power systems,” in *2006 IEEE PES Power Systems Conference and Exposition*, pp. 2206–2211, IEEE, 2006.
- [119] D. Kottick, M. Blau, and D. Edelstein, “Battery energy storage for frequency regulation in an island power system,” *IEEE Transactions on Energy Conversion*, vol. 8, no. 3, pp. 455–459, 1993.
- [120] C.-F. Lu, C.-C. Liu, and C.-J. Wu, “Effect of battery energy storage system on load frequency control considering governor deadband and generation rate constraint,” *IEEE Transactions on Energy Conversion*, vol. 10, no. 3, pp. 555–561, 1995.

- [121] S. Aditya and D. Das, “Battery energy storage for load frequency control of an interconnected power system,” *Electric power systems research*, vol. 58, no. 3, pp. 179–185, 2001.
- [122] M. Arita, A. Yokoyama, and Y. Tada, “Evaluation of battery system for frequency control in interconnected power system with a large penetration of wind power generation,” in *Power System Technology, 2006. PowerCon 2006. International Conference on*, pp. 1–7, IEEE, 2006.
- [123] P. Mercier, R. Cherkaoui, and A. Oudalov, “Optimizing a battery energy storage system for frequency control application in an isolated power system,” *IEEE Transactions on Power Systems*, vol. 24, no. 3, pp. 1469–1477, 2009.
- [124] A. M. Howlader, Y. Izumi, A. Uehara, N. Urasaki, T. Senjyu, A. Yona, and A. Y. Saber, “A minimal order observer based frequency control strategy for an integrated wind-battery-diesel power system,” *Energy*, vol. 46, no. 1, pp. 168–178, 2012.
- [125] T. Masuta and A. Yokoyama, “Supplementary load frequency control by use of a number of both electric vehicles and heat pump water heaters,” *IEEE Transactions on smart grid*, vol. 3, no. 3, pp. 1253–1262, 2012.
- [126] Y. Han, P. M. Young, A. Jain, and D. Zimmerle, “Robust control for microgrid frequency deviation reduction with attached storage system,” *IEEE Transactions on Smart Grid*, vol. 6, no. 2, pp. 557–565, 2014.
- [127] I. Chidambaram and B. Paramasivam, “Optimized load-frequency simulation in restructured power system with redox flow batteries and interline power flow controller,” *International Journal of Electrical Power & Energy Systems*, vol. 50, pp. 9–24, 2013.
- [128] T. S. Gorripotu, R. K. Sahu, and S. Panda, “Agc of a multi-area power system under deregulated environment using redox flow batteries and interline power flow controller,” *Engineering Science and Technology, an International Journal*, vol. 18, no. 4, pp. 555–578, 2015.
- [129] A. Pappachen and A. P. Fathima, “Load frequency control in deregulated power system integrated with smes–tcps combination using anfis controller,” *International Journal of Electrical Power & Energy Systems*, vol. 82, pp. 519–534, 2016.
- [130] R. Shankar, K. Chatterjee, and R. Bhushan, “Impact of energy storage system on load frequency control for diverse sources of interconnected power system in deregulated power environment,” *International Journal of Electrical Power & Energy Systems*, vol. 79, pp. 11–26, 2016.
- [131] Y. Arya, N. Kumar, and S. Gupta, “Optimal automatic generation control of two-area power systems with energy storage units under deregulated environment,” *Journal of Renewable and Sustainable Energy*, vol. 9, no. 6, p. 064105, 2017.

- [132] P. Kumar, D. P. Kothari, and Ibraheem, "Recent philosophies of automatic generation control strategies in power systems," *IEEE transactions on power systems*, vol. 20, no. 1, pp. 346–357, 2005.
- [133] O. I. Elgerd and C. E. Fosha, "Optimum megawatt-frequency control of multiarea electric energy systems," *IEEE Transactions on Power Apparatus and Systems*, no. 4, pp. 556–563, 1970.
- [134] T. E. Bechert and N. Chen, "Area automatic generation control by multi-pass dynamic programming," *IEEE Transactions on Power Apparatus and Systems*, vol. 96, no. 5, pp. 1460–1469, 1977.
- [135] F. Beaufays, Y. Abdel-Magid, and B. Widrow, "Application of neural networks to load-frequency control in power systems," *Neural Networks*, vol. 7, no. 1, pp. 183–194, 1994.
- [136] Y. Karnavas and D. Papadopoulos, "Agc for autonomous power system using combined intelligent techniques," *Electric power systems research*, vol. 62, no. 3, pp. 225–239, 2002.
- [137] Z. Al-Hamouz and H. Al-Duwaish, "A new load frequency variable structure controller using genetic algorithms," *Electric Power Systems Research*, vol. 55, no. 1, pp. 1–6, 2000.
- [138] I. Kocaarslan and E. Çam, "Fuzzy logic controller in interconnected electrical power systems for load-frequency control," *International Journal of Electrical Power & Energy Systems*, vol. 27, no. 8, pp. 542–549, 2005.
- [139] E. Ejegi, J. Rossiter, and P. Trodden, "A survey of techniques and opportunities in power system automatic generation control," in *Control (CONTROL), 2014 UKACC International Conference on*, pp. 537–542, IEEE, 2014.
- [140] D. Trudnowski, M. Donnelly, and E. Lightner, "Power-system frequency and stability control using decentralized intelligent loads," in *Transmission and Distribution Conference and Exhibition, 2005/2006 IEEE PES*, pp. 1453–1459, IEEE, 2006.
- [141] B. S and V. L, *Convex optimization*. Cambridge university press, 2004.
- [142] S. Boyd, N. Parikh, and E. Chu, *Distributed optimization and statistical learning via the alternating direction method of multipliers*. Now Publishers Inc, 2011.
- [143] D. K. Molzahn, F. Dörfler, H. Sandberg, S. H. Low, S. Chakrabarti, R. Baldick, and J. Lavaei, "A survey of distributed optimization and control algorithms for electric power systems," *IEEE Transactions on Smart Grid*, vol. 8, no. 6, pp. 2941–2962, 2017.
- [144] C. Zhao, U. Topcu, and S. H. Low, "Optimal load control via frequency measurement and neighborhood area communication," *IEEE Transactions on Power Systems*, vol. 28, no. 4, pp. 3576–3587, 2013.

- [145] C. Zhao, U. Topcu, N. Li, and S. Low, “Design and stability of load-side primary frequency control in power systems,” *IEEE Transactions on Automatic Control*, vol. 59, no. 5, pp. 1177–1189, 2014.
- [146] E. Mallada, C. Zhao, and S. Low, “Optimal load-side control for frequency regulation in smart grids,” *IEEE Transactions on Automatic Control*, vol. 62, no. 12, pp. 6294–6309, 2017.
- [147] X. Zhang and A. Papachristodoulou, “A real-time control framework for smart power networks: Design methodology and stability,” *Automatica*, vol. 58, pp. 43–50, 2015.
- [148] D. J. Shiltz, S. Baros, M. Cvetković, and A. M. Annaswamy, “Integration of automatic generation control and demand response via a dynamic regulation market mechanism,” *IEEE Transactions on Control Systems Technology*, vol. 27, no. 2, pp. 631–646, 2017.
- [149] J. Köhler, M. A. Müller, N. Li, and F. Allgöwer, “Real time economic dispatch for power networks: A distributed economic model predictive control approach,” in *2017 IEEE 56th Annual Conference on Decision and Control (CDC)*, pp. 6340–6345, IEEE, 2017.
- [150] D. D. Siljak, *Decentralized control of complex systems*. Courier Corporation, 2011.
- [151] S. S. Stanković and D. D. Šiljak, “Contractibility of overlapping decentralized control,” *Systems & Control Letters*, vol. 44, no. 3, pp. 189–200, 2001.
- [152] A. İftar, “Decentralized estimation and control with overlapping input, state, and output decomposition,” *Automatica*, vol. 29, no. 2, pp. 511–516, 1993.
- [153] X.-B. Chen and S. S. Stanković, “Decomposition and decentralized control of systems with multi-overlapping structure,” *Automatica*, vol. 41, no. 10, pp. 1765–1772, 2005.
- [154] X.-B. Chen and S. S. Stankovic, “Overlapping decentralized approach to automation generation control of multi-area power systems,” *International Journal of Control*, vol. 80, no. 3, pp. 386–402, 2007.
- [155] I. Ngamroo, Y. Mitani, and K. Tsuji, “Application of smes coordinated with solid-state phase shifter to load frequency control,” *IEEE Transactions on applied superconductivity*, vol. 9, no. 2, pp. 322–325, 1999.
- [156] D. Menniti, A. Pinnarelli, N. Scordino, and N. Sorrentino, “Using a facts device controlled by a decentralised control law to damp the transient frequency deviation in a deregulated electric power system,” *Electric power systems research*, vol. 72, no. 3, pp. 289–298, 2004.
- [157] P. Khayyer and Ü. Özgüner, “Decentralized control of large-scale storage-based renewable energy systems,” *IEEE Transactions on Smart Grid*, vol. 5, no. 3, pp. 1300–1307, 2014.

- [158] R. H. Byrne, T. A. Nguyen, D. A. Copp, B. R. Chalamala, and I. Gyuk, "Energy management and optimization methods for grid energy storage systems," *IEEE Access*, vol. 6, pp. 13231–13260, 2018.
- [159] M. Shiroei, A. M. Ranjbar, and T. Amraee, "A functional model predictive control approach for power system load frequency control considering generation rate constraint," *International Transactions on Electrical Energy Systems*, vol. 23, no. 2, pp. 214–229, 2013.
- [160] A. M. Ersdal, L. Imsland, and K. Uhlen, "Model predictive load-frequency control," *IEEE Transactions on Power Systems*, vol. 31, no. 1, pp. 777–785, 2016.
- [161] M. Diehl, R. Amrit, and J. B. Rawlings, "A lyapunov function for economic optimizing model predictive control," *IEEE Transactions on Automatic Control*, vol. 56, no. 3, pp. 703–707, 2010.
- [162] J. M. Maciejowski, *Predictive control: with constraints*. Pearson education, 2002.
- [163] A. Jokic, M. Lazar, and P. Van den Bosch, "Price-based optimal control of power flow in electrical energy transmission networks," *Lecture Notes in Computer Science*, vol. 4416, p. 315, 2007.
- [164] R. J. Abraham, D. Das, and A. Patra, "Load following in a bilateral market with local controllers," *International Journal of Electrical Power & Energy Systems*, vol. 33, no. 10, pp. 1648–1657, 2011.
- [165] P. Bhatt, R. Roy, and S. Ghoshal, "Optimized multi area agc simulation in restructured power systems," *International Journal of Electrical Power & Energy Systems*, vol. 32, no. 4, pp. 311–322, 2010.
- [166] K. S. Parmar, S. Majhi, and D. Kothari, "Lfc of an interconnected power system with multi-source power generation in deregulated power environment," *International Journal of Electrical Power & Energy Systems*, vol. 57, pp. 277–286, 2014.
- [167] N. Atic, D. Rerkpreedapong, A. Hasanovic, and A. Feliachi, "Nerc compliant decentralized load frequency control design using model predictive control," in *Power Engineering Society General Meeting, 2003, IEEE*, vol. 2, pp. 554–559, IEEE, 2003.
- [168] E. E. Ejegi, J. A. Rossiter, and P. Trodden, "Model predictive load frequency control of a two-area deregulated power system," in *Control Conference (ECC), 2015 European*, pp. 1044–1049, IEEE, 2015.
- [169] T. Mohamed, H. Bevrani, A. Hassan, and T. Hiyama, "Decentralized model predictive based load frequency control in an interconnected power system," *Energy Conversion and Management*, vol. 52, no. 2, pp. 1208–1214, 2011.
- [170] P. Mc Namara, R. Meere, T. O'Donnell, and S. McLoone, "Control strategies for automatic generation control over mt dc grids," *Control Engineering Practice*, vol. 54, pp. 129–139, 2016.

- [171] A. N. Venkat, I. A. Hiskens, J. B. Rawlings, and S. J. Wright, “Distributed mpc strategies with application to power system automatic generation control,” *IEEE transactions on control systems technology*, vol. 16, no. 6, pp. 1192–1206, 2008.
- [172] M. Ma, H. Chen, X. Liu, and F. Allgöwer, “Distributed model predictive load frequency control of multi-area interconnected power system,” *International Journal of Electrical Power & Energy Systems*, vol. 62, pp. 289–298, 2014.
- [173] X. Liu, Y. Zhang, and K. Y. Lee, “Robust distributed mpc for load frequency control of uncertain power systems,” *Control Engineering Practice*, vol. 56, pp. 136–147, 2016.
- [174] P. R. B. Monasterios and P. Trodden, “Low-complexity distributed predictive automatic generation control with guaranteed properties,” *IEEE Transactions on Smart Grid*, 2017.
- [175] P. R. B. Monasterios, B. Hernandez, and P. A. Trodden, “Nested distributed mpc,” *IFAC-PapersOnLine*, vol. 50, no. 1, pp. 11822–11828, 2017.
- [176] E. Ejegi, J. Rossiter, and P. Trodden, “Distributed model predictive load frequency control of a deregulated power system,” in *2016 UKACC 11th International Conference on Control (CONTROL)*, pp. 1–6, IEEE, 2016.
- [177] M. Ma, C. Zhang, X. Liu, and H. Chen, “Distributed model predictive load frequency control of the multi-area power system after deregulation,” *IEEE transactions on Industrial Electronics*, vol. 64, no. 6, pp. 5129–5139, 2016.
- [178] R. M. Hermans, A. Jokić, M. Lazar, A. Alessio, P. P. Van den Bosch, I. A. Hiskens, and A. Bemporad, “Assessment of non-centralised model predictive control techniques for electrical power networks,” *International journal of control*, vol. 85, no. 8, pp. 1162–1177, 2012.
- [179] A. M. Ersdal, L. Imsland, K. Uhlen, D. Fabozzi, and N. F. Thornhill, “Model predictive load–frequency control taking into account imbalance uncertainty,” *Control Engineering Practice*, vol. 53, pp. 139–150, 2016.
- [180] A. M. Ersdal, D. Fabozzi, L. Imsland, and N. F. Thornhill, “Model predictive control for power system frequency control taking into account imbalance uncertainty,” *IFAC Proceedings Volumes*, vol. 47, no. 3, pp. 981–986, 2014.
- [181] K. Baker, G. Hug, and X. Li, “Optimal integration of intermittent energy sources using distributed multi-step optimization,” in *Power and Energy Society General Meeting, 2012 IEEE*, pp. 1–8, IEEE, 2012.
- [182] K. Baker, J. Guo, G. Hug, and X. Li, “Distributed mpc for efficient coordination of storage and renewable energy sources across control areas,” *IEEE Transactions on Smart Grid*, vol. 7, no. 2, pp. 992–1001, 2016.
- [183] G. K. Larsen, N. D. van Foreest, and J. M. Scherpen, “Distributed control of the power supply-demand balance,” *IEEE Transactions on Smart Grid*, vol. 4, no. 2, pp. 828–836, 2013.

- [184] G. K. Larsen, N. D. van Foreest, and J. M. Scherpen, “Distributed mpc applied to a network of households with micro-chp and heat storage,” *IEEE Transactions on Smart Grid*, vol. 5, no. 4, pp. 2106–2114, 2014.
- [185] K. T. Jan Bendtsen and J. Stoustrup, “Hierarchical model predictive control for resource distribution,” in *Decision and Control (CDC), 2010 49th IEEE Conference on*, pp. 2468–2473, IEEE, 2010.
- [186] K. Trangbæk, M. Petersen, J. Bendtsen, and J. Stoustrup, “Exact power constraints in smart grid control,” in *Decision and Control and European Control Conference (CDC-ECC), 2011 50th IEEE Conference on*, pp. 6907–6912, IEEE, 2011.
- [187] F. Berkel, D. Görges, and S. Liu, “Load-frequency control, economic dispatch and unit commitment in smart microgrids based on hierarchical model predictive control,” in *52nd IEEE Conference on Decision and Control*, pp. 2326–2333, IEEE, 2013.
- [188] F. Kennel, D. Gorges, and S. Liu, “Energy management for smart grids with electric vehicles based on hierarchical mpc,” *IEEE Transactions on industrial informatics*, vol. 9, no. 3, pp. 1528–1537, 2013.
- [189] A. Parisio, E. Rikos, G. Tzamalīs, and L. Glielmo, “Use of model predictive control for experimental microgrid optimization,” *Applied Energy*, vol. 115, pp. 37–46, 2014.
- [190] A. Parisio, E. Rikos, and L. Glielmo, “A model predictive control approach to microgrid operation optimization,” *IEEE Transactions on Control Systems Technology*, vol. 22, no. 5, pp. 1813–1827, 2014.
- [191] S. R. Cominesi, M. Farina, L. Giulioni, B. Picasso, and R. Scattolini, “A two-layer stochastic model predictive control scheme for microgrids,” *IEEE Transactions on Control Systems Technology*, vol. 26, no. 1, pp. 1–13, 2017.
- [192] D. B. Nguyen, J. M. Scherpen, and F. Bliëk, “Distributed optimal control of smart electricity grids with congestion management,” *IEEE Transactions on Automation Science and Engineering*, vol. 14, no. 2, pp. 494–504, 2017.
- [193] K. Edlund, J. D. Bendtsen, and J. B. Jørgensen, “Hierarchical model-based predictive control of a power plant portfolio,” *Control Engineering Practice*, vol. 19, no. 10, pp. 1126–1136, 2011.
- [194] R. Halvgaard, L. Vandenberghē, N. K. Poulsen, H. Madsen, and J. B. Jørgensen, “Distributed model predictive control for smart energy systems,” *IEEE Transactions on Smart Grid*, vol. 7, no. 3, pp. 1675–1682, 2016.
- [195] K. Worthmann, C. M. Kellett, P. Braun, L. Grüne, and S. R. Weller, “Distributed and decentralized control of residential energy systems incorporating battery storage,” *IEEE Transactions on Smart Grid*, vol. 6, no. 4, pp. 1914–1923, 2015.

- [196] C.-F. Lu, C.-C. Liu, and C.-J. Wu, "Dynamic modelling of battery energy storage system and application to power system stability," *IEE Proceedings-Generation, Transmission and Distribution*, vol. 142, no. 4, pp. 429–435, 1995.
- [197] J. M. Guerrero, N. Berbel, J. Matas, J. L. Sosa, and L. G. De Vicuña, "Droop control method with virtual output impedance for parallel operation of uninterruptible power supply systems in a microgrid," in *APEC 07-Twenty-Second Annual IEEE Applied Power Electronics Conference and Exposition*, pp. 1126–1132, IEEE, 2007.
- [198] J. M. Guerrero, M. Chandorkar, T.-L. Lee, and P. C. Loh, "Advanced control architectures for intelligent microgrids—part i: Decentralized and hierarchical control," *IEEE Transactions on Industrial Electronics*, vol. 60, no. 4, pp. 1254–1262, 2012.
- [199] J. M. Guerrero, J. C. Vasquez, J. Matas, M. Castilla, and L. G. de Vicuña, "Control strategy for flexible microgrid based on parallel line-interactive ups systems," *IEEE Transactions on industrial Electronics*, vol. 56, no. 3, pp. 726–736, 2008.
- [200] E. W. Kimbark, *Direct current transmission*, vol. 1. John Wiley & Sons, 1971.
- [201] N. Chaudhuri, B. Chaudhuri, R. Majumder, and A. Yazdani, *Multi-terminal direct-current grids: Modeling, analysis, and control*. John Wiley & Sons, 2014.
- [202] A. Sumper, F. D'Áz-González, O. Gomis-Bellmunt, *et al.*, *Energy storage in power systems*. John Wiley & Sons, 2016.
- [203] Z. M. Salameh, M. A. Casacca, and W. A. Lynch, "A mathematical model for lead-acid batteries," *IEEE Transactions on Energy Conversion*, vol. 7, no. 1, pp. 93–98, 1992.
- [204] S. Aditya and D. Das, "Application of battery energy storage system to load frequency control of an isolated power system," *International journal of energy research*, vol. 23, no. 3, pp. 247–258, 1999.
- [205] M. Ceraolo, "New dynamical models of lead-acid batteries," *IEEE transactions on Power Systems*, vol. 15, no. 4, pp. 1184–1190, 2000.
- [206] K. Van den Bergh, E. Delarue, and W. D'haeseleer, "Dc power flow in unit commitment models," *TME Work. Pap. Environ. Tech. Rep.*, 2014.
- [207] M. K. Petersen, K. Edlund, L. H. Hansen, J. Bendtsen, and J. Stoustrup, "A taxonomy for modeling flexibility and a computationally efficient algorithm for dispatch in smart grids," in *2013 American control conference*, pp. 1150–1156, IEEE, 2013.
- [208] D. S. Callaway and I. A. Hiskens, "Achieving controllability of electric loads," *Proceedings of the IEEE*, vol. 99, no. 1, pp. 184–199, 2010.
- [209] M. Farina, P. Colaneri, and R. Scattolini, "Block-wise discretization accounting for structural constraints," *Automatica*, vol. 49, no. 11, pp. 3411–3417, 2013.

- [210] E. G. Gilbert and K. T. Tan, "Linear systems with state and control constraints: The theory and application of maximal output admissible sets," *IEEE Transactions on Automatic control*, vol. 36, no. 9, pp. 1008–1020, 1991.
- [211] P. A. Trodden and J. M. Maestre, "Distributed predictive control with minimization of mutual disturbances," *Automatica*, vol. 77, pp. 31–43, 2017.
- [212] "National Grid ESO LFDD 09/08/2019 Incident Report ofgem." [https://www.ofgem.gov.uk/system/files/docs/2019/09/eso\\_technical\\_report\\_-\\_final.pdf](https://www.ofgem.gov.uk/system/files/docs/2019/09/eso_technical_report_-_final.pdf).
- [213] "Drax britains." <https://www.drax.com/energy-policy/britains-blackout/#chapter-1/>.
- [214] E. D. Medagoda and P. W. Gibbens, "Multiple horizon model predictive flight control," *Journal of Guidance, Control, and Dynamics*, vol. 37, no. 3, pp. 946–951, 2014.
- [215] X. Chen, M. Heidarinejad, J. Liu, and P. D. Christofides, "Composite fast-slow mpc design for nonlinear singularly perturbed systems," *AIChE Journal*, vol. 58, no. 6, pp. 1802–1811, 2012.
- [216] M. Ellis, M. Heidarinejad, and P. D. Christofides, "Economic model predictive control of nonlinear singularly perturbed systems," *Journal of Process Control*, vol. 23, no. 5, pp. 743–754, 2013.
- [217] M. Wogrin and L. Glielmo, "An mpc scheme with guaranteed stability for linear singularly perturbed systems," in *49th IEEE Conference on Decision and Control (CDC)*, pp. 5289–5295, IEEE, 2010.
- [218] J. P. Koeln and A. G. Alleyne, "Robust hierarchical model predictive control of graph-based power flow systems," *Automatica*, vol. 96, pp. 127–133, 2018.
- [219] J. P. Koeln, H. C. Pangborn, M. A. Williams, M. L. Kawamura, and A. G. Alleyne, "Hierarchical control of aircraft electro-thermal systems," *IEEE transactions on control systems technology*, vol. 28, no. 4, pp. 1218–1232, 2019.







$$\begin{aligned}
B^c = & \begin{bmatrix} 0 & 0 & 0 & 0 \\ 0 & 0 & 0 & 0 \\ \frac{\tau_{1,1}}{Tg1} & 0 & 0 & 0 \\ 0 & 0 & 0 & 0 \\ \frac{\tau_{1,2}}{Tg2} & 0 & 0 & 0 \\ 0 & \frac{1}{Tb1} & 0 & 0 \\ 0 & 0 & 0 & 0 \\ 0 & 0 & 0 & 0 \\ 0 & 0 & 0 & 0 \\ 0 & 0 & \frac{\tau_{2,3}}{Tg3} & 0 \\ 0 & 0 & 0 & 0 \\ 0 & 0 & \frac{\tau_{2,4}}{Tg4} & 0 \\ 0 & 0 & 0 & \frac{1}{Tb2} \\ 0 & 0 & 0 & 0 \end{bmatrix}; \bar{B}^c = \begin{bmatrix} \frac{-Kp1}{Tp1} & \frac{-Kp1}{Tp1} & 0 & 0 \\ 0 & 0 & 0 & 0 \\ \frac{\chi_{1,1}}{Tg1} & \frac{\chi_{1,2}}{Tg1} & \frac{\chi_{1,3}}{\alpha_{12}Tg1} & \frac{\chi_{1,4}}{\alpha_{12}Tg1} \\ 0 & 0 & 0 & 0 \\ \frac{\chi_{2,1}}{Tg2} & \frac{\chi_{2,2}}{Tg2} & \frac{\chi_{2,3}}{\alpha_{12}Tg2} & \frac{\chi_{2,4}}{\alpha_{12}Tg2} \\ 0 & 0 & 0 & 0 \\ 0 & 0 & 0 & 0 \\ 0 & 0 & 0 & 0 \\ 0 & 0 & 0 & 0 \\ \frac{\alpha_{12}\chi_{3,1}}{Tg3} & \frac{\alpha_{12}\chi_{3,2}}{Tg3} & \frac{\chi_{3,3}}{Tg3} & \frac{\chi_{3,4}}{Tg2} \\ 0 & 0 & 0 & 0 \\ \frac{\alpha_{12}\chi_{4,1}}{Tg4} & \frac{\alpha_{12}\chi_{4,2}}{Tg4} & \frac{\chi_{4,3}}{Tg4} & \frac{\chi_{4,4}}{Tg4} \\ 0 & 0 & 0 & 0 \\ 0 & 0 & 0 & 0 \end{bmatrix}; \tilde{B}^c = \begin{bmatrix} \frac{-Kp1}{Tp1} & 0 \\ 0 & 0 \\ 0 & 0 \\ 0 & 0 \\ 0 & 0 \\ 0 & 0 \\ 0 & 0 \\ 0 & 0 \\ 0 & 0 \\ 0 & \frac{-Kp2}{Tp2} \\ 0 & 0 \\ 0 & 0 \\ 0 & 0 \\ 0 & 0 \\ 0 & 0 \end{bmatrix}
\end{aligned} \tag{A.2}$$

$$C^c = \begin{bmatrix} \beta 1 & 0 & 0 & 0 & 0 & 0 & 0 & 0 & 1 & 0 & 0 & 0 & 0 & 0 & 0 & 0 \\ 0 & 0 & 0 & 0 & 0 & 0 & 0 & 1 & 0 & 0 & 0 & 0 & 0 & 0 & 0 & 0 \\ 0 & 0 & 0 & 0 & 0 & 0 & 0 & 0 & -\alpha_{12} & \beta 2 & 0 & 0 & 0 & 0 & 0 & 0 \\ 0 & 0 & 0 & 0 & 0 & 0 & 0 & 0 & 0 & 0 & 0 & 0 & 0 & 0 & 0 & 1 \end{bmatrix} \tag{A.3}$$

$$D^c = \begin{bmatrix} (\chi_{3,1} + \chi_{4,1}) & (\chi_{3,2} + \chi_{4,2}) & -\frac{1}{\alpha_{12}}(\chi_{1,3} + \chi_{2,3}) & -\frac{1}{\alpha_{12}}(\chi_{1,4} + \chi_{2,4}) \\ 0 & 0 & 0 & 0 \\ -\alpha_{12}(\chi_{3,1} + \chi_{4,1}) & -\alpha_{12}(\chi_{3,2} + \chi_{4,2}) & (\chi_{1,3} + \chi_{2,3}) & (\chi_{1,4} + \chi_{2,4}) \\ 0 & 0 & 0 & 0 \end{bmatrix} \tag{A.4}$$

### A.1.2 Deregulated Power System Model - No BESS

$$A^c = \begin{bmatrix} \frac{-1}{Tp1} & \frac{Kp1}{Tp1} & 0 & \frac{Kp1}{Tp1} & 0 & \frac{-Kp1}{Tp1} & 0 & 0 & 0 & 0 & 0 \\ 0 & \frac{-1}{Tt1} & \frac{1}{Tt1} & 0 & 0 & 0 & 0 & 0 & 0 & 0 & 0 \\ \frac{-1}{R1Tg1} & 0 & \frac{-1}{Tg1} & 0 & 0 & 0 & 0 & 0 & 0 & 0 & 0 \\ 0 & 0 & 0 & \frac{-1}{Tt2} & \frac{1}{Tt2} & 0 & 0 & 0 & 0 & 0 & 0 \\ \frac{-1}{R2Tg2} & 0 & 0 & 0 & \frac{-1}{Tg2} & 0 & 0 & 0 & 0 & 0 & 0 \\ T12 & 0 & 0 & 0 & 0 & 0 & -T12 & 0 & 0 & 0 & 0 \\ 0 & 0 & 0 & 0 & 0 & \frac{\alpha_{12}Kp2}{Tp2} & \frac{-1}{Tp2} & \frac{Kp2}{Tp2} & 0 & \frac{Kp2}{Tp2} & 0 \\ 0 & 0 & 0 & 0 & 0 & 0 & 0 & \frac{-1}{Tt3} & \frac{1}{Tt3} & 0 & 0 \\ 0 & 0 & 0 & 0 & 0 & 0 & \frac{-1}{R3Tg3} & 0 & \frac{-1}{Tg3} & 0 & 0 \\ 0 & 0 & 0 & 0 & 0 & 0 & 0 & 0 & 0 & \frac{-1}{Tt4} & \frac{1}{Tt4} \\ 0 & 0 & 0 & 0 & 0 & 0 & \frac{-1}{R4Tg4} & 0 & 0 & 0 & \frac{-1}{Tg4} \end{bmatrix} \quad (A.5)$$

$$B^c = \begin{bmatrix} 0 & 0 \\ 0 & 0 \\ \frac{\tau_{1,1}}{Tg1} & 0 \\ 0 & 0 \\ \frac{\tau_{1,2}}{Tg2} & 0 \\ 0 & 0 \\ 0 & 0 \\ 0 & 0 \\ 0 & \frac{\tau_{2,3}}{Tg3} \\ 0 & 0 \\ 0 & \frac{\tau_{2,4}}{Tg4} \end{bmatrix}; \bar{B}^c = \begin{bmatrix} \frac{-Kp1}{Tp1} & \frac{-Kp1}{Tp1} & 0 & 0 \\ 0 & 0 & 0 & 0 \\ \frac{\chi_{1,1}}{Tg1} & \frac{\chi_{1,2}}{Tg1} & \frac{\chi_{1,3}}{\alpha_{12}Tg1} & \frac{\chi_{1,4}}{\alpha_{12}Tg1} \\ 0 & 0 & 0 & 0 \\ \frac{\chi_{2,1}}{Tg2} & \frac{\chi_{2,2}}{Tg2} & \frac{\chi_{2,3}}{\alpha_{12}Tg2} & \frac{\chi_{2,4}}{\alpha_{12}Tg2} \\ 0 & 0 & 0 & 0 \\ 0 & 0 & \frac{-Kp2}{Tp2} & \frac{-Kp2}{Tp2} \\ 0 & 0 & 0 & 0 \\ \frac{\alpha_{12}\chi_{3,1}}{Tg3} & \frac{\alpha_{12}\chi_{3,2}}{Tg3} & \frac{\chi_{3,3}}{Tg3} & \frac{\chi_{3,4}}{Tg2} \\ 0 & 0 & 0 & 0 \\ \frac{\alpha_{12}\chi_{4,1}}{Tg4} & \frac{\alpha_{12}\chi_{4,2}}{Tg4} & \frac{\chi_{4,3}}{Tg4} & \frac{\chi_{4,4}}{Tg4} \end{bmatrix}; \tilde{B}^c = \begin{bmatrix} \frac{-Kp1}{Tp1} & 0 \\ 0 & 0 \\ 0 & 0 \\ 0 & 0 \\ 0 & 0 \\ 0 & 0 \\ 0 & \frac{-Kp2}{Tp2} \\ 0 & 0 \\ 0 & 0 \\ 0 & 0 \end{bmatrix} \quad (A.6)$$

$$C^c = \begin{bmatrix} \beta 1 & 0 & 0 & 0 & 0 & 1 & 0 & 0 & 0 & 0 & 0 \\ 0 & 0 & 0 & 0 & 0 & -\alpha_{12} & \beta 2 & 0 & 0 & 0 & 0 \end{bmatrix} \quad (A.7)$$

$$D^c = \begin{bmatrix} (\chi_{3,1} + \chi_{4,1}) & (\chi_{3,2} + \chi_{4,2}) & -\frac{1}{\alpha_{12}}(\chi_{1,3} + \chi_{2,3}) & -\frac{1}{\alpha_{12}}(\chi_{1,4} + \chi_{2,4}) \\ -\alpha_{12}(\chi_{3,1} + \chi_{4,1}) & -\alpha_{12}(\chi_{3,2} + \chi_{4,2}) & (\chi_{1,3} + \chi_{2,3}) & (\chi_{1,4} + \chi_{2,4}) \end{bmatrix} \quad (\text{A.8})$$

## A.2 Chapter 4

### A.2.0.1 Transformation Matrices

$$V = \begin{bmatrix} I_1 & 0 & 0 \\ 0 & I_2 & 0 \\ 0 & I_2 & 0 \\ 0 & 0 & I_3 \end{bmatrix}; \quad M = \begin{bmatrix} I_1 & 0 & 0 & 0 \\ 0 & \frac{1}{2}I_2 & \frac{1}{2}I_2 & 0 \\ 0 & 0 & 0 & I_3 \end{bmatrix}; \quad U * V = I_n \quad (\text{A.9})$$

